Universidade do Minho
Escola de Engenharia

Leslie Edith Alejo Guerra

Seismic behaviour and strengthening of barrel vaults of Augustinian churches in Mexico

January 2022

Seismic behaviour and strengthening of barrel vaults of Augustinian churches in Mexico

Leslie Edith Alejo Guerra

UMinho | 2022

Universidade do Minho
Escola de Engenharia

Leslie Edith Alejo Guerra

Seismic behaviour and strengthening of barrel vaults of Augustinian churches in Mexico

Doctoral Thesis
Civil Engineering

Work developed under supervision of
Professor Paulo B. Lourenço
Doctor Nuno Mendes
Professor Guillermo Martínez Ruiz

January 2022

Acknowledgments

This thesis has been performed at the University of Minho in collaboration with the Michoacan University of Nicolas of Hidalgo. The author acknowledges the economic support provided by CONACyT (Consejo Nacional de Ciencia y Tecnología– Mexico), within the scope of the call CONACyT-Alianza FiiDEM 2016 (291111), fellowship 439857/268696, CVU 446408.

I would like to express my gratitude to my supervisors not only for the academic contributions but also for the emotional support. To Professor Paulo B. Lourenço, thank you for your guidance and for that "just in the right moment" conversation, it was very important to me; to Doctor Nuno Mendes, thank you for all the knowledge you shared with me and for your endless patience; to Professor Guillermo Martínez, thank you for the introduction to this field and for the encouragement from the distance. This work would not have been possible without the support of several people who were directly or indirectly involved. To Doctor Juan Cabrera Aceves, thank you for the inspiration and for always taking the time to answer my emails with interesting information. To Doctor Carlos E. Mendoza, I appreciate the geometrical data provided, it was essential for this research. To MSE Rodolfo Gaytán, thank you for organizing and carrying out the dynamic identification campaign for the case study. To Father Manuel Belman, thank you for the empathy regarding this investigation and for granting us access to the building during the performed tests.

To my friends Laura, Pablo, Mary and Diego, thank you for the trust and support when I made the decision to start this adventure. To my former boss and teacher, Doctor J. Jesús Alvarez Sereno, thank you for the support, the advice, the teaching and the friendship. To the friends I made during this experience, Ioana, Giorgos, Fabio, Nicoletta, María Pia, Telma and Pilar, thank you for making my journey more pleasant and enjoyable. To my fellow Mexicans, Rafa, Isis, Diego, Daniel and Daniel, thank you for making me feel that there was a "*cachito*" (small piece) of Mexico in Portugal. To my family in Guimaraes, Rafa, Elesban, Xinyu, Meera and Antonio, I will always be grateful for having met you. Thank you for sharing not only your knowledge but also your shoulders, for taking care of me when necessary and for allowing me to grow wiser by your side. Thank you to my family, my father, my mother and my siblings, you have always been there to tell me that I can reach my goals, to push me when I need to be pushed and to celebrate when the time to celebrate comes. Thank you, from the bottom of my heart, for the unconditional support to all my craziness in life. Finally, and especially, I want to thank Alberto for all the emotional support, for the time invested in checking my work, for the interesting discussions and suggestions and for never letting me believe that I could not do it. All my gratitude to you.

STATEMENT OF INTEGRITY

I hereby declare having conducted this academic work with integrity. I confirm that I have not used plagiarism or any form of undue use of information or falsification of results along the process leading to its elaboration.

I further declare that I have fully acknowledged the Code of Ethical Conduct of the University of Minho.

Resumo

Os conventos do século XVI são um exemplo significativo do rico e variado Património Cultural Mexicano, difundido em mais de metade do país. As construções agostinianas caracterizam-se por projetos muito ambiciosos, com naves únicas, atingindo até 70 m de comprimento e mais de 13 m de largura, cobertas por abóbadas de berço. Concebido maioritariamente para suportar cargas estáticas verticais, este sistema de cobertura demonstrou ser extremamente vulnerável a eventos sísmicos moderados. O México está localizado numa zona com elevada sismicidade e vários Estados estão em perigo sísmico constante. A maioria dos conventos mexicanos do século XVI estão situados nesses Estados. Recentemente, após os terremotos de Chiapas e Puebla em 2017, várias dessas estruturas, pertencentes à *"La Ruta de los Conventos"* (A Rota dos Conventos), foram severamente danificadas.

O principal objetivo da presente tese é fornecer informações valiosas sobre o comportamento sísmico das igrejas agostinianas de nave única do período colonial e apoiar a sua preservação através da análise de técnicas de reforço adequadas para prevenir os danos causados por sismos. Assim, foi selecionado um caso de estudo relevante, nomeadamente o templo de Santo Agostinho, localizado no centro histórico da cidade de Morelia (Michoacan), reconhecida como Património Cultural pela UNESCO desde 1991. Foi realizada uma inspeção visual da igreja e ensaios de identificação dinâmica utilizando vibração ambiental. Foi desenvolvido um modelo numérico 3D FEM detalhado no programa DIANA, adotando uma abordagem de macro-modelação, e calibrado relativamente às frequências naturais identificadas experimentalmente. O *Modal Assurance Criterion* (MAC) validou a precisão do modelo calibrado. Por forma a avaliar o desempenho sísmico da igreja, foram realizadas análises dinâmicas não lineares (NLDA) e análises estáticas não lineares (POA). Após a determinação da capacidade da estrutura, foram definidas e analisadas seis configurações de reforço usando a POA, tendo por objetivo avaliar a melhoria da capacidade sísmica. A análise do edifício não reforçado demonstrou que a igreja suportaria o sismo de projeto, de acordo com o mapa de perigosidade sísmica produzido pelo INEEL, embora apresentando um fator de segurança baixo. A abóbada de berço, os arcos transversais, a cúpula, a fachada, o presbitério e a abóbada de aresta são os elementos mais vulneráveis, apresentando mecanismos de colapso característicos e semelhantes aos identificados durante os levantamentos pós-sismo. As técnicas de reforço adotadas produziram um incremento máximo na capacidade estrutural de 92% e 57% na direção transversal e longitudinal, respetivamente.

Palavras-chave: Construções agostinianas; abóbada de berço; modelo FEM; análise não linear dinâmica; análise não linear estática.

Abstract

Convents from the 16th century are a significant example of the rich and varied Mexican Cultural Heritage, widespread in more than half of the country. Among them, Augustinian constructions are characterised by very ambitious projects, with single naves, reaching up to 70 m in length and more than 13 m in width, covered by barrel vaults. Being conceived mostly to stand vertical static loads, this roofing system is particularly concerning and proved to be extremely vulnerable against moderate seismic events. Mexico is located in a highly seismic area known as the ring of fire and several states are under a constant seismic hazard. The majority of the Mexican convents from the 16th century is located in these states. Recently, after the earthquakes of Chiapas and Puebla of 2017, several of these structures, belonging to "*La Ruta de los Conventos*" (The Route of the Convents), were severely damaged.

The main objective of the present thesis is to provide valuable insight into the seismic behaviour of Augustinian single-nave churches from the colonial period and support their preservation by analysing suitable strengthening techniques to prevent or reduce the damage caused by earthquakes. To achieve it, a relevant case study was selected, namely the temple of *San Agustin*, located in the historic city centre of Morelia (Michoacan), recognised as Cultural Heritage by UNESCO since 1991. An accurate visual inspection of the church and dynamic identification tests, using ambient vibration, were carried out. A detailed numerical 3D FEM model was developed in the environment of the DIANA software, adopting a macro-modelling approach, and calibrated to the experimentally identified natural frequencies. The Modal Assurance Criterion (MAC) validated the accuracy of the updated model. In order to evaluate the seismic performance of the church, nonlinear dynamic analyses (NLDA) and pushover analyses (POA) were performed. After determining the capacity of the structure, six strengthening configurations were defined and analysed using POA, aiming at improving the seismic capacity. The analysis of the unreinforced building demonstrated that the church would stand the expected earthquake, according to the hazard map by INEEL, although presenting a low safety factor. The barrel vault, transverse arches, dome, façade, presbytery and groin vault are the most vulnerable elements, presenting collapse mechanisms and damage scenarios similar to those identified during post-earthquake surveys. The strengthening techniques adopted produced a maximum increment in the structural capacity of 92% and 57% in transverse and longitudinal direction, respectively.

Keywords: Augustinian constructions; barrel vault; FEM model; nonlinear dynamic analysis; pushover analysis.

Contents

Index of figures

Index of tables

Chapter 1
Introduction

1.1. Motivation

Mexico boasts a varied and rich built Cultural Heritage (CH), encompassing the legacy of numerous and advanced pre-Hispanic civilizations as well as the peculiar results of the graft of European models into this enduring cultural background. Convents from the 16th century constitute numerous and prominent examples of Mexican Heritage. Built under the supervision of the Mendicant friars of the Franciscan, Dominican and Augustinian orders, the convents were widespread in more than half of the country by 1580 (Waldinger, 2013).

As stressed by Chanfón (1996), a Mexican architect active in the field of conservation, a society is identified by its culture. CH assets, although objective evidence of individualism, contribute to build over time this common culture. Protecting CH is, therefore, equivalent to protecting an identity factor: each generation has the duty of conserving it and transmitting it to the following ones. Ironically, human-

generated activities often contribute to CH deterioration and destruction rather than to its preservation, and this has been a constant in the timeline of many countries (Krauze, 2013). Anthropogenic actions as structural and architectural alterations, increment of operational loadings, lack of maintenance and conservation, inadequate interventions, wars or conflicts, urbanization and even tourism and cultural attraction are potentially detrimental for CH. Noteworthy examples of events that caused CH losses in the world are the large fires of Rome in 64 (Barrett, 2020), of London in 1666 (Alagna, 2004), or of Moscow in 1812 (Schönle, 2021) or the fatal earthquakes that struck Lisbon in 1755 (Mendes-Victor et al., 2008) and San Francisco in 1906 (Fradkin, 2006). Mexico is not an exception. The transition between ending and beginning of social/political eras often came along with the destruction of many emblematic buildings, under the flag of "order and progress", making way to new constructions, claiming to bring the latest fashions and technologies for the era (Ruiz Razura & Fregoso Torres, 2020). In this context, great CH buildings from Mexico city were destroyed (Tovar de Teresa, 1990). Similarly, in Guadalajara city centre, after the Mexican Revolution and following the desire of establishing a modern civil state separated from the power of the religion, the total or partial demolition of valuable religious buildings was common (Cabrales Barajas, 2015). Besides the intentional destruction, the ignorance about the importance of CH overshadows its real value and reduces the economical investments in preservation (CCSEM 2014), leading to neglection, lack of maintenance and, ultimately, abandonment to factors that trigger the decay of the materials and, thus, of the structure itself. On the other hand, even when investments in preservation are made, poor knowledge of the traditional structural systems and null or inadequate training of the involved stakeholders may result in improper interventions. **Figure 1-1** shows some examples of severely damaged Mexican CH along time.

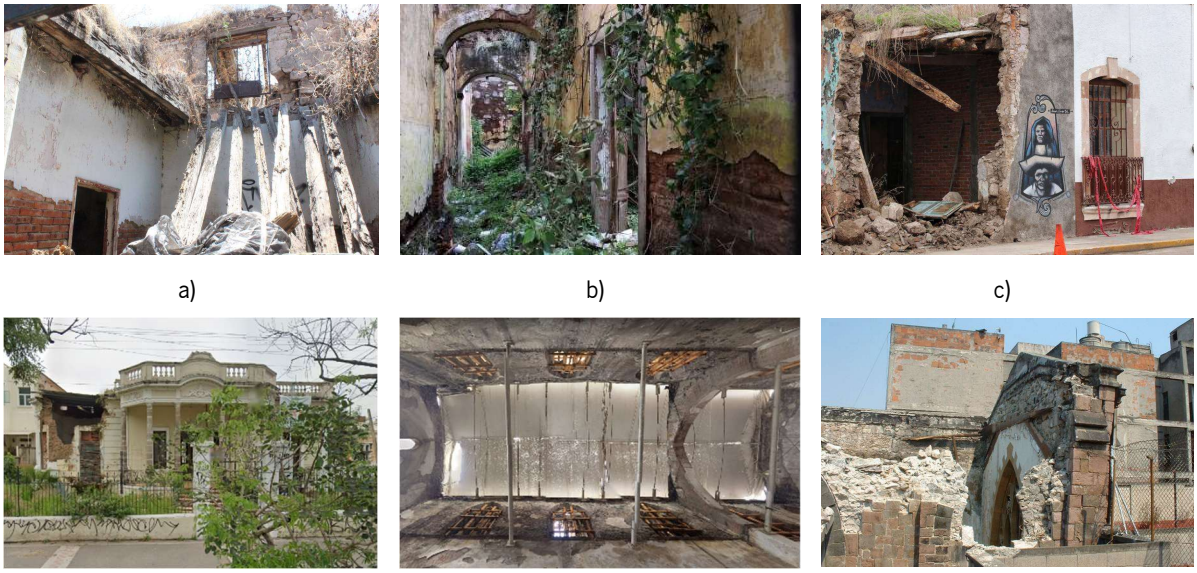

a) b) c)

d) e) f)

Figure 1-1. Long-term deterioration of Cultural Heritage. Ancient houses at Morelia historical city centre: a) picture by Luna (2019); b) and c) pictures by Maldonado (2019a, 2019b). d) *Castiello* house at Guadalajara historical city centre (Google Maps, 2021). Old Christ Church in Mexico city: e) missing roof (Google Maps, 2019); f) back wall of the presbytery (Piñón, 2014).

Such anthropogenic actions contribute to further weakening CH that is already threatened by environmental actions, through physical weathering and natural disasters, mainly earthquakes. Building collapses due to earthquakes can lead to many human losses. Indeed, according to Statista Research Department (2016), five of the ten natural extreme events that have caused more harm to humanity, in terms of deaths, are earthquakes, as shown by the red bars in **Figure 1-2**. If the two tsunamis shown in the figure are considered also (they were generated by earthquakes), then the count adds to seven out of ten more deadly disasters.

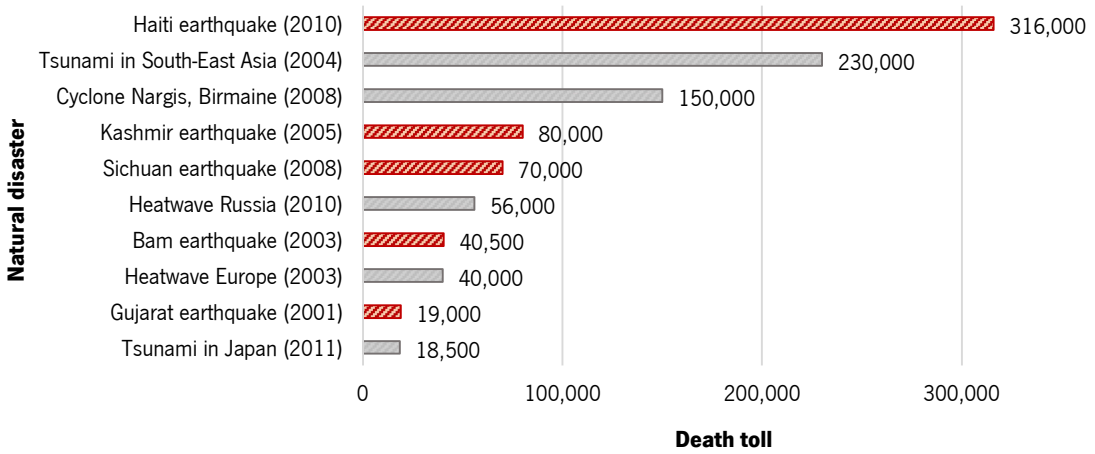

Figure 1-2. The worst natural hazards of the 21st century, based on the number of deaths: earthquakes in red [adapted from (SRD, 2016)].

Mexico, as well, is located in a highly seismic area. **Figure 1-3** shows the exposition of the heritage to earthquakes by overlapping the location of the CH sites in the list of UNESCO with the seismicity map of the country. Oaxaca and Michoacan are the regions with the higher seismic activity, followed by Morelos, Puebla and part of Veracruz. Mexico state, Tlaxcala and Hidalgo are also characterised by a significant seismic hazard (Meli, 2011).

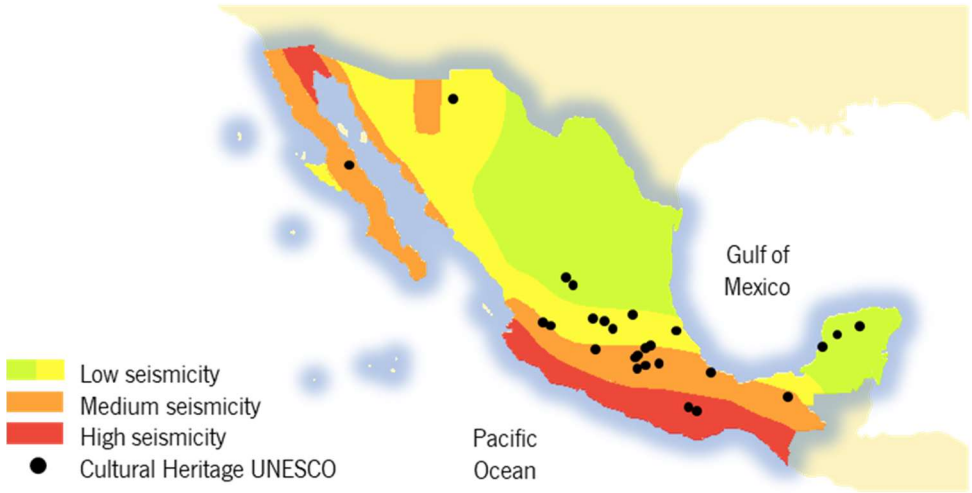

Figure 1-3. Location of the Mexican CH by UNESCO (2020a) overlapping the seismicity map of the country [adapted from (INEEL, 2017)].

The majority of the convents from the 16th century are located in seismic areas and demonstrated to be extremely vulnerable to seismic actions. Considering Mexican seismic history, many of them have been subjected to several earthquakes during their lifetime. In the period between 1568 and 1870, 21 earthquakes with intensity higher than VIII (Modified Mercalli scale) are documented. In the period between 1805 and 2000, the monitoring of the seismicity allowed to record 36 important strokes with magnitudes higher than 7.5 (Mw). After 2000, 38 events with magnitudes higher than 6.4 have been documented (Cotilla-Rodríguez et al., 2019; SSN, 2021). According to Forbes Mexico (2021), the eight most catastrophic earthquakes that the country has ever suffered, ordered by magnitude, are: M = 8.6, Oaxaca, 1787; M = 8.2, Chiapas, 2017; M = 8.1, Michoacan, 1985; M = 7.8, Guerrero, 1957; M = 7.5, Guerrero, 2012; M = 7.2, Baja California, 2010; M = 7.1, Puebla, 2019; and M = 7.0, Mexico state, 1912. Post-earthquake surveys in the last decades recorded a large number of convent buildings that suffered significant damages. For example, in the recent seismic events of Chiapas and Puebla, on September 8 and 19 of 2017 respectively, the temple of *San Juan Bautista* in Morelos, the temple of *la Virgen del Patrocinio* in Oaxaca and the Augustinian ex-convent of Malinalco in Mexico suffered mainly, partial collapses. Most of the structures belonging to "The Route of the Convents" (*La Ruta de Los Conventos* in Spanish) were severely damaged. Earthquakes, indeed, are a constant threat to this typology of CH, as it mainly comprises unreinforced masonry buildings. These structures were conceived mostly to present structural capacity for vertical static loads (Lourenço et al., 2011). However, they are highly vulnerable against moderate seismic events (Bothara & Brzev, 2011). An important percentage of churches present a typical single nave covered by barrel vaults supported by longitudinal bearing walls. The compressive behaviour of vaults allows the use of materials with low tensile strength. Nevertheless, the capacity of this structural element can be affected by horizontal displacements at the supports, leading to the formation of hinges and, in extreme cases, partial or total collapse (ICOMOS/ISCARSAH, 2003). This characteristic damage under lateral loads consists of cracking at one side of the intrados as well as at the opposite side on the extrados (see **Figure 1-4**a). In addition, the vertical component of an earthquake produces the vertical vibration of the vault. The downward displacement of the crown generates extra horizontal thrust, which contributes to the opening of the higher part of the walls. This action can be the cause of cracking appearing at the intrados of the crown and at the extrados haunches (see **Figure 1-4**b).

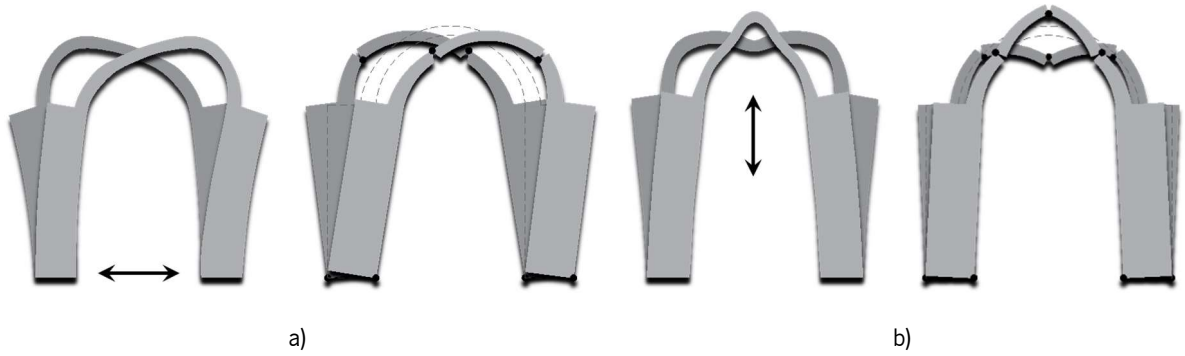

a) b)

Figure 1-4. Damage in barrel vaults caused by the earthquake: a) failure mechanism due to horizontal displacements; b) failure mechanism due to vertical displacements [adapted from (Meli, 2011)].

The majority of the damage presented in a vault roofing system is due to the movement of the supports, influenced by their considerable height, allowing out-of-plane vibrations and causing cracks. Besides the supports system (walls and buttresses), the shape and the span of the vault are also important factors for the structural behaviour (Meli, 2011; Meli & Peña, 2004). Many interventions carried out in the past were inappropriate due to incorrect assumptions. However, nowadays, the focus of the conservation aims to a deep understanding of the building (Roca et al., 2019), suggesting intervention procedures to be respectful of the aesthetics, the functions, the original structure and its strength, ductility and stiffness. Usually, the peculiarity of each case leads to specific requirements and solutions, limiting the generalisation to more case studies (Hamid et al., 1994). Therefore, as stressed in recommendations, such as the ISCARSAH by ICOMOS, each case should be studied in depth to better replicate its structural behaviour. Nonetheless, due to the contemporaneity of these churches in Mexico, most of them built in a short time interval during the 16th century, with similar geometrical characteristics and architectural features (buildings typologies), there is the possibility that the detailed analysis of few representative case studies and the identification of effective remedial measures may lead to a generalised solution.

The interest of asset managers and institutions, such as INAH (National Institute of Anthropology and History), in protecting and restoring Mexican churches from the 16th century, when necessary, has been growing in the last years, also due to the increased awareness of society and the concern of multidisciplinary scholars. Some studies (Chávez & Meli, 2007, 2010) were specifically devoted to this type of buildings and various strengthening techniques have been analysed. However, at this stage, more research is needed to deepen the understanding of their structural behaviour and the effectiveness of traditional and innovative strengthening techniques.

1.2. Objectives

The main objective of the present thesis is to provide valuable insight into the seismic behaviour of a type of Mexican CH, namely single-nave churches from the colonial period, and to support their cost-effective preservation, by analysing suitable strengthening techniques to prevent or reduce the damage caused by earthquakes. A detailed description of the features of such buildings is firstly provided together with an attempt to frame the evolution of this architectonical typology within the wider history of western architecture, between the 16th and 19th centuries. The main differences between the Mexican and the European churches are stressed, being this an essential step towards the understanding of the peculiarities of Mexican CH and the development of a tailored preservation strategy. The existence of a large number of assets with common features supports the idea of performing a detailed analysis of a representative building to infer information on the structural behaviour, the vulnerability and the effectiveness of remedial measures that can be generalised to other cases.

Hence, a relevant case study is selected, namely, the single-nave temple of San Agustin, dated back to the 16th century, located in the historic centre of Morelia, capital of Michoacan and listed as CH. This building is representative of several CH assets distributed all over the country and especially in areas with medium and high exposure to seismic hazards. The church presented some damage due to an earthquake in 2014. In order to address the sources of uncertainties typical of existing building diagnosis, an accurate characterisation of the case study geometry, material properties and structural details is carried out, by means of: 1) a thorough reconstruction of the building past events; 2) a detailed geometrical and damage survey; 3) an extensive dynamic identification campaign, focused mainly on the barrel vault.

For the seismic assessment and the design of the structural strengthening, the Finite Element Macro-modelling approach is selected. The analysis procedures investigated are pushover analysis and non-linear time history analysis. The characteristics of seismic hazard in Mexico, with specific attention to the southern area of the country, is analysed and 8 seismic records are selected to perform the analyses. These records were registered at different stations during earthquakes that induced significant damage to religious CH. Such a detailed and broad assessment aims at deepening the knowledge on the seismic behaviour of this class of single nave Mexican churches, improving the understanding of their structural capacity and their collapse mechanisms that, due to the differences with European CH, are expected to be distinct. This paramount investigation paves the way for tailor-made mitigation of Mexican CH vulnerabilities, liberated from the uncritical acceptance of solutions developed in another context, due to

a lack of knowledge. Indeed, this investigation aims to produce valuable information for the stakeholders that are involved in Mexican CH preservation, supporting with evidence their decision-making in terms of remedial measures.

In the definition of the strengthening techniques, specific attention is paid to the barrel vaults whose vulnerability in this type of church is a major concern. An optimisation of economic resources allocation is pursued by testing and comparing six different schemes: three schemes made of individual techniques (tie-rods, textile-reinforced mortar, TRM, at the intrados, stiffeners connected through TRM at the extrados) and three schemes obtained through combinations of individual strengthening measures.

The present thesis is just a step towards the achievement of the aforementioned objectives, therefore, after discussing the main conclusions, future research topics are proposed for a fruitful continuation of this work.

1.3. Outline and organization

In order to achieve the aforementioned objectives, this thesis is organised into seven chapters as follows:

- **Chapter 1** contains a brief introduction to the work with the motivation, objectives and outline of this research.
- **Chapter 2** aims at providing valuable insight into the origin and the evolution in time of Mexican built heritage with specific attention to the colonial period, namely from 1519 to 1810. This peculiar heritage is strongly characterized by hybridization between the buildings of Europe, mainly from Spain, and the local pre-Hispanic cultures and traditions. Therefore, similarities and differences between European and Mexican historic buildings are stressed, introducing main features, damage scenarios, heterogeneities and structural behaviour.
- **Chapter 3** describes the seismic hazard in Mexico, explaining how the country belongs to the Circum-Pacific Belt, the tectonics involved and how this affects, mostly, the south of the Mexican territory. Among the many existing records of great earthquakes that hit Mexico, five strokes are selected due to their magnitude, the damages caused to the built environment and the impact on society. Based on the provisions of the Mexican Construction code, eight seismic records from different stations are presented, considering the site effects, and adopted to perform the seismic assessment of this study.
- **Chapter 4** introduces the case study selected in this thesis as a significant and representative example of Mexican single-nave churches from the colonial period. This case study, San Agustin church, dates back to the 16th century and is located in Morelia, a city considered cultural heritage since 1991. In order to better represent its behaviour, dynamic identification tests are performed and a 3D FEM model is calibrated, obtaining more accurate results.
- **Chapter 5** reports the results of the assessment through 8 non-linear time history dynamic analyses considering three components of the earthquake (lateral in the transverse direction, lateral in the longitudinal direction and vertical). Besides the dynamic analyses, pushover analyses in the four horizontal directions (+X, -X, +Y, -Y) are also performed. The results are discussed and compared with the post-earthquake damage survey of Mexican heritage.
- **Chapter 6** evaluates and discusses six different schemes of strengthening for the barrel vault: tie-rods located at the impost line of both the transverse arches; layers of textile-reinforced mortar (TRM) at the intrados of the barrel vault; and stiffeners at the extrados of the barrel vault

connected through TRM. Three of the strengthening schemes are presented as individual techniques and three are presented as combinations of them. The comparisons are carried out in terms of damage, load capacity and displacements of the structure.

- **Chapter 7** summarises the main conclusions of the work and presents future lines for the research.

A schematic diagram of the thesis main body organisation is shown in **Figure 1-5**.

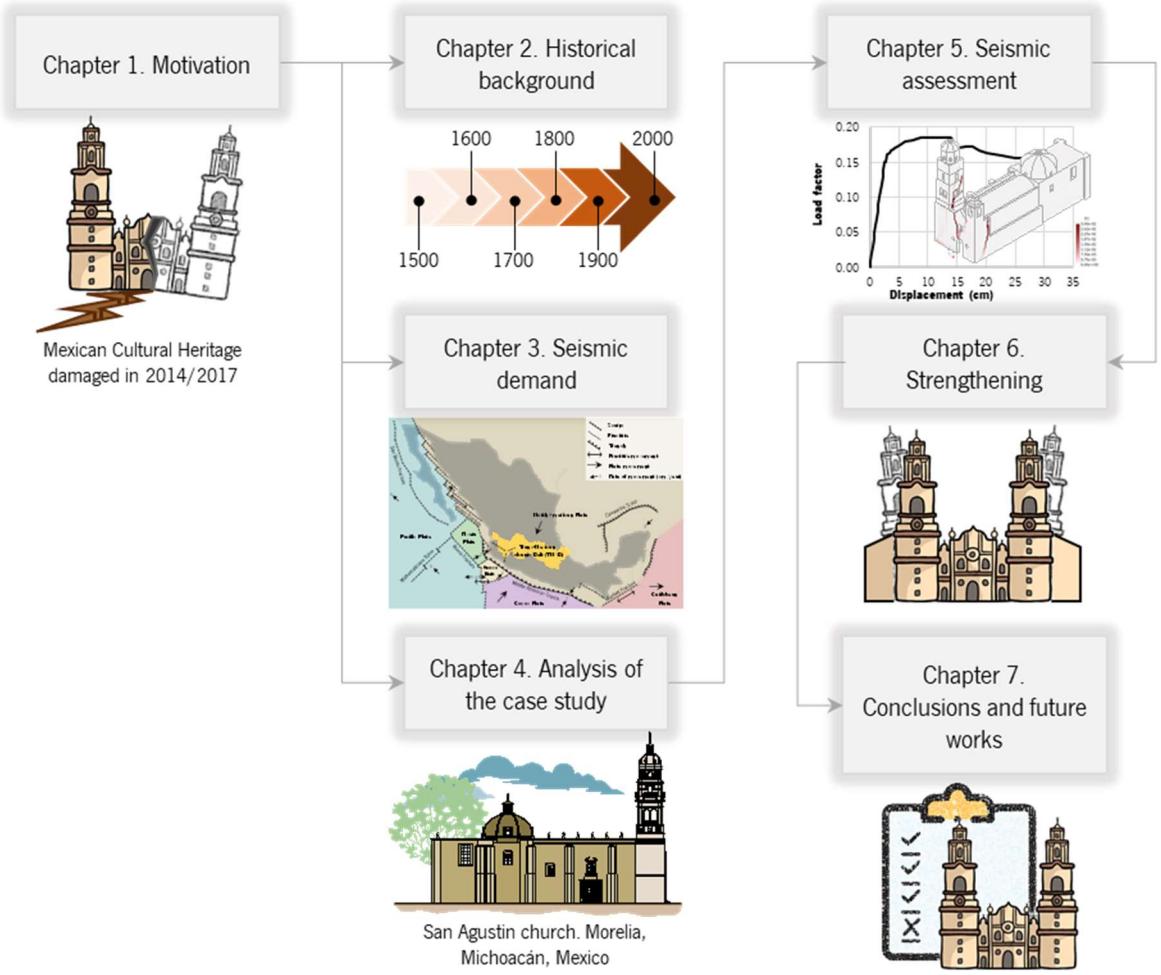

Figure 1-5. Diagram of the organization of the thesis.

Chapter 2
Historical Background

2.1. Introduction

Historical investigation is important as a part of the scientific and multidisciplinary approach necessary to understand the Built Heritage. Through the historical context, it is possible to understand the built heritage origin and evolution in time, being a valuable source of information in order to know characteristics, damage, heterogeneities, or even structural behaviour. The present chapter aims at providing a general overview of the historical context regarding the colonial period in Mexico. The styles developed in architecture during this stage, which in the country ranges from 1519 to 1810, are strongly characterised by a hybridisation between the models coming from Europe (mainly from Spain) and the local pre-Hispanic cultures and traditions. Therefore, the analysis of Mexican heritage requires a first introduction to the European influence, presented next, in Section 2.2, followed by a description of the Mexican Colonial Built Heritage, presented in Section 2.3.

2.2. European Influence in the Colonial Architecture

The Colonial era in Latin America ranges from 1492 (arrival of the first Columbus expedition) to the 19th century. During this period, new architectural elements and features were compulsory introduced, although their realization was often filtered by a process of imitation and adaptation to the indigenous traditions. This brought the evolution of unique local variants of the contemporary architectural styles developed in Europe. The comparison with European models, in fact, allows to understand and appreciate the evolution of the main architectural solutions in countries like Mexico. Therefore, in the present section, a brief overview of the European architecture is presented, with specific attention to Spain, as principal base design of the Mexican colonial styles.

2.2.1. Gothic

Religious beliefs have played an important role in the history of humanity, closely linked to the development in the different areas (politics, economy, education, etc.). Through years, religion has also assumed an outstanding influence in architecture. Evidence of this are the historical remaining buildings that show the relevance of the spirituality for the social life.

The term Gothic architecture refers to a style that originated in France during the 12th century and diffused to the rest of Europe. The style flourished until the 15th century when it was supplanted by the Renaissance. Since the Renaissance emerged as an alternative style with a brand-new aesthetic and way of building, the passage from Gothic was not synchronous everywhere and in some areas the Gothic continued during the 16th century.

The most significant achievements of Gothic architecture are related to religious buildings, namely churches, cathedrals and abbeys. These structures were designed to generate emotions that usually led to fearful respect for the holy supremacy through the magnificence of the buildings (Von Simson, 1988). Gothic religious architecture is mainly characterised by the use of pointed arches, cross ribbed vaults, flying buttresses, towers, pinnacles and tall spires, and high-pitched roofs. The elements present a significant height, which together with the extensive use of light contributes to the sense of magnificence. Although such features can be identified in many of the still existing examples (**Figure 2-1**), due to the long-time span in which the Gothic evolved, several variants of the style emerged with particular regional

characteristics. Each variant holds a rich historical background and its understanding deserves a deep study and a complete explanation of its specificities, see **Table 2-1** for selected examples.

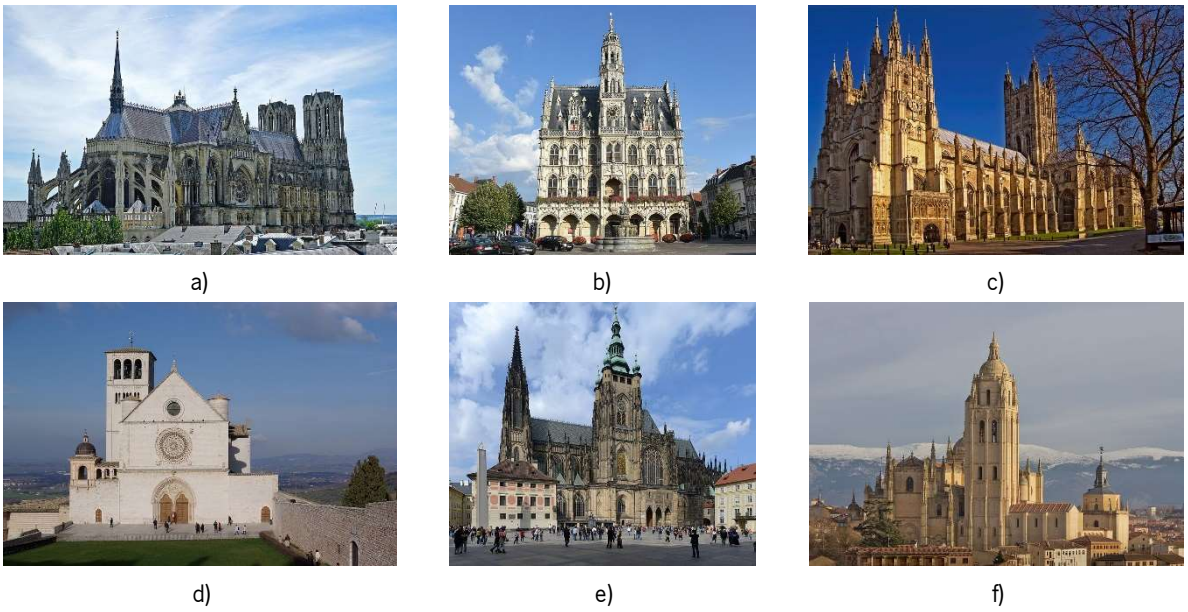

a) b) c)

d) e) f)

Figure 2-1. Examples of the different variants of the Gothic Style in Europe: a) French [Reims Cathedral by (Garitan, 2015)]; b) Brabantine [Oudenaarde City Hall (Hermans, 2016)]; c) English [Canterbury Cathedral (McCallum, 2006)]; d) Italian [Basilica of San Francesco of Assisi (Werner, 2009)]; e) German [Cathedral of Prague (Alvesgaspar, 2016)]; and f) Spanish [Cathedral of Segovia (Delgado, 2012)].

Table 2-1. Architectonic variants of the Gothic style.

Gothic variant	Architectonic examples
French Gothic	Notre-Dame Cathedral, Reims Cathedral (**Figure 2-1**a), Chartres Cathedral, and Amiens Cathedral
Brabantine Gothic	Brussels, Oudenaarde (**Figure 2-1**b) or Leuven City Hall
English Gothic	Westminster Abbey, Canterbury Cathedral (**Figure 2-1**c) or Salisbury Cathedral
Italian Gothic	Basilica of San Francesco of Assisi (**Figure 2-1**d), the church of Santa Maria della Spina in Pisa or the basilica of Sant'Antonio of Padua
German Gothic	cathedrals of Cologne, Strasbourg, Prague (**Figure 2-1**e) or Freiburg
Spanish Gothic	Monastery of San Juan de los Reyes in Toledo, the Royal Chapel of Granada, the cathedral of Segovia (**Figure 2-1**f) or the cathedral of Sevilla

Most of the buildings mentioned above are the result of a long construction process. Thus, they do not belong to a pure style, and are rather a combination of several styles.

In Spain, the Gothic arrived quite early, already in the 12th century, due to the connection with France through the pilgrimage routes. In this time, the actual Spain territory was divided into three main kingdoms

in the north, namely Navarre, Aragon and Castille, whereas the south was still ruled by Muslims. The evolution of Gothic architecture coincided with the completion of the "*Reconquista*". The coexistence of Muslim and Christians, with mutual influences since the 11th century, produced a peculiar style called Mudejar (Autorino, 1994). Between the 13th and the 15th century, this style is characterised by a combination of the influence of European Gothic architecture with Hispano-Islamic tradition. In Spain, the Mudejar religious buildings are both basilica and single nave, usually in brick masonry and with large use of wood and plaster (Autorino, 1994). Flat timber ceilings, sometimes carved and painted, are used with characteristic decorative geometric patterns (e.g. the so-called "*artesonados*", in **Figure 2-2**a, and "*alfarjes*", in **Figure 2-2**b). A typical architectural feature is the horseshoe arch, presented in **Figure 2-2**c. Mudejar art is especially evident in the decorative elements: ceramics [e.g. so called "*azulejos*" (tiles)] and woodwork.

a) b) c)

Figure 2-2. Typical elements of the Mudejar style: a) *Artesonado* on the ceiling of the Throne Room of the *Aljafería* (palace) in Zaragoza (Ecelan, 2004); b) *alfarjes* on the Hall of the Ambassadors of the Alcazar of Seville (Gordon, 2007); and c) typical horseshoe arch from the Mudejar style (Farlex, 2012).

The diffusion of the Mudejar style among Spain is due to the monumental model represented by the Muslim palaces in the newly conquered cities and the employment of skilled Mudejar craftsmen working for Christian patrons. Along the centuries, the palaces built in this style became the symbol of the Spanish Crown, such as the "Alcazar of Seville", and a way to communicate the new power, legitimating the style in the Christian kingdom. Also, in religious architecture, the Mudejar style was also justified by the need of adapting the monumental buildings to the needs of the new ruling class, for instance converting mosques into churches.

Gothic architecture reached, during the centuries, a high level of complexity, which testifies the development of a reliable structural design methodology. Although this methodology was different from

the modern scientific approach, it allowed to face a series of challenging tasks related with stereotomy, weight-lifting, centring and dimensioning. Learning a series of rules was likely to be the most important part of the training for a master builder. Unfortunately, only a small number of contemporary written sources offer an insight into such body of knowledge. The Album by Villard the Honnecourt illustrates the classic Gothic era without mentioning any structural detail. Besides that, the other remained documents mainly belong to the late-Gothic period. Among them the so-called treatises enclose information about particular aspects of design or structural matters related to specific buildings [e.g. the "treatises" of Enrique Egas, Francisco de Colonia or Rodrigo Gil de Hontañón and the expertise on structural problems of Milan (Ackerman, 1949) or Gerona (Huerta, 1998)] (Huerta, 2002).

The first architects and craftsmen who moved from Europe to Mexico were used to late-Gothic construction techniques and aesthetic. They introduced locally the body of knowledge developed in the previous centuries and trained the indigenous workers. Thus, even though the development of the colonial Mexican heritage coincided with the European Renaissance era, a strong Gothic influence is evident. Therefore, understanding and preservation of colonial heritage benefits from a more in-depth analysis of the characteristics of the Gothic architecture in terms of structural behaviour and vulnerability. In this regard, the Canterbury Cathedral, in which the structural assessment was carried by a team of the University of Minho (Karanikoloudis et al., 2020), is selected as a typical example of the Gothic. A brief description of the case study is provided hereafter.

2.2.1.1. Canterbury cathedral

Canterbury Cathedral is one of the most prestigious buildings of the United Kingdom and holds the title of UNESCO World Heritage since 1988. This Cathedral resulted from a long construction evolution (1070 to 1834). Considering the alterations and reconstructions, the Cathedral is a mixture of Romanesque, early-Gothic and Decorated Gothic styles (**Figure 2-3**). The description of such structure requires a historical background of its origin. During the Anglo-Saxon era, St. Agustin was declared the first Archbishop of Canterbury. By the year of 597, he established the first cathedral in the north-east of the city. This marked as well the starting period of the construction process that finished in 1070 and which can be divided in four phases (Collinson et al., 1995). Phase I (597-740): the church was a single nave and the altar was located at the apse; and the west, north and south façades were porches (porticus). Phase II (740-760): partial additions to the previous church; near the south-east corner of the nave, a detached building was constructed to be used as a baptistery and mausoleum for the archbishops. Phase III (9th or 10th century): an extensive campaign to enlarge of the cathedral was carried out. Part of the

growth focused on the widening of the foundations; porches were integrated into side aisles and the length of the cathedral increased from 23 m to 49 m (this phase was the prequel of a reorganization in order to incorporate monastic buildings). Phase IV (ended at 1067): the cathedral became bipolar by adding a major west polygonal apse, replacing the previously demolished squared west front; two towers were added at the eastern corners, lateral hexagonal stair towers were built in the west front and the arcade walls were strengthened; the total length increased to 75 m and the width to 31 m. In 1067, a great fire consumed the monastic complex, including the church.

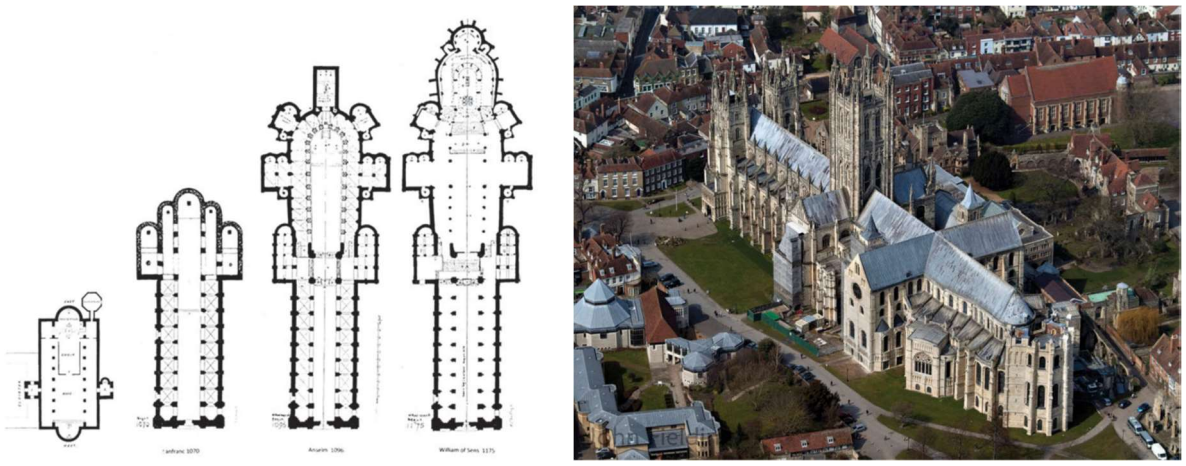

a) b)

Figure 2-3. a) Evolution of the construction process of the Canterbury Cathedral (Collinson et al., 1995); and b) southeast aerial view (photo by John Fielding 2013).

In 1070, the remains were demolished in order to rebuild the new cathedral with a Norman style, under the supervision of the Archbishop Lanfranc. In 1077, the new Norman cathedral was already in place; a tower, one transept, the crossing and a steeple were constructed. The distribution of the nave was in eight bays and the west front stood out with two twin towers crown with gilded pinnacles (Collinson et al., 1995; Dudley, 2010). An extension resulted from adding a new choir in 1096 by the Archbishop Anselm, who demolished the previous one and the underground crypts in order to increment the length to 58 m in east direction, counting from the crossing. The new construction included the ambulatory, chevette chapels, three level altars and an attaching chapel of the Holy Trinity. However, after almost 80 years, this choir was devastated due to a fire. The reconstruction was commissioned to Willian of Sens, who in 1096, not only rebuilt but also increased the choir height by 3.7 m starting the transition from the Romanesque to the Gothic style (Collinson et al., 1995). The bad state of the original nave (from 1077) motivated the project of demolition and reconstruction, and in 1378 the Archbishop Sudbury had started this modification. However, the process was stopped due to his decease in 1381. A year after, the "Synod

earthquake" (May 21st, 1382), estimated as 5.8 magnitude in the Richter scale, caused severe damage at the Cathedral's bell tower and cloister. During the period 1391-1411, Prior Thomas Chillenden was in charge of the reconstruction that included the nave and the transepts following a Perpendicular Gothic style, characterised by an emphasis on vertical lines. Thus, more slender elements replaced all piers and the side walls in the aisles disappeared to be rebuilt with the new characteristics, lierne vaults with bosses were used as a roofing system, raised to align with the choir roof. Alterations to the structure took place until 1834, mainly regarding the towers: in 1430 the demolition of the square tower at the crossing and the reinforcement of the piers, in order to support the new bigger tower (more than 70 m height) completed in 1504; the south-west tower was replaced in 1459; the north-west tower's spire remained until 1705; due to structural deficiencies, the tower was demolished in 1834 and replaced with a twin of the south-west tower. This was the last important modification to the current monument (Collinson et al., 1995; Willis, 1845). The intervention in the 20th century has been directed to the conservation of the structure as a cultural heritage, continuing up to the present time.

2.2.2. Renaissance

The term Renaissance refers to a cultural movement originated in centre of Italy, as a revival in the study of classical antiquity, during the 15th century, promoted by the renaissance humanists. This renovated interest culminated in the definition of new rules for architecture, arts and decoration inspired by the survived classical examples of roman era and justified by the authority of the ancient writers, especially Vitruvius.

In Spain, for all the arts, the passage from Gothic to Renaissance happened in the early decades of the 16th century. Already before 1520s architects and craftsman began to use Renaissance ornamental characteristics, but in a system of rules which was still Gothic (Bury, 1976). However, the real introduction of the new style was fostered by the diffusion of treatises describing the classical rules and their reinterpretation by the Italian architects and intellectuals (e.g. the works of Leon Battista Alberti, Giovanni Giocondo, Cesare Cesariano, Sebastiano Serlio, etc.), followed by the first treatises on the topic by Iberian authors (e.g. Diego de Sagredo, Alonso de Vandelvira, Hernan Ruiz, Francisco de Holanda, Juan de Are, etc.). In this process, two different approaches emerged. First, a style which reflected the survival of local late-Gothic traditions interacting with the new classical taste that culminated in the so-called Plateresque.

Then, and in parallel to this, the diffusion of a sober and severe style, more rooted in the classical instances promoted by the Renaissance and, thus, called Purist.

The term Plateresque refers to the application of heavy decorations and ornaments, resembling the work of the silversmiths ("*plata*" means silver in Spanish). These are used to cover the architectural elements as arches, columns, pilasters and jambs, with stone carving, stuccos, ironworks and woodworks (Compean, 2015). Significant examples of Plateresque in Spain are in Salamanca (e.g. the façade of the University, the new Cathedral in **Figure 2-4**a, the Convent of *San Esteban*) and in Seville (façade of the Town Hall / "*Ayuntamiento*" in **Figure 2-4**b and Royal Chapel in the Cathedral). Prominent artists of this style were Damian Forment, Andris de Najera, Vasco de la Zarza, Alonso Berruguete, Diego de Siloe and Felipe Vigarny.

a) b)

Figure 2-4. Examples of Renaissance style architecture in Spain: a) New Cathedral of Salamanca (Jentges, 2010); b) façade of the Town Hall / "*Ayuntamiento*" in Seville (Anual, 2010).

The introduction of Renaissance in Spain coincided with the ascent of the country after the union of the Castile and Aragon kingdoms, the final conquest of the Emirate of Granada and the colonisation in America. The need for an international legitimisation of the power led first to tighten the relationship with the Papacy, promoting the Crown as champion of the Christianity, and then to build a direct reference to the Roman Empire. This was even more evident after the death of Ferdinand II of Aragon and the union of the Spanish Crown to the so-called Holy Roman Empire by his heir, Charles V of Habsburg. In a period strongly influenced by Renaissance humanism, the adoption of an architectural style which recalls the classicism aimed at presenting the Holy Empire as the new Roman Empire. Associated to this identification, a sense of superiority developed with the legitimization of the imperialistic aims and the centralization of power (Autorino, 1994). Moreover, this strategy implied the rejection and the elimination of the Islamic influence. In this regard, the attitude toward Moriscos (Muslims converted to Christianism)

and Mudejars (Muslims living in the Christian kingdom without conversion) quickly changed. After the conquering of Granada, a tolerant attitude was evident, typical of the previous centuries where Christians and Muslims had to coexist and cooperate. After that, in less than a century, the Crown introduced the imposition of mass baptism, the confiscation of properties and, finally, the mass expulsion between 1609 and 1616. This new policy was justified politically by the new role of the Crown as embodiment of the Christendom, but also economically. Although, since the Moriscos were traditionally active in several activities, they became, with time, less important, making their presence in Spain no longer needed (Autorino, 1994).

In this scenario, the Purist style was introduced and developed, and it is probably no coincidence that its main examples are close to the centre of the power and directly connected with the king, first Charles V and then Philippe II, as the Palace of Charles V in Granada, the Taverna hospital in Toledo, the monastery of *San Lorenzo* at El Escorial (**Figure 2-5**) and the Cathedral of Valladolid (Bury, 1976).

Figure 2-5. Examples of Purist style architecture in Spain: monastery of *San Lorenzo* at El Escorial (Segundo, 2009).

The purist style required the definition of a new set of rules and aesthetic, and was supported by the activity of well-educated artists and intellectuals, in some cases trained directly in Italy, among them Diego de Sagredo, Bartolomé Bustamante, Pedro Machuca, Juan Bautista de Toledo, Juan de Herrera de Maliaño. Philippe II strongly promoted its diffusion and the monastery of El Escorial became a symbol of

it, so much so that it was also called *Escorial* style, or *Herrerian* style, after Juan de Herrera who completed the construction and was appointed Inspector of Monuments of the Crown in 1579. The political and cultural programme of the Habsburg House was also reflected on the creation of a new capital, Madrid, where this style was consolidated and largely represented, becoming the court style. This further developed, after the last third of the 16th century, into a Mannerist style characterized by geometric rigor, absence of decoration and magnificence of the clean volumes. Its peculiar combination of architectural features from different traditions, such as the Spanish, the Flemish, the Italian and the Central European, reflected an evolution, linked to the new Spanish Empire and the so-called Spanish Golden Age.

The interest of the Renaissance intellectuals for the classicism promoted also the study of technology. This fostered the diffusion of technical literature in the form of treatises. These documents are particularly important not only for art historians but also for the professionals involved in structural preservation, as some of them contain graphic rules and rules of proportions for static purposes. Such rules were most probably part of the body of knowledge shared within the trades of bricklayer, architect, master builder and the other professions involved in the construction process. Among the most important treatises produced in Spain, it is worth mentioning the ones from Rodrigo Gil de Hontañón (1500-1577) and Ginés Martínez de Aranda (1550-1600).

The work of Gil de Hontañón is particularly relevant as he contributed to the design and the construction of several cathedrals and major buildings in Spain. Thus, the rules presented in his book are the result of a practical activity. Hontañón stands at the crossroads between the late-Gothic tradition of the period of his education and of his father, a famous master builder as well, and the new forms and rules of the Renaissance. He tries to reconcile these two instances in his treatise. Relying on a centuries-old tradition, he is confident when provides trustworthy rules for the design of Gothic vault, buttresses and towers (Huerta, 2002). He also tries to open up to the humanism and the Renaissance approach by analysing such elements according to analogies with the human body (e.g. a ribbed vault that mimics the hand, a tower draws inspiration from a man standing, etc.) (Huerta, 2002). However, when he presents the peculiar elements of the new style, like round arches and barrel vaults, he fails to provide general rules and admits that after discussing with other Spanish and foreigner architects he found no agreement. The late-Gothic rules that he masters still hold for the typical structural elements of the early Renaissance style. Hontañón himself is, indeed, a master of the Plateresque style. But it is evident to him that the new forms bring new problems for the professionals and require more investigation. Apparently, Gil de Hontañón never designed a barrel vault in one of his buildings and the rules he suggested for this

structural system have an experimental character, maybe the results of an experimentation he performed (Huerta, 2002). The need for new rules holding for the new systems together with a new attitude toward science encouraged the experimentation and a progressive mathematization of the debate about structural design during the 16th and the 17th century, laying the foundation for the modern scientific structural science.

2.2.3. Baroque

The Baroque style was developed in Europe in a time of religious and political fracture, after the Council of Trent (1545-1563), which produced a change in the Catholic liturgy and practices triggered by the Protestant Reformation. The style firstly appeared in Italy in the beginning of the 17th century, as one of the means to face such reformation (Bailey, 2003). One of the main aims was the communication of religious themes through the emotional involvement of the popular audience by creating a new face for Catholic Church. The Jesuits order was particularly involved in its development and diffusion. The Baroque did not introduce a brand-new way of building with respect to the Renaissance, as the basic architectural elements were preserved but made more spectacular, increasing the height, the size and the number of ornaments. It resulted in the proliferation of decorative elements forming a new rhetorical aesthetic with strong symbolic value aimed at creating illusions and surprise (Compean, 2015).

Politically, Spain was, in the beginning of the 17th century, at the top of its rise, in the midst of the Spanish Golden Age. Under the reign of Philip III (r. 1598-1621), the empire was experiencing the so-called *"pax hispanica"*, a long period of peace that promoted the economic and cultural growth. However, by the 1630s the Iberian Peninsula was involved in the events culminated in the Thirty years' war. The sequence of revolts of Catalans, Portuguese and Dutch, in some cases with the direct support of France, endangered and reduced the extension of the Spanish empire. In the second half of the 17th century, the decline of the Habsburg monarchy started, whose last king was Carlos II (r. 1665-1700) and, even, if slowly, also the decline of the country itself started (Escobar, 2017). Baroque influence reached Spain in this time. Since 1680s, the contribution of a family of artists, the Churriguera, to the development of Spanish Baroque was so important that this is often called Churrigueresque. This style emerged in the late 17th century and was characterized by heavy decorations with stuccos and gold especially in the "retablos" (decorated panels above and behind an altar), by the use of the Solomonic columns of the Composite order and of the "*estipites*" (type of column or pilaster), aiming at an anticlassical twisted movement of

the elements. In Churrigueresque, the intricate and exaggerated decoration tends to cover and hide all the structural elements as columns and walls (Compean, 2015). Some of the main examples of the Spanish Baroque include the façade of the University of Valladolid, the Hospice / *"Hospicio" de San Fernando*, in Madrid (**Figure 2-6**a), the Cathedral of our Lady of the Pillar in Zaragoza (**Figure 2-6**b), the Palace of *San Telmo* in Seville (**Figure 2-6**c) and the façade of the Cathedral of Saint Mary in Murcia (**Figure 2-6**d).

Together with this elaborated Baroque, a soberer international style characterises some projects commissioned by the Crown, as at the Royal Palace. In 1730s, similarly to the rest of Europe, Rococo, namely an elaborated theatrical evolution of the Baroque, appeared. A few examples were realised before the 1760s, when neoclassical influence spread inducing a gradual return to sobriety.

a) b) c) d)

Figure 2-6. Examples of Baroque style architecture in Spain: a) Hospice / *"Hospicio" de San Fernando*, in Madrid (Alvesgaspar, 2014); b) Cathedral of our Lady of the Pillar in Zaragoza (Deth, 2016); c) Main façade of the Palace of *San Telmo* in Seville (Jebulon, 2012); and d) Cathedral of Saint Mary in Murcia (Tango, 2014).

2.3. Colonial Built Heritage in Mexico

Mexico is a country with a very rich cultural history, standing out the Olmeca, the Tolteca, the Maya and the Mexica (known as Aztecs) cultures. Less known but not less important are the Teotihuacans, the Zapoteca, the Mixteca and the Chichimeca cultures (among others) (Fernández Fernández, 1999). Until 1519, before the arrival of the Spaniards, the coexistence of these people was based on the military power, which also marked the limitation of the territory and the greatness of the constructions. Remains of the magnificence of these civilizations are found in archaeological sites, such as Texcoco, la Venta, Teotihuacan, Cempoala, Chichen Itza, Mitla, Uxmal or el Tajin. Pre-Columbian monumental buildings demonstrate the existence of well-trained masons able to use efficiently rudimentary stone tools for labour-intensive construction. These structures also testify the existence of constructive strategies assuring building stability against seismic events (e.g. wall corner pieces, ashlars, coursing, thick walls, lack of continuous vertical joints and mosaic of different size stones voluntarily not in a regular pattern) (Ibarra-Sevilla, 2013).

The colonial era starts in Mexico in 1519 and constitutes a strong turning point for the forms of the architecture. To provide a better insight into the development of built heritage in Mexico, it is necessary to analyse the characteristics and the organisation of the society in the colony.

2.3.1. Construction in the 16th century

In order to regulate the trade and the immigration between Spain and the New World in 1503, the "*Casa de Contratación*" was established in Seville. It was in charge of granting travel permits (Autorino, 1994). Moreover, after 1509, the Spanish Crown restricted the individuals eligible for emigration, in order to keep the homogeneity in the ruling class of the colonies, by rejecting several classes of applicants (e.g. Muslims and Jews or their descendants). Between 1493 and 1600 almost 55,000 Spaniards emigrated legally. Nonetheless, there was also consistent illegal emigration, proved by literary sources, estimated in no less than 150,000 people, during the first century of the colony. Already in 1570, in fact, Spanish America counted around 118,000 European inhabitants (Autorino, 1994). Among them, three categories of people are essential for the analysis of the evolution of the architecture: 1) the patrons who commissioned the buildings; 2) the master builders and the expert craftsman involved in the design and the construction; 3) the manpower.

2.3.1.1. Patrons

Commonly, the patrons of monumental buildings included members of the clergy, nobles and city administrators. In Mexico, these categories are all represented and participate in the commission of buildings. However, the specific characteristics of the colonial enterprise made that, nowadays, the heritage outside Mexico City is composed almost only of religious buildings. In the beginning of the colonial era, for the Spanish and the Papal courts, influenced by the Renaissance humanism, the New World was not just a territory to exploit, but a place where it was possible to build an ideal society, impossible in Europe, aiming at the unity of faith and state ("one fold under one pastor") (Autorino, 1994).

The political unity under a single empire looked possible considering that the only other European conquerors were the Portuguese and Charles V married Isabel of Portugal, linking the two empires. Similarly, the Church promoted the religious unity and all the other religions were banned from the colonies, appointing the Inquisition, from 1570s, to prevent the diffusion of other doctrines contrary to Catholic faith. The strong connection between Spanish Crown and Papacy provided to the first the legitimisation for the empire. Through the power of patronage, granted by the Papacy, the Crown achieved the authority over the priests and the monastic orders participating in the colonial enterprise but also the duty of promoting and supporting economically the missionary activities in the new territories. However, the colonisation was not just a matter of reorganisation of a conquered territory, it required a cultural, spiritual and ideological subjugation. The Church, at the end of the 15th century and in the 16th century, had the instruments and the experience to do that better than the Crown (Autorino, 1994). The missionary activities were, thus, used also to promote the new political power, making the conquest, the new social order and the new hierarchy accepted by the indigenous population. The religious buildings became, thus, also a political symbol of the occupation. This explains both the magnificence of religious constructions, not related with the actual number of inhabitants of the settlements, and the lack of administrative monumental buildings.

By 1580, the expansion of the Spanish territory was in parallel with the expansion of the mendicant orders (Waldinger, 2013). Currently, Mexico has 27 Cultural Heritage plus 2 mixed sites (Cultural-Natural) in the list of World Heritage by UNESCO. **Table 2-2** reports this list and highlights in bold the 11 sites developed in the 16th century, during the period of the colonization. It is easy to contrast the current location of this Cultural Heritage, in **Figure 2-7**, against the path followed by the expansion sought by the friars and thus, the construction of the religious centres and the cities around them. The identification of the patrons is important in the study of the architectural forms. In literary sources, it was common to give credit and recognition for artistic production not to the ones who physically produced it but to the designers of the

decoration and to the patrons who commissioned it. The patrons, especially if members of the clergy, were in charge of validating the architectural product, especially in terms of iconography, decorations and related symbolism. By accepting the finished work, the patrons legitimised any adopted solution and let the results become a model for future reference. This process was essential for the diffusion of the European models, as the patrons were commonly ordering the forms, they were familiar with. In addition, this process contributed to the development of a colonial hybrid style, as variants and reinterpretations of the original model in light of indigenous culture were tolerated or even appreciated. In this regard, it is worth mentioning the example of Juan de Palafox y Mendoza, Bishop of Puebla de los Angeles since 1642. He supervised several art commissions including the erection of Puebla Cathedral. Under his guidance, local indigenous and mestizo artists developed a peculiar local variant of the Churrigueresque. His genuine interest in the indigenous culture is reflected in the treatise "*Historia de las Virtudes del Indio*" that he dedicated to King Philippe IV. In the beginning of the 16th chapter he wrote: *"And as for the practical and mechanical arts the Indigenous are exceptionally talented, especially in painting, gilding, carpentry, masonry, other stonework and architecture; they are not only good at these professions, but they master each line of work"* [translated by Maxine Compean (Compean, 2015)].

Table 2-2. World Heritage List for Cultural Heritage in Mexico by (UNESCO, 2020b), part 1.

No.	Name of the site	Inscription date
1	Pre-Hispanic City and National Park of Palenque	1987
2	**Historic Centre of Mexico City and Xochimilco**	1987
3	Pre-Hispanic City of Teotihuacan	1987
4	**Historic Centre of Oaxaca and Archaeological Site of Monte Albán**	1987
5	**Historic Centre of Puebla**	1987
6	**Historic Town of Guanajuato and adjacent Mines**	1988
7	Pre-Hispanic City of Chichen-Itza	1988
8	Archaeological Zone of Paquimé, *Casas Grandes*	1998
9	**Historic Centre of Morelia**	1991
10	El Tajin, Pre-Hispanic City	1992
11	**Historic Centre of Zacatecas**	1993
12	**Earliest 16th-Century Monasteries on the Slopes of Popocatepetl**	1994
13	Rock Paintings of the Sierra de San Francisco	1993
14	Pre-Hispanic Town of Uxmal	1996
15	**Historic Monuments Zone of Querétaro**	1996
	In **bold** the sites built in the 16th century during the colonization period.	

Table 2-3. World Heritage List for Cultural Heritage in Mexico by (UNESCO, 2020b), part 2.

No.	Name of the site	Inscription date
16	*Hospicio Cabañas*, Guadalajara	1997
17	**Historic Monuments Zone of Tlacotalpan**	1998
18	**Historic Fortified Town of Campeche**	1999
19	Archaeological Monuments Zone of Xochicalco	1999
20	Ancient Maya City and Protected Tropical Forests of Calakmul, Campeche (*)	2002
21	Franciscan Missions in the Sierra Gorda of Querétaro	2003
22	Luis Barragán House and Studio	2004
23	Agave Landscape and Ancient Industrial Facilities of Tequila	2006
24	Central University City Campus of "*Universidad Nacional Autónoma de México*" (UNAM)	2007
25	**Protective town of San Miguel and the Sanctuary of Jesús Nazareno de Atotonilco**	2008
26	*Camino Real de Tierra Adentro*	2010
27	Prehistoric Caves of Yagul and Mitla in the Central Valley of Oaxaca	2010
28	**Aqueduct of Padre Tembleque Hydraulic System**	2015
29	Tehuacán-Cuicatlán Valley: originally habitat of Mesoamerica (*)	2018

(*) Mixed site: Cultural and Natural.

In **bold** the sites built in the 16th century during the colonization period.

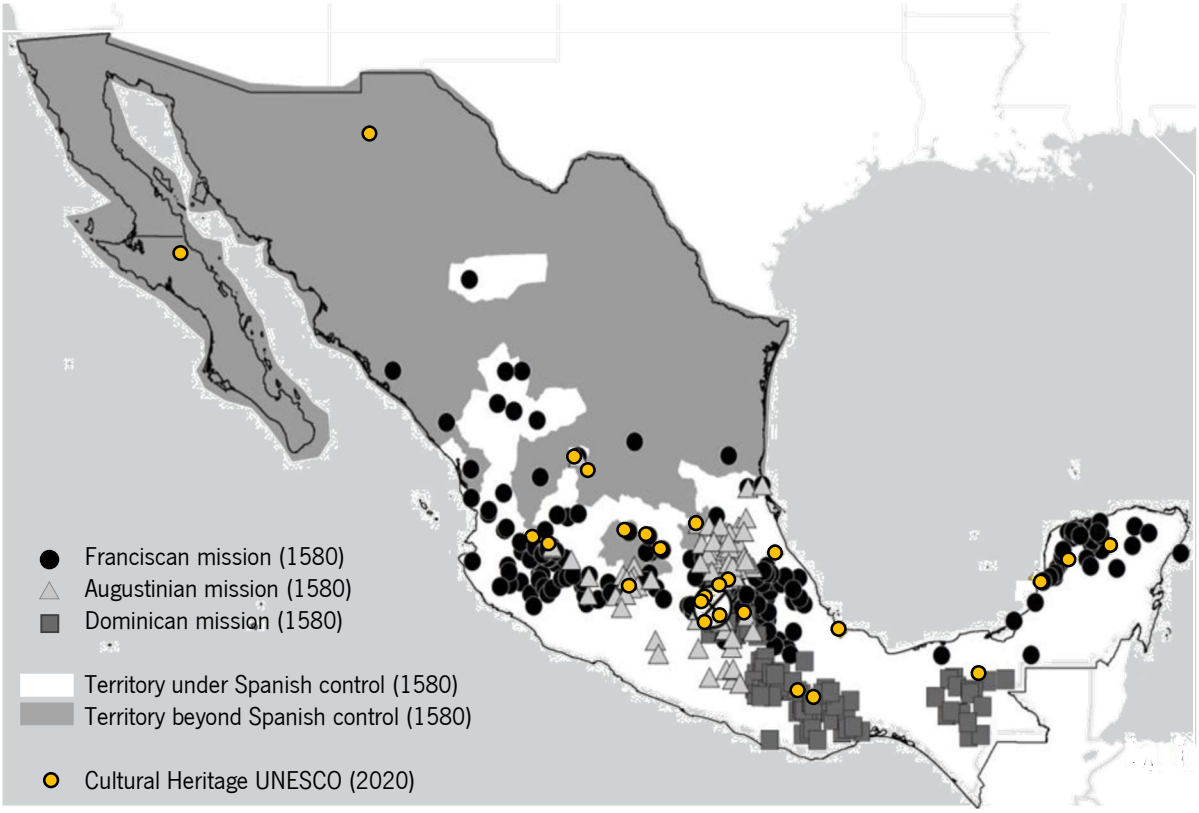

Figure 2-7. Establishment of Missions and Spanish Military control in 1580 (Waldinger, 2013) overlapping the location of the Cultural Heritage in Mexico by 2020 (UNESCO, 2020b).

The patrons of the religious buildings were mainly members of the Church: mendicant orders or secular clergy. The Franciscans and the Dominicans were the first orders to arrive in Mexico. They carried out evangelization towards the east and the west of Mexico City. The Augustinian arrived later (García & Peña, 2014; Kubler, 1983). Most of the UNESCO sites in the 16th century, are related to the Franciscans and the Augustinian missions (**Figure 2-7**), though, by the end of the colonial era, Dominican was the second largest order with more missions over the Augustinians, while the Franciscans were the largest order.

Until 1550 the role of the secular clergy was less important, as these were few in number and not adequately trained. Later, the secular clergy acquired more influence at the expenses of the mendicant orders whose power was restricted by the Crown. The secular clergy was active at the end of the century in a context where the new system was already established. They had potentially more time to supervise the construction. At this stage, also the so-called *"encomenderos"* order the commission of religious buildings. They were soldiers rewarded with *"encomiendas"*, namely lands and indigenous people to administer. To receive the *"encomienda"*, in fact, they were committed to contribute to the construction of a religious building on the area. For them the patronage on religious building was also a way to show the social status.

2.3.1.2. Master builders and manpower

Some friars could have been designers, for instance Juan de Alameda, who came to Mexico in 1528 with the bishop Zumarraga, or Francisco de Tembleque, who designed the aqueduct from Zempoala to Otumba. But most of the friars were probably not experienced in construction and design. In addition, their number was not enough to carry out the conversion and the construction at the same time: until 1536, there were only 60 friars in Mexico, and in the 1580s they were 5 or 6 hundreds spread into 400 religious establishments (Autorino, 1994).

Until 1570s there are no news of architects in Spanish America and, in the first stage of the colonization, not many craftsmen were willing to move there, as demonstrates the request of the Crown to the *Casa de Contratación* to provide craftsmen. The first builders who went to the New World were involved directly in the work and in the training of the locals. Indeed, the erection of the religious buildings required the construction of structural systems and elements for which the indigenous workforce was not familiar to. Similarly, the decoration was following an iconography unknown to them. The 16th century is, thus, characterised by a process of symbiosis and culture transfer: on one side the Spanish advanced technology, master builders and new demands, combined, on the other side, with the locally available materials and workers. According to (Kubler, 1983), this symbiosis resulted in very experienced

indigenous workers by 1560, whose production is an important reason to justify the study of the 16th century Mexican architecture.

Augustinians are particularly active in the use of Spanish craftsmen to train indigenous people in construction. For instance, documents in the late 1530s report that the Augustinians at Tiripitio, Michoacan, appointed Spanish craftsmen to train the local people. However, before 1550 these masters were living only in big cities with large settlements of Spaniards. They could move to other places for specific jobs. This process of training promoted the diffusion of the traditional forms of art that the craftsmen were familiar with. As mentioned, the body of knowledge was mainly a set of rules whose reliability was proven in the previous centuries, and transmitted from the master to the disciples. It is not possible to estimate the origin of the craftsmen who participated to the training of the local workers. However, according to the data available, by 1600, 38% of the legal emigrants originated from Andalucía (by 1509 they were 60%). Moreover, there are evidences of Moriscos that emigrated illegally. It is possible that artists from south of Spain, particularly if former Muslims, brought to the colonies the influence of the Mudejar style that was still strong in the beginning of the 16th century.

The professions involved in the construction process at that time, in Spain, were collected in the trades of bricklayer (*"albañil"*), and architect and master builder (*"alarife"*). Each position had a specific training and role. In the New World, instead, the small number of skilled workers and the need of a numerous manpower in short time, made the training process and the differences among workers less well defined. Only with the decrees/ *"ordenanzas"* of the 18th century in Mexico, the construction trade was changed into an art. However, the *"ordenanzas"* aimed to protect and support the hierarchy and the social system, namely the members of the guild, allowing only the Spaniard to be Masters of Architecture. Even though, apparently, indigenous people and mestizos were excluded from the profession, there are evidences of indigenous people that trained themselves attending lessons in the artist studios and finally owned their own studios, as Francisco Martínez Gudiño or the Xuárez family (Compean, 2015). Agustín Hernández de Solís is another example of mestizo architect that had a relevant role in the development of the colonial Baroque.

In the hierarchy, below the craftsmen, a large number of workers were involved in the construction process. Most, if not all, of them were indigenous workers. Their activities as stone carvers and masons were described, for instance, in 16th century by Fray Bernardino de Sahagún, in the Florentine Codex (Ibarra-Sevilla, 2013).

2.3.2. Renaissance

During the first century of the colonisation, two main periods of built environment transformation emerged: 1) immediately after the Spanish arrival to the region (1530s); 2) during the reorganisation of the settlements (second third of 16th century). In the first period, the original towns saw a superimposition of the new buildings over the indigenous monuments that were dismantled and/or reconfigured (García & Peña, 2014), together with a transformation of the open spaces according to the new needs and traditions of the new social and religious order (such as churches, palaces and administrative buildings). In this period, the building activities required more physical strength than refined skills. Thus, local workers were involved and, probably, iron tools were not used yet.

In the second period, some settlements were abandoned, and entire communities were relocated to new sites after a series of epidemic events (e.g. in 1576). The phenomenon started in the 1540s as the Viceroy authorised the first relocations. New settlement architecture and urbanism were designed as archetypes of the future, reflecting an analogous phenomenon happening in Spain with the definition of a Renaissance Court style [see (Wyrobisz, 1980)]. In this period, also new monasteries and churches were spread over the country. The expansion of Christianity and colonisation produced a large program of monastic complexes building commissioned by the mendicant orders. Two religious building typologies were developed and coexisted within the same monastic ensemble: one for the Spanish minority and another originally built almost exclusively for indigenous people (Flores Marini, 1966). The former assumes the traditional forms of a church whereas the latter has small or no similarities to the European models. The religious space for local is a peculiar architectural solution of Latin America and especially of Mexico, mixing local tradition of sacred space with the new Christian needs. This typology consists of a large platform devoted to liturgical and educational activities (atrium) and an open chapel. Originally, indigenous people opposed to the idea of a covered space for the sanctuaries. Since these elements lack in the European tradition, the architectonical solutions resulted from local experimentation and creativity. However, subsequently, new churches, more traditional, were built and the open chapels were either dismantled or reused as porches. The open chapels (e.g. at Teposcolula, Oaxaca in **Figure 2-8**) are single nave buildings, with orientation of the long axis in north-south instead of the classic east-west. In order to facilitate evangelisation, the west side is open on the atrium were numerous people could attend the ceremony (Kirakofe, 1995).

a) b)

Figure 2-8. Open chapel from *San Pedro* convent in Teposcolula, Oaxaca (HA 2018): a) west façade; and b) roof plan and elevation.

Although during the colonial era thousands of churches were built over a large and varying territory, the short period of construction, the common origin of the promoter of the constructions and the shared phases of evolution led to a set of similar characteristics. Though it is possible to find churches with a latin-cross floor plan, most of them present a single rectangular nave (**Figure 2-9**). The single nave church is typical for the mendicant orders in Europe and has several advantages: 1) easy definition of the footprint; 2) low complexity in the construction process; 3) no need for large quantity of columns, which are expensive and difficult to make; 4) suitable for any kind of roofing system; 5) no expertise required for the workers. The churches built at the beginning of the colonization have a simple façade without bell towers. However, many of them underwent subsequent interventions, such as the addition of bell towers, attached to the main wall of the façade, or the superimposition of new decorative elements (Peña et al., 2016). The façade in a colonial church is commonly composed of the main wall, one or two towers and the frontispiece. In general, there are two openings: the main door (5 to 8m height) and a window for the choir loft (circular or rectangular). The bell tower is composed of a square section basement, a belfry (up to three bodies) and a small dome. At the basement, there are small openings for the staircase and, sometimes, the third body of the belfry is similar to a lantern. The barrel vault is the most common system for the nave roof, though some churches were also constructed with ribbed vaults. The apse is normally covered with a smaller quadripartite vault and, when present, a hemispherical dome covers the transept bay. The choir loft forms an intermediate floor in the first bay of the nave (García & Peña, 2014).

Stone masonry was the most common material even in the pre-colonial era, due to the abundance of local stones, thus, new settlements largely relied on the use of it. As a consequence, it is possible to find different patterns of blocks, varying from extremely heterogeneous (rubble) to fairly regular stone masonry

(Peña et al., 2016; Peña & Manzano, 2015). When necessary for the construction of monumental churches, stones were moved even for 100 km (López-Doncel et al., 2016).

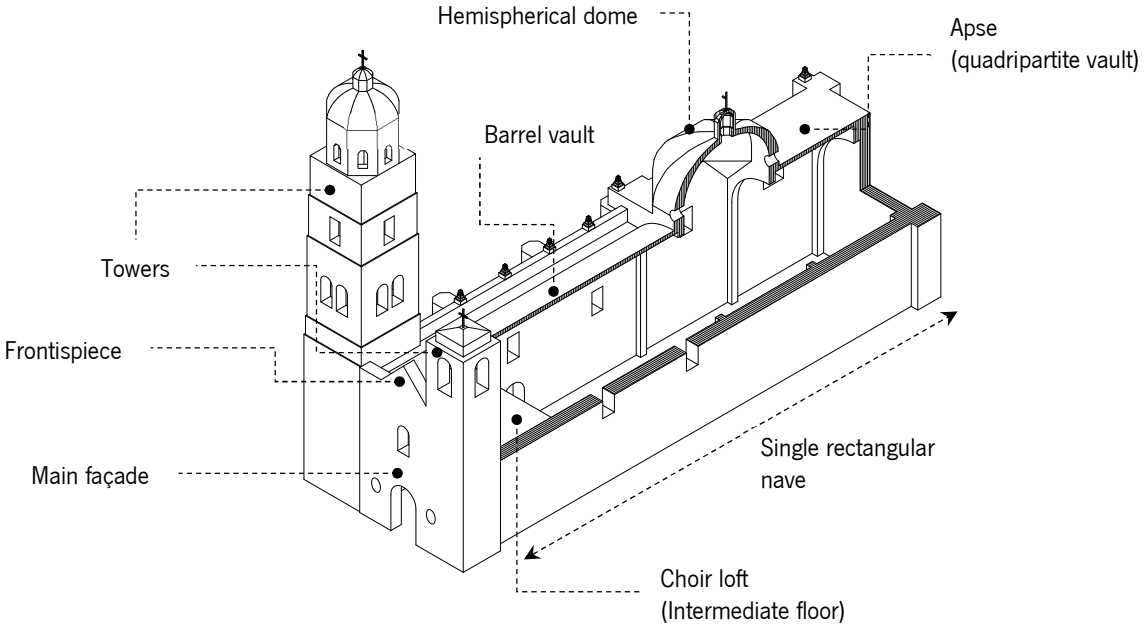

Figure 2-9. Characteristics of a colonial church with a single rectangular nave (San Agustin church, Morelia, Michoacan).

2.3.3. Baroque

It is possible to identify two tendencies in Mexican Baroque. On one side, in Mexico City, many examples of Baroque architecture are strongly influenced by the Spanish models, as the *Sagrario Metropolitano* (**Figure 2-10**a), a small church adjoining the cathedral. Mexico City is in this phase a metropolis, culturally extremely active and connected with Spain. Here, many artists came from Europe to work, importing new influences as Lorenzo Rodriguez and Jerónimo de Balbás. Also, local artists were formed and set their studios in Mexico City, as Pedro de Arrieta.

On the other side, the rest of the New World is a kind of "periphery" for this centre. The periphery produces a hybrid architecture that embraces the Baroque style but reinterprets it in light of pre-Hispanic traditions. Puebla de los Angeles is one of the main centres where this style was developed and spread influencing the neighbouring states. Examples of this hybrid styles are the façade of *Hospital of Acámbaro* in Guanajuato (**Figure 2-10**b), the façade of the Temple of *Santa Mónica* in Hidalgo and the church of *Santa María Tonantzintla* in San Andrés Cholula, Puebla (**Figure 2-10**c). The analysis of the iconography

of the last example explains clearly this process of hybridisation through the influence of local pre-Hispanic traditions. The name itself, Tonantzintla, refers to Tonantzin, the goddess of corn. The decorative elements of the church, as local flowers and fruits, perfectly fit the baroque forms but do not allude to Christian themes rather to the goddess myth. This phenomenon has been identified in general in the Mexican Christian iconography.

a) b) c)

Figure 2-10. Examples of the two tendencies in Mexican Baroque in Mexico: a) *Sagrario Metropolitano* in Mexico city (Mathias, 2013); b) façade of *Hospital of Acámbaro* in Guanajuato (López & Biosca, 2012); c) church of *Santa María Tonantzintla* in San Andrés Cholula, Puebla (Alejcasvi, 2009).

When the friars train native artists and craftsmen to represent Christian symbols and images, the indigenous populations recognise and interpret some of them based on their own tradition and meanings. They were familiar with typical Christian symbolism as water, blood, flowers and fruits. The result is a hybrid symbolism implemented in architecture that does not follow completely the logic of the Catholic counter-reformation and introduces joy and serenity within the decorations. This is evident in the *"retablos"*, as in the churches of Santa Clara and Santa Rosa in Querétaro (**Figure 2-11**a) or in the *Santuario de Ocotlán*, in Ocotlán, Tlaxcala (**Figure 2-11**b), where there is a tendency to fill all the space with patterns and ornaments with many local flowers, figures with indigenous physiognomy and abundance of colour. Some scholars proposed different names as *Mestizo* style or *Tequitqui* for the hybrid style completely developed in the country. The former term has some racist implication, which prevents its diffusion whereas the second, coined by the art historian José Moreno Villa, is a Nahuatl term that means "tributary". The hybridisation typical of Tequitqui began in the 16th century but continued after the introduction of Baroque in 17th and 18th century. To support the differences between Spanish Style and Hybrid Mexican style it is worth mentioning the so called Temple of *Santo Domingo* in Puebla (**Figure**

2-11c), where Spanish artists produced decorations in the Churrigueresque style whereas in the *Capilla del Rosario* (**Figure 2-11**d) the decorations present the hybrid characteristics (Compean, 2015).

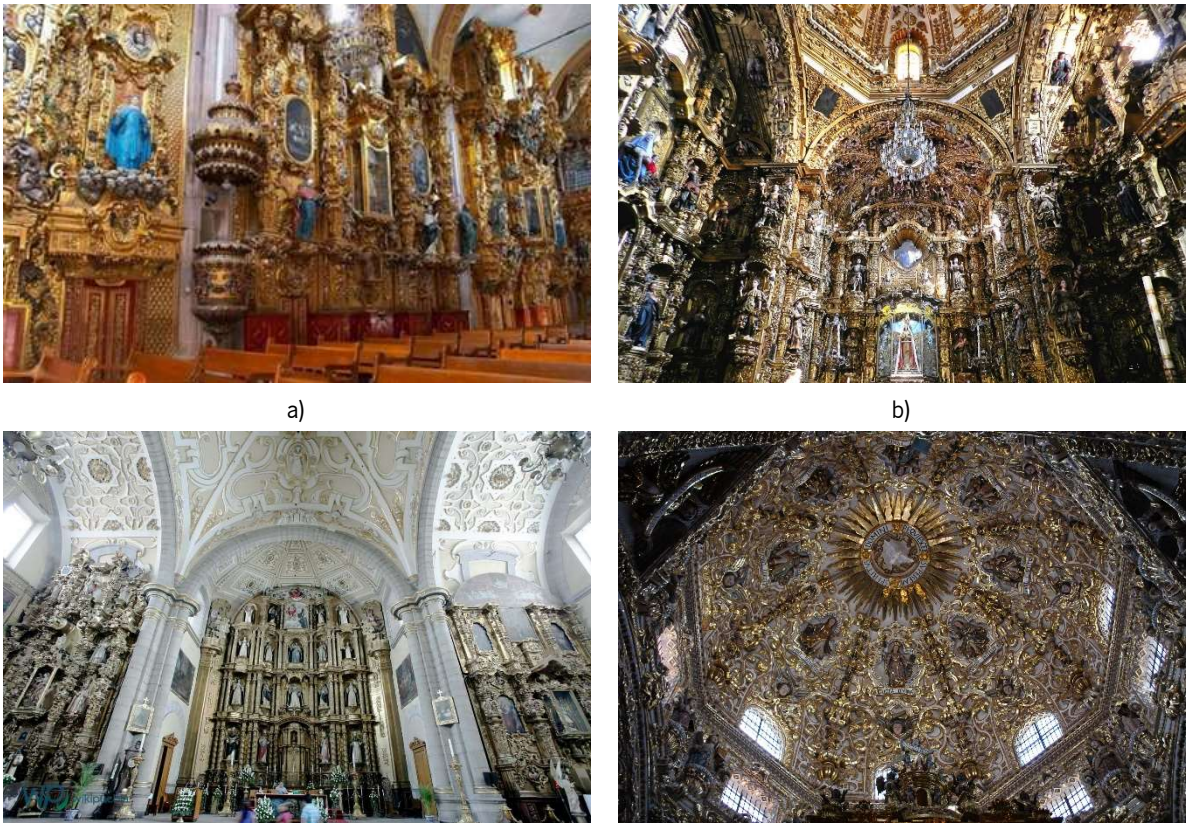

a) b) c) d)

Figure 2-11. Hybrid symbolism in the Mexican baroque: a) interior of the church of *Santa Rosa* in Queretaro (J. F. Zavala, 2019); b) interior of the *Santuario de Ocotlán*, in Ocotlán, Tlaxcala (Turismo Tlaxcala, 2020); c) interior of the Temple of *Santo Domingo* in Puebla (Aguila, 2010); d) dome of the *Capilla del Rosario* (Linares Garcia, 2010).

2.3.4. Non-Religious Heritage

As already mentioned, Mexican heritage is characterised by a lack of non-religious monumental buildings within the cities, excluding the case of Mexico City. However, it is worth mentioning a series of counter-examples composed of public or private buildings. The non-religious heritage of Mexico is characterised by a relevant historical and aesthetic value. Most of these building nowadays host libraries, museums, governmental uses or belong to university campus. Some of them were Haciendas, namely properties of large territories used for agriculture. More than the religious heritage, this kind of buildings underwent modifications and stratifications during their history, gaining, in some cases, their value

especially because of this and at the same time, being more at risk of deterioration, due to the incompatible changes in the use and the inadequate interventions during their life. As an example, it is worth mentioning our Lady of the Conception of Chapingo (**Figure 2-12**a and b), an important hacienda purchased by the Society of Jesus from the Marquis Francis of Medina, treasurer of the Royal Mint (Soria et al., 2011). The actual aspect of the *hacienda* results from the modifications required by the Company between 1699 and 1767, and the modifications carried out in the 1880s when the owner was the General Manuel González (at that time President of Mexico), after a period when the hacienda underwent several changes of ownership, and finally after the 1920s to adapt it to the requirements of a College, the National School of Agriculture. A very peculiar non-religious site is the so-called Palace of Cortés, in Cuernavaca, Morelos (**Figure 2-12**c and d). This is an example of the first period of the built environment transformation, as the building, erected in 1526 as fortified residence for the conqueror Hernan Cortés, stands on a pre-Hispanic Aztec structure. The original Spanish late-Gothic forms of the building are still evident due to the few subsequent interventions.

a) b)

c) d)

Figure 2-12. *Hacienda* of Our Lady of the Conception of Chapingo: a) 1923, inauguration of the National School of Agriculture (Fierro Gossman, 2014); b) actual rectory of the Autonomus University of Chapingo (Martinez Ramos, 2012). Palace of Cortés, in Cuernavaca, Morelos: c) frontal view of the building (Rene, 2017); d) façade of the Palace (Zamora, 2009).

Few examples of non-religious buildings from Plateresque style survived, as the house of the *"Caballero Águila"* in San Pedro Cholula, Puebla (**Figure 2-14**a). More numerous are the building from the second half of the 17th century in Baroque style. Some worthy examples are in Santiago de Querétaro [e.g. the government building and the "*Casa de la Marquesa*" (**Figure 2-14**b)], in Puebla [e.g. la *Casa de los Muñecos* (**Figure 2-14**c)], in Morelia [e.g. the government building (**Figure 2-14**d)] and in Mexico City (e.g. the palace of the Count of Heras and Soto, the palace of Iturbide, the house of the Count of Miravalle, the palace of the Count of San Mateo of Valparaíso, the house of the "*Azulejos*", the palace of the Counts of *Valle de Orizaba*). Finally, it is worth mentioning a series of buildings commissioned by viceroys or administrators that date back to the 18th and early 19th century, thus, at the turn of Mexican Independency. Such buildings present the typical architectural features of the neo-classic revival style. Many of them are located in Mexico City as the Chapultepec Castle (**Figure 2-14**a), the Palace of Mining (*Palacio de Minería*) (**Figure 2-14**b), the Palace of the Marquis *del Apartado* (**Figure 2-14**c) and the Palace of the Count *de Buenavista* (**Figure 2-14**d). Others host the government building of the states as in San Luis Potosí and in Coahuila.

Figure 2-13. a) House of the "*Caballero Águila*" in San Pedro Cholula, Puebla (Ayuntamiento de San Pedro Cholula, 2020); b) "*Casa de la Marquesa*" (Contreras, 2019); c) "*Casa de los muñecos*" in Puebla (Mexch, 2008); and d) Michoacan government building in Morelia (Rodríguez López, 2006).

a) b)

c) d)

Figure 2-14. a) Chapultepec Castle in Mexico city (Historia Civil, 2019); b) Palace of Mining in Mexico city (Thelmadattar, 2008); c) Palace of the Marquis *del Apartado* (Fierro Gossman, 2020); d) Palace of the Count *de Buenavista* (GOB MX, 2016).

2.3.5. Augustinian Convents

A specific section on Augustinian convents is presented, as this is the focus of the present work. The Augustinian friars arrived to Mexico in 1533. Together, with the other mendicant orders, they were in charge of the evangelization in the new territories. This fact also made the 16th century an important period in terms of architectural development, considering 1550s as the decade of major experimentation and construction. This order was established, mostly, in the central region of the country. Until 1810, they settled 140 missions in the New Spain (Waldinger, 2013). Grouped by State, **Table 2-4** presents the location of 65 Augustinian structures, whose construction was made between 1530 and 1620 (Kubler, 1983).

Table 2-4. Construction activities registered during the period 1530-1620 [adapted from (Kubler, 1983)].

Location	State	Location	State	Location	State
Yuriria	Guanajuato	Acolman	Mexico	Ajuchitlan	Morelos
Ocotlan	Jalisco	Culhuacan	Mexico	Atlatlahuca	Morelos
Tonala	Jalisco	Malinalco	Mexico	Jonacatepec	Morelos
Acatlan	Hidalgo	Mexico	Mexico	Ocuituco	Morelos
Actopan	Hidalgo	Ocuilan	Mexico	Tlayacapan	Morelos
Atotonilco el Grande	Hidalgo	San Felipe	Mexico	Totolapan	Morelos
Ayotzingo	Hidalgo	Zacualpa Mines	Mexico	Yecapixtla	Morelos
Chapantongo	Hidalgo	Charo	Michoacan	Zacualpan Amilpas	Morelos
Chapulhuacan	Hidalgo	Copandaro	Michoacan	Oaxaca	Oaxaca
Epazoyucan	Hidalgo	Cuitzeo	Michoacan	Atlixco	Puebla
Huejutla	Hidalgo	Huango	Michoacan	Chiautla	Puebla
Ixmiquilpan	Hidalgo	Jacona	Michoacan	Chietla	Puebla
Lolotla	Hidalgo	Morelia	Michoacan	Huatlatlauca	Puebla
Metztitlan	Hidalgo	Parangaricutiro	Michoacan	Pahuatlan	Puebla
Molango	Hidalgo	Patzcuaro	Michoacan	Puebla	Puebla
Singuilucan	Hidalgo	Tacambaro	Michoacan	Tantoyuca	Veracruz
Tezontepec	Hidalgo	Tingambato	Michoacan	Alcozauca	Guerrero
Tlanchinol	Hidalgo	Tiripitio	Michoacan	Atlixtac	Guerrero
Xochicoatlan	Hidalgo	Tlazazalco	Michoacan	Chilapa	Guerrero
Zacualtipan	Hidalgo	Tzirosto	Michoacan	Pungarabato	Guerrero
Panuco	Zacatecas	Ucareo	Michoacan	Tlapa	Guerrero
Zacatecas	Zacatecas	Undameo	Michoacan		

The Augustinian religious architecture is characterised by their ambitious projects that, in many cases, led to long periods of construction (Kubler, 1983). Thus, it is likely to find, in several cases, combination of architectonical styles and materials, or to identify elements added to the complexes much later than the initial building. **Figure 2-15** shows the case of San Agustin, in Morelia as an example of the explained above, with different materials and architectural styles.

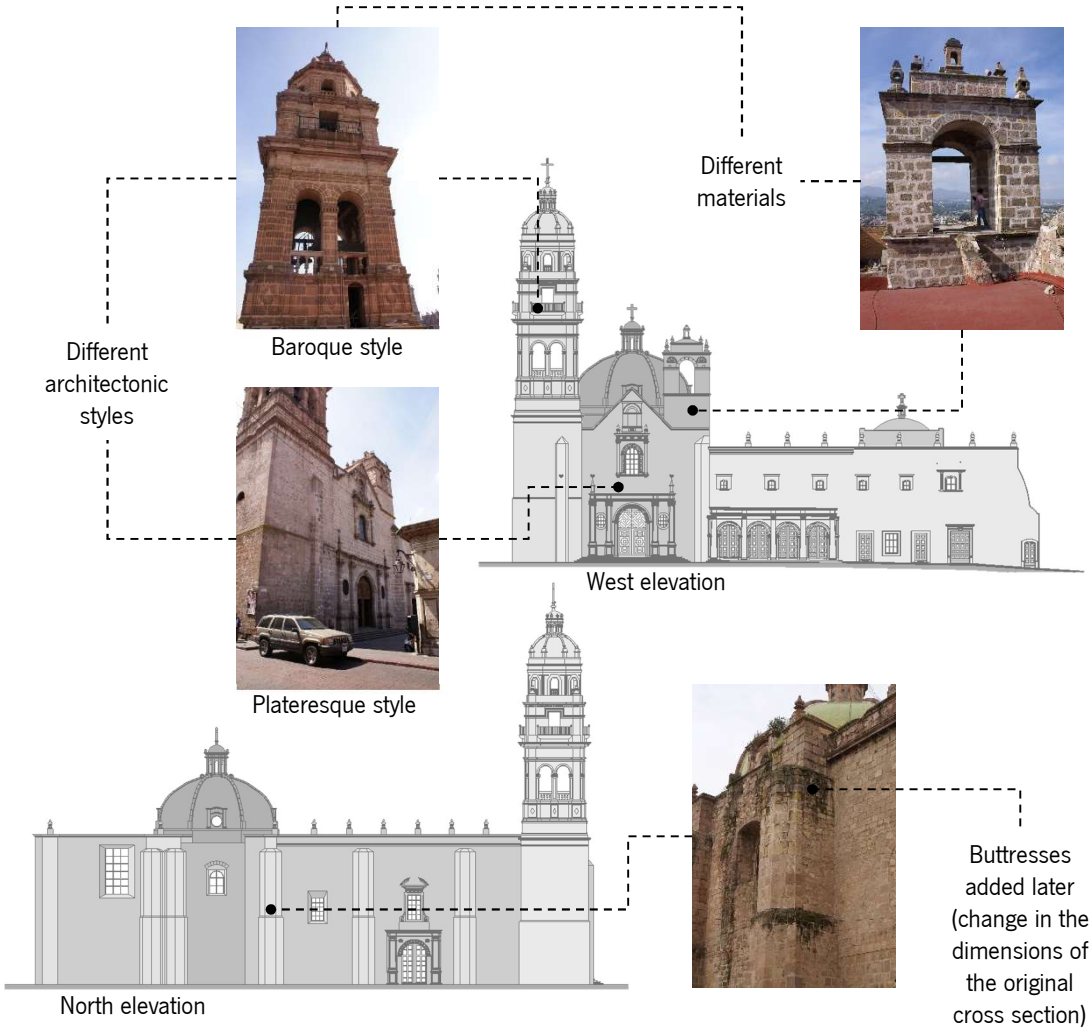

Figure 2-15. San Agustin church in Morelia, Michoacan.

Besides a couple of aqueducts [at Epazoyucan and Tiripetio (Kubler, 1983)], convents were by far, the most notorious type of structures built by this order. In general, convents, including the Augustinian ones, were not only dedicated to spiritual purposes. They were also active centres that promoted the organization and development of the population from 16th to 18th centuries. Thus, their importance lies as well in the social role during this period. Among the most notable uses, it is possible to mention: 1) population and urbanization centres; 2) defence and protection fortresses; 3) agricultural, artisan and economic promotion institutes; 4) elementary and higher education centres; 5) the main convents also operate as hospitals (Chauvet, 1966).

As a general rule, it is possible to clearly identify the characteristic elements of a convent, independently of the order: atrium, atrial cross, posa chapels (four quadrangular buildings located at the ends of the atrium), open chapels, convent, orchard and church (Flores Marini, 1966). **Figure 2-16** shows a perspective of the now ex-convent of Epazoyucan, Hidalgo (Orellana, 1966) pointing out the typical

elements listed above. However, this "general rule" was not definitive and it is also likely to find cases where the conditions drove differences in configuration.

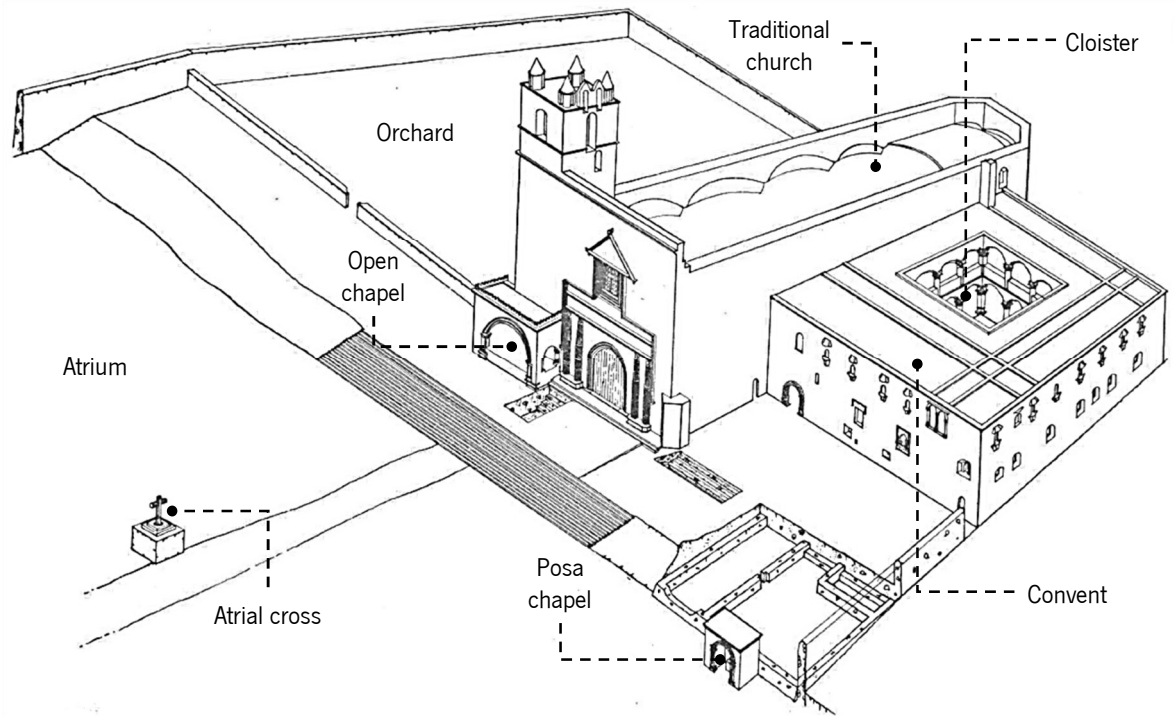

Figure 2-16. Perspective of the Augustinian complex from the 16th century located in Epazoyucan, Hidalgo (Orellana, 1966).

The atrium was a large yard delimited by a perimeter wall, often with a likely military crenelated decoration, though the function was not related to war purposes. This area emerged as a response to the opposition of the population to be in closed spaces for the ceremonies or as a sort of substitute during the church construction (since Augustinian projects were long in the execution). It is directly associated to other three elements: the atrial cross, the posa chapels and the open chapel. Together as a compound, became in many cases, the analogy of a conventional church, but in an open space. With this approach, the open chapel worked as the presbytery, the atrium as the nave and the posa chapels as the lateral chapels. However, it is also possible to attribute other functions to the atrium (e.g. social, administrative or fiscal functions) (Brenišínová, 2016; Flores Marini, 1966; Kubler, 1983).

The plans of a typical convent tend to be similar to secular constructions of the period. The spaces were organized around the squared disposition of the cloister and had direct communication through the doors of each room. The main façade, in general, follows the plane of the church façade (usually facing to the west) and could be accentuated by a series of openings in the way of a portal or an open chapel. In the second level, it is notable the irregular disposition of the windows (Kubler, 1983). In order to highlight the

fact that the distribution of the elements was not a strict statute, **Figure 2-16** illustrates the particular case of Epazoyucan (Orellana, 1966), where: 1) the plane of the convent façade does not follow the plane of the church façade; and 2) the open chapel is attached to the church façade. Likewise, other cases with such similar differences exists.

A great number of Augustinian cloisters were covered by barrel vaults. By the decade of 1530, their inner façades where heavy, the buttresses were solid and massive and, instead of large arcades, the openings were small and well separated (e.g. Jonacatepec in **Figure 2-17**a, Ocuituco in **Figure 2-17**b, Tlayacapan and Totolapan). However, by the end of the 16th century, the stylisation of this space is notable. The buttresses are more elaborated and a double rhythm in the openings of the second level is introduced (e.g. Actopan in **Figure 2-17**c, Copandaro, Cuitzeo in **Figure 2-17**d and Ixmiquilpan) (Kubler, 1983).

a) b) c) d)

Figure 2-17. Examples of Augustinian cloisters: a) and b) by the decade of 1530; c) and d) by the end of the 16th century. a) Jonacatepec, Hidalgo (MX GOB 2018); b) Ocuituco, Morelos (Schaefer, 2014); c) Actopan, Hidalgo (INAH TV, 2017); d) Cuitzeo, Michoacan (Ambriz, 2017).

As above-mentioned, single nave churches are the most numerous religious constructions of the period (Brenišínová, 2016; Kubler, 1983), and Augustinian churches are not excluded. It is possible to identify two types of plans based on the single nave shape: 1) with rectangular or squared presbytery; or 2) trapezoidal presbytery. Augustinian temples can reach total dimensions between 60 and 70 m, which was possible thanks to the roof system (Kubler, 1983). Most of these churches were covered with a barrel

vault along the nave, which also gave the possibility to cover spans bigger than 13 m. In Mexico, this type of roof results similar to a tunnel and, several cases, due to the infill on the haunches, the extrados becomes an almost flat surface interrupted only by the longitudinal elevation of the crown of the vault (e.g. Yuriria in **Figure 2-18**a and Atotonilco *el Grande* in **Figure 2-18**b).

a)

b)

Figure 2-18. Extrados as a flat surface interrupted only by the longitudinal elevation of the crown of the vault: a) Yuriria, Guanajuato (Wallfisch, 2016); b) Atotonilco *el Grande*, Hidalgo (Hernandez, 2019).

Ribbed cross vaults where reserved for the presbytery and the transept, in case of existence (e.g. Yuriria in **Figure 2-18**a) (García & Peña, 2014; Kubler, 1983; Niell & Sundt, 2015). Due to the simultaneous use of two different roof systems (barrel and ribbed cross vaults) the levels of the windows were in a different position: at the presbytery, they were over the level of the impost, while in the nave they were at a much lower level of the impost.

Table 2-5 shows some proportions found in selected Franciscan and Augustinian churches. Rodrigo Gil de Hontañón (Cabrera, 2011) recommended a range for the height level of the roof system between 18

and 21.30 m (from the floor to the key stone), while for the span length a dimension between 9 to 10 m, meaning a ratio from 1:2.0 to 1:2.3. The three Augustinian cases, presented in the column Ratio Span/Height (Span/H) in **Table 2-5**, are under the proposed value. Thus, these structures had a lower height for the actual span. Analysing more in depth, the comparison Franciscan-Augustinian churches show that: 1) the ratio Span/Total thickness of the walls (Span/t_{total}) is within a range of 2.56 to 4.30, being Yecapixtla the most robust construction; 2) in general, the nave length and span of the Augustinian constructions are larger than Franciscan; 3) the span can be over 13 m; and 4) on average, the height of the vaults is around 22 m (from the floor to the key stone).

Table 2-5. Proportions for some Franciscan and Augustinian constructions. Adapted from (Kubler, 1983).

Franciscan constructions (Rib vault)						**Augustinian constructions (Barrel vault)**					
Location	Span length (m)	Ratio Span/ t_{total}	Nave length (m)	Height H (m)	Ratio Span/H	Location	Span length (m)	Ratio Span/ t_{total}	Nave length (m)	Height H (m)	Ratio Span/H
Atlixco	11.00	1:2.25	43.20	-	-	Tiripitio	10.80	-	51.00	-	-
Huaquechula	11.40	-	46.30	19.12	1:1.68	Acolman	12.50	1:3.12	-	-	-
Tochimilco	11.70	1:3.85	53.10	24.31	1:2.08	Tezontepec	12.50	-	50.50	-	-
Tula	11.90	1:2.82	48.80	20.10	1:1.69	Atotonilco el Grande	13.00	1:3.82	61.60	21.00	1:1.62
Cholula	12.00	1:3.55	53.15	21.00	1:1.75	Yuriria	13.50	1:3.30	-	-	-
Zempoala	12.50	1:4.17	50.50	-	-	Yecapixtla	13.50	1:2.56	-	-	-
Tepeaca	12.80	1:3.20	53.60	21.70	1:1.70	Ixmiquilpan	14.40	1:4.00	66.90	25.50	1:1.77
Huejotzingo	13.02	1:3.25	57.37	21.90	1:1.68	Actopan	14.57	1:4.30	65.40	22.21	1:1.54
Puebla ca.	13.20	1:4.00	-	-	-	Cuitzeo	15.00	-	70.00	-	-

t_{total}: Total sum of both the thickness of the Gospel and the Epistle walls.

In general, the churches were oriented on the east-west direction. The west façade was the main one, the north led to a cemetery or a lateral yard, the south led to a corridor for the cloister and the east led to the presbytery. In large complexes, it was possible to find rooms between the corridor of the cloister and the Epistle wall of the church (e.g. Atotonilco *el Grande* in **Figure 2-19**a and Actopan in **Figure 2-19**b). When these spaces were directly connected to the church, its function was as lateral chapels or baptisteries (e.g. Ixmiquilpan in **Figure 2-19**c). In other cases, they were only connected to the cloister. Most Augustinian churches adopted a plane façade, possibly losing the diagonal buttresses located in the frontal corners. An indication of these buttresses can be seen in Acatlán (**Figure 2-19**d). At some churches the buttresses look like they were carefully designed, since the heads are combined with the cornice in a continuous band (e.g. Yecapixtla). However, the size and disposition of the buttresses were

not always like this and a great number of Augustinian churches present a variation that looks like improvisation. The variation in number distribution, size and even shape, can be noticed in the four cases of **Figure 2-19.**

The choir was designed as a large balcony in the internal part of the main façade. In the majority of the cases, the length is similar to the span of the nave, keeping a square or almost square proportion on the plan. Although in general this element was built with masonry, there are cases where it rests on a wooden framework or is made completely of wood in modest churches or provincial areas. The presence of the choir implies that the greatness of the nave can only be observed from the centre of the church.

The towers appeared in the second half of the 16th century and are characteristics from the Augustinian constructions (Kubler, 1983). They are an important constituent in the composition of the façade.

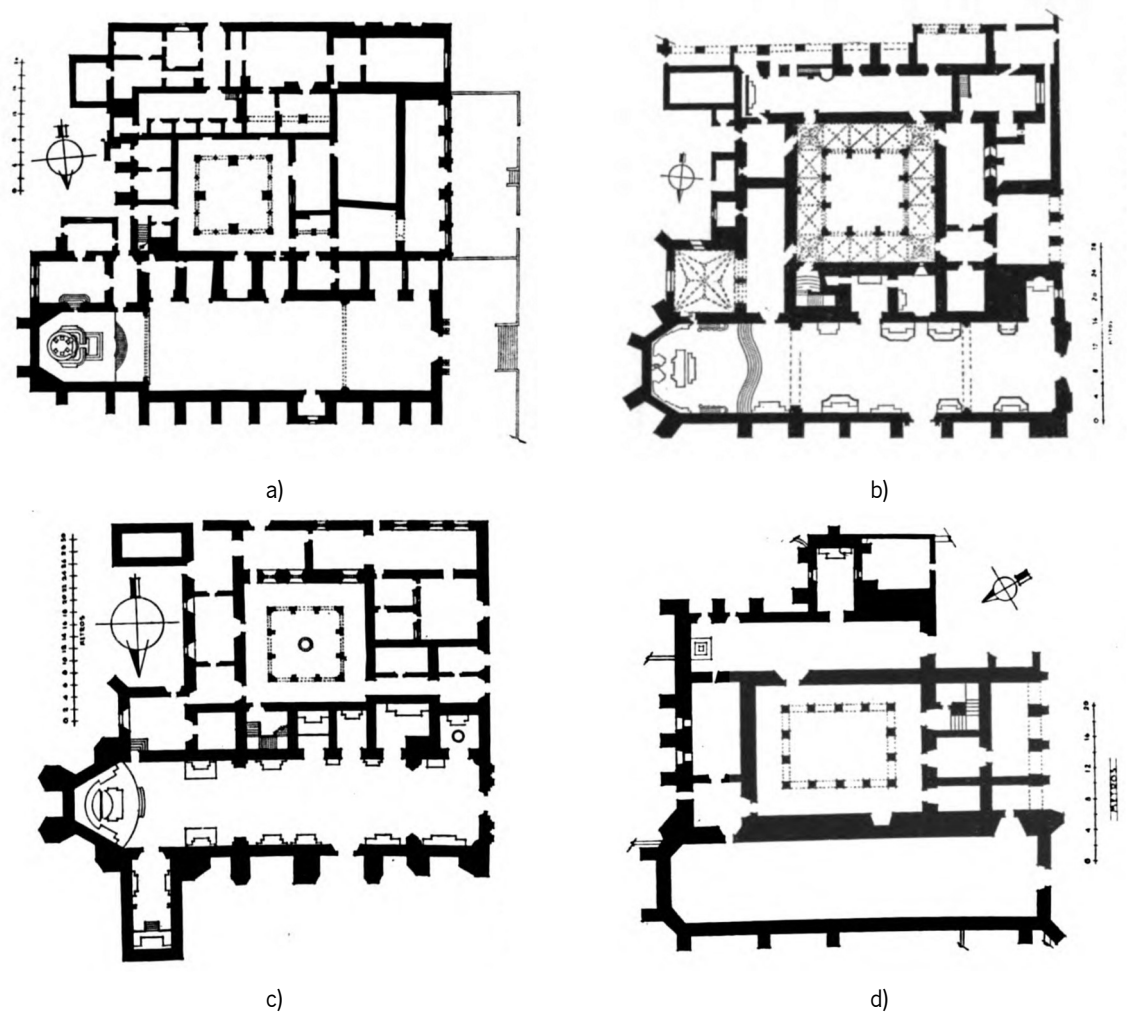

Figure 2-19. Plans of Augustinian convents (Kubler, 1983): a) Atotonilco *el Grande*, Hidalgo; b) Actopan, Hidalgo; c) Ixmiquilpan, Hidalgo; d) Acatlan, Hidalgo.

2.4. Conclusions

The present chapter provides an introduction to the main characteristic of the Mexican Heritage, in order to explain its value and analyse its development during the colonial era. The goal is to address the historical relationship between the European architectural styles (especially from Spain) and the forms of architecture that flourished in Mexico.

Considering the span of time in which the Spanish colonization took place, an analysis of the architectural styles produced in Europe was described: 1) Gothic; 2) Renaissance; and 3) Baroque. Gothic started in the 12th century and lasted until the end of the 16th, which allowed the spreading of the style (from the latest period) to the new conquered lands. It is possible to see some resemblance in the construction techniques and aesthetic due to the first architects and craftsmen that moved from Europe to Mexico. Several studies in the literature focus on searching the relations in the constructions from the New World in agreement to the European treatises, such as the one from Rodrigo Gil the Hontañón. Nonetheless, some studies point out that modifications to the "rules" were made, depending on the local context, for instance the seismicity, which led to more robust structural characteristics. The Renaissance, trying to revive the classical architecture in Europe, occurred in parallel in the colonies, considering that this period started in the early decades of the 16th century, same period when the Aztec Empire was conquered and the territory became the New Spain. From this period, the Plateresque style is one that immigrated to the new lands, becoming as well, a source of inspiration that, together with the local culture, created important examples of architecture such as the Metropolitan Cathedral. Regarding the Baroque, the style reached Spain at the beginning of the 17th century. Although the independency of the New Spain happened in 1810, the cultural transmission did not stop with the political separation of the countries. In this period, important monuments were erected, such as the house of the *"Azulejos"*, in Mexico City.

Explanations of how the architectural styles evolved and how the constructive process was performed in the new lands respond not only to the global history production but also to the local influence. Thus, the creation and diffusion of colonial styles depended on foreign knowledge and on regional sources and cultural traditions, resulting in interesting symbiosis of the immigrant and the local expertise. Therefore, it is possible to compare the local heritage with the heritage around the world, tracking connections through history. It is important to highlight that the local territory was much centralized, meaning that the strongest and "purest" influence of the European culture was localized in Mexico City. In this regard, architectural influence was blurred with distance.

In the case of the religious architecture, the constructions under the management of the mendicant orders are a good example. These constructions from the 16th century clearly expose the hybridization of the styles in the architecture and the decorative elements (e.g. the altars or the so called *"retablos"*). The complexes managed by the different orders present similarities; however, Augustinian architecture was characterised by very ambitious projects. Flourishing between 1530 and 1620, Augustinian convents were stablished mostly in the central region of the country. Big projects and long construction processes resulted from these developments: according to Kubler (1983), the temples can reach total dimensions between 60 and 70 m thanks to the roof system, which also allows bigger spans than 13 m. The majority of the constructions present barrel vaults as roof system on the nave of the church as well as the cloister. The evolution of the constructive process can be noticed in the stylisation of the spaces. One clear example in cloisters is the massive buttresses and the small openings evolving to more elaborated buttresses and double rhythm openings on the second level.

Chapter 3
Seismic Demand Definition

3.1. Introduction

In geographic terms, Mexico is located between the latitudes 15° and 30° and the longitudes 86° and 116°. Two-thirds of the country and 90% of the coastline area on the Gulf of Mexico are located in the tropics. The geographical characteristics of Mexico are varied, including the large southwest coastline bordering the Pacific Ocean, dry and hot regions in the north, the high central mountainous region, including Mexico City, and the flat and heavy vegetation regions of the southern and eastern coast of the Gulf of Mexico. The most easterly section of Mexico includes the Yucatan Peninsula, a flat limestone tableland, which is rich in Mayan culture and tradition (Cook et al., 2000). **Figure 3-1** shows the classification of the four principal climatic areas and the respective average annual relative humidity.

In general, the risk (R) is a function of hazards (H), vulnerability (V) and exposure (E), according to the equation: R = H x V x E. Mexico is a country subjected to several hazards, due to its peculiar geological

nature. Central Mexico presents an offshore subduction zone, a volcanic belt, high seismic activity in a great part of the country and a variety of complex local structures (Lomnitz & Castaños, 2006). Recognising the high level of hazard and aiming at avoiding the loss of built heritage, Mexico needs a correct assessment and reduction of the vulnerability of the buildings, as this is a direct consequence of risk reduction.

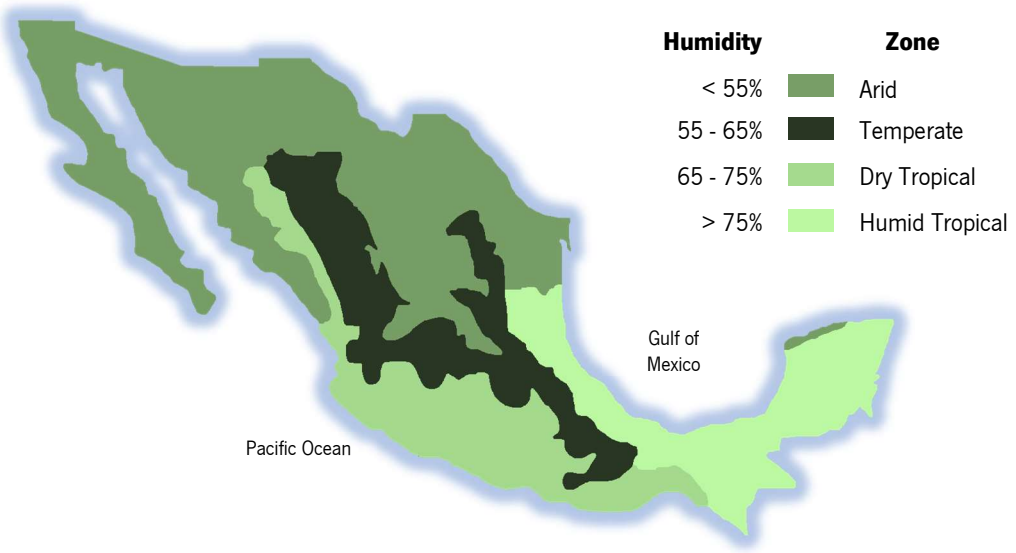

Figure 3-1. Climatic classifications in Mexico [adapted from (Cook et al., 2000)].

Recent earthquakes have caused the collapse and severe damage of even modern buildings, projected in accordance with the established seismic codes at the moment of the design. Earthquakes that strongly affect new buildings, combined with the need for housing and infrastructure in developing countries, may overshadow the interest for a correct understanding and assessment of the heritage building conditions, excluding some glaring case studies (e.g. the Mexico City cathedral). The design and assessment of contemporary buildings are of great importance, but certainly, a global effort to reduce the vulnerability of the built heritage is needed as well. In this regard, the National Institute of Anthropology and History (INAH) and the National Institute of the Beauty Arts (INBA), both in Mexico, including the acknowledgement of UNESCO, are trying to bring more attention to the built cultural heritage and its ability to foster the local economic development. In this regard, routes and associations have been founded to connect and preserve the monuments while the scientific community is also showing a greater interest in the topic. It is noted that INAH is the official bureau devoted to the preservation of historic properties built before 1900, while the preservation of the relevant architecture from the 20th century is promoted and supervised by the INBA.

3.2. Seismicity

The Circum-Pacific Belt, also known as the Ring of Fire, is an area in the shape of a line of 40,000 km around the Pacific Ocean. It is distinguished by having most of the active volcanos in the world and sites with the highest seismic activity, which also affect the neighbouring areas. The Ring of Fire surrounds almost totally the Pacific Ocean (**Figure 3-2**). Its extension covers the coasts of South America, Mexico and California to Alaska; then it continues through the Aleutian Islands, before heading south through Japan and the East Indies. Most of the seismic energy on the planet is released in this region, this is the reason why around 80% of the earthquakes in the world occur in this zone (Yin et al., 2019). The geology has explained how the interaction between the tectonic plates is the cause of this aspect. In the specific case of the Circum-Pacific Belt, the plates with major extension in the interaction are: Antarctic Plate, Nazca Plate, South American Plate, Cocos Plate, Caribbean Plate, North American Plate, Juan de Fuca Plate, Pacific Plate, Filipino Plate and Australian Plate (**Figure 3-3**). According to (EN 2020), since 1800, not only great volcanic events had happened within this area (e.g. the eruptions of Mount Tambora in 1815, Krakatoa in 1883, Novarupta in 1912, Mount Saint Helens in 1980, Mount Ruiz in 1985, and Mount Pinatubo in 1991), but also several of the largest earthquakes recorded in history (e.g. the earthquakes of San Francisco in 1906, Chile in 1960 and 2010, Alaska in 1964, Mexico in 1985 and 2017, Japan in 2011, or the devastating tsunami that occurred in Thailand in 2004).

Mexico is located in one of the most seismic areas in the world. Although there are some local faults along some states, they are considered less dangerous and, in this particular case, the high seismicity is attributed to the interaction between five tectonic plates: North American, Cocos, Pacific, Rivera and Caribbean plates (**Figure 3-4**). Most of the continental territory is located on the North American plate, while the Baja California peninsula belongs to the Pacific Plate. In the Pacific coastal strip, the interaction relies on the Rivera Plate, the Cocos Plate and the Caribbean Plate. It is worth to mention that the Trans-Mexican Volcanic Belt results from the interaction between the Cocos and Rivera plates subducted beneath the North American plate and a large majority of the intraplate seismicity is located in this area, where, according to (Suárez et al., 2019), 40% of the population of Mexico lives.

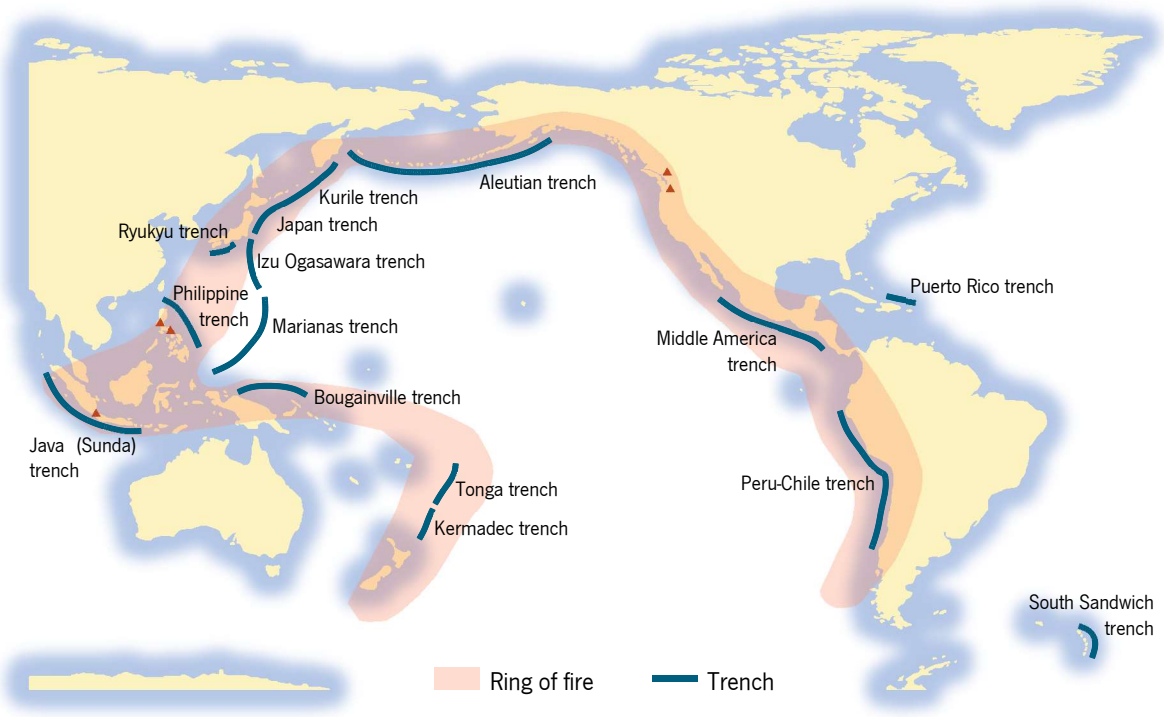

Figure 3-2. Circum-Pacific Belt also known as Ring of Fire [adapted from (Gringer, 2009)].

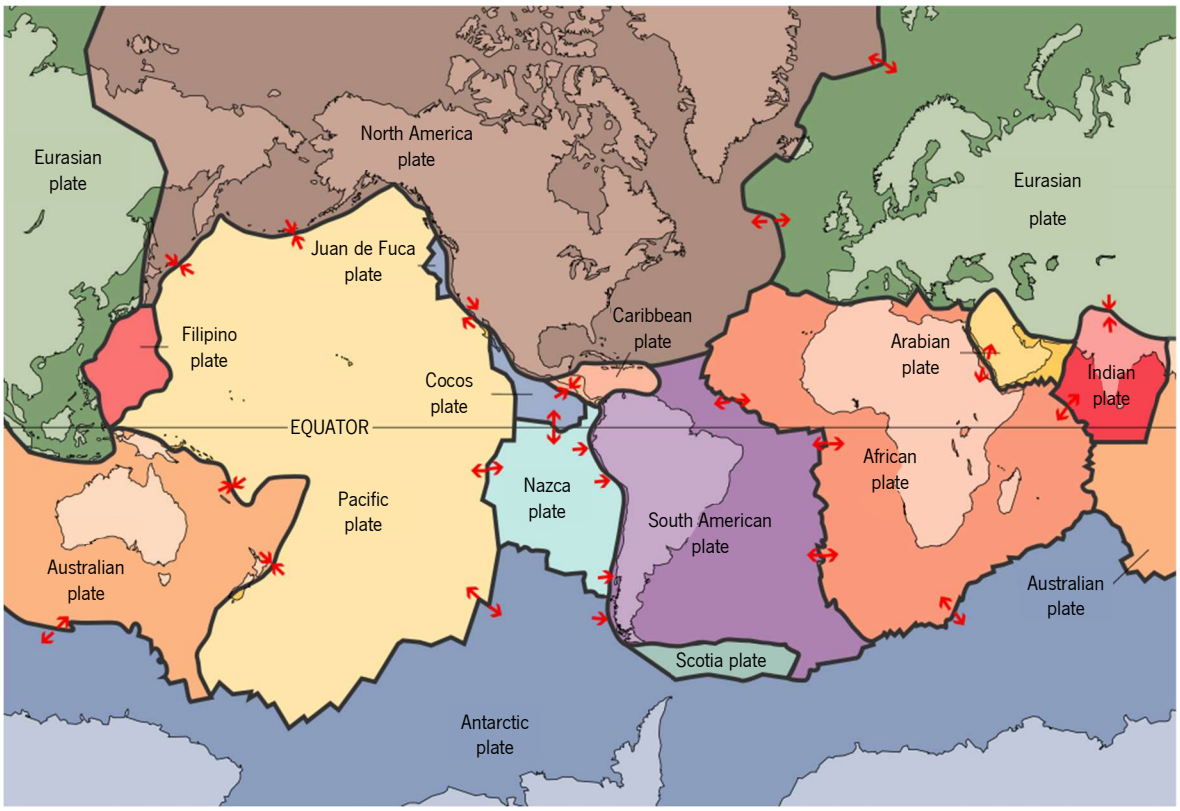

Figure 3-3. World tectonic plates [adapted from (USGS, 1996)].

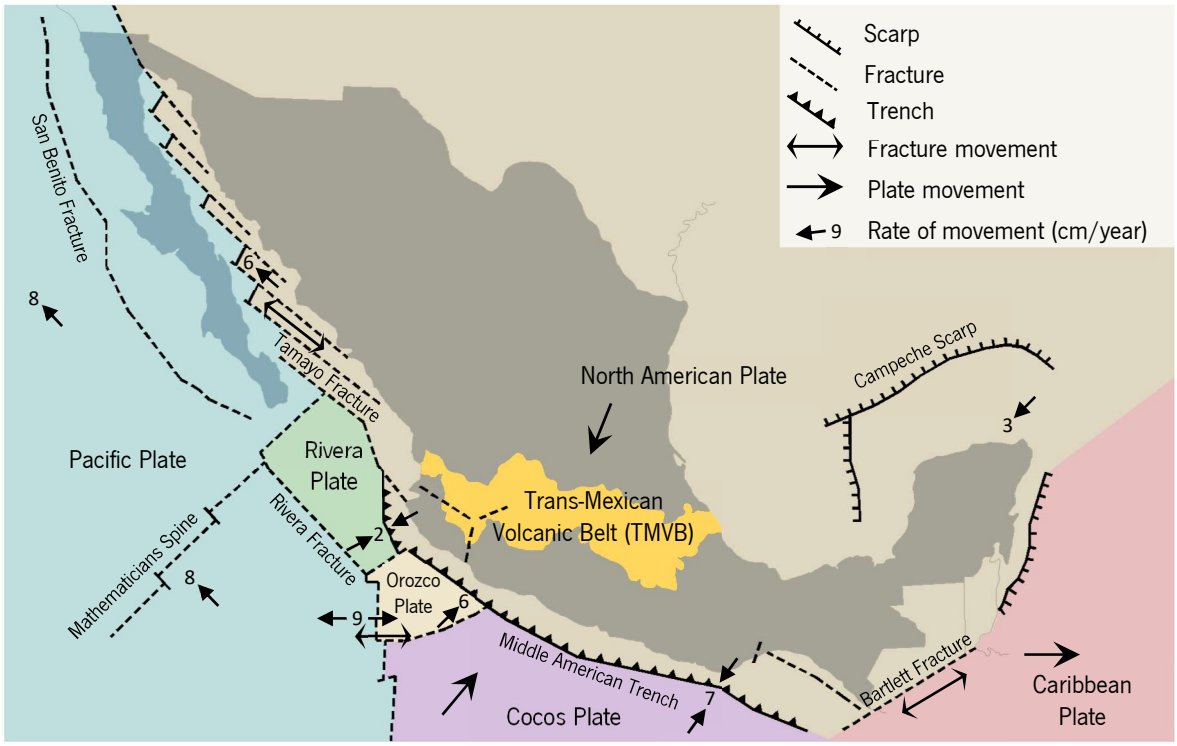

Figure 3-4. Tectonic plates affecting Mexican seismicity [adapted from (Rhoda & Burton, 2012)].

Although the epicentre zones are located mostly on the Pacific coast, Mexico City has become an important seismic receptor, due to its proximity to the fault, being able to experience the effects of the earthquakes. These effects are further increased due to the nature of the ground: the city was built on what used to be a lake.

The studies of seismicity in Mexico started at the beginning of the last century, with the inauguration of the National Seismic Network, in 1910. Nonetheless, earthquakes in previous times were documented in the historical records of the country. Currently, the Seismic Network counts 35 seismic stations under the management of the Geophysics Institute (IG) of the Autonomous National University of Mexico (UNAM), which operates the National Seismologic Service (*SSN - Servicio Sismológico Nacional*, in Spanish). The SSN reports an occurrence of 4 earthquakes per day with a magnitude M > 3. The Seismic Alert System of Mexico (SASMEX - *Sistema de Alerta Sísmica Mexicano,* in Spanish) is operated by the Centre of Instrumentation and Seismic Records (*CIRES – Centro de Instrumentación y Registro Sísmico*, in Spanish). The CIRES has stations in the seismic regions of the subduction area between the Cocos Plate and the south of the Trans-Mexican Volcanic Belt (TMVB), specifically in the states of Jalisco, Colima, Michoacan, Guerrero, Puebla and Oaxaca. In the North of Mexico, the Centre for Scientific Research and Higher Education, at Ensenada, focuses its studies on the seismic activities of the Gulf of California

(namely the San Andreas fault) and the north-west Seismic Network. Besides these three large research groups, with investigations concentrated in the seismicity of Mexico, some other universities are developing regional systems to monitor seismic behaviour.

According to the National Institute of Electricity and Clean Energies (INEEL 2017), the country is divided into four zones, which aims to provide the seismic action parameters to implement in the structural design (**Figure 3-5**):

- **Zone A**: There are no historic registered earthquakes and there have not been seismic movements in the last 80 years. A Peak Ground Acceleration (PGA) higher than 0.1 g due to earthquakes is not expected.
- **Zone B and C**: They are intermediate zones. The earthquakes registered are not frequent or the PGA is not higher than 0.7 g.
- **Zone D**: Strong earthquakes have been reported in this zone. The occurrence is highly frequent and the PGA can exceed 0.7 g.

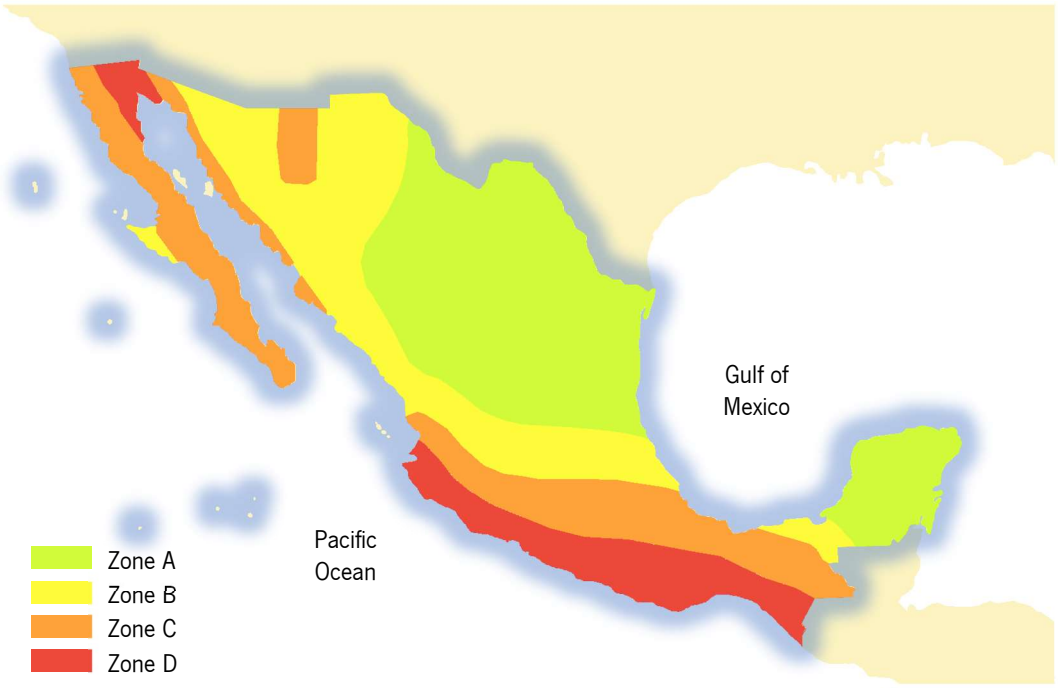

Figure 3-5. Seismic regions in Mexico [adapted from (INEEL 2017)].

Another classification, developed by SSN, divides the territory into three zones (**Figure 3-6**):

- **Seismic zone**: located in the south and south-west of the country. This region includes the states of Mexico, Colima, Michoacán, Guerrero, Morelos, Oaxaca, south of Veracruz, Chiapas, Jalisco, Puebla and Mexico City.
- **Peniseismic zone**: This area includes the western Sierra Madre mountains, the plains of Sonora, Sinaloa, Nayarit and the transverse region going from the south of Durango to the centre of Veracruz.
- **Non-seismic zone**: The north and northeast of the country belong to this region as well as the Yucatan peninsula.

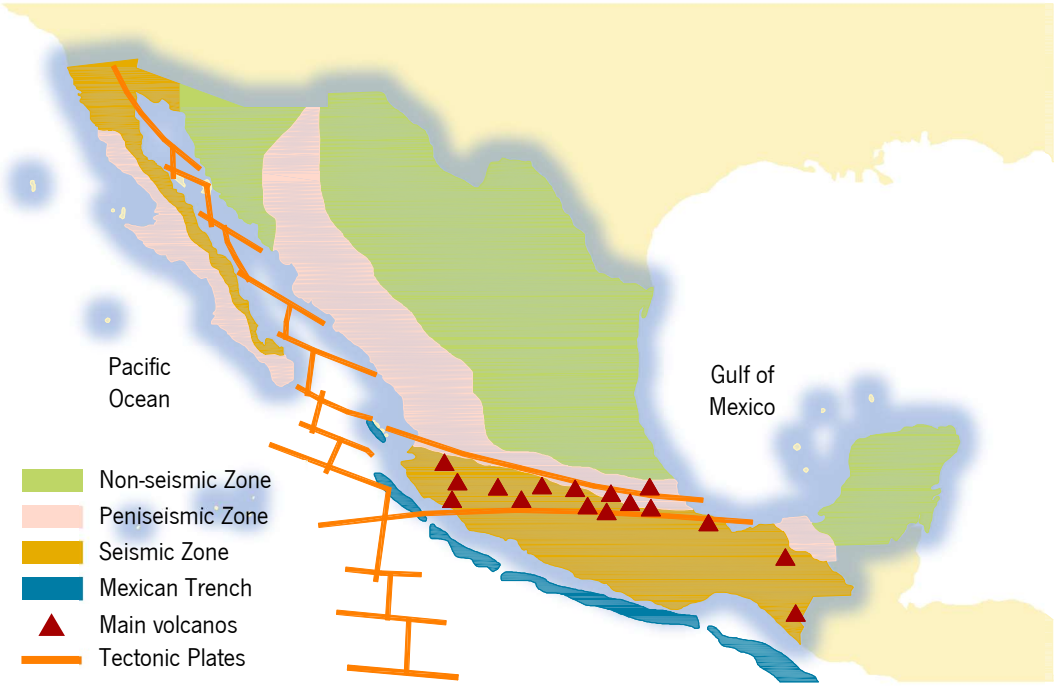

Figure 3-6. Seismic regions in Mexico [adapted from (UNAM, 2017)].

Thus, the areas with major seismic activity are located on the western coast of the country along plate edges, which contact is known as Trench. The geographic areas where earthquakes higher than M = 7 (Richter scale) have not to happen in the last 50 years or more, accumulating elastic energy, are known as seismic gaps. These zones are considered the areas with higher seismic hazard: Guerrero gap (almost 100 years); Jalisco gap (approximately 70 years); and Chiapas gap (more than 300 years).

According to the Mexican Geological Services (SGM 2017), on average, in the country, earthquakes are likely to happen:

- **Magnitude M>= 7.5**: Once every ten years.
- **Magnitude M>= 6.5**: Five every four years.
- **Magnitude M>= 4.5**: Hundred every year.

The most destructive earthquakes in the history of Mexico reached a magnitude of 8.1 and 7.6 on September 19th and 20th, respectively, in 1985. These two events demonstrated that the knowledge of the phenomena was not sufficient. As a consequence, they became the starting point for the development of studies and the basis for a new design code that takes seismicity as a very important topic.

Recently, on September 7th, 2017 an earthquake of magnitude 8.2 occurred, and on September 19th same year, another earthquake with magnitude 7.1 devastated the country again, reaching high levels of damage. The epicentre of the first shake was located in the cost of the Gulf of Tehuantepec, 140 km to the southwest of Pijijiapan, Chiapas (latitude: 14.76°; longitude: -94.10°), at a depth of 45.9 km. More than 6,000 aftershocks were reported by the end of the month, including two with a magnitude higher than 6.1. The epicentre of the second shake was located 12 km to the southeast of Axochiapan, Morelos (latitude: 18.34°; longitude: -98.67°), at a depth of 51.2 km. By the end of the month, more than 30 aftershocks were reported. In these cases, the higher magnitude was 4.0 (SSN 2021).

The SNN reports every year a map with the annual seismic activity. As shown in **Figure 3-7**, the maps from 2016 to 2019 confirm what was previously referred to. The major seismic activity is located in the southwest of the country, on the coastline of the Pacific Ocean. In 2016, six earthquakes with a magnitude higher than 6.0 are reported. In 2017, four earthquakes with a magnitude higher than 6.0 were also reported. In 2018 and 2019 three such earthquakes are reported each year.

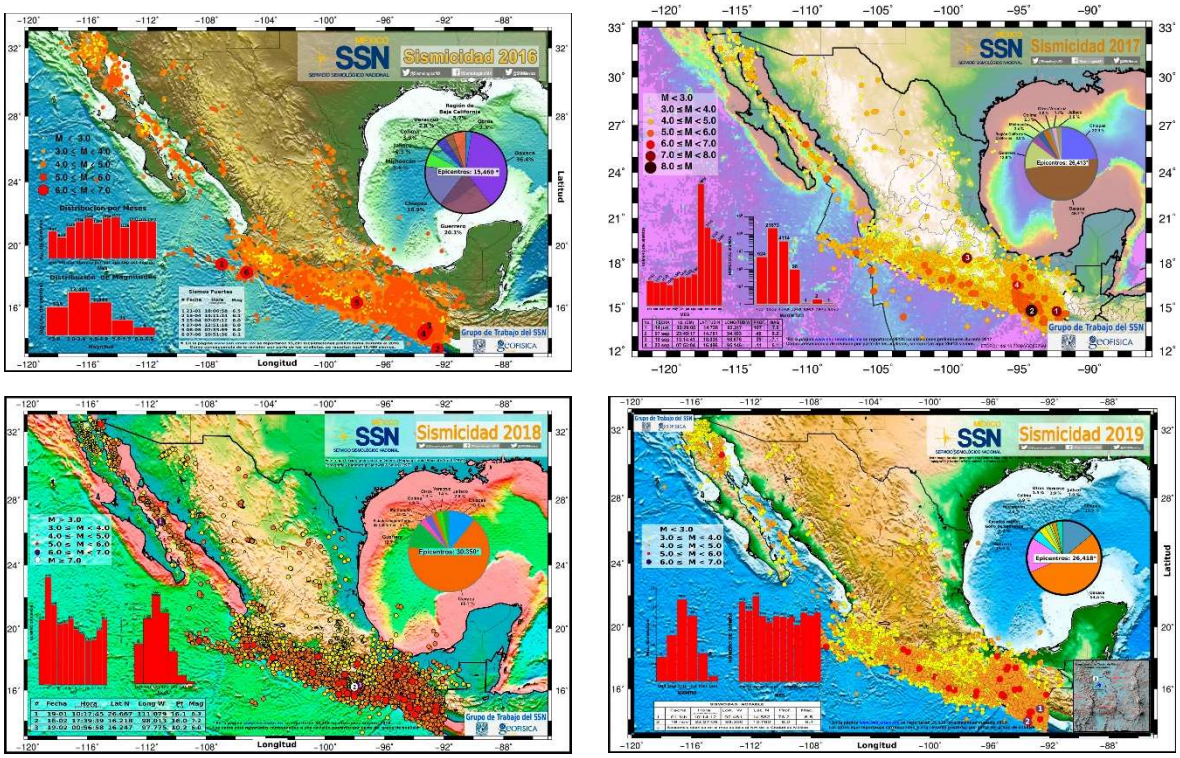

Figure 3-7. Seismicity maps from 2016 to 2019 (SSN 2020).

Reports of the damage surveys carried out after some of the past events allowed to collect information regarding the characteristics and the main issues related to cultural heritage conservation in Mexico (Klingner, 2006). Such reports are essential sources to evaluate the behaviour of the heritage buildings against strong earthquakes and to identify the main issues to tackle to strengthen and protect them.

On June 15th, 1999, a 7.0 Mw earthquake occurred near Tehuacan (Puebla). It caused 14 casualties, more than 400 injuries and severe damages in buildings, including more than 700 monuments in the states of Puebla, Tlaxcala, Guerrero, Oaxaca, Veracruz and Morelos. A team of engineers carried out a series of surveys after June 19th (Jimenez et al., 1999). In the area affected by the earthquake, there are many historical buildings and Puebla City, the capital of the state, is included in the UNESCO monument list. Many churches from 16th to 19th century are in the area, typically cross-shaped, with barrel-vaulted aisles with main arches and a central dome, in general, reinforced with buttresses. Churches with more than one nave have large pilasters. The façades present one or two bell towers. The materials adopted are adobe, bricks and stone blocks. All the structural elements are thick and, overall, the state of conservation was good. During the surveys the following damage patterns were identified: 1) longitudinal cracks along the barrel vault crown, eventually followed by two additional cracks between the crown and the base (severe damage) due to the outwards movements of the support walls (*La Compañía* church, in Puebla); 2) cracks along the meridians of the domes, due to the lack of restraint at the base (*San Juan*

Bautista church, in Acatlan); 3) cracking and failure of the buttresses following the previous damage scenarios; 4) shear damage around the openings of the belfry causing, in some cases, the collapse of the tower (*San Agustin* church, in Puebla; *Nuestra Senora de Los Remedios* church in Cholula, Puebla); 5) diagonal crack due to the detachment of the tower from the façade (Tlacotepec church); 6) fall of ornamental elements. The performance of the churches against this event was significantly worse than other types of buildings, irrespective of the moderate seismic action. **Figure 3-8** shows a sketch of the common damages presented in a technical report by the CENAPRED (Alcocer et al., 1999).

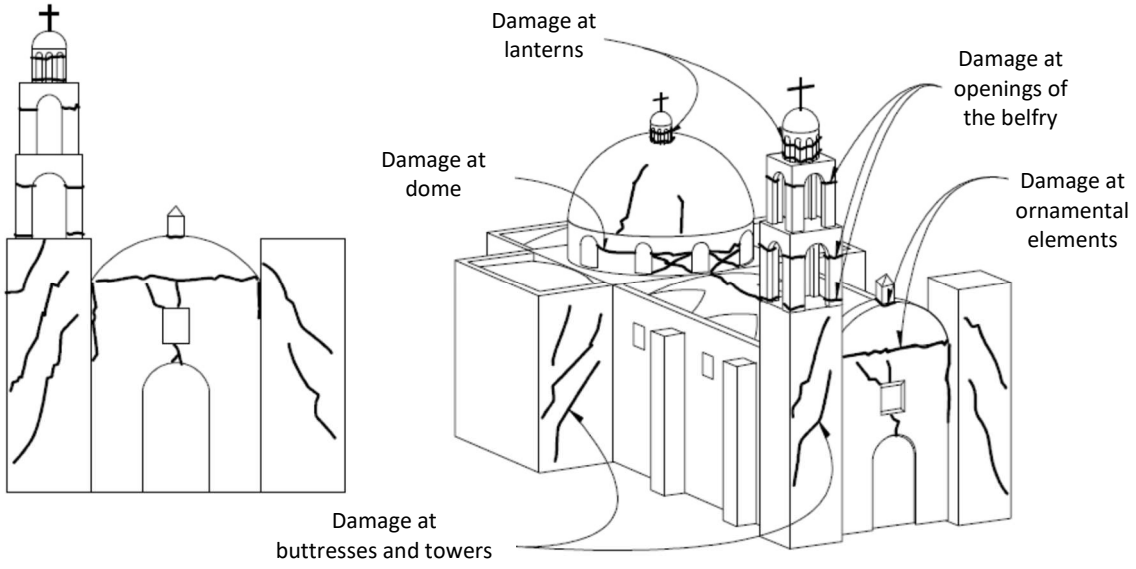

Figure 3-8. Common damage observed in churches due to the earthquake on June 15th, 1999 [adapted from (Alcocer et al., 1999)].

After the earthquake in Tecoman (7.6 Mw), on January 21st, 2003, the Earthquake Engineering Research Institute (US), the National Centre for Disaster Prevention (CENAPRED) and the Mexican Society for Earthquake Engineering (SMIS) provided reports about the state of damage of the buildings (Klingner, 2006). The earthquake caused 17 casualties and more than 500 injuries, moreover, it damaged almost 14,000 structures, of which almost 3,000 collapsed. Regarding the heritage, many churches were affected, but they presented only light damages (e.g. stuccos and plaster spalling, damages in non-structural elements or fine cracking at walls). The only monument that suffered more severe damage was the church of *San Pedro*, located at Coquimatlan, which underwent severe shear damage in the walls and the cupolas and the partial collapse of the main dome. The south bell tower collapsed. Also, the north bell tower was damaged in the columns, with the permanent rotation over one of them. However, the structure was considered reparable. The surveys involved the municipalities of Colima, Manzanillo, Villa de Álvarez, Comala, Coquimatlan, Tecoman, Ixtlahuacan and Armeria (Colima). Furthermore, the close

states of Jalisco (especially Ciudad Guzman, Melaque, Barra de Navidad and Cihuatlan) and Michoacan were visited.

The epicentre of the earthquake on September 19th, 2017 was registered at the south of the TMVB. It is considered as an intraplate earthquake of an intermediate depth, produced by tensional stresses along the Cocos plate. Including on the list of losses, the cultural heritage suffered severe damage, mainly in the state of Morelos (due to its proximity to the epicentre), where it is located the path known as The Convents Route, "*La Ruta de Los Conventos*" in Spanish (Pérez-Gavilán et al., 2018). **Figure 3-9** shows some of the severely damaged structures observed in the inspection.

a) b) c)

Figure 3-9. Damage in the historical heritage: a) Santo Domingo de Guzman, Tlaquiltenango; b) Santiago Apostol, Jiutepec; c) Santo Domingo de Guzmán, San Andres Hueyapan. Pictures from (Pérez-Gavilán et al., 2018).

3.3. Earthquakes records

It is known that the average of the periods in heritage buildings is low due to the large stiffness of structures with very thick walls and elements. In the particular case of the San Agustin church, in Morelia, which is adopted as a case study in this work, the frequency of the vertical mode of the vault is equal to 3.71 Hz (T = 0.27 s) (more details are presented in Chapter 4). Due to these aspects, research on records of past earthquakes with high amplitudes close the vertical vault period was done. An example is presented in **Figure 3-10**. The response spectra correspond to the records of the earthquake that

occurred on September 7th, 2017. The name of the station is HUAMELULA (HUAM), located in the state of Oaxaca (latitude: 16.03°; longitude: -95.67), managed by the Engineering Institute of UNAM. As shown, the maximum spectral accelerations (Sa) for the three components are with periods lower than 0.5 s.

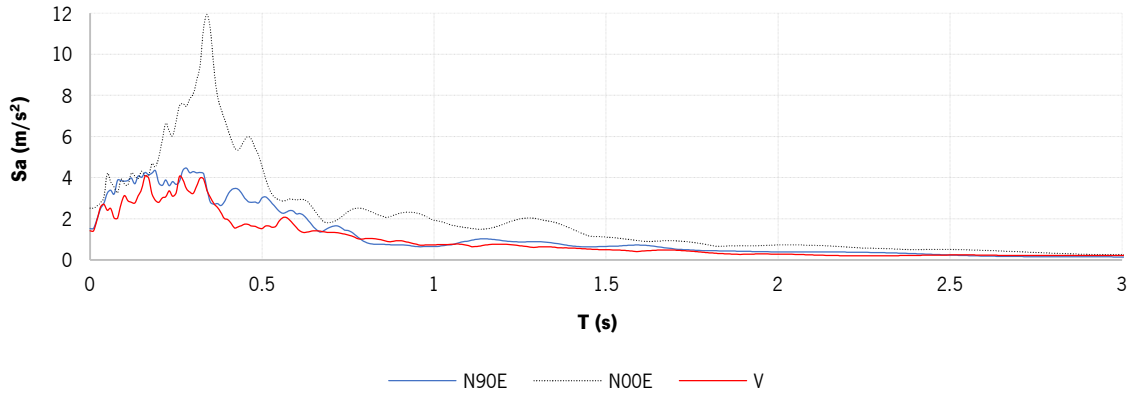

Figure 3-10. Response spectra for the record HUAM1709 (two horizontal and vertical components).

Figure 3-11 shows the location of the epicentres of five strong important earthquakes in Mexico, with magnitude Mw higher than 7.0, that were considered to perform the analyses in this study and are discussed below in the text:

1. Michoacan: September 19th, 1985. Mw = 8.1
2. Puebla: Jun 15th, 1999. Mw = 7.0
3. Colima: January 21st, 2003. Mw = 7.2
4. Chiapas: September 8th, 2017. Mw = 8.2
5. Puebla: September 19th, 2017. M = 7.1

Figure 3-11. Location of epicentres of the adopted earthquakes (Mexico).

3.3.1. Michoacan: September 19th, 1985 (Mw = 8.1)

This event was an important earthquake in the country, not only due to the magnitude but also due to the learnings about the seismicity in Mexico. The epicentre was located on the coast of Michoacan State (18.081° latitude: -102.942° longitude), at a depth of 15km (subduction area). The earthquake showed that the country was not ready to face a hazard of this magnitude. The losses included 13,000 damaged buildings and 500 collapses, leading to 6,000 deaths, 20,000 injuries and economic losses of 4,500 million dollars. Even if the institutional organization and the crisis management was poor, the social response was relevant and civil associations were created, and indeed, they still exist nowadays. In 1986, the needs exposed by this event led to the development of a National System for Civil Protection and further studies, in order to better understand the seismicity of the country. As a result, several improvements emerged such as the definition of seismic risk macro-zoning; methodologies to evaluate the vulnerability, mainly in essential buildings; reconstruction programs and development of techniques for structural rehabilitation; seismic instrumentation and alert systems; better understanding of the dynamic behaviour of the structures; enhancement of the construction and structural design codes; and

professional updating (Sánchez Pérez, 2007). 36 stations from the Strong Motion Network (RAII-UNAM) recorded this event in different parts of the country.

3.3.2. Puebla: June 15th, 1999 (Mw = 7.0)

The epicentre of the earthquake of June 15th, 1999 was located in Tehuacan, the state of Puebla (18.18° latitude: -97.51° longitude), at a depth of 69 km (intraplate area). This event is particularly important due to the damages induced in historical monuments: mainly churches, government palaces and convents built between the 16th and the 19th century, most of them located in the states of Puebla and Morelos. It was estimated that around 1,300 monuments were affected by this seismic event, in many cases as a result also of the lack of maintenance (Alcocer et al., 1999). 43 stations from the RAII-UNAM recorded this event in different parts of the country.

3.3.3. Colima: January 21st, 2003 (Mw = 7.6)

Relevant by its magnitude, the epicentre of this earthquake that occurred on January 21st, 2003 was located at the coast of the state of Colima (18.60° latitude: -104.22° longitude), at a depth of 9 km (subduction area). The earthquake caused damages to historical heritage in the states of Colima and Jalisco. The towers, together with the façades and the connection between them were reported as the more vulnerable elements. In some cases, cracks along the vaults were also described. 38 stations from the RAII-UNAM recorded this event in different parts of the country.

3.3.4. Chiapas: September 8th, 2017 (Mw = 8.2)

The epicentre of the earthquake of September 8th, 2017 was located at the cost of the Gulf of Tehuantepec, Chiapas (14.76° latitude: -94.10° longitude), at a depth of 45.9km (subduction area). Most of the damages in buildings caused by this earthquake were reported in Mexico City, Puebla and Oaxaca. It is considered the largest earthquake in more than a century (Sahakian et al., 2018; Sarlis et al., 2018). 73 stations from the RAII-UNAM recorded this event in different parts of the country.

3.3.5. Puebla: September 19th, 2017 (Mw = 7.1)

The seismic event of September 19th, 2017 occurred only 12 days after the previous one (September 8th, same year) and 32 years after an earthquake that left a mark in the history of the country (September 19th, 1985). The epicentre was located in the state of Puebla (18.33°latitude: - 98.67° longitude) at a depth of 51.2 km (intraplate area). Most of the damages were reported in Puebla, Morelos, Guerrero and Mexico City and neighbouring states (Sahakian et al., 2018; Sarlis et al., 2018). 73 stations from the RAII-UNAM recorded this event in different parts of the country.

3.4. Discussion. Seismic Demand

In order to consider the effect of the site, the records measured at several stations (located at different distances to the epicentres) were analysed. The five events previously mentioned were recorded by 263 stations in the country. This number was shortened to 50 signals by defining a radius of influence of 200 km for each event. The response spectra of the signals were evaluated. Finally, 30 records presented maximum spectral accelerations for periods lower than 0.5 s, the list is in **Table 3-1**.

Table 3-1. List of records reduced due to the radius of influence and the maximum structural response. Maximum PGA recorded by the seismic stations.

	Date	Magnitude	Station	Identification	State	PGA (cm/s²)
1	19/09/1985	Mw = 8.1	Zihuatanejo airport	AZIH	Guerrero	153.93
2	19/09/1985	Mw = 8.1	Caleta de Campos	CALE	Michoacan	140.68
3	19/09/1985	Mw = 8.1	La Union	UNIO	Guerrero	165.29
4	19/09/1985	Mw = 8.1	Villita Margen Derecha	VILE	Michoacan	125.17
5	19/09/1985	Mw = 8.1	Zacatula	ZACA	Michoacan	262.23
6	15/06/1999	Mw = 7.0	Chila de las Flores	CHFL	Puebla	110.4
7	15/06/1999	Mw = 7.0	Serdan City	CSER	Puebla	199.13
8	15/06/1999	Mw = 7.0	Faculty of Medicine, Oaxaca	OAXM	Oaxaca	89.1
9	15/06/1999	Mw = 7.0	Raboso	RABO	Puebla	162.58
10	21/01/2003	Mw = 7.6	Caleta de Campos	CALE	Michoacan	28.08
11	08/09/2017	Mw = 8.2	Huamelula	HUAM	Oaxaca	251.73
12	08/09/2017	Mw = 8.2	Faculty of Medicine, Oaxaca	OAXM	Oaxaca	268.82
13	08/09/2017	Mw = 8.2	University of Oaxaca	OXCU	Oaxaca	195.79
14	08/09/2017	Mw = 8.2	Jalapa del Marques	OXJM	Oaxaca	275.78
15	08/09/2017	Mw = 8.2	Technological Institute of Oaxaca	OXTO	Oaxaca	213.25
16	08/09/2017	Mw = 8.2	Xoxocotlan	OXXO	Oaxaca	217.7
17	08/09/2017	Mw = 8.2	Rio San Francisco, Puebla	RFPP	Puebla	22.97
18	08/09/2017	Mw = 8.2	San Alejandro, Puebla	SAPP	Puebla	45.77
19	08/09/2017	Mw = 8.2	Salina Cruz	SCRU	Oaxaca	293.29
20	19/09/2017	Mw = 7.1	IDEI yard 5	CUP5	Mexico city	58.84
21	19/09/2017	Mw = 7.1	Huamuxtitlan	HMTT	Guerrero	170.47
22	19/09/2017	Mw = 7.1	Nicolas Bravo, Puebla	PBP2	Puebla	98.68
23	19/09/2017	Mw = 7.1	Habana Park, Puebla	PHPU	Puebla	141.71
24	19/09/2017	Mw = 7.1	La Paz Hill, Puebla	PZPU	Puebla	119.97
25	19/09/2017	Mw = 7.1	Raboso	RABO	Puebla	154.69
26	19/09/2017	Mw = 7.1	Rio San Francisco, Puebla	RFPP	Puebla	183.95
27	19/09/2017	Mw = 7.1	San Alejandro, Puebla	SAPP	Puebla	205.97
28	19/09/2017	Mw = 7.1	SISMEX Puebla	SXPU	Puebla	139.18
29	19/09/2017	Mw = 7.1	Primary School Emiliano Zapata, Tehuacan	THEZ	Puebla	166.5
30	19/09/2017	Mw = 7.1	South Tonalapa	TNLP	Guerrero	65.97

For the sake of clarity, **Figure 3-12** shows the response spectra for the 30 records mentioned. According to the Mexican codes (NTC-2017), a minimum of 8 records of past earthquakes must be used to perform a time history analysis. The response of the structure must consider simultaneously both horizontal-

orthogonal components. It is known that due to the characteristics of the historical structures, the vertical component of the earthquakes may play an important role in the performance of the ancient buildings, due to the considerable density of the masonry and presence of joints. **Figure 3-13** to **Figure 3-15** presents the 8 response spectra of the selected records.

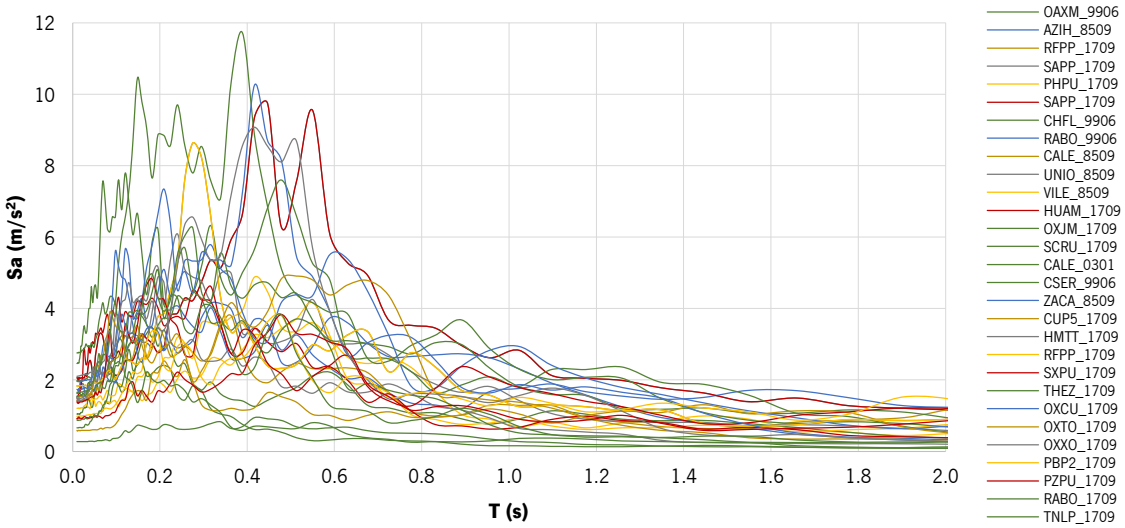

Figure 3-12. Response spectra of the 30 records. Component N90W (the legend presents the identification of the station and the data, year and month, of the record, according to **Table 3-1**).

The higher values for the spectral acceleration were selected, considering the three components (N90W, N00E and Vertical). For the component N90W, the higher values of spectral acceleration (Sa) are within a range of 4 to 12 m/s^2 and periods (T) around 0.2 to 0.6 sec. For the component N00E, the higher values of Spectral acceleration (Sa) are within a range of 4 to 13 m/s^2 and periods (T) around 0.2 to 0.6 sec. For the vertical component, the higher values of spectral acceleration (Sa) are within a range of 1.5 to 8.5 m/s^2 and periods (T) around 0.1 to 0.5 s.

Table 3-2 shows the characteristics of the seismic records presented in **Figure 3-13** to **Figure 3-15**. From the original list, one record from 1999 was selected. The station was located in the state of Oaxaca and presented a PGA of 89.1 cm/s^2. Five records from the earthquake of September 8th, 2017 were selected. The accelerometers were located in Oaxaca and Puebla and they present a maximum PGA of 293.0 cm/s^2. Two records from the earthquake of September 19th, 2017 were selected. The stations were located in Puebla and they present a maximum PGA of 184.0 cm/s^2. These records were selected based on the maximum spectral acceleration related to structural periods lower than 0.5 s.

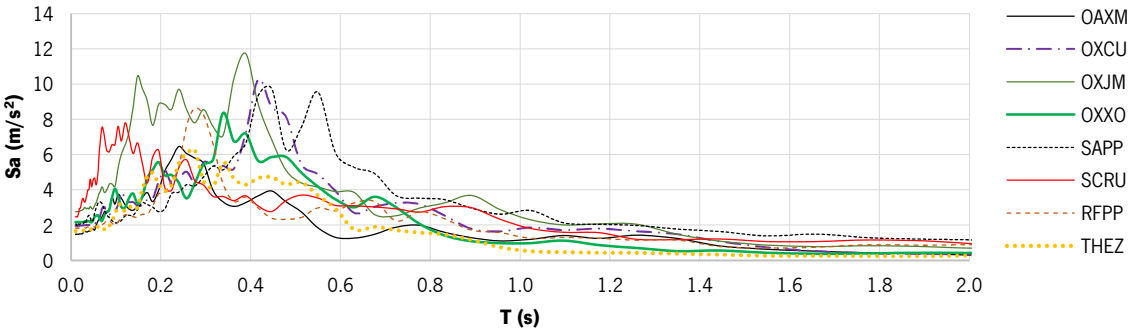

Figure 3-13. Response spectra for the 8 selected records. Component N90W.

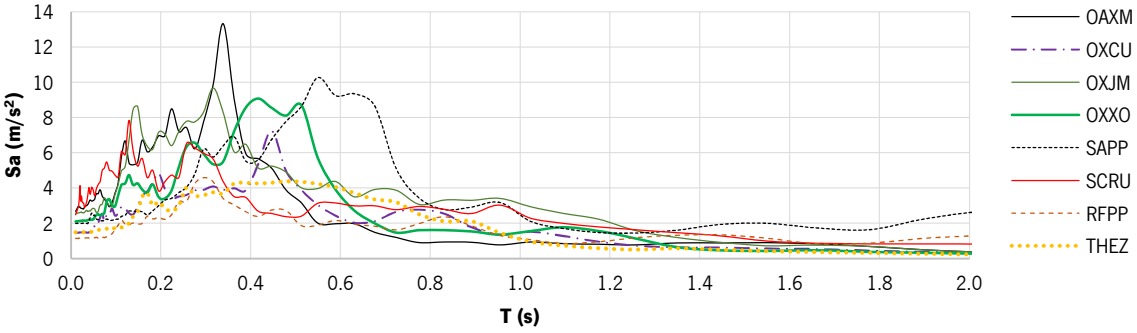

Figure 3-14. Response spectra for the 8 selected records. Component N00E.

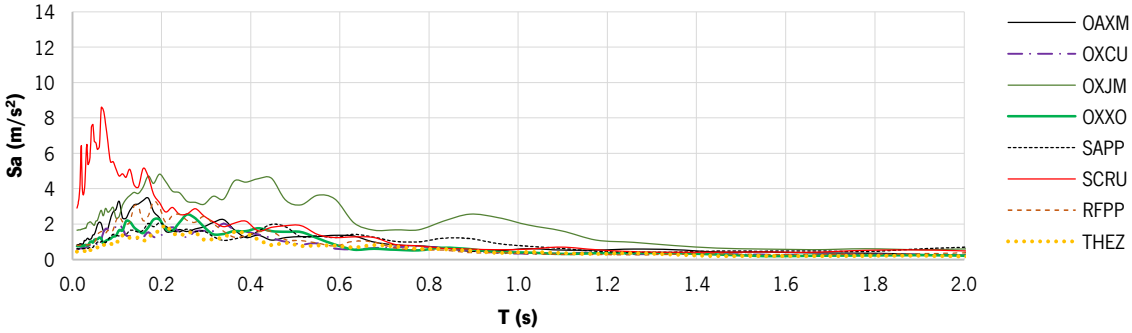

Figure 3-15. Response spectra for the 8 selected records. Vertical component.

Table 3-2. List of the selected earthquakes to perform the dynamic analysis.

	Date	Magnitude	Station	Identification	State	PGA (cm/s²)	DE (Km)	t (s)
1	08/09/2017	Mw = 8.2	Faculty of Medicine, Oaxaca	OAXM	Oaxaca	268.8	380	167
2	08/09/2017	Mw = 8.2	University of Oaxaca	OXCU	Oaxaca	195.8	377	165
3	08/09/2017	Mw = 8.2	Jalapa del Marques	OXJM	Oaxaca	275.8	235	173
4	08/09/2017	Mw = 8.2	Xoxocotlan	OXXO	Oaxaca	217.7	376	194
5	19/09/2017	Mw = 7.1	San Alejandro, Puebla	SAPP	Puebla	45.8	93	73
6	08/09/2017	Mw = 8.2	Salina Cruz	SCRU	Oaxaca	293.3	197	179
7	19/09/2017	Mw = 7.1	Rio San Francisco, Puebla	RFPP	Puebla	184.0	93	94
8	19/09/2017	Mw = 7.1	Primary School Emiliano Zapata, Tehuacan	THEZ	Puebla	166.5	137	128

PGA: Peak Ground Acceleration; DE: Distance to the Epicentre; t: duration of the earthquake.

3.5. Conclusions

Mexico is a country with high seismic hazards. The conditions that surround its geography imply a constant presence of telluric movements. The Seismic Institute from UNAM reports that 80% of the seismic activity in the country is located in its southwest and the most seismic states are Jalisco, Colima, Michoacan, Guerrero, Oaxaca and Chiapas. Due to their proximity to the subduction area between the Rivera and Cocos plates under the North American plate. Most of the strong earthquakes in the history of Mexico has been recorded with epicentre within this area. It is important to mention as well the intraplate seismicity at the TMVB and the tensional earthquakes generated at the continental area.

Mexico has learnt through the effects of strong earthquakes that seismicity is a very important issue. After the event on September 19th, 1985, and the devastation provoked, studies and research about earthquakes increased. This was also a starting point for a new design code that changed completely the parameters and the process for structural design. New types of analysis were implemented and seismic performance of buildings started to be considered as one of the most important parts of the design, particularly in areas of relevant seismicity.

The north of the country is exposed rarely to seismic action, and thus, the design can be simpler than in southern Mexico. Each state has developed its own codes for structural design. Nonetheless, it is normal to refer to the code established for Mexico City, which has been a reference to the seismic studies. However, it should be noticed that these codes calibrate the spectra of design for new buildings and the

past modifications does not include special sections to the study of the cultural heritage structural behaviour.

In the present work, seismic records that occurred in Mexico were adopted. The SSN recorded events that occurred from the beginning of the last century, such as: the earthquake on September 19th, 1985; the earthquake on June 15th, 1999; the earthquake on January 21st, 2003; the earthquake on September 7th, 2017; and the earthquake on September 19th, 2017. In order to select records, the spectral acceleration of the records was evaluated and the number of records was reduced, taking into account the period of the vertical mode of the case study adopted in this study (San Agustin Church). First, 30 records were selected, considering their three components. Finally, and taking into account the Mexican codes (NTC-2017), 8 seismic records were selected, including the two horizontal and the vertical components.

Chapter 4
San Agustin Church: History and model updating

4.1. Introduction

As stated in the previous chapters, the preservation of built heritage in Mexico is an open issue. On one side, regardless of the outstanding value of many historical buildings in the country, there is still limited knowledge of traditional construction techniques and material behaviour. On the other side, the condition survey and the vulnerability assessment should be tasks of strategic importance considering the exposition to major hazards, as earthquakes. Indeed, past earthquakes proved that traditional unreinforced masonry (URM) structures have a poor performance for seismic actions, as highlighted in post-event surveys [e.g. (Alcocer et al., 1999; Reyes et al., 2003)] or in seismic assessment studies from the literature [e.g. (Meli & Peña, 2004; Peña et al., 2016; Peña & Manzano, 2015)].

During the Colonial period, thousands of churches have been built in a large territory. However, due to the short span of this period, most of these buildings present similar characteristics, as described in Chapter 2. Therefore, an in-depth analysis of a relevant example of this typology is truly beneficial, providing an insight into the seismic behaviour of a large class of buildings and allowing to test retrofitting techniques that can be largely applied to Mexican Heritage.

The aim of the present thesis is to contribute to the appreciation of the built heritage in Mexico (specifically the single nave churches from the 16th century) and to address the lack of attention to the needs for their conservation. In this regard, the Church of San Augustin, located in Morelia, Michoacan, has been taken as a case study due to its relevance and the possibility to perform in-depth surveys and testing campaigns. The accessibility to the building is essential to carry out a seismic assessment using advanced numerical analysis tools. Access allows obtaining a sufficient level of knowledge regarding the geometry, the materials, the structural system details and the state of conservation. For the present case study, the historic context and the characteristics of the building have been investigated both through literature review (Cabrera, 2011; Nuñez Gaona, 2015) and in situ surveys. In-situ experimental campaigns have been carried out, in the past, by the Michoacan University of Saint Nicholas of Hidalgo (Nuñez Gaona, 2018) and, recently, for the present study.

The seismic behaviour of the church, together with other case studies located in Morelia, has been previously investigated by the authors (Alejo et al., 2014; M. Zavala et al., 2014), using a simplified 2D rigid element model of the transverse section of the nave. Such studies pointed out the significant vulnerability of this particular building. Furthermore, damage induced in the building by the 7.2 magnitude earthquake of Guerrero, on April 18th, 2014, drew attention to the safety condition of the building, recommending further analyses (Nuñez Gaona, 2015, 2018). In this regard, the present work relies on a set of refined numerical models calibrated based on a new and larger experimental campaign.

4.2. The Church of San Agustin

The church of San Agustin is one of the 249 recognized monuments of great relevance in the city centre of Morelia, capital of Michoacan in Mexico (UNESCO, 2013b). Identified as the most ancient construction of the city (1550) (Cabrera, 2011), the building was built by the Augustinian friars, during the evangelization of the new lands conquered by the Spaniards. In this period, the Augustinian friars promoted the edification of several convents in the South of the country, including the actual state of

Michoacan (Kubler, 1983). The church is, therefore, an example of the constructive and architectural style of the buildings erected by the order. Indeed, the case study is a single nave church with a vaulted roofing system, a common typology in Mexico and in Morelia itself. In **Figure 4-1**, it is possible to identify the location of the city in the country and, on a bigger scale, the area included in the UNESCO Heritage List since 1991. In the same figure, the location of the other single nave churches with vaulted roofing, built in Morelia during the 16th to 18th century, is shown.

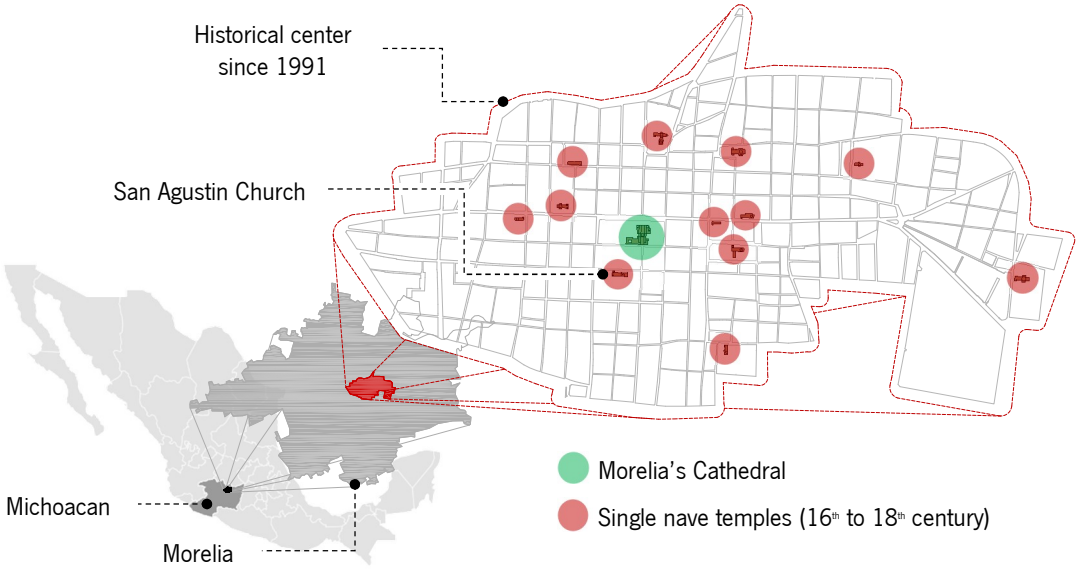

Figure 4-1. Historical centre in Morelia city. Adapted from (UNESCO, 2013a).

4.2.1. Geometric properties

The complex of San Agustin was built in two main phases, resulting in different styles, as evident in the west façade (**Figure 4-2**a): 1) the Plateresque style in the main body, started in 1550; 2) the Baroque style in the bell tower, finished in 1667 (Espejel, 2015). **Figure 4-2** shows these elements in the building.

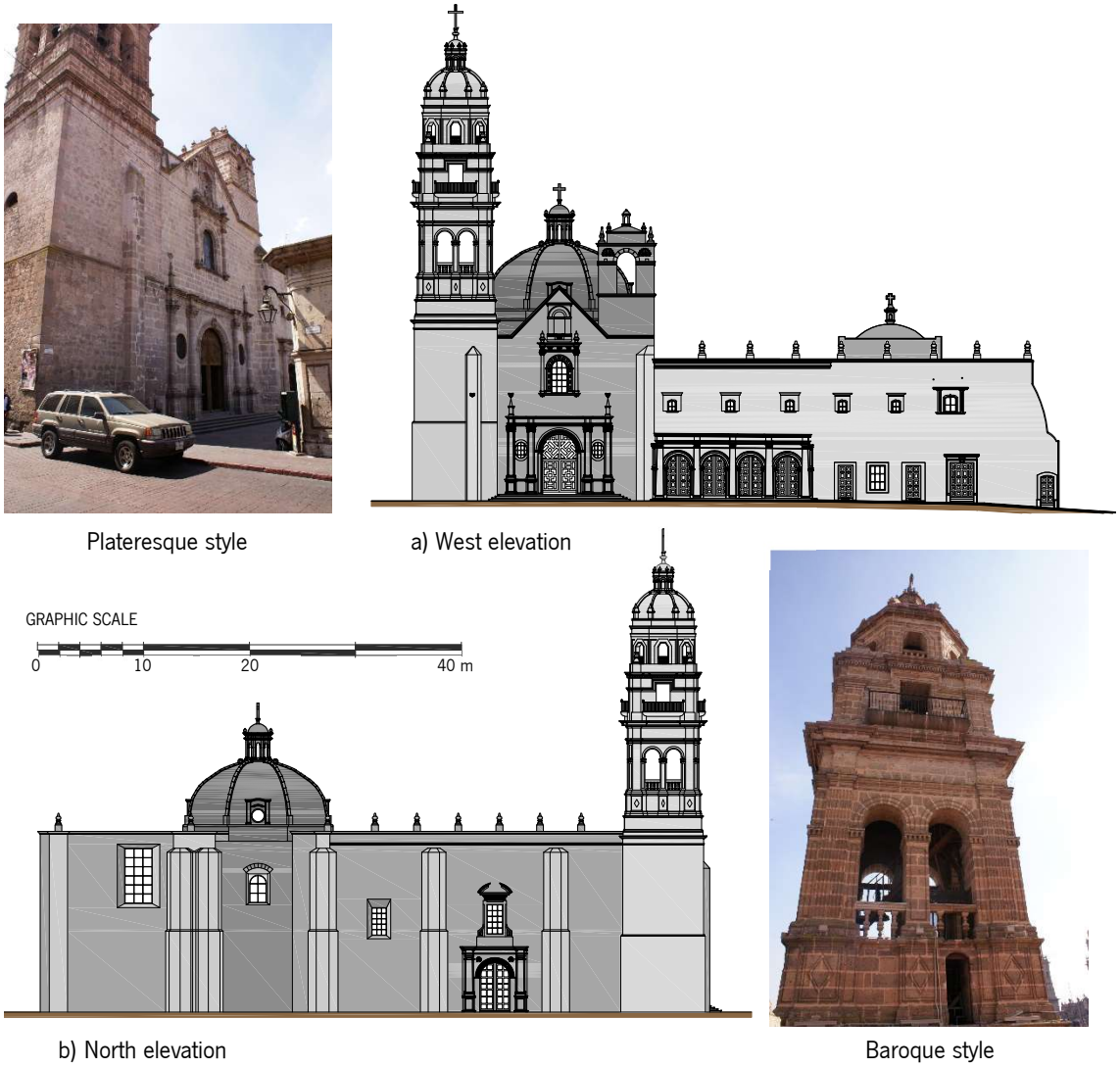

Figure 4-2. Elevations of San Agustin Church.

After the nationalisation of the compound, in the second part of the 19th century, the church and the rest of the convent were separated by closing the door between the nave and the north corridor of the cloister (number 6 in **Figure 4-3**) and the door between the ante-sacristy and the east corridor of the cloister (number 7 in **Figure 4-3**). Currently, the complex is still divided into two main bodies, namely: the church, belonging to the secular clergy; and the former convent cloister, nowadays used as a student house, under the administration of the Michoacan University of Saint Nicholas of Hidalgo.

The church is composed of five main parts: 1) vestibule; 2) north tower; 3) south tower; 4) nave; and 5) presbytery. In **Figure 4-3** the distribution of these main areas is shown using different colours. The plan of the church respects a proportion of approximately 1:5, being approximately rectangular with 58 m in the longitudinal direction and 11 m in the transverse direction.

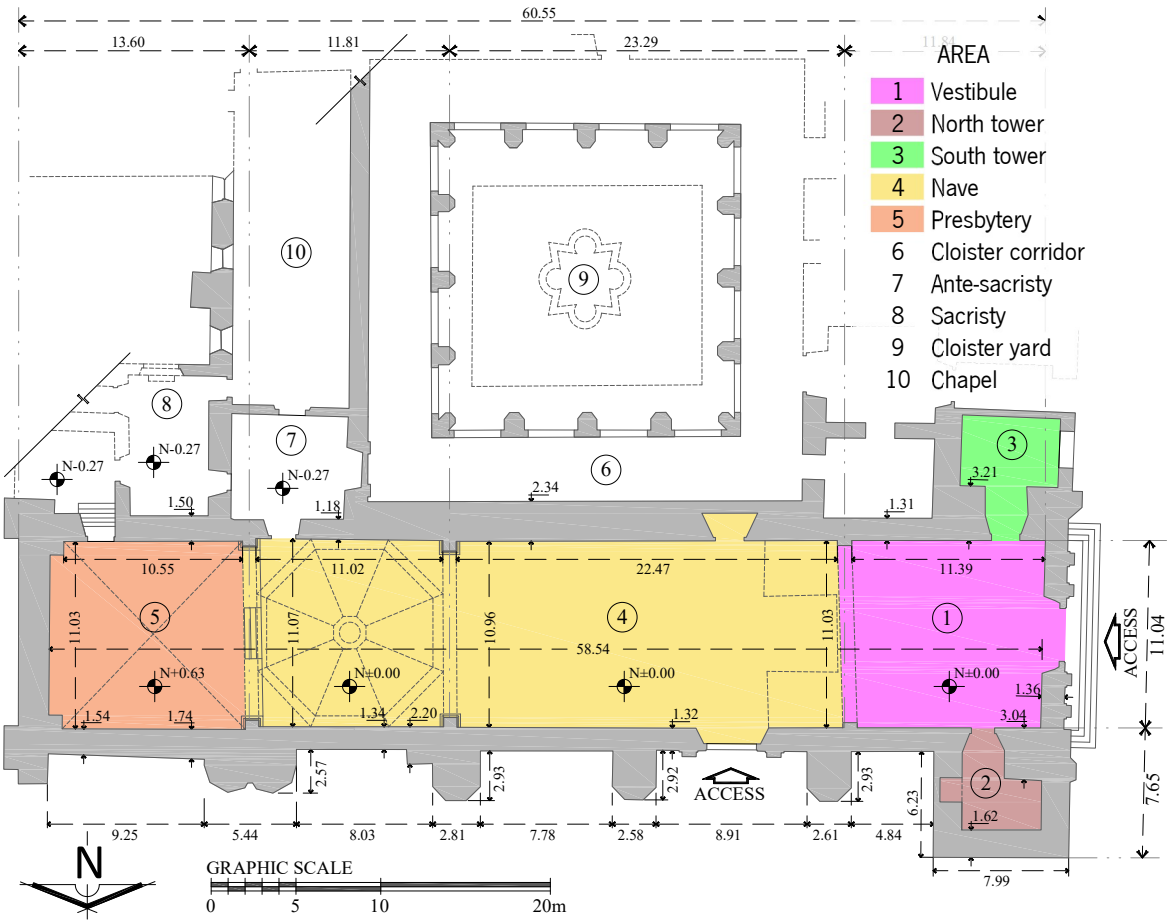

Figure 4-3. Architectural plan. Nave and cloister of San Agustin church in Morelia, Michoacan, Mexico.

The stone masonry walls of the church present different thicknesses. The south wall is shared with the cloister and it is thicker than the north wall (ranging from 1.18 m to 2.34 m). The north wall thickness varies from 1.32 m to 1.74 m but it is stiffened by four buttresses (**Figure 4-2**b). The original buttresses were later enlarged with a poorly connected addition, evident from the abrupt variation in the dimension of the cross-section (Cabrera, 2011). The wall shared between the nave and the north tower is 3.04 m thick, whereas the wall between the nave and south tower is 3.2 m thick.

The roofing system is composed of a cast-in-situ barrel vault in the nave, a groin vault in the presbytery and an octagonal cloister vault in-between (**Figure 4-4**). The secondary groin vault is the result of an extension of the apse in 1840 (Espejel, 2015). It was not possible to perform a direct inspection of the foundation during the survey. However, inspections on similar historical buildings in the area refer that the depth of the foundation is commonly around 10% of the structure height. That ratio would suggest a foundation of approximately 1.60 m for San Agustin church, considering the vault crown as the highest point.

The visual survey allowed to distinguish three masonry types in the structure (**Figure 4-4**): 1) M_{Vault}, a rubble quarry masonry with a high content of mortar located at the vaults (cast-in-situ as a concrete); 2) M_{North}, regular masonry with good bonding, located in the lower section of the north tower, the north wall, the apse and the east part of the south wall. The dome was considered with this type of masonry as well; finally, 3) M_{South}, ashlar masonry located in the west part of the south wall, the façade, the south tower and the upper section of the north tower.

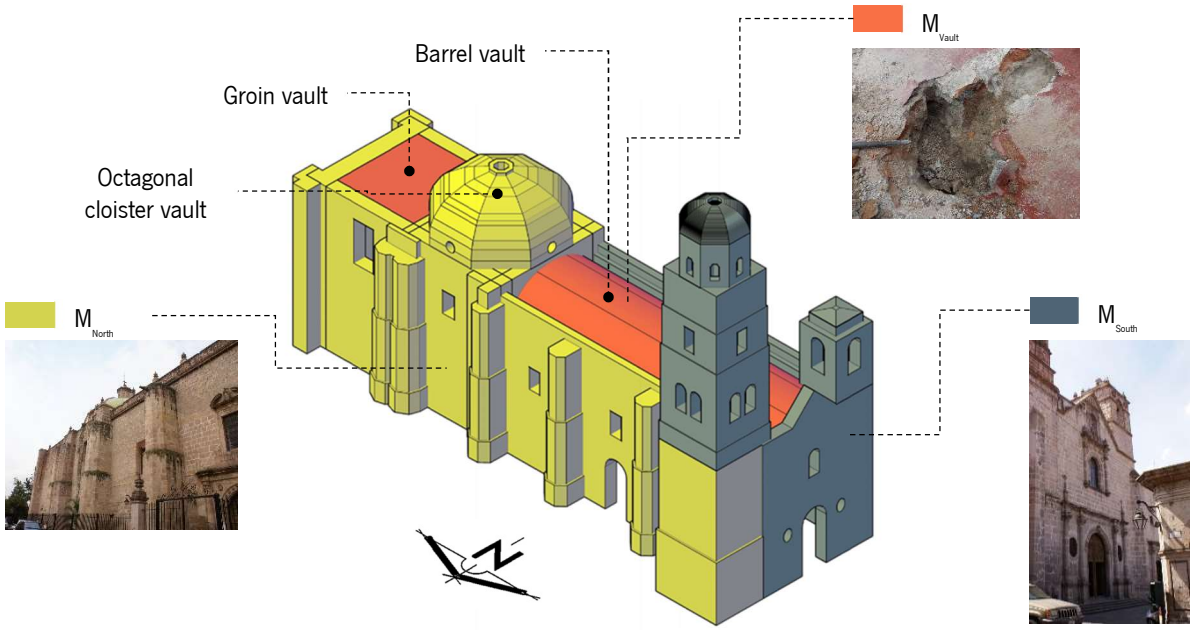

Figure 4-4. Distribution of the materials in different parts of the structure.

San Agustin church presents features belonging to both the typologies of central Mexico's churches outlined by (García & Meli, 2008; Meli & Peña, 2004; Peña et al., 2016) and described in Chapter 2. On one side, the south tower is short, the plan is a simple rectangle and the walls are reinforced with buttresses. On the other side, the façade is slender, the north tower is 40.9 m high and presents several openings, the vault span is quite significant, and the walls are not as thick as the typical examples in the areas with the highest seismic hazard.

4.2.2. Damage survey

The building suffered deterioration, due to the lack of funds and maintenance, affecting not only the aesthetic but also the structural safety. Significant damage was caused by the 7.2 magnitude earthquake

of Guerrero, on April 18th, 2014. After the event, a crack appeared along the vault crown at the intrados, going from the dome to the choir loft, where it changes from the longitudinal to the transverse directions and goes down to the walls (**Figure 4-5**). This pattern is likely due to the larger stiffness of the western part of the building caused by the two towers (north and south) and the choir loft. This latter element acts as a horizontal diaphragm at 7.15 m from the ground. **Figure 4-5**c shows the division of the crack while **Figure 4-5**d emphasizes the crack going down to the north wall.

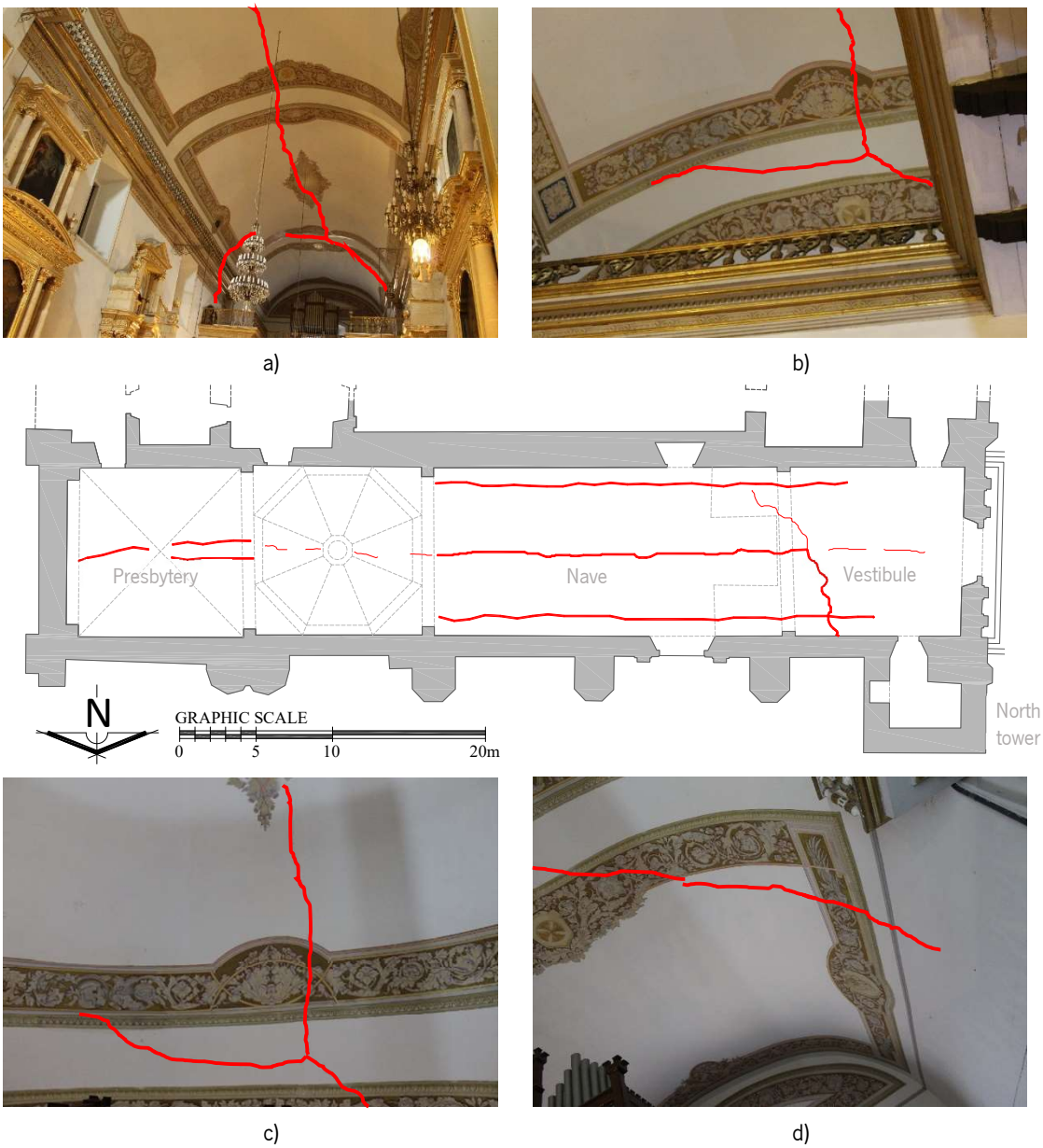

Figure 4-5. Damage at the intrados of the vaults: a) longitudinal and transverse cracking; b) change of crack direction; c) crack leading to the north wall; d) damage at presbytery's groin vault.

Moreover, two longitudinal cracks affect the intrados of the barrel vault at the haunches (**Figure 4-6**a). This symmetrical pattern is likely due to the lateral thrust generated by the vault and the presence of filling material on the roof. **Figure 4-6**b shows also material deterioration around the crack due to moisture, more evident in the rainy season, with changes in the coloration of the painting. A double crack affects the middle of the small groin vault over the presbytery (east-west), dividing this part of the building into two macro-elements (**Figure 4-6**c to e).

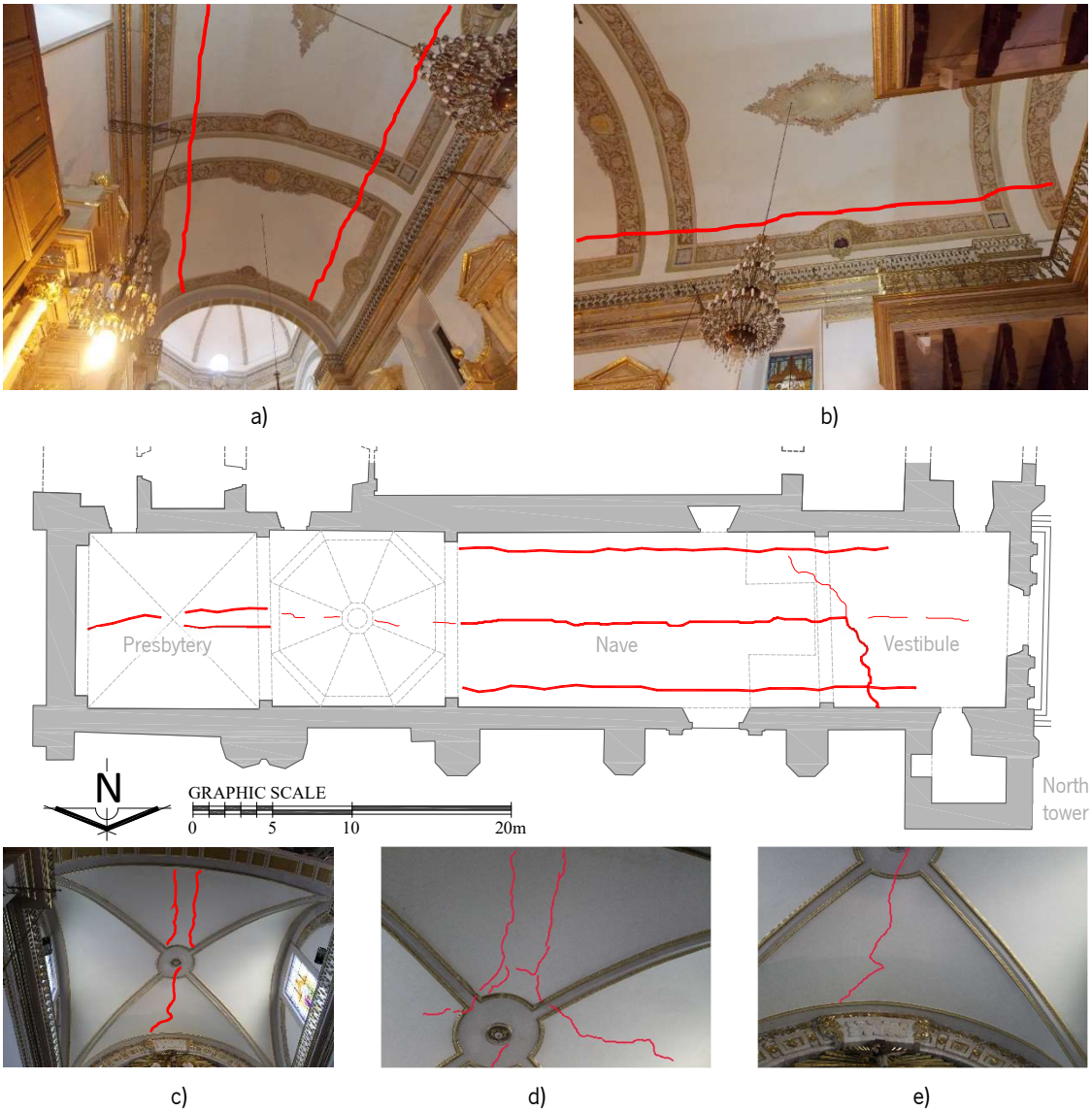

Figure 4-6. Damage at the intrados of the vaults: a) and b) nave's barrel vault; c), d) and e) presbytery's groin vault.

A survey of the walls confirmed that the original buttresses were later reinforced. The poor connection between the more recent masonry jacket and the rest of the north wall presents several cracks, mainly along the joints (**Figure 4-7**). Nevertheless, some of these cracks might also be caused by the lateral

thrust of the barrel vault, since the higher damage is located at the vault's level. The building presents other types of damage, such as cracking at the base of the buttresses (**Figure 4-8**a and **Figure 4-8**b), loss of verticality at the edge of a buttress (**Figure 4-8**c) and vertical cracking (**Figure 4-8**d). Furthermore, some stones have been replaced, as shown in **Figure 4-8**e. The main façade presents two types of damage: 1) cracks due to the interaction with the towers; and 2) damage caused by environmental agents, as the presence of vegetation, the loss of material or deformations on the decorative elements (**Figure 4-9**a). These are worsened by the lack of maintenance or by the interventions using non-compatible materials, for instance, covering the missing parts of the ashlars, as in **Figure 4-9**.

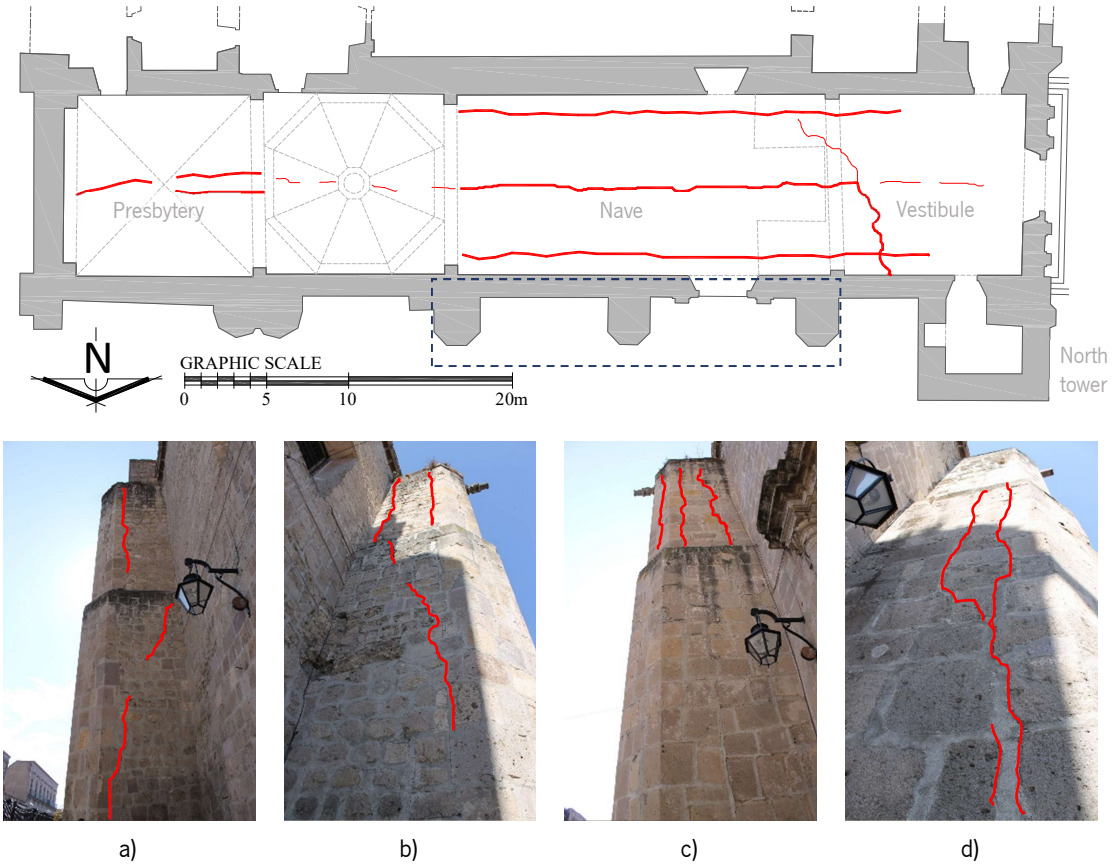

Figure 4-7. Damage at the buttresses: a) to e) vertical cracking.

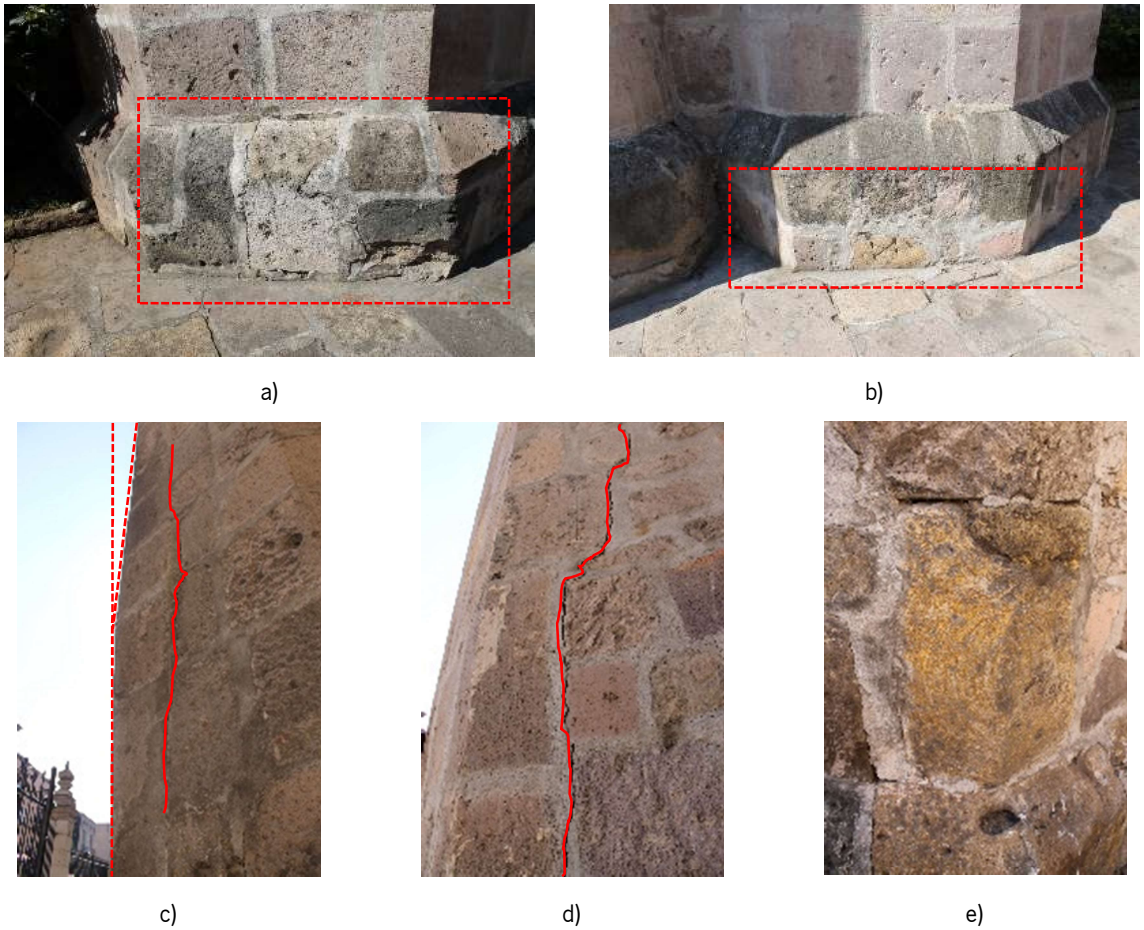

Figure 4-8. Damage in buttresses: a) and b) detachment of masonry at the basement; c) loss of verticality at the edge and vertical crack; d) vertical crack; and e) replacement of damaged units.

Figure 4-9. Damage in the west façade: a) cracks in the connection tower-façade and at the decorative elements; b) cracks in the frame door, exfoliation at the base of the pilaster and marks of previous interventions.

4.3. Dynamic identification tests

Much information can be obtained by understanding the dynamic behaviour of structures. Within the existing methodologies for identifying the dynamic properties of a building, it is possible to highlight forced and environmental vibration techniques. Both methods have gained strength in the last decades for existing masonry buildings, as shown in the literature (Masciotta et al., 2017; Taleb et al., 2012).

Based on the resonant approach, forced vibration testing methodology works through the application of dynamic harmonic excite a specific part of the building (Taleb et al., 2012). Forced vibration can be produced mechanically and several types of equipment have been successfully used in the field, for instance, the eccentric mass shakers which excite with harmonic sinusoidal forces within a specific frequency range, like the one used by Taleb et al. (2012) to induce forced vibration to an unreinforced building rehabilitated by dampers in Algiers (Algeria). However, the applicability of forced vibration tests to large and complex masonry structures is often limited, due to the required equipment to induce the excitation and the possible negative effects that the forced vibration can cause to the masonry structure.

On the other hand, the environmental vibration testing methodology is based on ambient excitation, through the movement induced in the building by sources such as the wind, pedestrians, vehicle traffic, among others (Masciotta et al., 2017). These vibrations are not controlled, but they can be recognized as a stationary random process, enough to excite several modes of structural vibration (Taleb et al., 2012). Ambient vibrations are an inexpensive and always available source that can excite the modes of the structure in the low-frequency range.

Dynamic identification can be carried out according to either forced vibration or ambient vibration testing, in which the former usually leads to more controlled and accurate results (Masciotta et al., 2017; Masciotta & Ramos, 2019; Taleb et al., 2012). In the process of the Data Acquisition (DAQ) real physical conditions are converted into digital numeric values, thus, the vibrations of the structure can be visualised as a plot in a computer and further processed and manipulated. DAQ systems include three main components: 1) sensors that transform physical parameters to electrical signals; 2) signal conditioning circuitry that prepares the electrical signals to be converted to digital values; and finally, 3) converters that change the original signals into digital values

It is well known that for the study of Cultural Heritage structures it is better to apply non-destructive and non-invasive techniques, including for monitoring. Indeed, forced vibration techniques are often less suitable for historical buildings, due to the recommendations of conservation to which are subjected this type of structure. Thus, for this study, the experimental campaigns consisted of the acquisition of the

environmental vibrations caused mainly due to wind, traffic loads and the movement of the soil, among others.

4.3.1. Test Planning

Dynamic identification tests were carried out, aiming at estimating the dynamic properties (frequencies, mode shapes and damping ratios) and, subsequently, updating a numerical model of the church. The ambient vibrations were recorded simultaneously through 4 tri-axial accelerometers, FBA ES-T (10 V/g, frequency range from 0.15 to 1000 Hz, dynamic range ± 0.5 g) (**Figure 4-10**a). The wired accelerometers were connected through Belden cables to two data acquisition (DAQ) systems connected in series (**Figure 4-10**b). The first DAQ receives the signal of each tri-axial accelerometer through a single cable and transmits it to the second DAQ, namely a GRANITE-12 24-bits analog-digital converter (KINEMETRICS, 2013), equipped with 12 channels.

a) b)

Figure 4-10. Equipment used in the dynamic identification tests: a) Force Balance Accelerometer; and b) Communication Centric Multi-Channel Recorder.

The Strong Motion Analyst (SMA) processing software (KINEMETRICS, 2019) was used to process the data. It is worth mentioning that the equipment was not fixed to the structure. Thus, no damage was induced to the building due to the testing campaign. For each different setup, three accelerometers were moved to a different position except one, which was kept fixed in the middle of the vault as a reference point (master-slave arrangement). Such a reference allowed the correlation among the signals of all setups. For the sake of clarity, the following terminology is used to identify the acquisitions: 1) a letter (A-D) indicating the position of the measurement; 2) a first number indicating the number of the setup (1-8); and 3) a second number separated by a comma (1-3) indicating the specific tri-axial accelerometer. For example, case D1,2 is referring to the second tri-axial accelerometer, from setup 1 and with location D (see the specification of locations in **Figure 4-11** and **Table 4-1**).

Table 4-1. Summary and organizations of the monitoring setups.

Location identification	Location	Number of setups
A	Barrel vault (transverse direction)	8
B	Barrel vault (longitudinal direction)	6
C	South wall	3
D	Perimeter choir loft wall	3

The discretization followed was based on the dimensions of the barrel vault. Eight divisions along the length and four divisions along the transverse direction were adopted. **Figure 4-11** shows the locations of the setups. The response of the structure was measured in three different parts of the building: 1) the extrados of the barrel vault with the accelerometer combinations A and B; 2) the south wall, with the accelerometer combinations C; and 3) the perimeter wall of the choir loft, with the accelerometer combinations D. Each setup was recorded 10 min with a 200 Hz sampling rate. The testing campaign was carried out in two days of acquisition (30/11/2018 and 19/12/2018) for the barrel vault (16 accelerometer combinations) and the lateral walls (6 accelerometer combinations), respectively. Due to the importance of other structural elements, it was planned to perform a testing campaign including the tower and the dome, which due to safety issues, was not permitted.

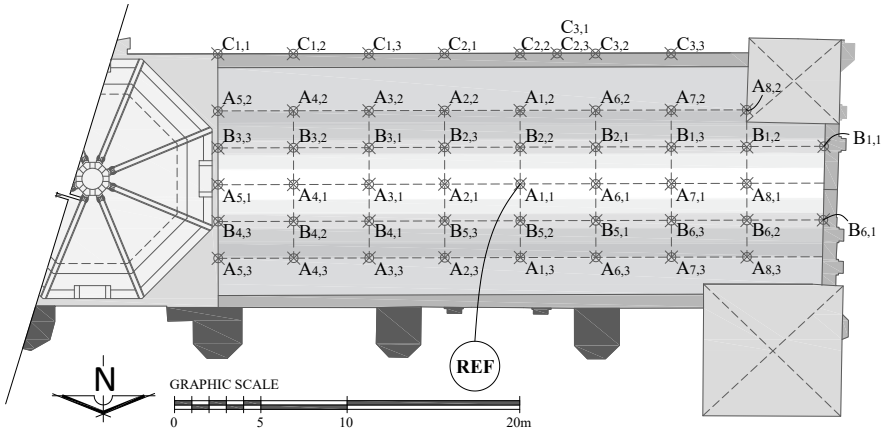

a) Roof plan. N + 16.80 m (higher point in barrel vault).

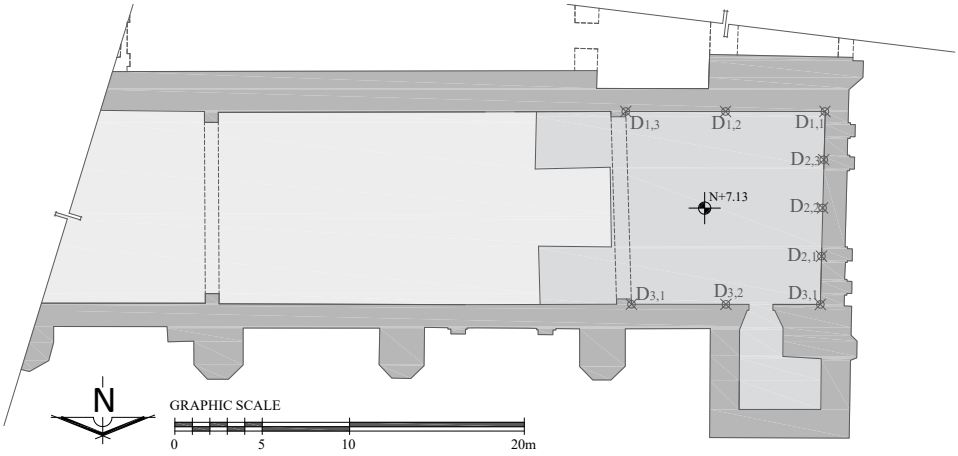

b) Choir loft plan N + 7.13 m

Figure 4-11. Accelerometer layout: a) at the extrados of the barrel vault and south wall; and b) at the perimeter wall of the choir loft (A – Transverse direction barrel vault; B – Longitudinal direction barrel vault; C – South wall; D – Perimeter choir loft wall).

4.3.2. Description of the results

Ambient vibration acquisitions are commonly processed assuming the input as a stationary random process to identify the system's modal parameters, and several dynamic identification algorithms have been developed with this purpose. Among them, the Enhanced Frequency Domain Decomposition (EFDD) algorithm (Brincker et al., 2001) has proven to be effective and has been implemented in commercial dynamic identification software, such as ARTeMIS Modal software (Ambient Response Testing and Modal Identification Software) (SVS, 2019), which has been adopted here.

The EFDD algorithm has been used to estimate the modal parameters of masonry structures either for condition assessment or to support the correct definition of the system stiffness for numerical modelling

(Kita et al., 2019; Masciotta et al., 2016; Scacco et al., 2019). The natural frequency and the damping ratio of each mode are estimated by transforming the corresponding Single-Degree-Of-Freedom (SDOF) System to the time domain obtaining, as a result, an SDOF Correlation Function: both modal parameters are obtained through simple regression analyses (Brincker et al., 2001; SVS, 2019). As seen in **Figure 4-12**, eight modes were identified in the range of 1-5 Hz. **Table 4-2** presents the results in terms of natural frequencies and damping ratios. For modes 1, 7 and 8, the quantification of the damping ratio was not reliable, due to a high statistical variation from random error sources.

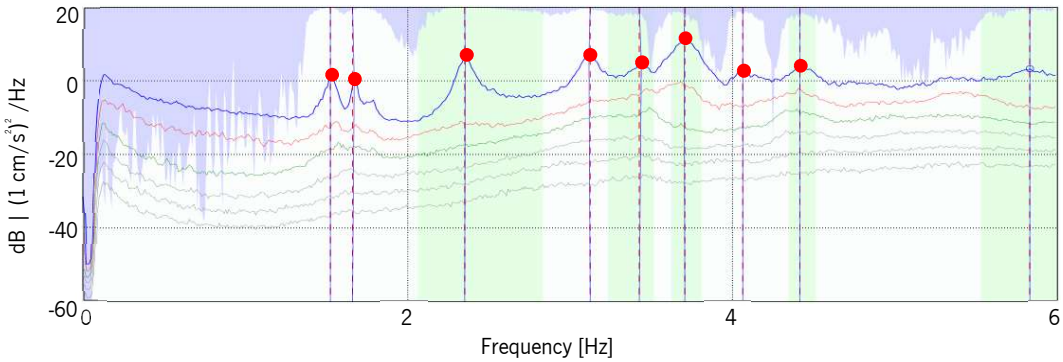

Figure 4-12. Modal features estimation: Enhanced Frequency Domain Decomposition (EFDD).

Table 4-2. Modal estimation results.

Mode	Frequency (Hz)	Damping ratio (%)	Mode	Frequency (Hz)	Damping ratio (%)
1	1.52	-	5	3.43	0.56
2	1.66	1.40	6	3.71	1.34
3	2.35	1.57	7	4.06	-
4	3.12	1.70	8	4.41	-

The first mode, presented in **Figure 4-13**a, involves mainly the north tower (not represented in the figure) and the north wall in the zone bounding the tower. With a frequency f= 1.52 Hz, the north tower can be considered as the most flexible element of the building, a logical assumption due to its height.

A frequency of f= 1.66 Hz was found for the second mode (**Figure 4-13**b). An out-of-plane deformation of the central and upper part of the north wall, likely due to the decrease of the cross-section in the upper third of the buttresses' height. In plan, it is possible to identify the influence of the north tower in this

mode, inducing a likely double curvature with an inflection point in the connection between the tower and the longitudinal wall.

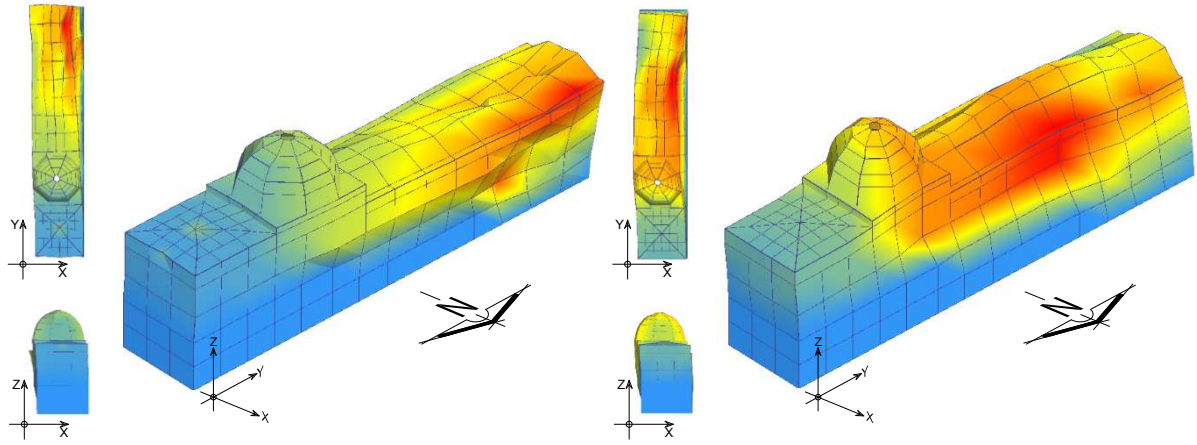

a) b)

Figure 4-13. a) Mode 1 (1.52 Hz); b) Mode 2 (1.66 Hz).

The third mode is a global and transverse mode with a frequency of f= 2.35 Hz. **Figure 4-14**a shows the movement of the central zone of the nave. The three images display the deformation of the upper part including the dome and part of the barrel vault. This characteristic movement seems to be affected by the presence of the towers and the choir loft, which provides additional stiffness to the west façade and allows the lateral displacement only at the central portion of the roof.

Mode 4 is a transverse mode with one point of inflection (**Figure 4-14**b), with a frequency of f= 3.12 Hz. In this case, the middle part of the dome and the west façade are the least excited parts of the building, while the maximum displacements affect the middle part of the barrel vault and, in the opposite direction, the groin vault that covers the presbytery.

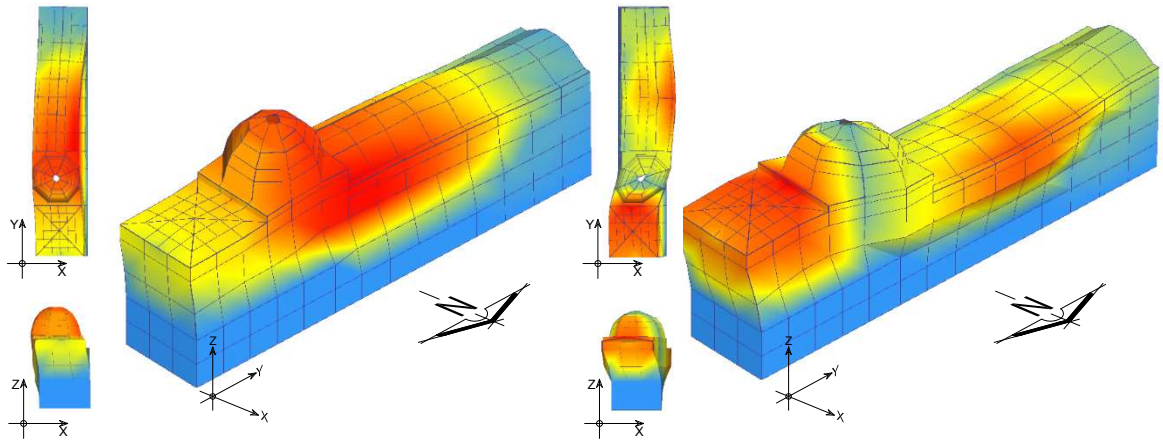

a) b)

Figure 4-14. a) Mode 3 (2.35 Hz); b) Mode 4 (3.12 Hz).

Increasing the complexity, **Figure 4-15**a shows that mode 5 is a transverse mode as well, but with two points of inflection, at the dome and at the point with a change of stiffness due to the choir loft, with a frequency of f = 3.43 Hz. The west façade (in the area of the south tower) and the groin vault present larger displacements in one direction while the central part of the barrel vault moves in the opposite direction.

In **Figure 4-15**b, mode 6 appears as the first vertical mode of the vault, with a frequency of f = 3.71 Hz. Once again, it is possible to notice that there is a stiffer zone corresponding to the west side of the nave, again due to the presence of the towers and the choir loft.

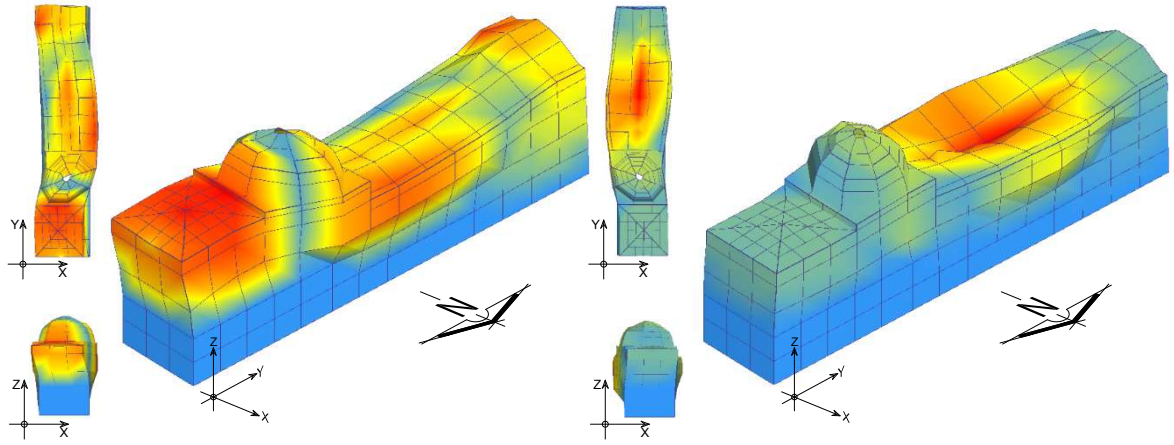

a) b)

Figure 4-15. a) Mode 5 (3.43 Hz); b) Mode 6 (3.71 Hz).

In **Figure 4-16**a, a second vertical mode in the barrel vault is found, with a frequency of f = 4.06Hz and very similar to mode 6. However, it is possible to notice that more structural elements are involved in mode 7: the length of the barrel vault implied is reduced to, approximately 3/5 of the total dimension of the nave; the dome and the groin vault, unlike mode 6, have also a significant displacement, even though the maximum is in the vertical direction of the barrel vault.

Finally, mode 8 is a transverse mode of the nave with inflection, coupled with a likely local movement of the north tower and a frequency of f = 4.414Hz. **Figure 4-16**b shows, in a clear way, an 'S' shape indicating the out-of-phase motion of the elements.

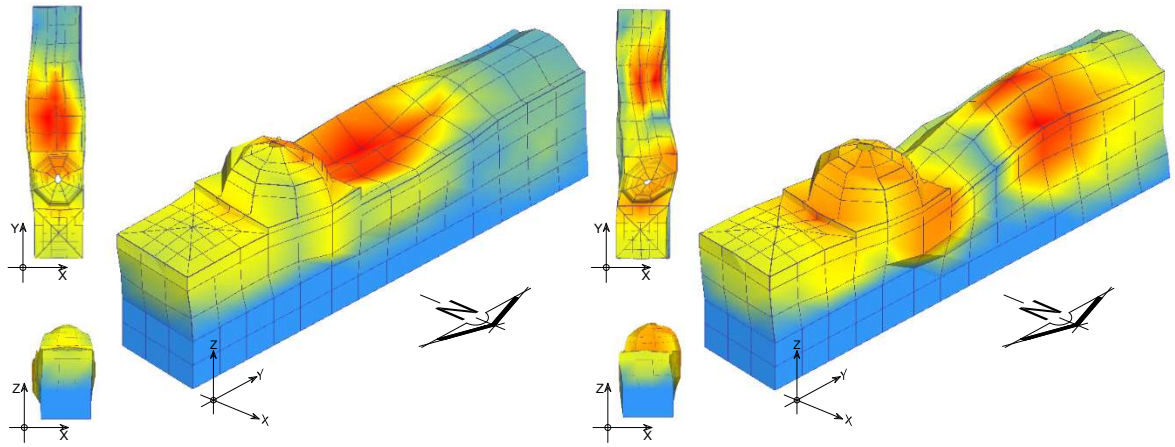

a) b)

Figure 4-16. a) Mode 7 (4.06 Hz); b) Mode 8 (4.41 Hz).

The dynamic identification results can be compared with a previous campaign carried out by Nuñez Gaona (2018). This past study limited the setups to a longitudinal line on the vault crown. However, one of the modes (3.71 Hz) identified by this author is consistent with the first vertical mode of the vault here presented (mode 6).

Due to the similarities among the religious heritage in Mexico, it is possible to compare the results with other case studies in literature, e.g. (Animas et al., 2015; Badillo-Almaraz et al., 2019; Ramírez-Cisneros et al., 2012). Based on such comparison, it is evident that the structure is quite flexible in some parts, mainly the north tower (first mode) and the lateral walls of the nave. As in other case studies, the transverse movement of the nave governs the first modes. The barrel vault is rather stiff compared to the previous elements, as its vertical modes appear only as numbers 6 and 7. The south longitudinal wall is stiffer than the north one, which can be related to the connection to the cloister, the thickness of the wall and the percentage of openings. The high longitudinal stiffness of the church is expected and confirmed by other case studies, as no longitudinal modes were identified.

4.4. Numerical modelling

Numerical models based on the Finite Element Method (FEM) have been successfully applied in the seismic assessment of historical structures, particularly through nonlinear static and dynamic analyses. FEM demonstrated to be a robust method, able to simulate and forecast the behaviour of the real system under seismic loads, being suitable for complex geometries and different material constitutive laws

(Bianchini et al., 2020; Endo et al., 2015; Karanikoloudis et al., 2020; Martínez et al., 2009; Ramírez et al., 2019). Three main modelling approaches can be adopted, according to the level of detail required (Lourenço, 1996): 1) detailed micro-modelling; 2) simplified micro-modelling; 3) macro-modelling.

The quality of a model is strongly dependent on the level of knowledge regarding the parameters of the system that affect its structural response. For URM structures, the most relevant parameters to investigate are the mechanical properties, geometry, structural details, connections and distribution of mass and stiffness (Lourenço et al., 2011). In contrast to new building design, for existing systems, such characteristics are unknown *a-priori* and they must be investigated limiting as much as possible the invasiveness. In this regard, a good combination of a detailed survey and a global dynamic identification demonstrated to be a powerful support to numerical model development. The former allows the definition of the geometry, the characteristics of the connections and the structural details and the identification of the actual damage patterns, whereas the latter allows an investigation of the stiffness of the structure and boundary conditions.

4.4.1. Preparation of models

The seismic assessment of the San Agustin church involved the preparation of partial models and a 3D numerical model of the whole church (**Figure 4-17**), based on FEM and using the software for structural analysis DIANA (DIANA, 2020).

The first model (**Figure 4-17**a), hereafter called M1, is a 2D simulation of a section of the nave, based on isoparametric plane stress elements with quadratic interpolation. The translation degrees of freedom at the base were restrained. Model M1 has 10,665 elements with 33,174 nodes. Then, aiming for a better insight into the global behaviour of the structure, a set of models in the 3-dimensional space were prepared using isoparametric solid elements with linear interpolation. First, the barrel vault was investigated considering the influence of the boundary conditions provided by the walls as external constraints (Model M2, **Figure 4-17**b) or simulating the walls themselves, the buttresses and the lower body of the north tower (Model M3, **Figure 4-17**c). Model M2 has 52,636 elements with 14,761 nodes, whereas Model M3 has 267,789 elements with 59,213 nodes. Finally, a 3D global model of the church was developed (Model M4, **Figure 4-17**d), using 407,022 elements with 91,953 nodes. The development of the different models, with a progressive improvement of the complexity in terms of the level of detail and number of elements, was adopted due to the low knowledge of the actual characteristics

of the vault and aims to evaluate its behaviour using different modelling approaches, in terms of dynamic characteristics for comparison with the identification carried out. It is worth to mention that due to uncertainties regarding the construction details, the backing in the models M1, M3 and M4 is not considered (conservative approach). The mass of the infill was defined as a densification of the material in the area of the haunches.

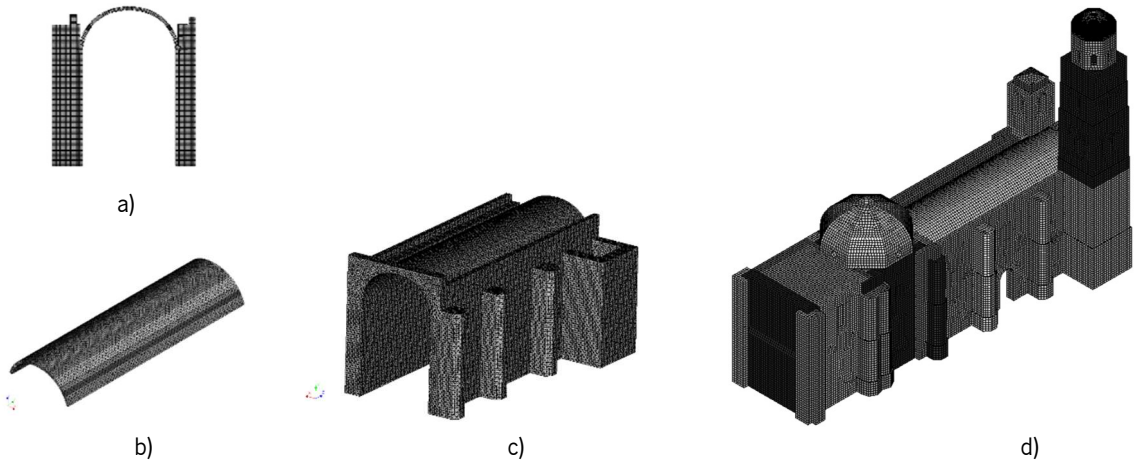

Figure 4-17. Partial and global models: a) M1, b) M2, c) M3 and d) M4.

4.4.2. Material properties

As previously mentioned, three different materials were identified based on visual inspection. The location of the materials is illustrated in **Figure 4-4**: M_{Vault}, a rubble quarry masonry with a high content of mortar located at the vaults (cast-in-situ as a concrete); M_{North}, regular masonry with good bonding, located in the lower section of the north tower, the north wall, the apse, the east part of the south wall and the dome; and M_{South}, ashlar masonry located in the west part of the south wall, the façade, the south tower and the upper section of the north tower. Due to the limited knowledge regarding the mechanical properties of the materials in Mexican Heritage, it was decided to base the study on similar cases, thus the characteristics were defined based on (Circolare n. 7, 2019).

Given the lack of experimental testing on-site and the uncertainty regarding the mechanical properties of the materials, the knowledge level considered was LC1, affecting the values with a confidence factor of 1.35 (Circolare n. 7, 2019). Furthermore, and in the case of M_{Vault}, both, the Young's modulus and the compressive strength were increased considering a corrective coefficient of 1.5, due to the presence of

mortar with good characteristics (Circolare n. 7, 2019). The tensile strength (f_t) in masonry is characterized by low values, typically within the limits of 0.1 to 0.2 MPa (Lourenço, 2008). The fracture energy values (tension and compression) were obtained based on the literature (Angelillo et al., 2014; Lourenço, 1996, 1998, 2009; Vasconcelos, 2005).

For the non-linear properties, a parabolic diagram defines the compressive behaviour, while an exponential diagram was adopted for tension (Lourenço, 1996). The mechanical properties of the materials are presented in **Table 4-3**. These properties correspond to the initial values adopted for the models. It is noted that the Young's moduli were updated in the calibration of the models in the next Section.

Table 4-3. Initial mechanical properties for the masonry (M).

Material	Linear parameters			Compressive parameters		Tensile parameters	
	E (GPa)	w (kN/m³)	*v*	f_c (MPa)	G_c (N/mm)	f_t (MPa)	G_f (N/mm)
$\mathbf{M}_{Vault}$	1.30	19	0.2	1.11	1.78	0.10	0.015
$\mathbf{M}_{North}$	1.74	22	0.2	1.93	3.08	0.15	0.023
$\mathbf{M}_{South}$	2.85	22	0.2	4.30	6.87	0.20	0.030

E: Young's modulus; w: specific weight; v: Poisson's ratio; f_c: compressive strength; G_c: compressive fracture energy; f_t: tensile strength; G_t: tensile fracture energy.

4.4.3. Model updating

The model updating process consists of tuning selected parameters to match specific numerical outputs with respect to the equivalent experimental ones (Elyamani & Roca, 2018). In this study, the experiment carried out was the dynamic identification and the target output of the updating process is the natural frequencies. Although not directly targeted, the modal components were used to assess the updating performance by calculating the Modal Assurance Criterion [(MAC values between numerical and experimental mode shapes), for more information see (Ewins, 2000)]. In the model updating, the Young's modulus values of the three materials were considered as the variables to calibrate.

In this regard, the first manual calibration was carried out based only on the sixth experimental mode, which involves mostly the barrel vault (vertical displacement). The results, in terms of Young's moduli, of the manually calibrated models (**Table 4-4**) show that when only a portion of the structure is investigated (Models M1 and M2), the stiffness of the vault is significantly lower than expected. This is clearly due to

the modelling strategy adopted since, for a more detailed model (M3), the values are closer to the expected ones. Therefore, in the final model (M4), the relevant structural elements were introduced and the three different material properties were tuned based on more mode shapes. Then, based on this preliminary result, the Douglas and Reid method (1982) was applied for the final calibration. Only the results of the calibration for model M4 are reported in **Table 4-5**, **Table 4-6** and **Figure 4-18**. The Rayleigh damping parameters, based on the calibrated frequencies, were $\alpha = 0.403/s$ and $\beta = 1.833E\text{-}03$ s.

Table 4-4. Young's modulus after manual calibration for a vault frequency of 3.71 Hz (specific weight was not calibrated). The average initial Young's modulus value of South and North walls is shown.

Material	Initial values	M1	M2	M3
	E (GPa)	E (GPa)	E (GPa)	E (GPa)
$\mathbf{M_{Vault}}$	1.30	0.30	0.17	3.60
$\mathbf{M_{Walls}}$	2.30	1.50	–	2.60

Table 4-5. Young's modulus after the calibration based on the (Douglas & Reid, 1982) method for model M4 (specific weight was not calibrated).

Young's modulus	$\mathbf{M_{Vault}}$	$\mathbf{M_{North}}$	$\mathbf{M_{South}}$
$\mathbf{E_{Inital}}$ **(GPa)**	1.30	1.74	2.85
$\mathbf{E_{Calibrated}}$ **(GPa)**	1.57	2.32	3.47

Due to the complexity of the model, it was possible to find numerically 4 out of the 8 modes reported in **Table 4-2**: mode 1, 2, 3 and 6. As previously mentioned, the dynamic identification was performed mainly at the barrel vault. This influenced the results for modes 1 and 2 since these two modes are related to the north tower, showing a low agreement with a MAC under 60%. It is suggested to extend a dynamic identification campaign to other parts of the building in order to have a better matching between the experimental modes and the numerical modes, after the calibration. Mode 3 shows a MAC of 85%. This mode is important since mass participation is highest.

Table 4-6. Modes after the calibration of model M4.

Experimental		Numerical			
Target Mode	**f_e (Hz)**	**f_n (Hz)**	**Δf (%)**	**MAC (%)**	**Mass participation (%)**
Mode 1	1.52	1.50	1.0	58.9	13.3
Mode 2	1.66	1.68	1.0	53.2	0.6
Mode 3	2.35	2.36	0.4	85.7	38.8
Mode 6	3.71	3.71	0.1	97.0	0.1
		Average	0.6	73.8	

Figure 4-18 shows the modes after the calibration. Two plans are included per each mode in order to better compare with the experimental results. Plan A1 includes the towers while Plan A2 does not (as in the dynamic identification tests). As was mentioned before mode 1 and mode 2 are local modes for the north tower (see **Figure 4-13** to compare with experimental results), mode 3 is a global mode in the transversal direction (see **Figure 4-14** to compare with experimental results), while mode 6 is a vertical mode for the barrel vault (see **Figure 4-15** to compare with experimental results).

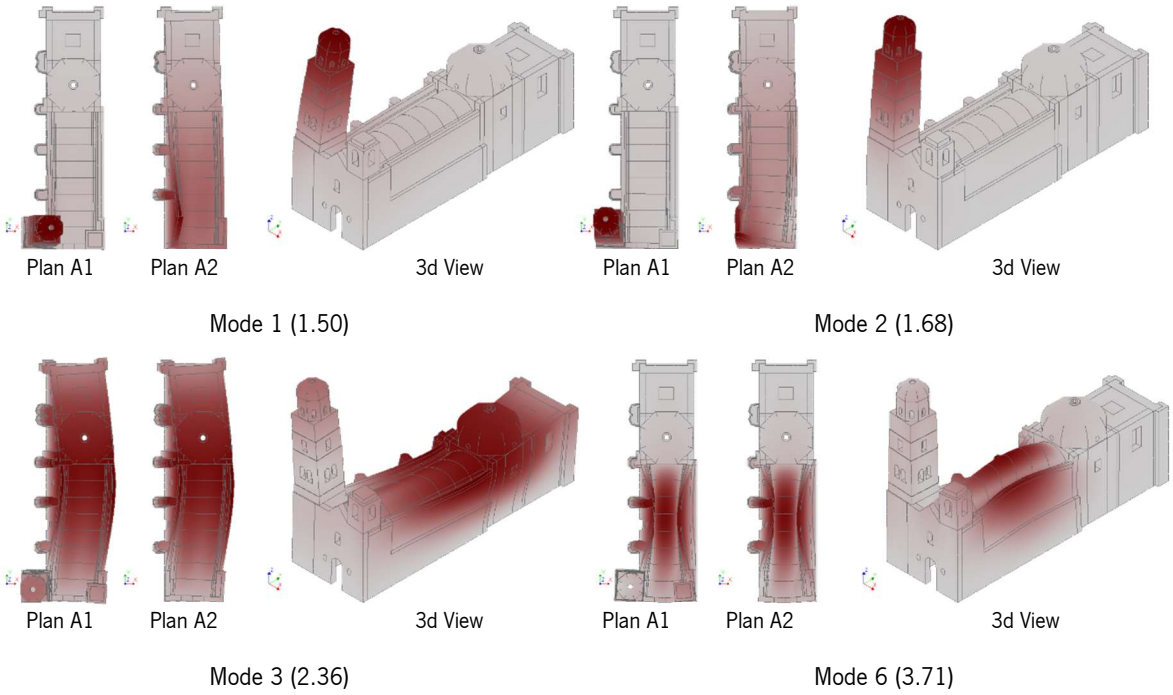

Figure 4-18. Modes after the calibration of model M4.

4.5. Conclusions

This chapter aims to introduce the San Agustin church, a building whose importance is associated with its historical background and with the fact that is located in a seismic area in Mexico (Michoacan). The building is part of the city centre of Morelia, which is a world cultural heritage site since 1991 (UNESCO, 1991). The lack of maintenance in this kind of buildings and the exposure to several hazards (i.e. environmental agents, aging and seismic events) affected its condition. The study of the mechanical properties of ancient buildings materials is a weakly unexplored topic in Mexico. Thus, in the development of the structural models, it was necessary to rely on parameters found in the literature and foreign codes (EN 1996-1-1, 2005; Lourenço, 1996; NTC, 2018; Vasconcelos, 2005).

An inspection of the church was carried out, which involved dynamic identification tests and damage surveys. Eight modes were identified in a range between 1-5 Hz. As expected, the lowest modes of the church are the ones related to the north tower (higher element in the building): mode 1 (1.52 Hz) and mode 2 (1.66 Hz). The first global mode presents the deformation of the main part of the nave (including the dome) in the transverse direction (2.35 Hz). The second transverse global mode (3.12 Hz) shows an inflection point in the area of the dome, depicting maximum deformations in opposite directions in the groin vault and the central zone of the nave, with a maximum in the north wall. Mode 5 (3.43 Hz) can be considered as a third transversal global mode while mode 6 (3.71 Hz) is the first vertical mode for the barrel vault. Mode 7 (4.06 Hz) appears as a second vertical mode for the barrel vault with some participation of the dome and finally, mode 8 (4.41 Hz) increases the complexity involving both the transverse and vertical direction.

The outcome of the dynamic identification allowed to calibrate the numerical model based on the frequencies and mode shapes. Due to the complexity of the model, four modes were identified and selected to calibrate the final 3D FEM model (407,022 elements with 91,953 nodes): mode 1, mode 2, mode 3 and mode 6, with an average difference between numerical and experimental frequencies lower than 1%. In order to verify the accuracy of the model, the Modal Assurance Criterion was applied, with an average acceptable result of 0.75.

The study of the Heritage in Mexico has still much to progress with knowledge from studies similar to the present one. Regarding the mechanical properties of the materials, the initial values obtained from the literature can be a good approximation when enough information is not available to perform the analysis. In this case, after the calibration of the model, it is possible to make a comparison between the initial values and the calibrated values. The differences found were about 20 and 30% higher than those from

the literature, which further confirm the adequacy of adopting reference values from established codes and recommendations.

Chapter 5
Seismic Assessment of San Agustin Church

5.1. Introduction

Design codes establish that buildings located in earthquake-prone areas should satisfy the technical requirements for seismic loads, since the destructive power of earthquakes can endanger their stability and safety and, consequently, cause human and economic losses. The codes have changed based on the experience obtained from earthquakes that occurred in the past and the resulted knowledge from research studies. However, in general, current design methods used in codes are not applicable to assess the seismic performance of historic masonry structures. It is well-known that low tensile strength and lack of box behaviour are characteristics that hinder and complicate the accurate analysis of Unreinforced Masonry (URM) buildings with flexible diaphragms (Lourenço et al., 2011). During the last decades, the

need of protecting ancient structures (not only to preserve them as part of the heritage but also as a way to protect the users) had led to the development of different strategies to analyse the seismic behaviour of URM buildings. Analytically, four main approaches can be followed, based on the characteristics of materials (e.g. linear or non-linear) and loading (e.g. static or dynamic) [for more information see (Roca et al., 2010, 2019)]. These methods can be listed, according to their complexity and computational burden, as follows: (1) linear static analysis; (2) linear dynamic analysis; (3) non-linear static, or pushover analysis (POA); (4) non-linear dynamic analysis (NLDA).

This chapter aims at the assessment of San Agustin church, based on two types of analysis: non-linear dynamic analysis (eight seismic records, previously defined in Chapter 3) and pushover analysis (four directions: +X; -X; +Y; -Y). In the following, the main results are described and supported by a general 3D view of the damaged building. The outcomes of the analyses are compared among them and with the typically expected failure mechanisms due to earthquakes.

Several investigations have been carried out in order to typify the behaviour of religious buildings against seismic hazards, by inspecting them after severe events. In Mexico, some examples of researches after earthquakes can be found in literature, e. g. (Meli & Peña, 2004; Peña et al., 2016; Peña & Chávez, 2016; Peña & Manzano, 2015). Fuentes et al. (2019) defined a classification of failure mechanisms in religious URM buildings, based on the Italian code (DPCM, 2015), and added as well new mechanisms due to the particularities of typical Mexican churches (choir loft and open chapels). Focusing on cases located in the states of Mexico, Morelos and Oaxaca, this study classifies the damages caused to URM religious buildings by the earthquakes of 2017. This classification is used here for comparison purpose. In order to carry out this comparison, it is necessary to identify the macro-elements that compose the building. A macro-element is known as an identified part of the building in terms of construction. It can coincide as well with an architectural and/or functional part (e.g. façade, apse, chapel). This type of macro-element is not independent of the building but it can present a specific and individual seismic behaviour (Doglioni et al., 1994).

Figure 5-1 shows a representation of the church decomposed in the possible macro-elements likely to be involved in activated mechanisms. Besides the typical outputs, the span is an important indicator for the analysis of the structural response of arched elements. Four transverse sections are considered (see **Figure 5-2**), the impost line of: (A) the east transverse arch; (B) the west transverse arch; (C) the middle section of the barrel vault; (D) the edge of the barrel vault, close to the connection with the main façade. Positive values in the plots indicate an increment in the span distance (opening). On the contrary, negative values in the plot indicate a decrement in the span distance (closing). The use of these indicators helps

to understand the process of the formation of hinges in the barrel vault, transverse arches and, consequently, in the dome.

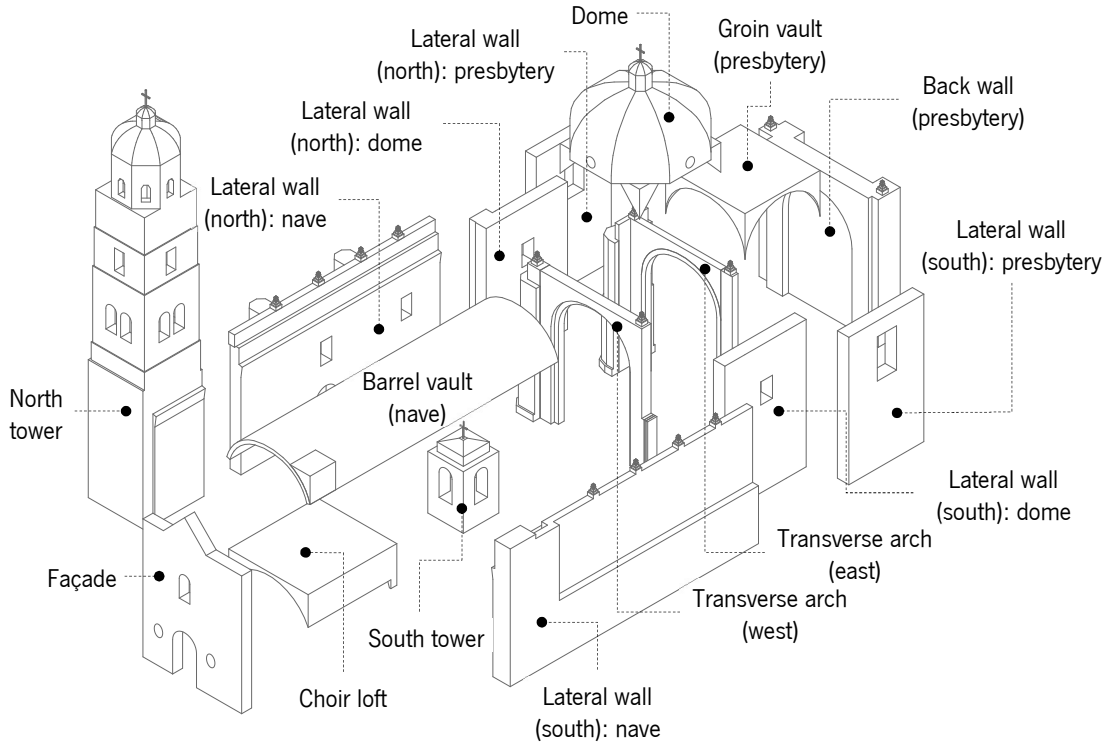

Figure 5-1. Representation of the building divided into macro-elements.

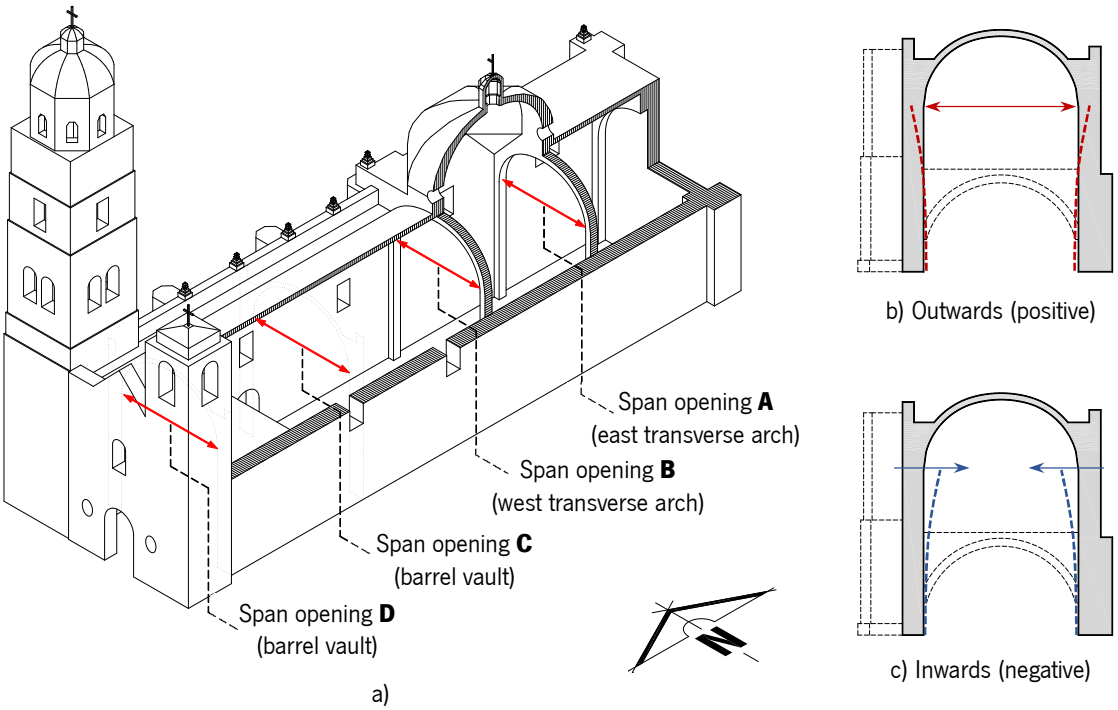

Figure 5-2. a) Axonometric view of the building indicating the four span opening indicators; b) outward displacement of the walls indicates a positive value in the plot; c) inward displacement of the walls implies a negative value in the plot.

The results obtained are expressed, mainly, in terms of principal strains and crack-widths. Although three components exist, only the E1 - tensile principal strains and Ecw1 – crack-width of the most opened crack is presented. For the sake of clarity, **Annex A** presents the inputs for each analysis; **Annex B** offers a detailed report of the state of damage for each analysis; **Annex C** shows graphical results of the different views of the building; and **Annex D** exposes graphical information of the failure mechanisms classification according to (DPCM 2015; Fuentes et al., 2019).

5.2. Nonlinear dynamic analysis (NLDA)

As described in **Chapter 3**, the structure was subjected to real earthquake records. The following Sections present its behaviour for eight different earthquakes, with the characteristics presented in **Table 3-2**. For each record, three components are considered: horizontal component applied in the transverse direction of the building (X direction); horizontal component applied in the longitudinal direction of the building (Y direction); and, vertical component applied in the direction of the gravity (Z direction). In **Annex A**, for each record, an individual graph of the three components is presented together with the corresponding acceleration spectra, in order to show the highest spectral accelerations in the frequency domain. An example is presented in **Figure 5-3**, where the horizontal component (X) of the record OAXM is accompanied by its spectrum. In this case, a duration of 30 s was considered as input for the analysis even if the original record has a duration of 167 seconds. However, the analysis only converged for the first 5.3 s (t_{eff}: effective time of analysis). Thus, the effective PGA (applied in the structure) is equal to 0.10 g.

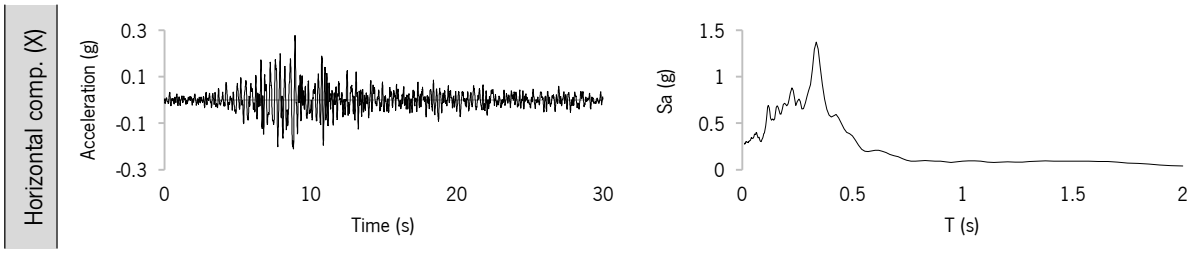

PGA = 0.28 g; PGA_{eff} = 0.10 g; t_{eff} = 5.3 s.

a)

Sa_{max} 1.37 g; T = 0.34 s

b)

Figure 5-3. Record OAXM. a) horizontal component (X); b) corresponding spectrum.

The resulting failure modes offer an insight into the expected mechanisms for typical Mexican single nave churches from the 16th century, subjected to comparable earthquakes. It is worth mentioning that the analyses did not complete any signal. The damage presented corresponds to the last converged step of each analysis. The duration of the applied input signals is presented in **Figure 5-29** and **Annex A**.

In nonlinear dynamic analysis, the Hilber-Hughes-Taylor (HHT) time integration method was adopted, with a time-step of 0.005 or 0.01 s, as a function of the signal. The iterative method used was Newton-Raphson regular, simultaneously satisfying the convergence norms for displacement (0.01) and force (0.01). The sparse Cholesky method was adopted to solve the system of equations.

Previously to the dynamic analysis, the model was evaluated under self-weight, considering this state as the initial conditions for the next dynamic analyses. Due to its self-weight, some cracks appear in the intrados of the crown in the transverse arches and some damage emerges in the façade, developed from the north base of the pediment. It is important to considerer that these damages continue developing when the seismic action is applied. A discussion of the damages is presented in the next Section, for the record OAXM. The subsequent sections provide a comparison with the first Section, reporting if needed, only major differences in the results. See the reports presented in **Annex B** for an exhaustive explanation of the results for each analysis.

5.2.1. OAXM. Oaxaca, Mexico. 09/08/2017. M=8.2

After the self-weight application, the NLDA with OAXM seismic record converged until 5.3 s. The first damage corresponds to Sabouret cracks at the perimeter of the groin vault, only at the extrados (**Figure 5-4a**). Together with the opening of the transverse arches, the dome cracks vertically (east, southeast and west meridional panels) with decreasing crack-width toward the top. A crack parallel to the north wall develops in the northwest corner at the base of the dome (**Figure 5-4b**). In the next time steps, damage appears in the connections between the choir loft and the lateral walls (**Figure 5-4c**) and a longitudinal crack opens in the crown of the groin vault. In the south wall, there is an in-elevation irregularity (due to the different height levels) that causes in-plane horizontal cracks at the top (**Figure 5-4d**). In-plane damage emerges in the façade as a result of the interaction with the towers, namely two vertical cracks running from both the bases of the pediment and growing in direction of the oval windows. In addition, typical shear cracks emerge from the window of the choir loft (**Figure 5-5a**). The response of the tower triggers a vertical crack in the north wall, along the connection with the buttress (**Figure 5-5b**). At the

intrados of the barrel vault damage emerges also from the interaction with the towers, plus longitudinal cracks develop at the crown (**Figure 5-5c**). At the extrados, hinges appear at the springers. The onset of diagonal cracks in the lateral walls of the presbytery, spreading from the corners of the window (**Figure 5-5d** and **e**), is likely due to the global transverse response of the building.

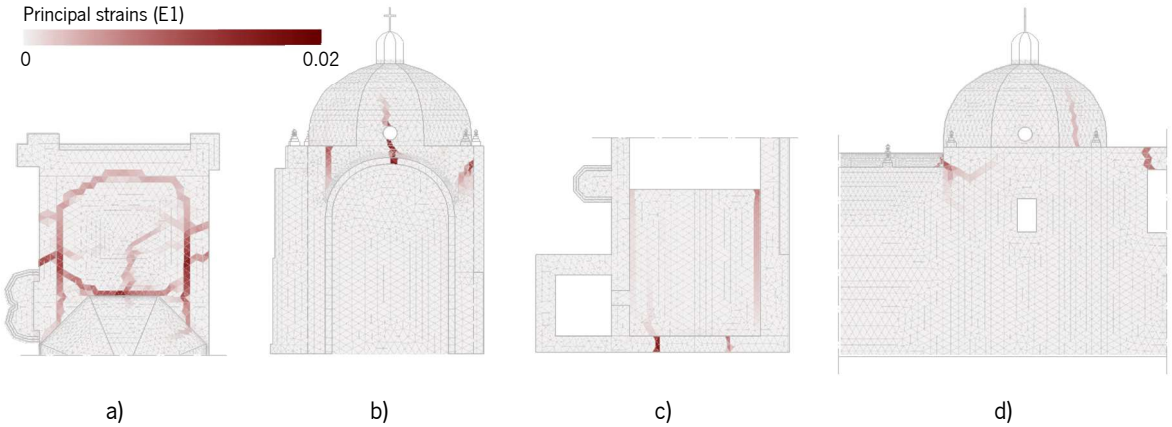

Figure 5-4. Damage in the building due to the action of the signal OAXM: a) groin vault (plan); b) transverse arch and dome (section-elevation); c) choir loft (plan); d) south wall (elevation).

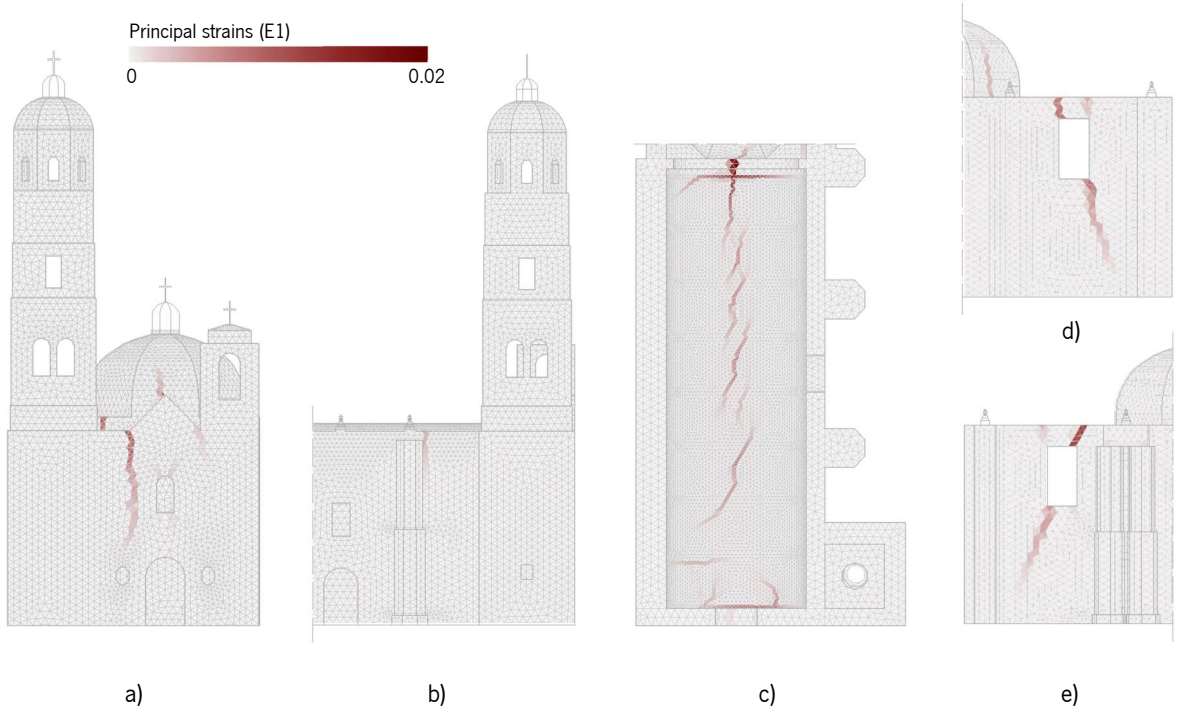

Figure 5-5. Damage in the building due to the action of the signal OAXM: a) façade (elevation); b) north wall (elevation); c) intrados barrel vault (plan); d) lateral wall presbytery (south elevation); e) lateral wall presbytery (north elevation).

The transverse response of the nave was analysed through the span openings, plotted in **Figure 5-6b**. Outward and inward deformation of the lateral walls causes damage along the building, as shown in **Figure 5-6a**. The groin vault, the transverse arches, the dome and the barrel vault are mainly affected. According to the output parameter, the span openings A, B and C reach the maximum opening at 5 s, before the analysis stops. In the case of the span opening D, the behaviour is different, since at this step no cracks are presented in the crown of the barrel vault (**Figure 5-6a**). The highest span opening suffered at section D occurs at 5.3 s, when a diagonal crack (30°) develops, located between the 3rd and 4th quarter of the barrel vault.

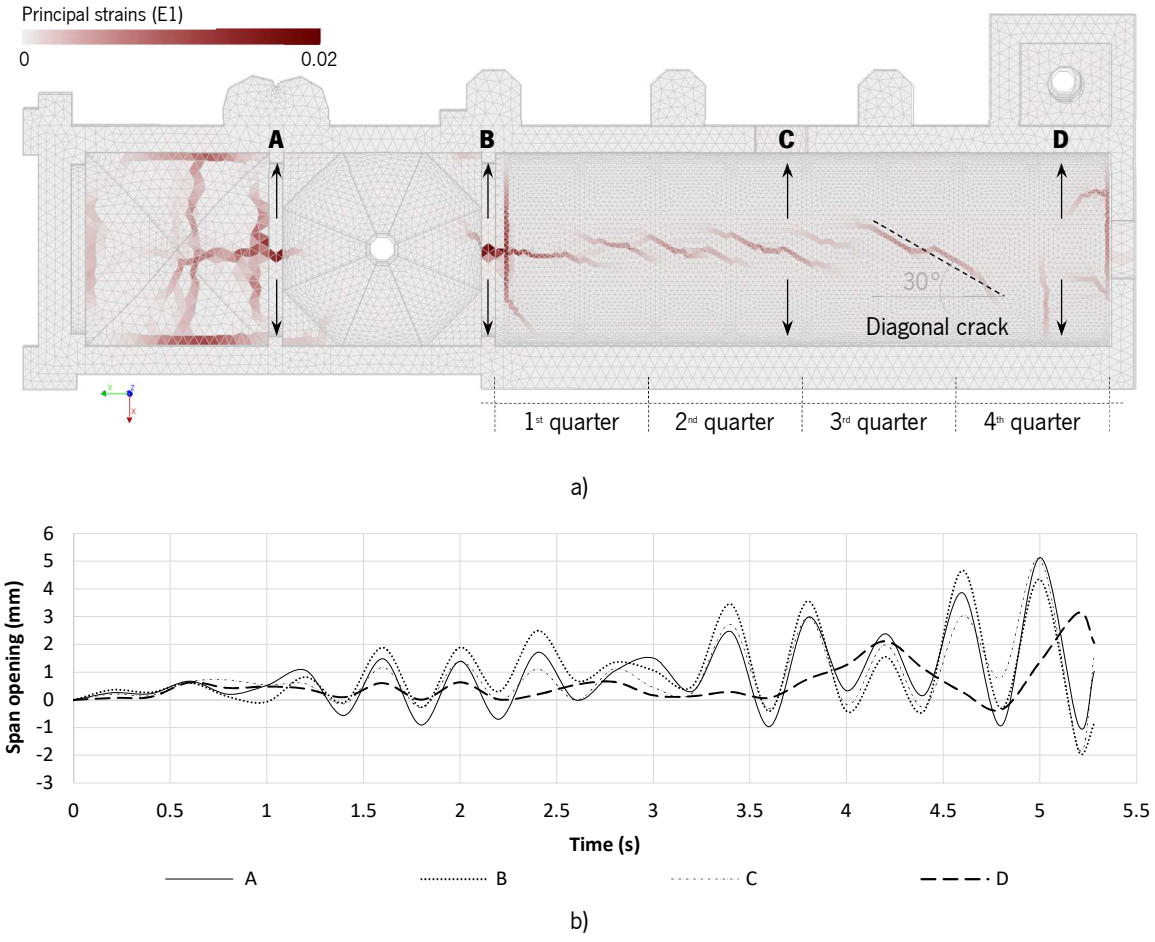

Figure 5-6. a) Damage at the intrados due to the OAXM record (last step converged); b) plot of the span openings A and B (transverse arches) and C and D (barrel vault).

5.2.2. OXCU. Oaxaca, Mexico. 09/08/2017. M = 8.2

The NLDA performed with the signal OXCU reached 4.1 s of the input. In terms of damage, similarities with the OAXM analysis were found: e.g. the Sabouret cracks in the groin vault, the damage in the northwest corner at the base of the dome; the cracks in the connections between the choir loft and the lateral walls; the compression area from the interaction of the nave and the south wall under the dome; in the façade, only the vertical crack developed from the north base of the pediment; and the diagonal cracks in the lateral walls of the presbytery. Major differences are related to the following aspects. Two hinges were detected at the crown of the transverse arches (**Figure 5-7a**). As consequence, the damage in the dome is higher than caused by the OAXM record, although causing cracks at the same three meridional panels (east, southeast and west) (**Figure 5-7a** and **b**). New damage develops in the back wall of the presbytery: a vertical crack parallel to the connection with the south wall emerges (**Figure 5-7b**). A significant longitudinal crack appears in the south haunch of the barrel vault, at the extrados (**Figure 5-7c**).

Figure 5-7. Damage in the building due to the action of the signal OXCU: a) transverse arch and dome (section-elevation); b) back wall (elevation); c) extrados barrel vault (plan).

At the intrados of the barrel vault, longitudinal cracks occurred, mainly at the 1st and 2nd quarter. The 3rd and 4th quarter present diagonal cracks of around 45° (**Figure 5-8a**). All the elements of the roofing system present longitudinal cracks, caused by the transverse deformation of the building. **Figure 5-8b**

shows that the maximum span openings for A, B, and C sections occur at 3.8 s. This is related to a longitudinal hinge located at the connection between the roof system and the south wall, mainly in the area of the presbytery and the dome. Regarding section D, the highest opening, detected at 3.6 s, is associated with the evolution of the vertical cracks both in the façade and in the connection between the north wall and the north tower.

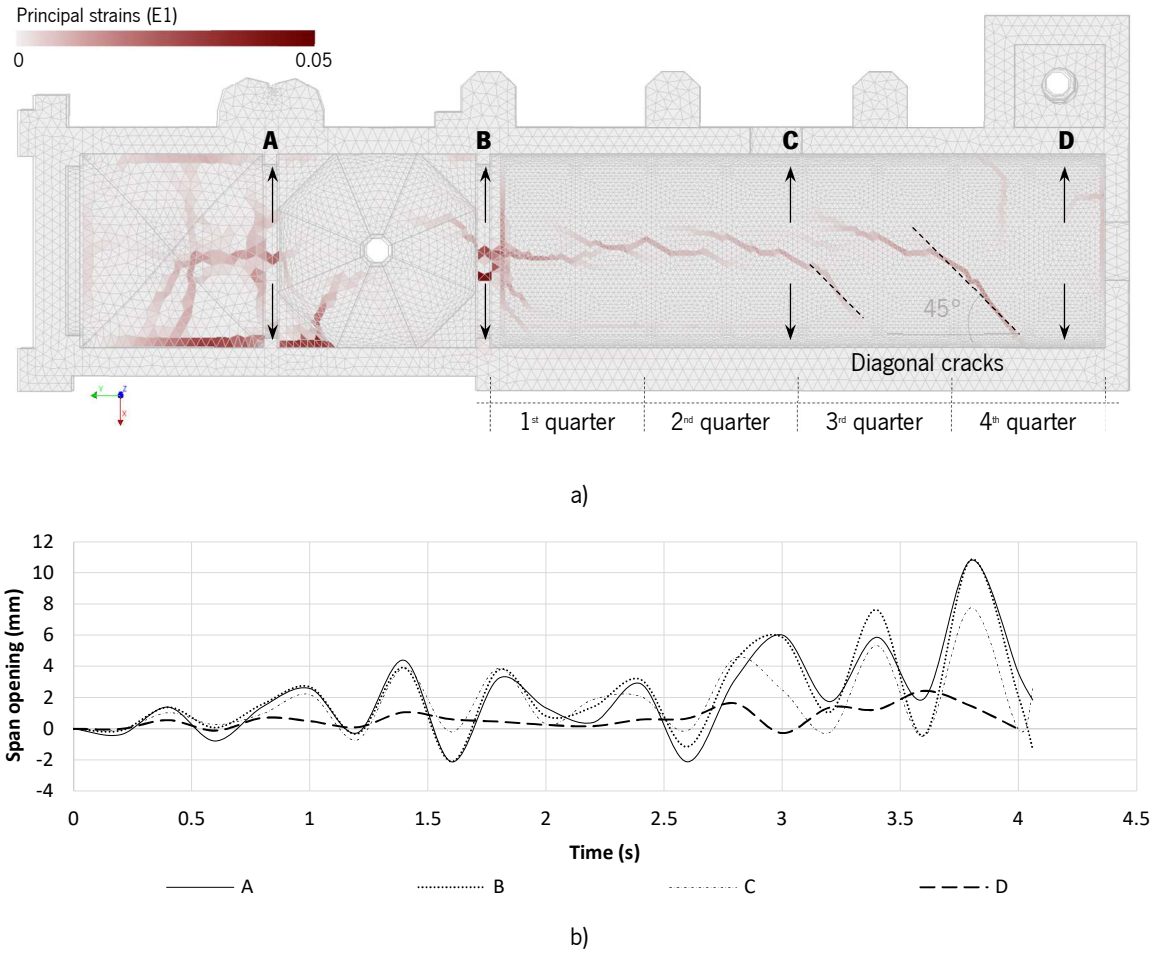

Figure 5-8. a) Damage at the intrados due to the OXCU record (last step converged); b) plot of the span openings A and B (transverse arches) and C and D (barrel vault).

5.2.3. OXJM. Oaxaca, Mexico. 09/08/2017. M = 8.2

This analysis was performed for 5 s of the input. The damage obtained is comparable to the previous analyses (OAXM and OXCU). The groin vault suffers the Sabouret cracks; the transverse arches present hinges at the crown; the dome is damaged in the east and west meridionals; the vertical crack in the

façade runs from the north base of the pediment; in the connection between the north wall and the tower presents a vertical crack; in the south wall, the interaction between the nave and the dome presents the same type of in-plane damage; the choir loft shows cracks in the connection with the lateral walls; the lateral walls of the presbytery present as well diagonal cracks. However, this analysis presents some differences: the east transverse arch presents two hinges at the crown while the east only one; the damage at the dome is lower than the damage observed in the two previous analyses; the diagonal crack at the south wall of the presbytery is larger than the damage emerged in the north side. **Figure 5-9a** shows the damage at the intrados of the roofing system due to the OXJM signal. The longitudinal damage in the 1st and 2nd quarter of the barrel vault consists of parallel cracks more similar to the ones caused by OAXM analysis, while the diagonal cracks seem to be different from both previous analyses (OAXM and OXCU).

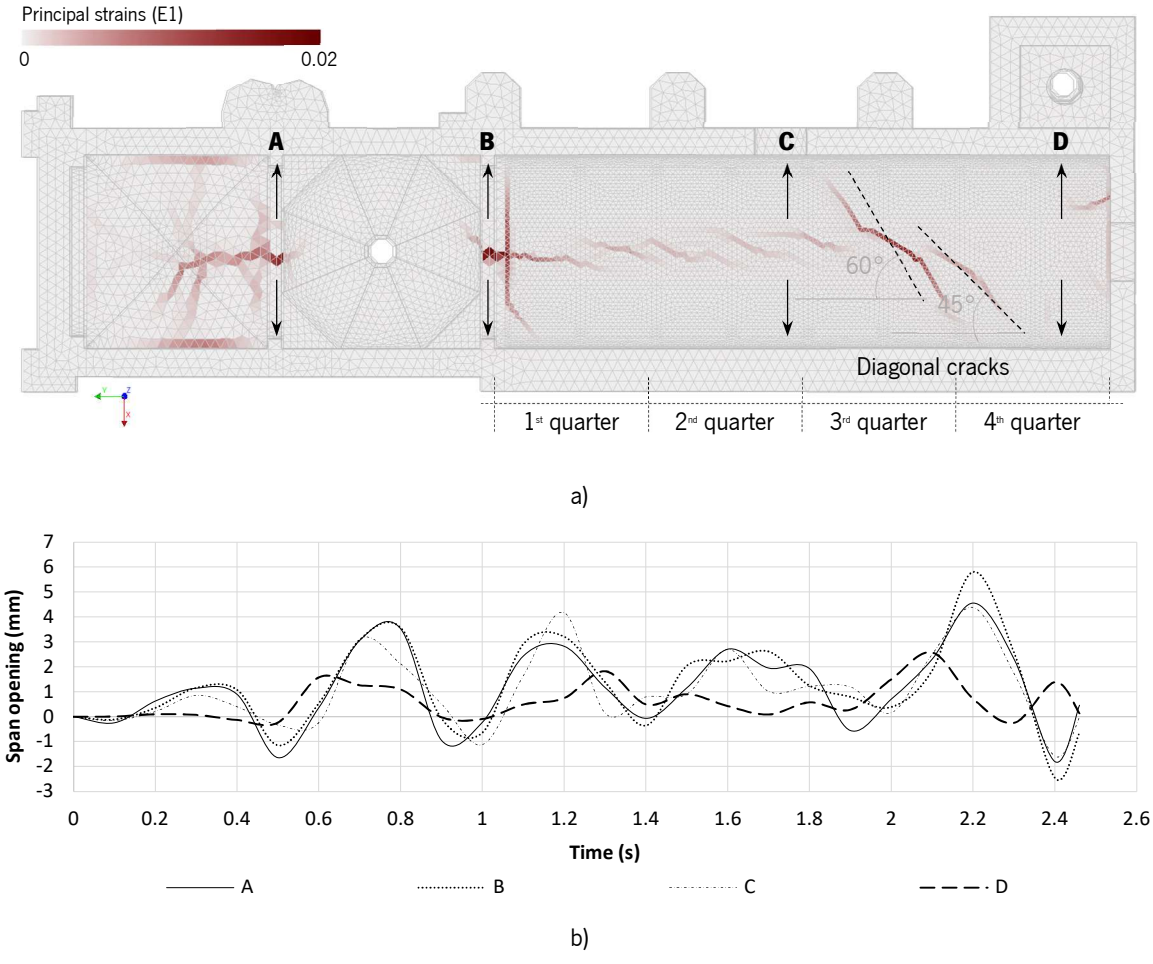

Figure 5-9. a) Damage at the intrados due to OXJM record (last step converged); b) plot of the span openings A and B (transverse arches) and C and D (barrel vault).

In **Figure 5-9b**, the plot of the span openings indicates a large opening around the 0.8 s, which corresponds to an evolution of the damage in the crown of the transverse arches, affecting mainly sections

A and B, but still detected at section C. Regarding section D, the first opening (0.6 s) is associated with the enlargement of the vertical crack located at the façade, increasing (0.7 s) due to the vertical crack at the connection between the north wall and the north wall. However, the highest openings for sections A, B, and C occurs at 2.2 s. This damage is related to the diagonal crack located in the 3rd and 4th quarter. At 2.1 s, section D shows a high value (smaller than the maximum for the other sections) related to the evolution of damage at the barrel vault and interaction with the south tower.

5.2.4. OXXO. Oaxaca, Mexico. 09/08/2017. M = 8.2

The OXXO earthquake was the fourth applied signal that caused a similar crack pattern. The main similarities are associated with the main damages described in the previous Sections, such as the cracks at the presbytery (groin vault and lateral walls), transverse arches and dome, façade, choir loft and barrel vault. Although differences exist, this Section (and the following ones) will focus on relating the damages with the span opening. **Figure 5-10a** presents a view of the final damage state for the seismic action OXXO while **Figure 5-10b** shows the plot of the span openings for the known indicators. At 1.2 s, the damage develops along the roofing system, and the span opening in sections A, B and C are affected by longitudinal cracks of the 1st and 2nd quarter of the nave and the cracks located at the crown of the transverse arches. At 1.6 s, sections A, B and C openings are in a range from 6 to 8 mm and damage occurs: 1) a diagonal crack appears, mainly in the 3rd quarter of the vault; 2) new hinges develop in the transverse arches; and 3) a diagonal crack opens at the south wall on the presbytery. At 2 s, a continuum hinge is developed in the longitudinal direction, namely at the connection of the groin vault with the south wall. This crack develops from there to the east-west meridional panel. Finally, in the crown of the west arch, a new hinge is also developed at this stage. Regarding the span opening at section D, the maximum values are lower than 2 mm. Two aspects identified in section D can be highlighted: around 1.5 s, a vertical crack develops at the connection of the north tower with the lateral wall; at 2.1 s, damage at the barrel vault increases and is connected to the crack of the north wall.

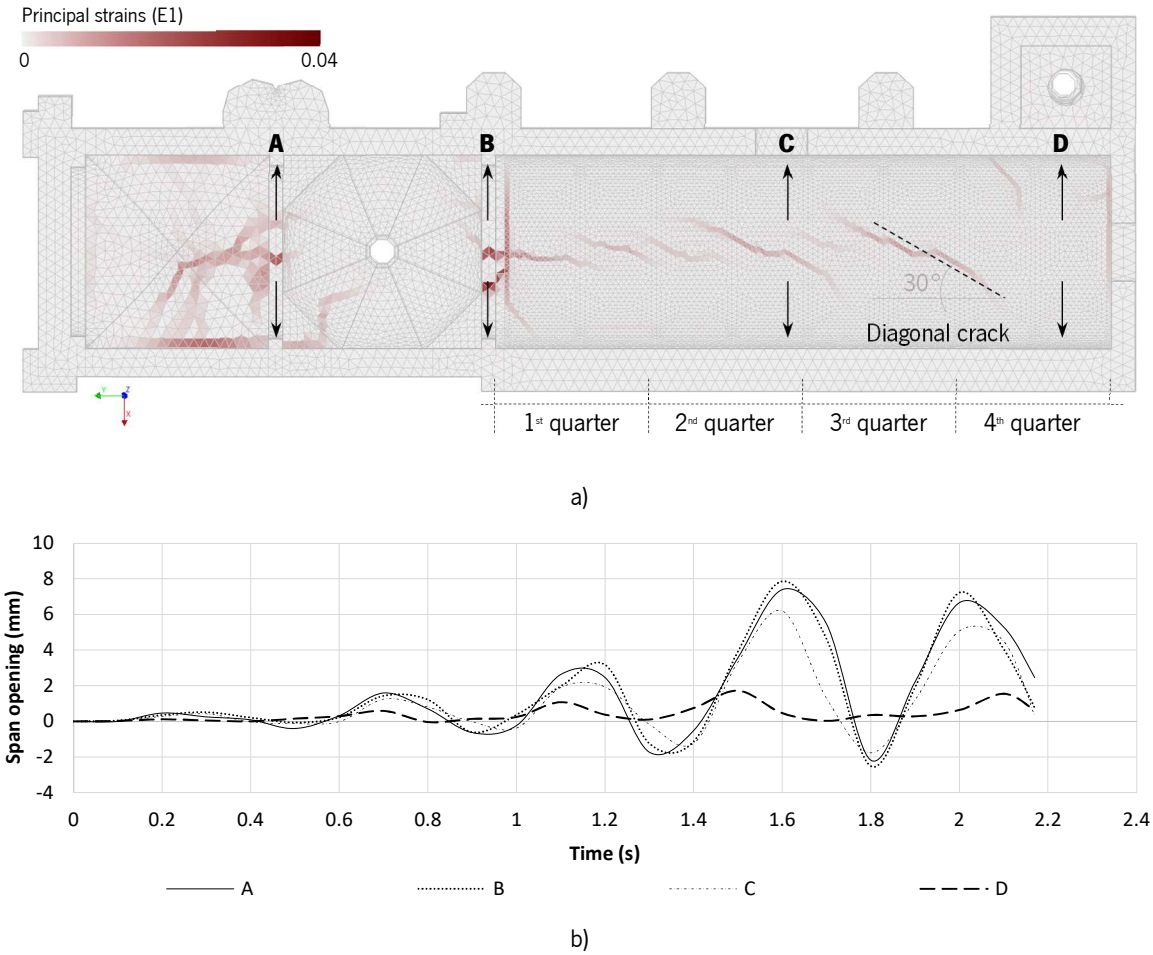

Figure 5-10. a) Damage at the intrados due to OXXO record (last step converged); b) plot of the span openings A and B (transverse arches) and C and D (barrel vault).

5.2.5. SAPP. Puebla, Mexico. 09/19/2017. M = 7.1

In the analysis performed with the record SAPP, a total duration of 8 s was reached. The maximum principal strains (E1) are higher than the ones obtained in the previous analyses. Around 4 s, all the span openings are almost synchronised, namely the peaks of the response. This is related to a sudden development of damage along the roofing system, creating longitudinal cracks at the barrel vault and the groin vault. At the same time, the hinges located at the crown of the arches increase their opening and damage appears at the dome, namely at the southeast meridian panel. A vertical crack at the connection of the north tower and the north wall appears, mainly affecting the span opening at section D. At this stage of the analysis, the principal strains (E1) reached maximum values of 0.03. From then on, the

analysis continues by opening and closing the same cracks, incrementing the principal strains to 0.07, as shown in **Figure 5-11a**.

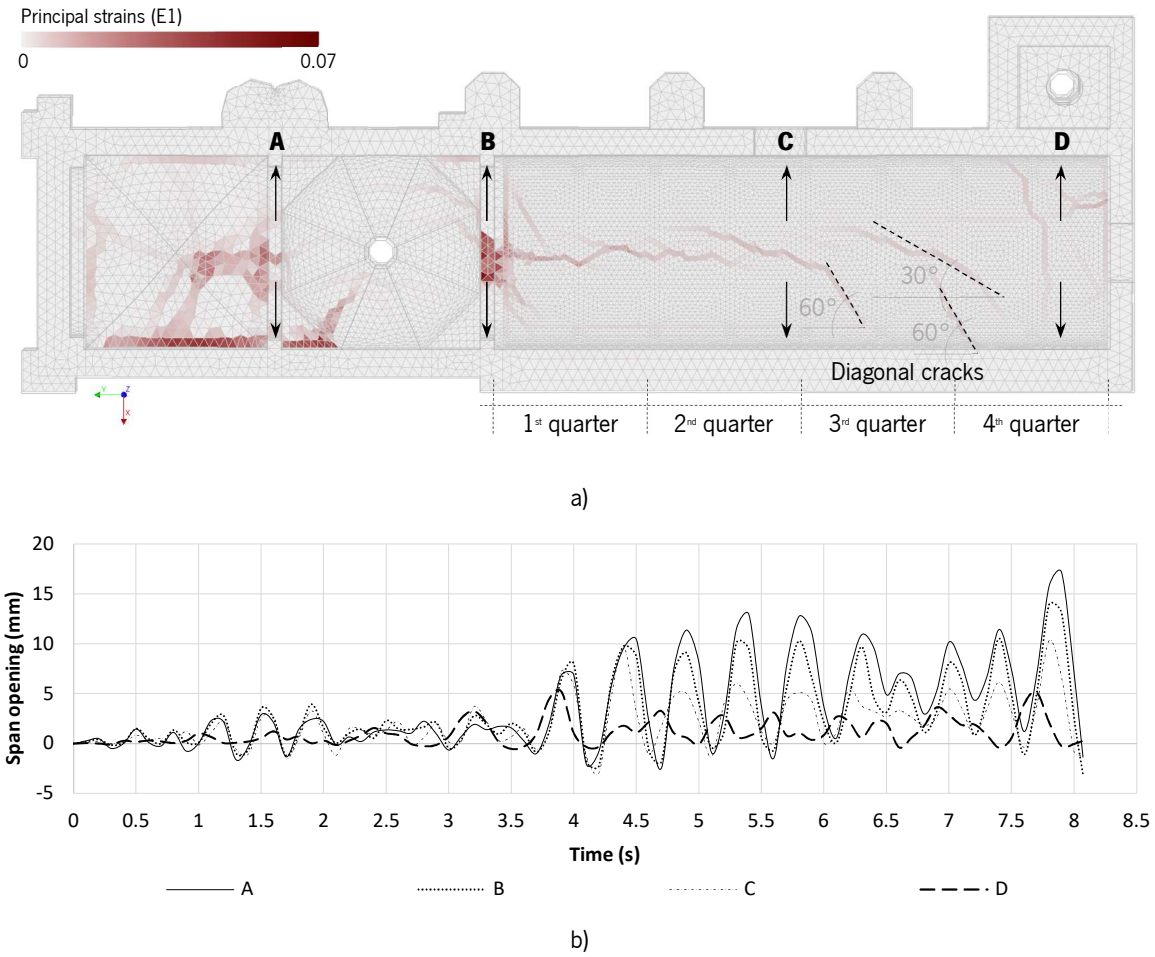

Figure 5-11. a) Damage at the intrados due to SAPP record (last step converged); b) plot of the span openings A and B (transverse arches) and C and D (barrel vault).

5.2.6. SCRU. Oaxaca, Mexico. 09/08/2017. M = 8.2

The analysis with the record SCRU converged until almost 12 s of the earthquake duration. According to the plot in **Figure 5-12b**, in the first 4.5 s of the analysis, the openings stay within a range of 2 mm. At this point, an early stage of damage is developed along the roofing system, namely, Sabouret cracks at the groin vault, hinges at the crown of the transverse arches that extend to the dome, and longitudinal cracks in the barrel vault. After 11 s, the highest opening is equal to 8 mm at section A, 6 mm at section B and almost 4 mm at section C. This is related to a sudden evolution of the damage: 1) a longitudinal

crack, located at the connection between the groin vault and the south wall; 2) a diagonal crack (located at the same wall); and 3) cracks at the southeast meridional panel of the dome. In addition, an evolution of the diagonal crack located within the 3rd and 4th quarter of the barrel vault is also observed. Regarding the span opening at section D, the maximum value is reached almost at the end of the plot, at around 11.8 s. At this point, the diagonal damage of the barrel vault reaches its ultimate state, developing vertical cracks in the north wall, at the connections with the buttress and the tower. A meaningful difference to the previous results is worth mentioning: the duration of the analysis is longer; therefore, the severity of the damage is not just due to a sudden deformation but, it is also a consequence of constant and continuous evolution.

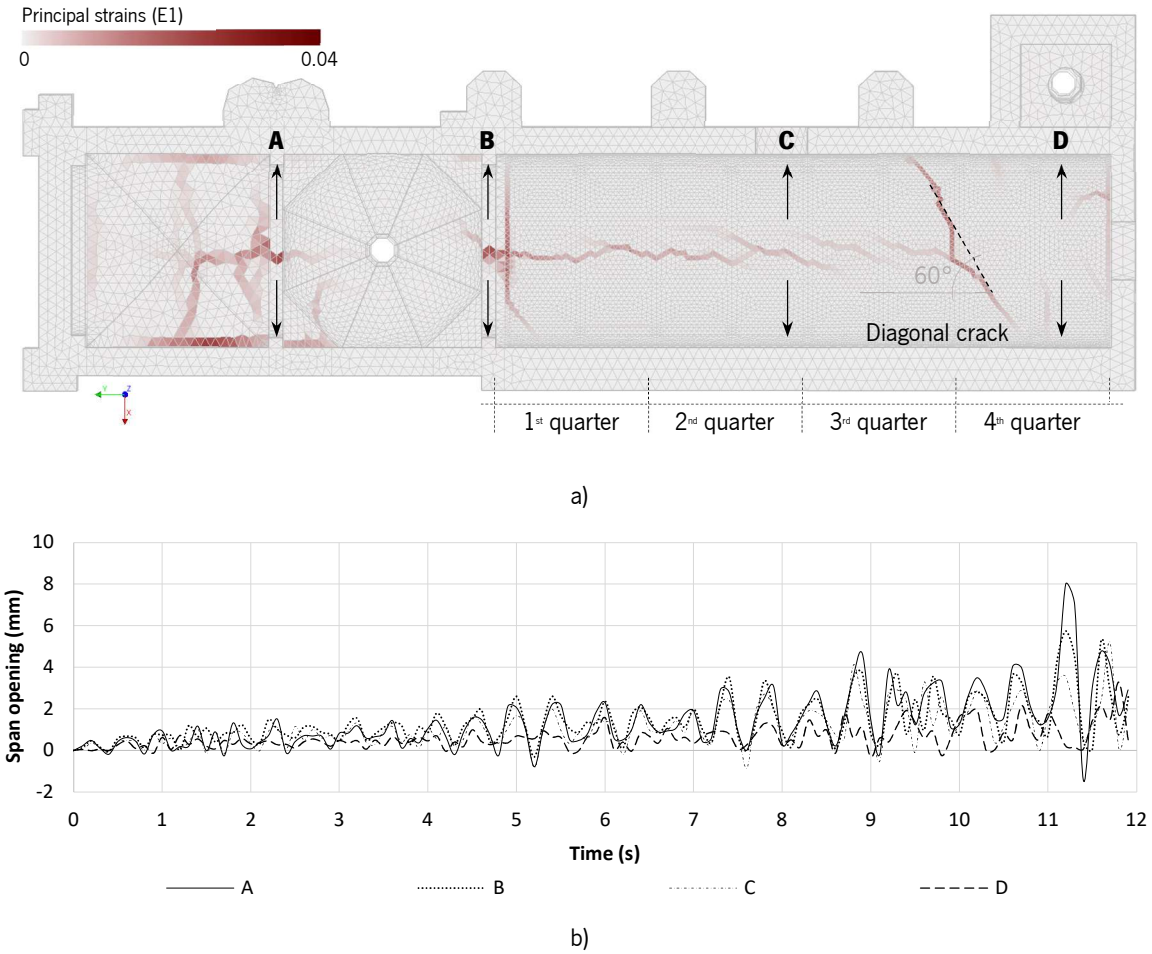

Figure 5-12. a) Damage at the intrados due to SCRU record (last step converged); b) plot of the span openings A and B (transverse arches) and C and D (barrel vault).

5.2.7. RFPP. Puebla, Mexico. 09/19/2017. M = 7.1

The results obtained for the analysis with the RFPP earthquake are similar to the ones obtained with the SCRU earthquake. For this analysis, the span openings stay lower than 2 mm until 5.5 s. After that, the oscillations reach values around 3 mm until at 11 s. During this part of the analysis, the damage evolves smoothly. It is at around 11.5 s that one of the maximum openings occurs, presenting a maximum value of almost 7 mm. This deformation results of the evolution of the damage located at the groin vault and the development of the diagonal crack located between the 3rd and 4th quarter of the barrel vault. The opening at section D, which occurred at 11.3 s, is related to damage at the barrel vault and its interaction with the south tower.

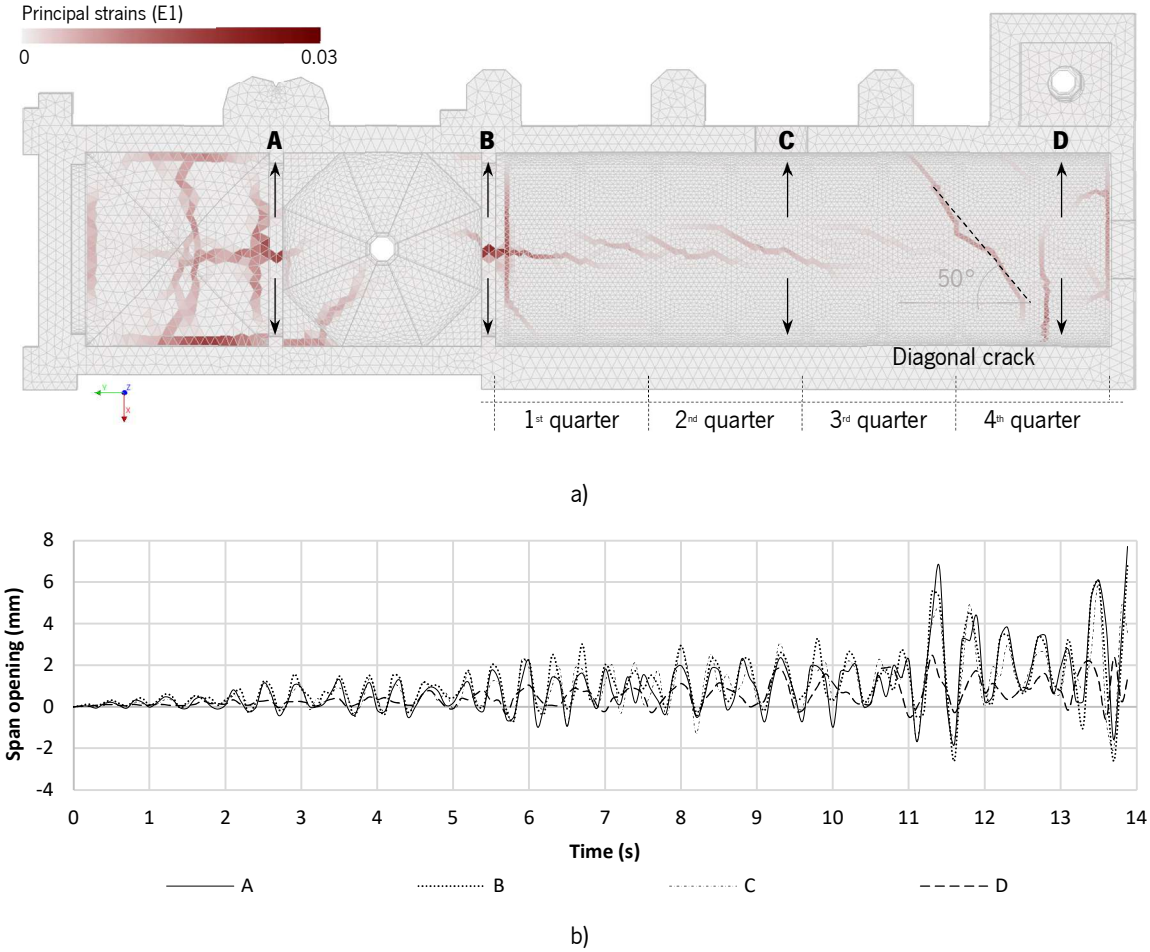

Figure 5-13. a) Damage at the intrados due to RFPP record (last step converged); b) plot of the span openings A and B (transverse arches) and C and D (barrel vault).

At 13.5 s, sections A, B and C reach values around 6 mm, which is associated with the development of the diagonal crack at the south wall of the presbytery, the damage emerging at the southeast meridional panel of the dome, and the evolution of the damage in the transverse arches and barrel vault. In the last step of the analysis, a second hinge appears at the crown of the east transverse arch causing an increase of the span opening at section A.

5.2.8. THEZ. Puebla, Mexico. 09/19/2017. M = 7.1

In the last NLDA, the THEZ earthquake was used (4.4 s of duration). This signal caused a significantly different response of the building. By looking at the damage in **Figure 5-14a** and the plot of the span openings (**Figure 5-14b**), it is possible to observe that the input acts as an impulse, producing most of the damage after the 4 s. Contrary to all the previous records, "X" cracks appear all along the barrel vault.

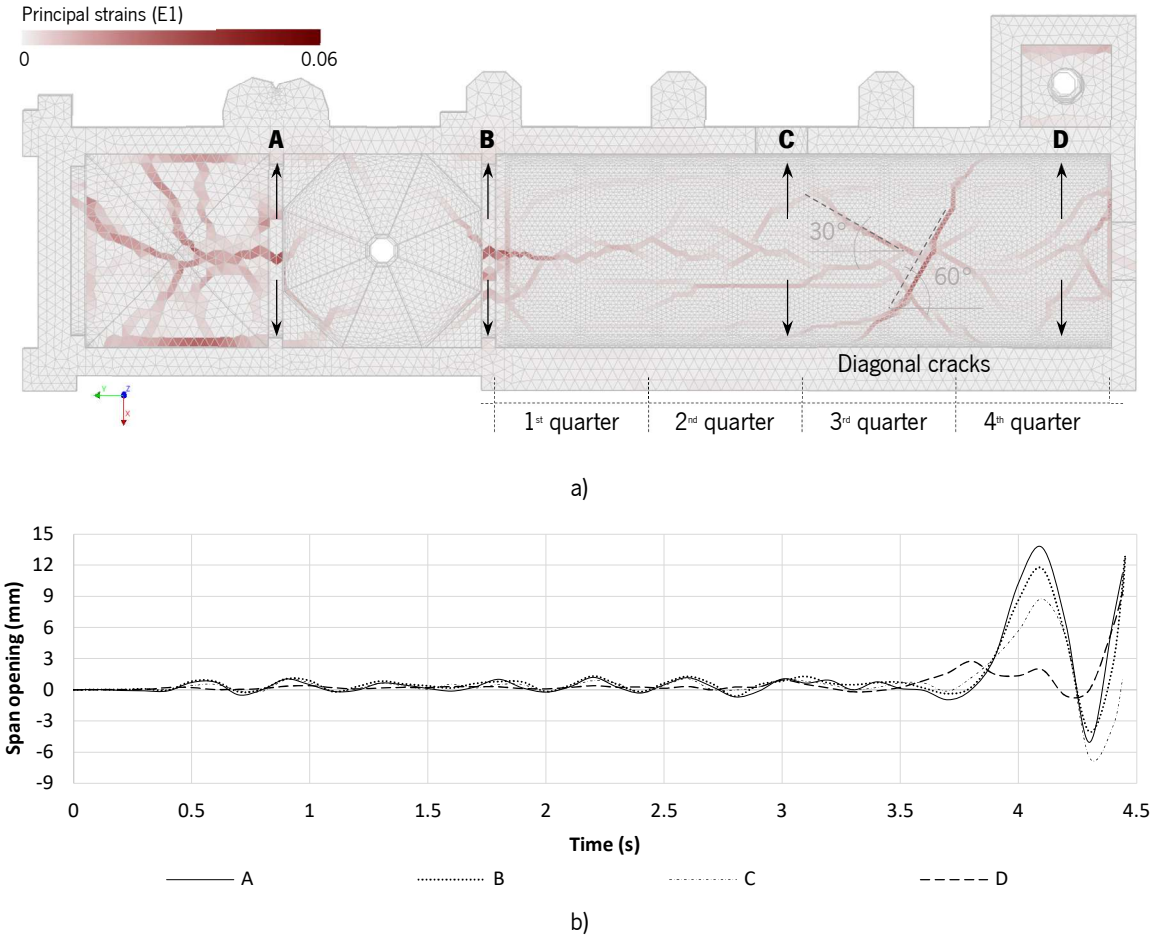

Figure 5-14. a) Damage at the intrados due to THEZ record (last step converged); b) plot of the span openings A and B (transverse arches) and C and D (barrel vault).

The first diagonal cracks occur at around 4 s and the X-shaped pattern is completed in the last step of the analysis. New damage emerges in the building under this record: horizontal cracks develop at the base of the internal face of the north wall (along the nave, the wall under the dome and the presbytery), while the south wall presents this type of damage at both faces (internal and external); the north tower is severely damaged at the belfry with horizontal cracks at the base of the windows and diagonal cracks; the dome suffers as well cracking following an X-shaped pattern that reaches six out of the eight meridional panels. In this way, this signal is extremely aggressive for this building. URM buildings were not designed to stand horizontal dynamic actions, mainly impulsive earthquakes, and the damage obtained from this analysis shows how fast a building of this type can suffer irreparable damages.

5.3. Pushover analysis (POA)

In comparison with the dynamic analysis, pushover analysis is a simplified nonlinear approach used to evaluate the seismic structural behaviour. In this study and in order to simulate ground motion, horizontal monotonic loads proportional to the mass were applied in four directions (+X, -X, +Y and -Y). This Section reports the results using three control points (**Figure 5-15**): (CP-1) top of the dome; (CP-2) top of the north tower; and (CP-3) top of the south tower. The outcome is a force–deformation relationship curve (capacity curve) useful to evaluate the maximum capacity of the structure. The load factor is normalised to the gravity; therefore, the values indicate the percentage of the self-weight applied horizontally. The displacements are presented in centimetres and the span openings in millimetres. The analysis was performed with a variable load step and the arc length control activated for all the model. The Secant (Quasi-Raphson) iterative method was used, satisfying the convergence norms for energy with a tolerance equal to 0.001. The parallel Direct Sparse method was adopted to solve the system of equations. A detailed report of the graphical results is shown in **Annex C**.

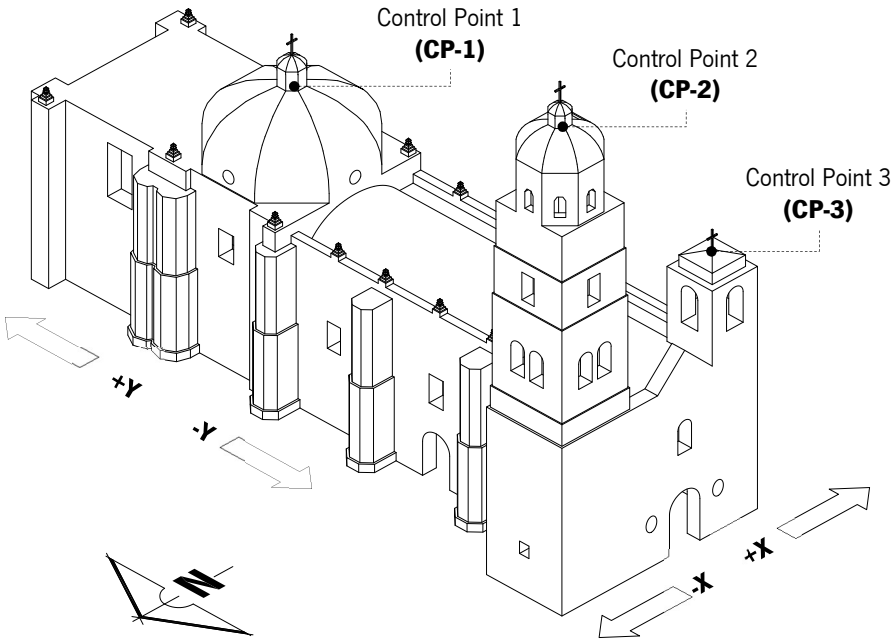

Figure 5-15. Sign convention adopted in the POA (+X, -X, +Y, -Y) and control points for the capacity curves: CP-1 (top of the dome), CP-2 (top of the north tower) and CP-3 (top of the south tower).

5.3.1. Pushover +X

The plot in **Figure 5-16** for the POA in the +X direction shows that the maximum capacity of the building, identified with a green indicator, reaching a load factor of 0.11. The related displacements for each control point are: CP-1 equal to 0.75 cm; CP-2 1 equal to 1.10 cm; and CP-3 equal to 2.39 cm.

Before reaching the maximum load capacity, the building shows an almost linear behaviour for CP-1 and CP-3 while CP-2 can be considered as totally linear. The post-peak trend, related to CP-1 and CP-3, is associated with the damage that occurred at these portions of the building, the last point corresponds to the largest deformations. The capacity curve CP-2 confirms a linear behaviour of the north tower as it unloads along the same path. The point reached at the final step of the analysis is identified with a red indicator in the figure.

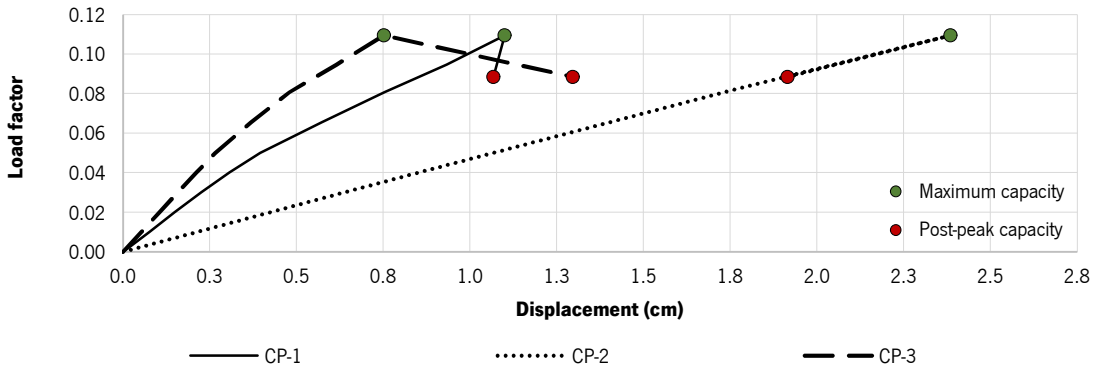

Figure 5-16. Capacity curves for the pushover in the positive X direction.

Figure 5-17a shows the graphical representation of the principal strains for the load factor equal to 0.11. Damage is localised at the east and west meridian of the dome, the groin vault and the intrados of the barrel vault. Maximum cracks of 5.5 mm are localised at the crown of the east transverse arch. **Figure 5-17b** depicts the principal strains values for the post-peak capacity indicated in the plot. The damage at the base of the dome is likely the reason for the evolution of the CP-1 curve, as well as the lack of damage detected in the north tower explains the linear behaviour shown by CP-2. However, major damage appears in the façade. A vertical crack that starts at the connection with the south tower can explain the sudden post-peak displacements for CP-3.

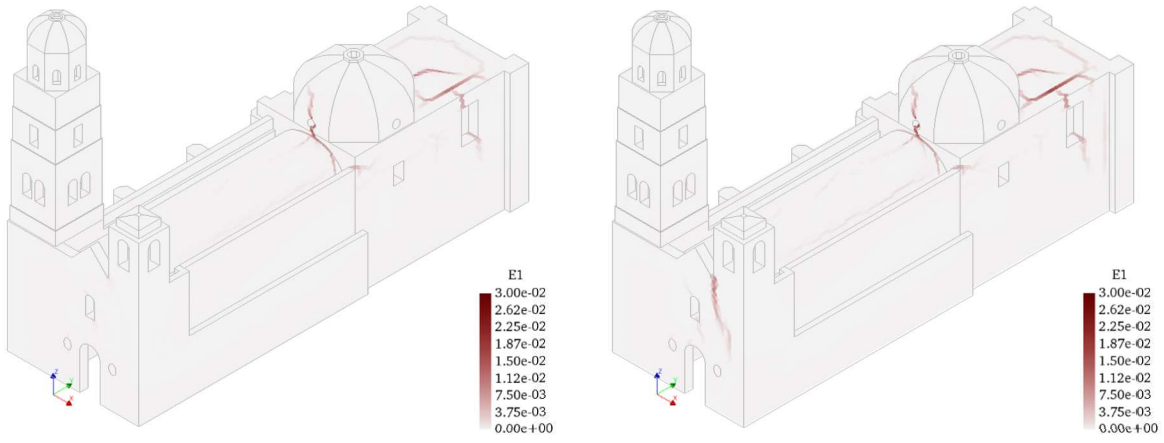

a) b)

Figure 5-17. Principal strains (E1) for the pushover analysis +X: a) maximum capacity of the building for the load factor equal to 0.11; b) post-peak capacity of the building for the load factor equal to 0.09.

In **Figure 5-18a**, the damage state related to the post-peak behaviour indicates damages at the intrados of the transversal arches, the barrel vault and the groin vault, including at its connection with the south wall. **Figure 5-18b** shows the plot for the span openings at the same sections used for the dynamic

analysis. Considering the image and the plot, it is clear that sections A and B present more damage, followed by section C. Section D presents the stiffer behaviour until the maximum capacity. After this point, a sudden crack opening occurs, which is associated with a brittle behaviour and is coherent with the crack of the façade, caused mainly due to the interaction with the south tower (**Figure 5-17b**).

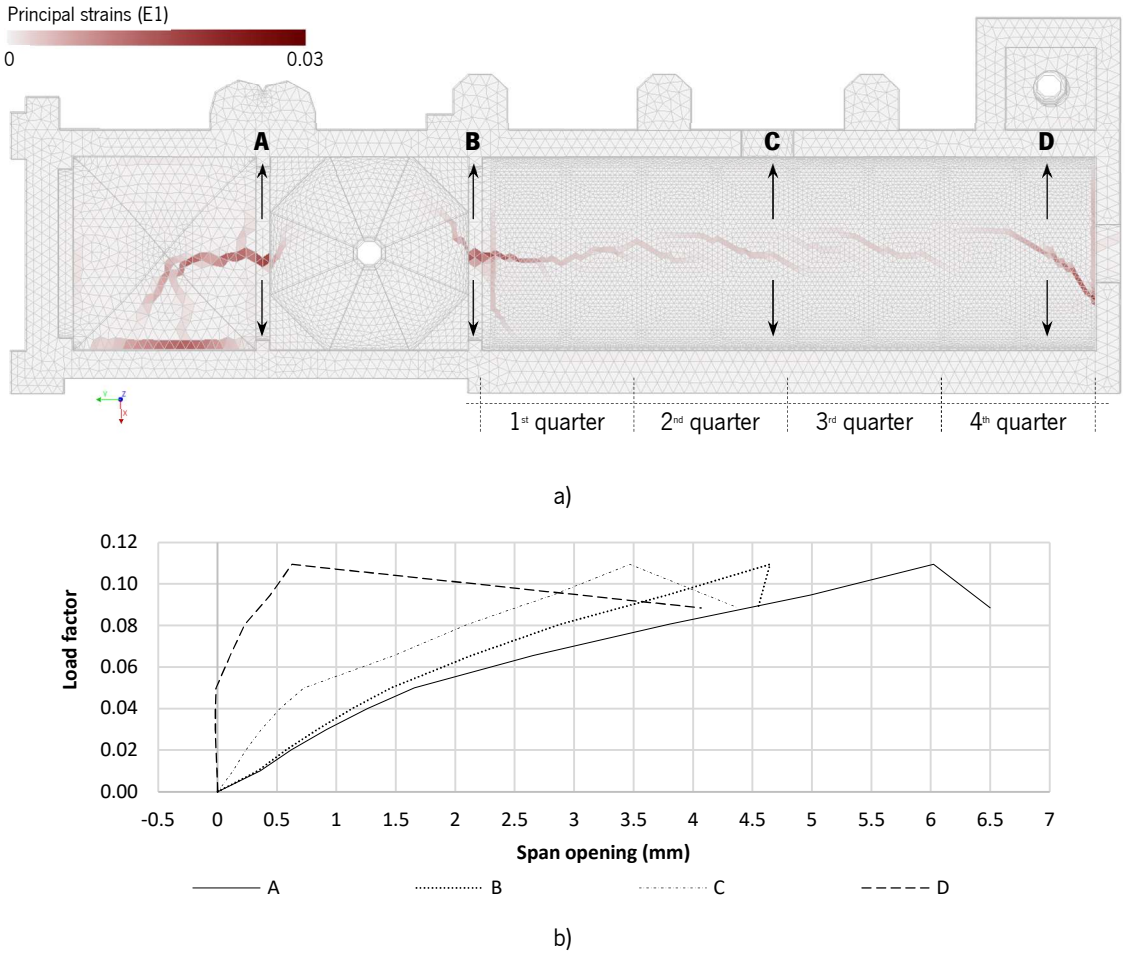

Figure 5-18. a) Damage at the intrados due to the pushover analysis +X (post-peak stage for the load factor equal to 0.09); b) plot of the span openings A and B (transverse arches), and C and D (barrel vault).

5.3.2. Pushover -X

The plot in **Figure 5-19** for the pushover analysis in -X direction indicates the maximum capacity of the building with a load factor equal to 0.14, increasing around 27% in comparison with +X pushover analysis. The related displacements for each control point are: CP-1 equal to 0.61 cm; CP-2 equal to 1.37 cm; and CP-3 equal to 5.71 cm. Similar to the results of the pushover in the +X direction, the behaviour of the

building remains almost linear until a sudden drop in the capacity. Damage is detected by all three control points. In the post-peak, after the red points (**Figure 5-19**), CP-2 continues the deformation while decreasing the capacity. Meanwhile, CP-1 and CP-3, keep approximately the same deformation with the decrement of the capacity (brittle response). In comparison with the maximum capacity of the +X pushover analysis, the displacements of the building in the -X direction decrease about 19% for CP-1, and increases about 25% for CP-2 and 39% for CP-3.

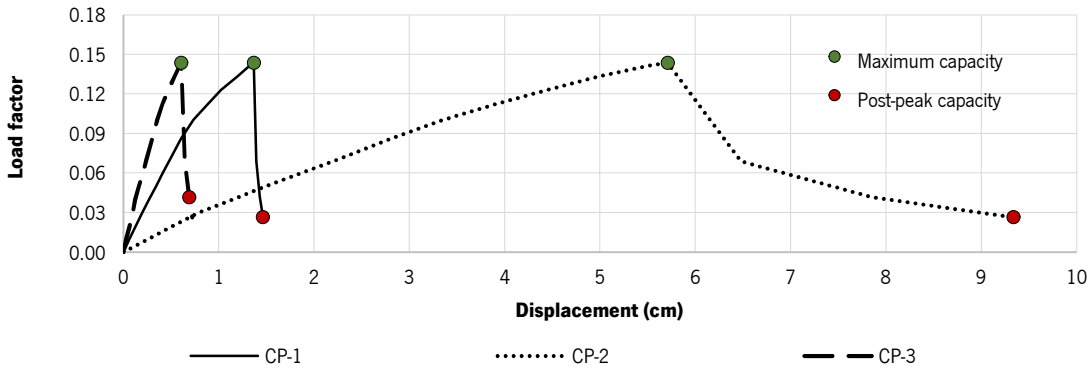

Figure 5-19. Capacity curves for the pushover in the negative X direction.

In **Figure 5-20a** the principal strains for the maximum capacity are presented. The highest damage appears on the west façade. A crack develops from the south base of the pediment, almost reaching the base of the wall and separating the front of the building in two parts. Once reached the red indicator for the post-peak behaviour (**Figure 5-20b**), a second crack appears in the same area but is located at the connection between the north tower and the façade. However, after this step, the capacity continues to drop until 0.03 while the displacement for CP-3, related to the north tower, increases to 9.34 cm.

Figure 5-21a shows the damage at the intrados of the vaults for the post-peak behaviour, indicated with a red point in the capacity curves in **Figure 5-19**. Cracks appear along the transversal arches, the barrel vault and the groin vault. A diagonal crack develops from the façade in the 4th quarter of the barrel vault, which corresponds to the one shown in **Figure 5-20b**. The plot of the span openings in **Figure 5-21b** depicts the major damage located in section D, reaching a deformation higher than 16 mm. This is consistent with the larger displacements shown by the CP-2 capacity curve. Regarding the other cases, the span openings at sections A and B present negative values, namely a closure of the span, until a load factor around 0.13. The post-peak behaviour shows no increment in the opening, keeping a constant value of approximately 0.5 mm until the end of the curve. The span opening at section C exhibits similar behaviour to the span opening at section D, but with displacements more than 50% smaller.

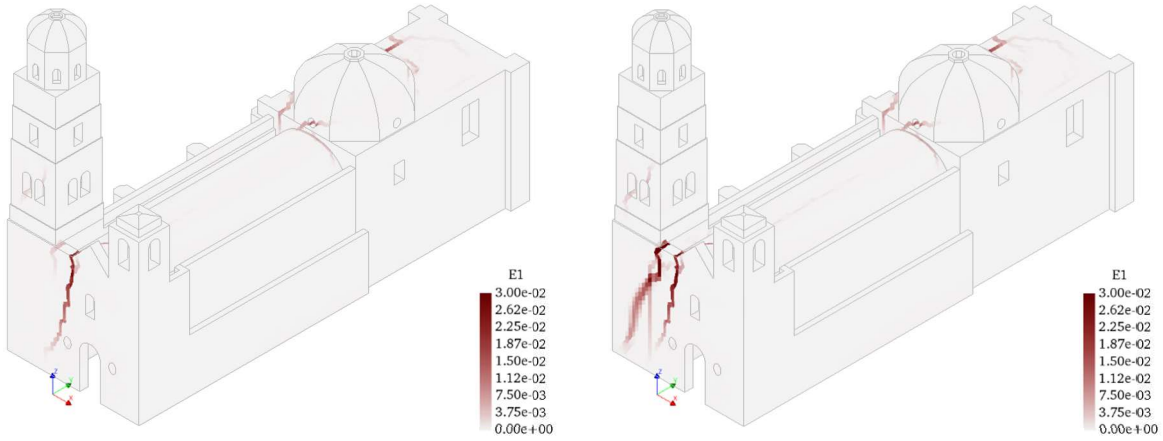

b) c)

Figure 5-20. Principal strains (E1) for the pushover analysis -X: a) maximum capacity of the building for the load factor equal to 0.14; b) post-peak capacity of the building for the load factor equal to 0.07.

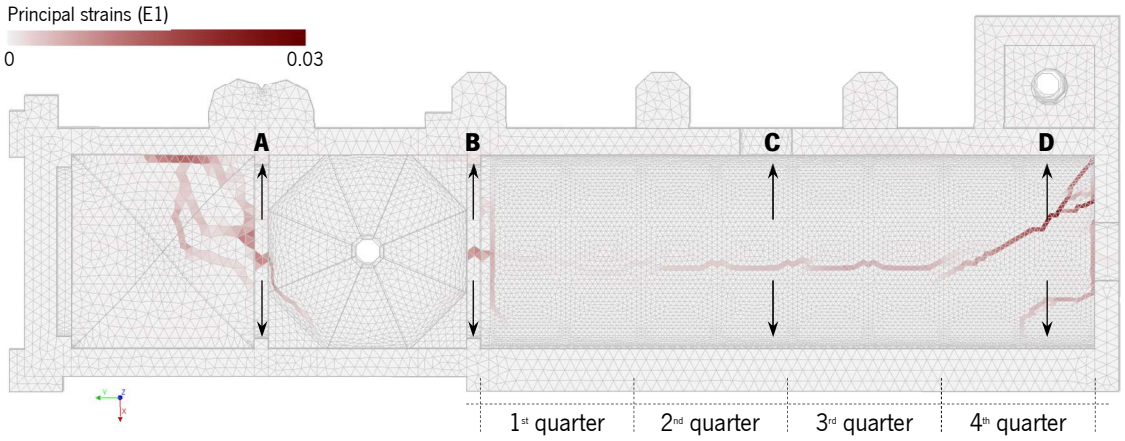

a)

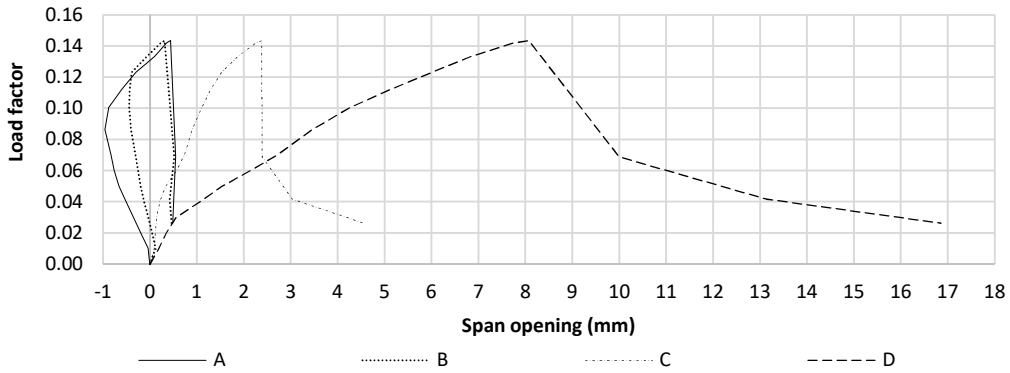

b)

Figure 5-21. a) Damage at the intrados due to the pushover analysis -X (post-peak stage for the load factor equal to 0.07); b) plot of the span openings A and B (transverse arches), and C and D (barrel vault).

5.3.3. Pushover +Y

The capacity curves for the POA in the positive Y direction are plotted in **Figure 5-22**. The maximum capacity, highlighted in green, reaches a load factor equal to 0.18, increasing about 80% in comparison with +X pushover analysis. The curves for CP-1 and CP-3 exhibit a linear behaviour compared to CP-2, which indicates that this direction is mainly affecting the north tower. This explains why the displacement related to the maximum load factor is lower than 1 cm for CP-1 and CP-3, while for CP-2 reaches 10 cm. In order to explain three relevant aspects of the response, three points are highlighted in the CP-3 capacity curve:

- **P1** for a load factor equal to 0.15: a sudden displacement of the tower is related to a vertical crack that appears at the façade, along the connection between the façade and the north tower (see **Figure 5-23a**).
- **P2** for a load factor equal to 0.17: at this point, the load factor approaches the plateau, reaching the maximum capacity while the displacements increase (see **Figure 5-23a**).
- **P3** for a load factor equal to 0.18: after the maximum capacity of the building, a drop in the load factor occurs, reducing about 6% (from 0.18 to 0.17). This change in the curve represents the onset of a mechanism of failure in the area of the presbytery. A diagonal crack develops in the north wall (presbytery). In the following steps of the analysis, a similar crack opens at the south wall (see **Figure 5-23b**).

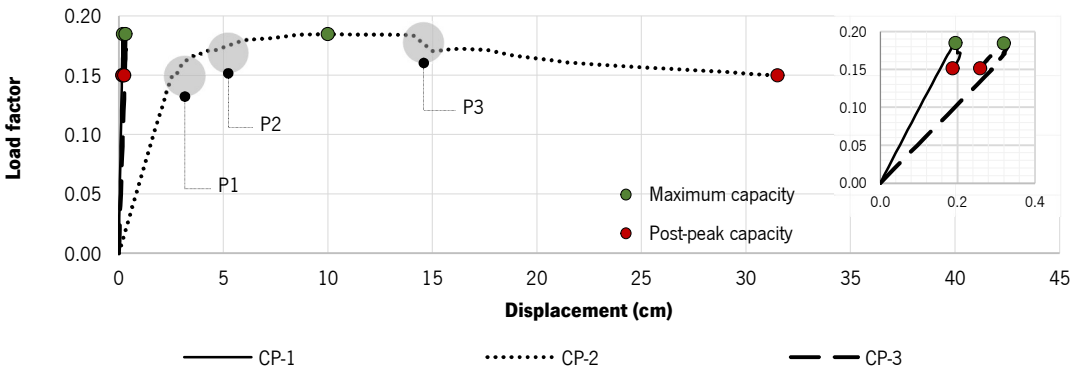

Figure 5-22. Capacity curves for the pushover in the positive Y direction.

Besides the indication of the points P1, P2 and P3, **Figure 5-23** shows the principal strains (E1) for the maximum capacity (a) and the post-peak capacity (b) of the structure. As already mentioned, this analysis

is mainly affecting the north tower, which exhibits the most severe damages at the area of the belfry. The damages presented at the maximum capacity increase notably at the post-peak, in which the same area is the most affected.

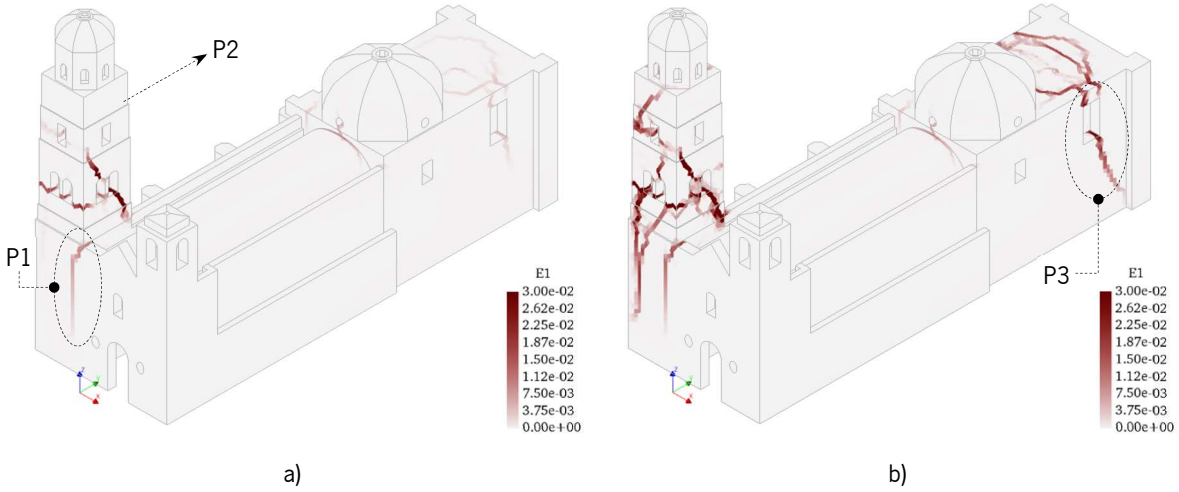

a) b)

Figure 5-23. Principal strains (E1) for the pushover analysis +Y: a) maximum capacity of the building for the load factor equal to 0.18; b) post-peak capacity of the building for the load factor equal to 0.15.

Figure 5-24a shows the principal strains for the intrados of the vaults related to the post-peak capacity (also shown in **Figure 5-23b**). The highest strains are located in the north tower, nonetheless, significant damages are located also in the crown (intrados) of the transversal arches, in the lateral walls of the presbytery and the groin vault.

In **Figure 5-24b**, until a load factor equals to 0.15 (P1), the span openings at sections A and B present a positive value, while section C is closing and D keeps a constant value practically equal to zero. Nonetheless, when the load factor reaches 0.15, the trend in the span opening changes drastically in the sections that are closer to the crack in the façade, whereas the farthest sections are barely affected by it. More in detail, sections D and C suffer a significant sudden opening, while sections B and A show negligible evidence of the damage onset. Also, at P2 (load factor equal to 0.17, before the maximum capacity), sections D and C present a change in the trend of the opening, whereas in sections B and A the opening continues to increase without significant variation. However, it is worth noting that for P3 the displacement at section A is much larger in comparison with the other sections. It is also possible to see that at the end of the curve, the state of damage developed in the structure changes the deformation path and it tends to recover from the displacement driven by the monotonic load.

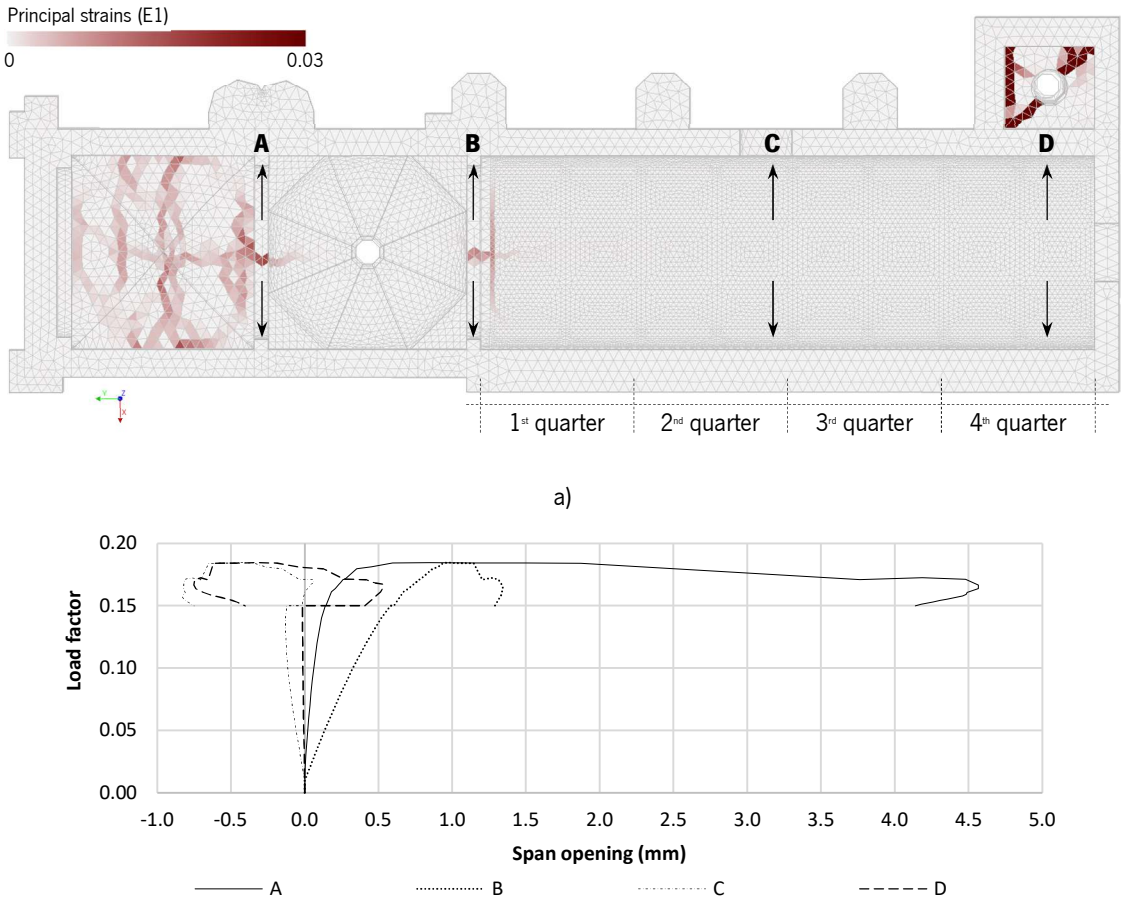

Figure 5-24. a) Damage at the intrados due to the pushover analysis +Y (post-peak stage for the load factor equal to 0.15); b) plot of the span openings A and B (transverse arches), and C and D (barrel vault).

5.3.4. Pushover -Y

For the pushover analysis in the negative Y direction, the capacity curves are plotted in **Figure 5-25**. The maximum capacity, indicated in green, reaches a load factor equal to 0.15, increasing around 72% in comparison with +X pushover analysis. The curve for CP-1 very low deformation when compared to CP-2 and CP-3. The -Y pushover is mainly governed by the west part of the building, as seen in the plot for CP-2 and CP-3 (curves related to the north and south tower, respectively).

The three points, indicated in the CP-3 curve, corresponding to the specific aspects described below:

- **P4** for a load factor equal to 0.07: a first diagonal crack appears in the barrel vault located between the third and fourth quarter with an inclination of approximately 60°. This damage crosses the barrel vault, from the south wall to the closest buttress in the north wall.

- **P5** for a load factor equal to 0.12: a second diagonal crack develops in the fourth quarter of the barrel vault with an inclination of 80° approximately. It develops from the southeast of the north tower to the south tower. The crack that appeared at P4 in the transverse direction of the vault continues in the vertical direction, reaching the south wall **Figure 5-26a**. Another vertical crack in the façade develops from the north base of the pediment.
- **P6** for a load factor equal to 0.13: as the load factor increases to 0.13, the north tower suffers a sudden diagonal crack in the area of the belfry that continues vertically along the first body of the tower. At the same time, a hinge develops in the connection of the façade and the barrel vault, and the cracks developed in P4 and P5 continue growing, producing as well, transverse damage in the loft choir.

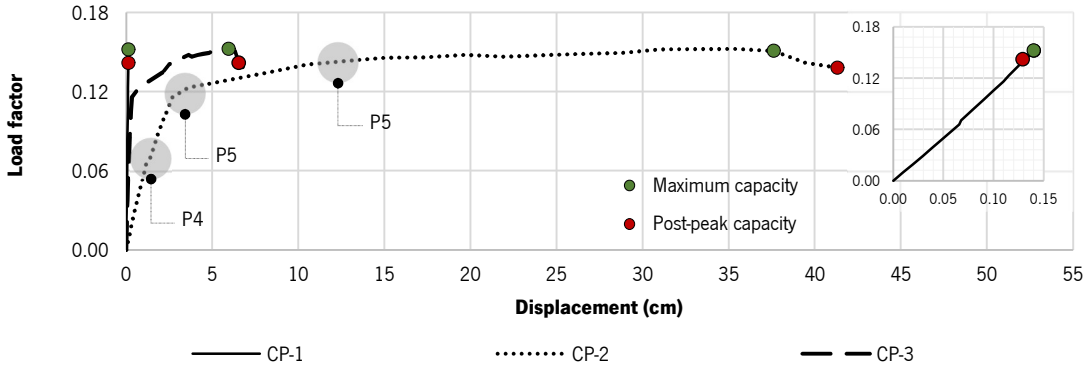

Figure 5-25. Capacity curves for the pushover in the negative Y direction.

Figure 5-26 depicts the principal strains for the maximum capacity (a) and the post-peak capacity (b) of the structure. From one point to the other, the strains increase about 18%. At these points, the three aspects highlighted in the capacity curve (P4, P5 and P6) already took place. **Figure 5-26a** shows the cracks in the façade and the south wall, which started at P4 and increased at P5, and the diagonal damage in the belfry of the north tower occurred in P6.

Sections A, B and C barely open or close until the load factor 0.07, while section D tends to open. With the development of P4, section D recovers the deformation and the rest continues with the previous tendency. Until P5 appears, the behaviour of the span openings follows an almost linear path. It is when it reaches a load factor equal to 0.12 that sections C and D change completely the direction and the span openings increase. When the analysis reaches 0.13 (P6), both sections C and D develop a large opening. Finally, section C develops an opening of almost 15 mm while section D only 7 mm.

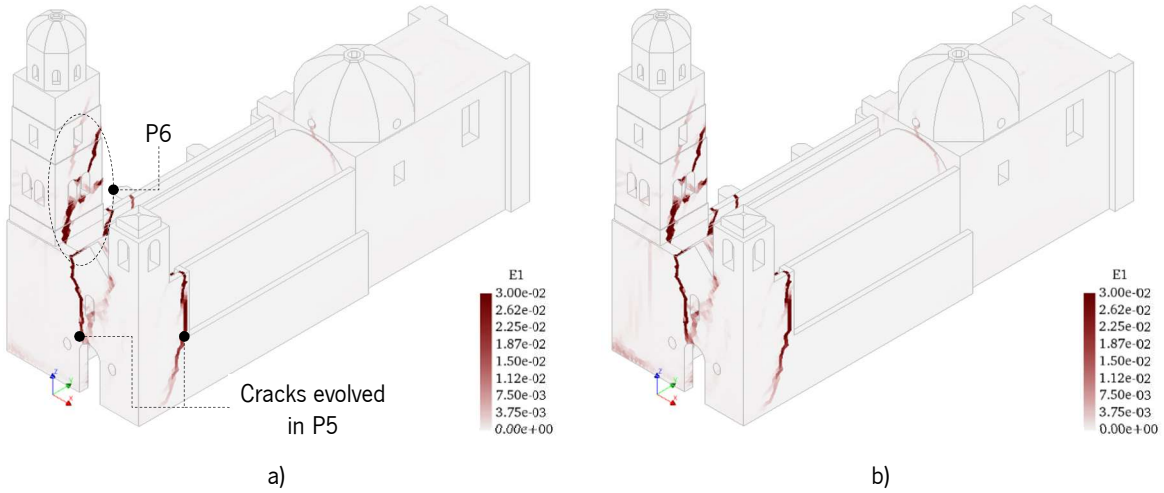

Figure 5-26. Principal strains (E1) for the pushover analysis -Y: a) maximum capacity of the building for the load factor equal to 0.15; b) post-peak capacity of the building for the load factor equal to 0.14.

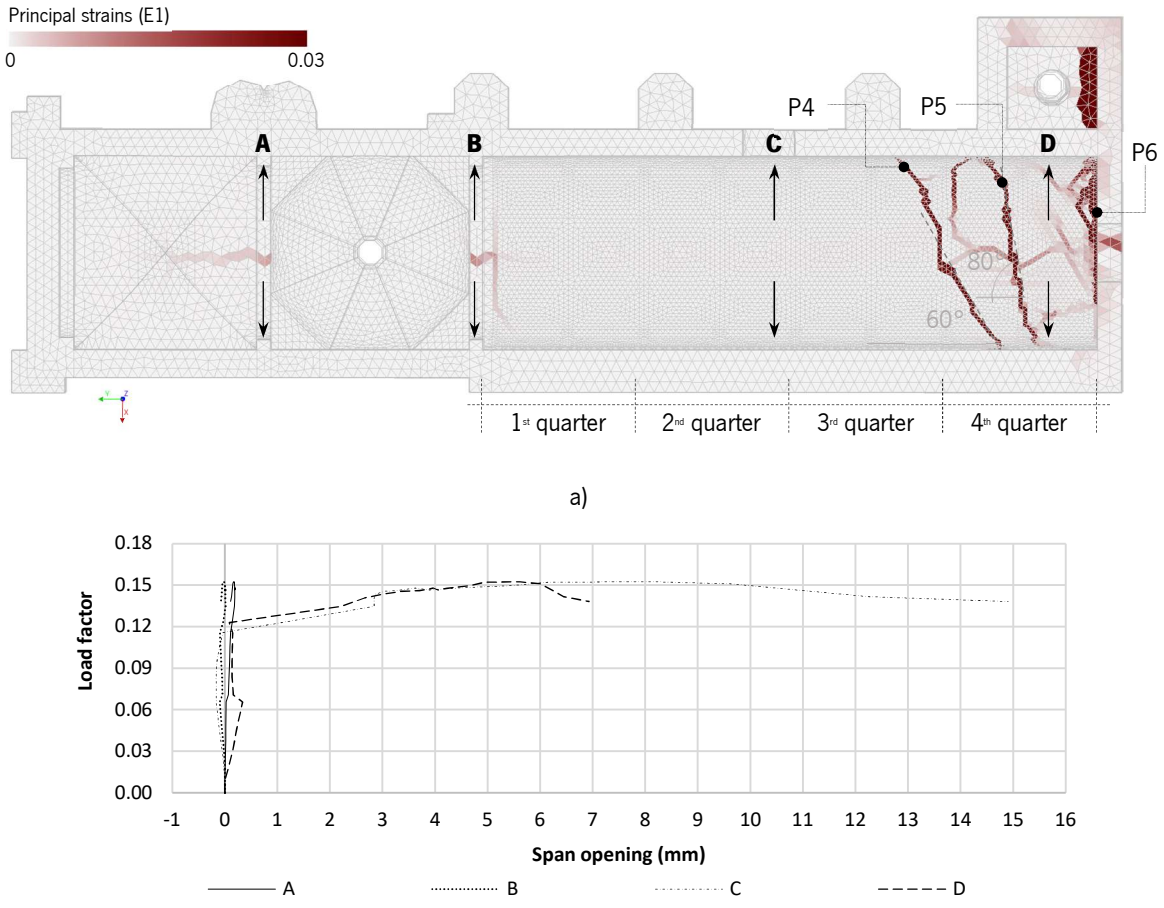

Figure 5-27. a) Damage at the intrados due to the pushover analysis -Y (post-peak stage for the load factor equal to 0.14); b) plot of the span openings A and B (transverse arches), and C and D (barrel vault).

5.4. Discussion of the results and comparison

In order to make a comparison of the results in terms of displacement, in **Figure 5-28** nine control points are identified, four macro-elements associated with the lateral displacements and five points at the roofing system related to the vertical displacement. In the case of the lateral displacements, the normalised values (maximum displacement on the top of the macro-element divided on the heigh) were compared for each analysis. For the vertical displacements, the comparison was done directly using the absolute values. The response of the building is also related to effective maximum peak ground acceleration (maximum applied acceleration in "g") and the duration of the analysis (in "s").

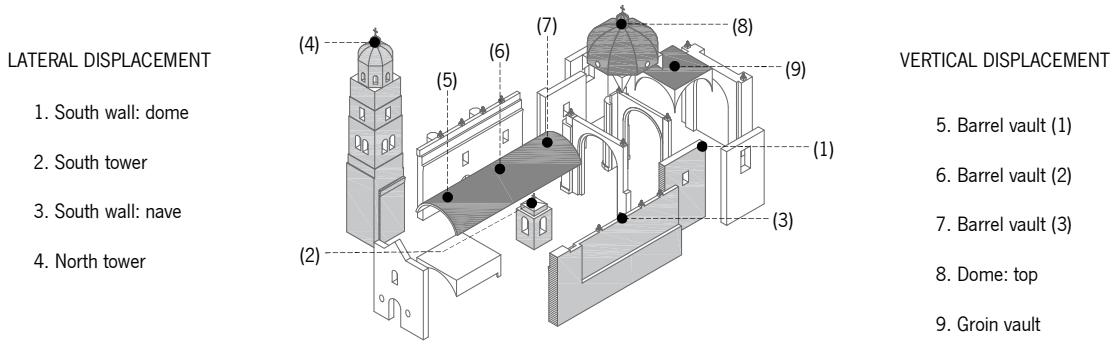

Figure 5-28. Control points for the analysis of the displacements. Lateral displacements related to the south wall under the dome (1), the south tower (2), the south wall in the nave (3) and the north tower (4). Vertical displacements related to the barrel vault (5-7), the dome (8) and the groin vault (9).

Figure 5-29 shows the normalised displacement in the transverse direction (X). For the south wall under the dome, the record causing more deformation is the signal SAPP with 0.15%. The record THEZ affects more the other three macro-elements. It is noted that the north tower presents a high displacement since the ratio overpass 0.40%. This aspect is consistent with the damages (in the north tower) mentioned in section 5.2.8.

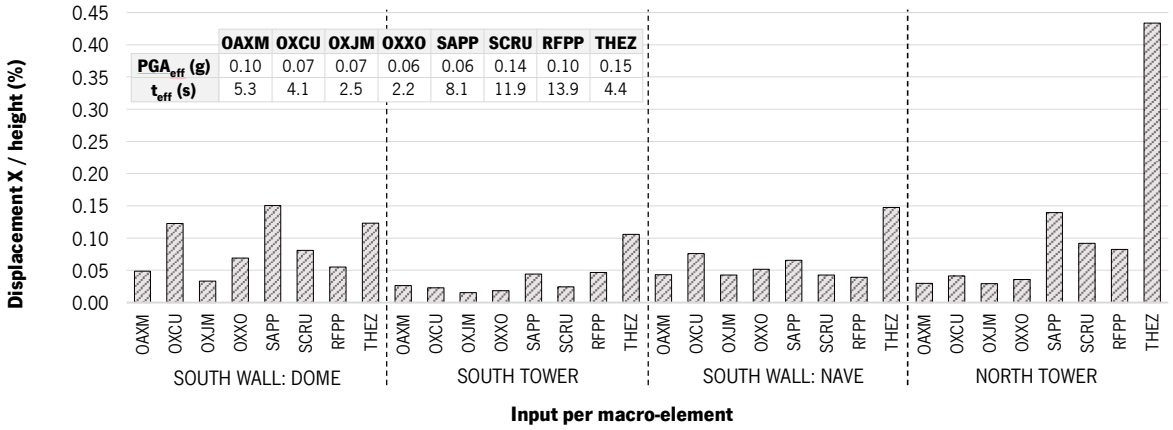

Figure 5-29. Maximum normalised displacement in the transverse direction (X). Eight records for four macro-elements: the south wall (dome), the south tower, the south wall (nave) and the north tower. In the table, it is specified the PGA_{eff} for the transverse component (X) and the length of each analysis (t_{eff}) in seconds.

In **Figure 5-30**, the normalised displacement in the longitudinal direction (Y) is presented. The same macro-elements are analysed. The south wall (nave) presents the lower values in comparison with the other macro-elements. The south wall (dome) keeps ratios lower than 0.02%. The behaviour of these two points is expected since they are located on the longitudinal wall. The south tower reaches a deformation of about 0.05% for RFPP and THEZ. The north tower becomes the element with higher displacements in the longitudinal direction (Y), in which the RFPP signal causes the highest displacement, although, it is lower than 50% of the displacement caused by THEZ in the transverse direction (X).

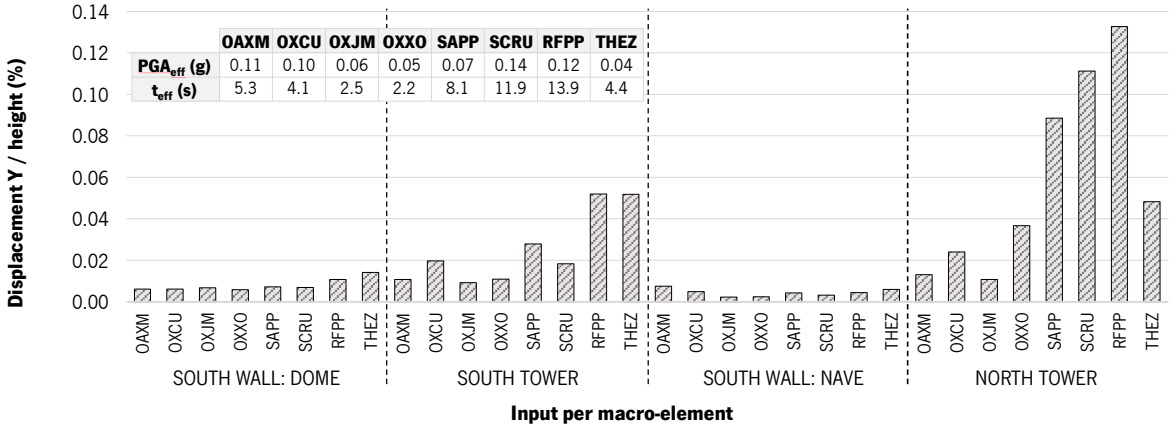

Figure 5-30. Maximum normalised displacement in the longitudinal direction (Y). Eight records for four macro-elements: the south wall (dome), the south tower, the south wall (nave) and the north tower. In the table, it is specified the PGA_{eff} for the longitudinal component (Y) and the length of each analysis (t_{eff}) in seconds.

Regarding the vertical displacements, **Figure 5-31** depicts the maximum values, positive and negative, reached in three points of the barrel vault, the dome and the groin vault. For the barrel vault (1), THEZ induces a maximum negative displacement around 9 mm, while on the positive side the maximum is reached by OAXM. The major deformation for this vault is located at point (3), with more than 12 mm for the signal SAPP. In comparison with the other macro-elements, the dome presents the lower displacements, being as well the signal SAPP the one generating a maximum of more than 5 mm of displacement. The groin vault presents the major negative displacements under the records SAPP and THEZ (about 15 mm).

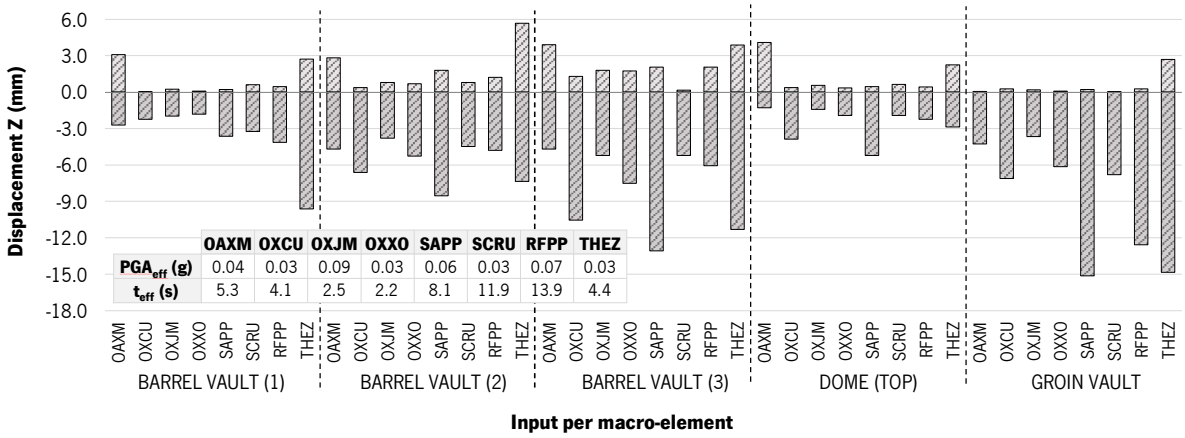

	OAXM	OXCU	OXJM	OXXO	SAPP	SCRU	RFPP	THEZ
PGA_{eff} (g)	0.04	0.03	0.09	0.03	0.06	0.03	0.07	0.03
t_{eff} (s)	5.3	4.1	2.5	2.2	8.1	11.9	13.9	4.4

Figure 5-31. Maximum (negative and positive) vertical displacement (Z) for five points in the roofing system: three points at the barrel vault, the dome and the groin vault. In the table, it is specified the PGA_{eff} for the vertical component (Z) and the length of each analysis (t_{eff}) in seconds.

In terms of qualitative analysis of the results, and according to a previous classification of the damage (DPCM, 2015; Fuentes et al., 2019), a failure mechanisms list is presented in **Table 5-1** and illustrated in **Annex D**. Thirty different cases are relevant for Mexican typical churches. Out of them, 20 may apply to the case of single nave temples. Thus, the remaining mechanisms are underlined in **Table 5-1**. The mechanisms obtained from the analyses are also identified.

Table 5-1. List of failure mechanisms adapted from (DPCM, 2015; Fuentes et al., 2019).

Relevant mechanisms for Mexican typical churches		Mechanisms affecting San Agustin church	
Mechanism	**Description of the failure mechanism**	**NLDA**	**POA**
M.1	Overturning of the **façade** (DPCM, 2015)		
M.2	Mechanisms in the pediment of the **façade** (DPCM, 2015)		
M.3	In-plane mechanisms in the **façade** (DPCM, 2015)	✓	✓
M.4	Prothyrum and narthex (DPCM, 2015)		
M.5	Transverse response of the **nave** (DPCM, 2015)	✓	✓
M.6	Shear mechanisms in **lateral walls** (DPCM, 2015)		
M.7	Longitudinal response of the **colonnade** (DPCM, 2015)		
M.8	Vaults of the **central nave** (DPCM, 2015)		
M.9	Vaults of the **lateral naves** (DPCM, 2015)		
M.10	Overturning of the end walls of the **transept** (DPCM, 2015)		
M.11	Shear mechanisms in the walls of the **transept** (DPCM, 2015)		
M.12	Vaults of the **transept** (DPCM, 2015)		
M.13	**Transverse arch** (DPCM, 2015)	✓	✓
M.14	**Dome and drum** (DPCM, 2015)	✓	✓
M.15	**Lantern** (DPCM, 2015)		
M.16	Overturning of the **presbytery** or **apse** walls (DPCM, 2015)	✓	✓
M.17	Shear mechanisms in the walls of the **presbytery** or **apse** (DPCM, 2015)	✓	
M.18	Vaults of the **presbytery** or **apse** (DPCM, 2015)	✓	✓
M.19	Roof elements: **nave** (DPCM, 2015)		
M.20	Roof elements: **transept** (DPCM, 2015)		
M.21	Roof elements: **apse** (DPCM, 2015)		
M.22	Overturning of the **chapels** (DPCM, 2015)		
M.23	Shear mechanisms in the **chapels** (DPCM, 2015)		
M.24	Vaults of the **chapels** (DPCM, 2015)		
M.25	Irregularity interactions (DPCM, 2015)	✓	✓
M.26	Exterior volumes (gable, pinnacles, statues) (DPCM, 2015)		
M.27	Bell **tower** (DPCM, 2015)	✓	✓
M.28	**Belfry** (DPCM, 2015)	✓	✓
M.29	**Choir loft** (Fuentes et al., 2019)	✓	✓
M.30	**Open chapel** (Fuentes et al., 2019)		

NOTE: the mechanisms underlined may not apply to single nave temples.

A more detailed summary of the results is presented in **Table 5-2** and **Table 5-3**. The first table shows the failure mechanisms obtained from the NLDA, organized according to the macro-element and the record. Only the record THEZ damaged the north tower with mechanisms that included the lower part of the tower and the belfry. The damage caused by RFPP to the south tower was classified as damage in the belfry. The eight records produced damage in the façade caused by the interaction with the towers, due to the geometrical irregularities. In addition, OAXM and THEZ records caused in-plane damage at the façade due to shear. Two types of damage were detected in the lateral walls (both north and south), in the parts of the nave and under the dome: M.5 due to the transverse response of the nave and M.25 due to the interaction of irregularities in the geometry, mainly regarding the in-elevation irregularity. In the case of the lateral walls of the presbytery and the back wall (when involved), the two damages developed are associated with the overturning of the presbytery and shear behaviour. The choir loft presented damages for the eight records, mainly related to the interaction with the lateral walls. The barrel vault presented typical damage as a result of the transverse response of the nave, likewise, the interaction of irregularities with other elements affected the stability of this element (e.g. diagonal cracks due to the separation of the façade, the towers, the choir loft and portions of lateral walls). Both transverse arches were affected by the transverse response, mainly due to the opening of the spans. The dome does not have a drum and, therefore, the damage appeared at the middle of the meridians, mainly in the area of the tension hoop in the eight analyses. The groin vault damage is classified as M.18 and it occurs for all records, with damage concentration at the corners and the crown.

Table 5-2. Failure mechanisms activated by the NLDA.

Macro-element of San Agustin church	Mechanisms activated by the signal:							
	OAXM	**OXCU**	**OXJM**	**OXXO**	**SAPP**	**SCRU**	**RFPP**	**THEZ**
North tower	-	-	-	-	-	-	-	M.27 & M.28
South tower	-	-	-	-	-	-	M.28	-
Façade	M.3 & M.25	M.25	M.25	M.25	M.25	M.25	M.25	M.3 & M.25
North lateral wall (nave)	M.5	M.5 & M.25	M.25	M.5 & M.25	M.25	M.5 & M.25	M.5	M.5 & M.25
North lateral wall (dome)	M.25	M.25	M.25	M.25	M.25	M.25	M.25	M.25
North lateral wall (presbytery)	M.16	M.16	M.16 & M.17	M.16	M.16	M.16	M.16	M.16
South lateral wall (nave)	M.25	M.25	M.25	-	M.25	-	M.25	M.5 & M.25
South lateral wall (dome)	M.25	M.25	M.25	M.25	M.25	M.25	M.25	M.25
South lateral wall (presbytery)	M.16	M.16	M.16	M.16	M.16	M.16	M.16	M.16
Choir loft	M.29	M.29	M.29	M.29	M.29	M.29	M.29	M.29
Barrel vault	M.5 & M.25	M.5 & M.25	M.5 & M.25	M.5 & M.25	M.5 & M.25	M.5 & M.25	M.5 & M.25	M.5 & M.25
East transverse arch	M.13	M.13	M.13	M.13	M.13	M.13	M.13	M.13
West transverse arch	M.13	M.13	M.13	M.13	M.13	M.13	M.13	M.13
Dome	M.14	M.14	M.14	M.14	M.14	M.14	M.14	M.14
Presbytery back wall	-	M.16	-	-	-	-	-	M.16
Groin vault	M.18	M.18	M.18	M.18	M.18	M.18	M.18	M.18

The failure mechanisms activated by the pushover analyses are compiled in **Table 5-3**. The damage located at the north tower occurred for the pushover analysis in -X, +Y and -Y directions, both in the lower part of the tower and the belfry. The analyses in X direction introduced shear in the façade. In addition, the four analyses showed damage due to the irregularities in the geometry, mainly at the towers. For the lateral walls under the dome and for the presbytery, the analysis in the +X direction affected the south side while the damage at the north side was caused by the load in the -X direction. In both cases, this damage contributed to the overturning of the presbytery. The lateral walls in the area of the nave showed damage only for the -Y pushover analysis. This damage is caused mainly due to the interaction of geometrical irregularities. The choir loft presented damages for three directions of the load (+X, -X and -Y). The barrel vault showed damages due to the transverse response of the nave and due to the interaction among macro-elements with significant geometry (irregularities). The transverse arches exhibited damage

mainly at the intrados of the crown for the four analyses. Cracks appeared in the meridians of the dome for the four analyses. Finally, the groin vault is also affected in the four cases.

Table 5-3. Failure mechanisms activated by the pushover analyses.

Macro-element of San Agustin church	Mechanisms activated by the analysis:			
	Pushover +X	**Pushover -X**	**Pushover +Y**	**Pushover -Y**
North tower	-	M.28	M.27 & M.28	M.27 & M.28
South tower	-	-	-	-
Façade	M.3 & M.25	M.3 & M.25	M.25	M.25
North lateral wall (nave)	-	-	-	M.25
North lateral wall (dome)	-	M.25	-	-
North lateral wall (presbytery)	-	M.16	M.16	-
South lateral wall (nave)	-	-	-	M.25
South lateral wall (dome)	M.25	-	-	-
South lateral wall (presbytery)	M.16	-	M.16	-
Choir loft	M.29	M.29	-	M.29
Barrel vault	M.5 & M.25	M.5 & M.25	-	M.5 & M.25
East transverse arche	M.13	M.13	M.13	M.13
West transverse arche	M.13	M.13	M.13	M.13
Dome	M.14	M.14	M.14	M.14
Presbytery back wall	-	-	-	-
Groin vault	M.18	M.18	M.18	M.18

Figure 5-32 shows a superimposed plot of the results for the eight NLDAs and the four directions of the POAs, in terms of principal strains (E1). The scale remains the same for both images to better compare the two sets of analyses in a graphical environment. It is understandable that despite the differences, the similarities allow to conclude that the POAs represent in a great percentage the behaviour of the building since it is able to reproduce important failure mechanisms. Regarding the differences, it is worth to mention that seismic actions are a source of uncertainties, and it is complicated to define a type of analysis that can reproduce in a completely accurate way their impact on the behaviour of a structure, in addition, the level of knowledge of a historical building can also bring assumptions.

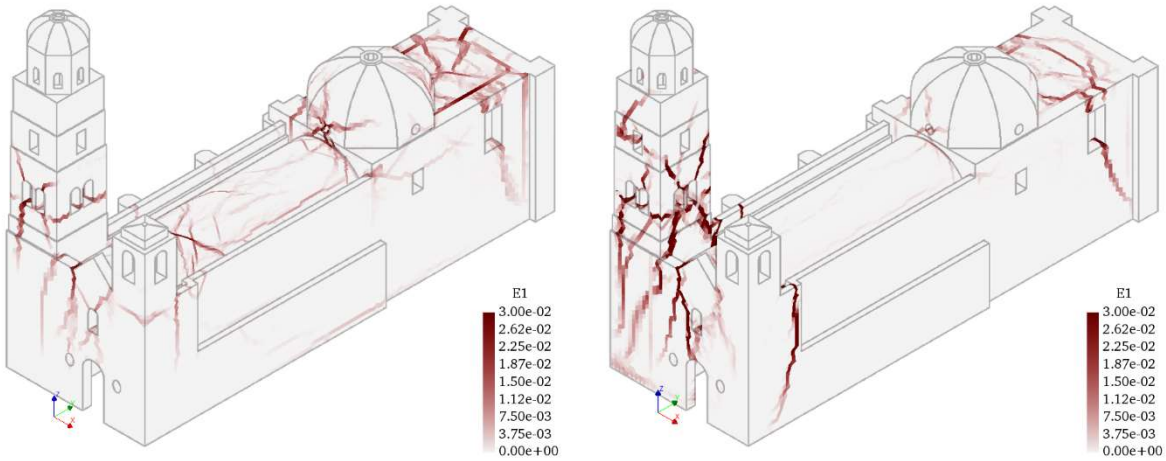

a) b)

Figure 5-32. Superimposed plot of maximum principal strains (E1) of a) NLDAs and b) POAs.

By comparing the two types of analyses (**Table 5-1**, **Table 5-2**, **Table 5-3** and **Figure 5-32**), it is demonstrated that the POAs performed in the four main directions are able to activate the mechanisms obtained from the NLDAs, except for M.17 (shear mechanism in the walls of the presbytery). However, this mechanism appeared only in one of the two lateral walls and only for one of the eight records, being thus less likely. It is worth noting that some of the macro-elements considered by (DPCM, 2015; Fuentes et al., 2019) are not present in this church (e.g. open chapel, pitched roof) or they are present but not considered in the model (e.g. exterior volumes, lanterns). Therefore, their collapse cannot be forecasted by these analyses. However, the analyses triggered in the San Augustin church model all the remaining mechanisms that are relevant for Mexican single nave temples, except for the following:

- M.1: Overturning of the façade.
- M.2: Mechanisms in the pediment of the façade.
- M.6: Shear mechanisms in lateral walls.

Experience demonstrated that the presence of the choir loft and connections between orthogonal walls can reduce the risk of overturning the façade, as it likely happened in the present case. The shear mechanisms, being in-plane, are mainly activated when the building presents a global behaviour, whereas the San Agustin church collapses due to local failures of its macro-elements.

Many studies have demonstrated that the use of FEM non-linear dynamic analysis to assess complex buildings is accurate since it can reproduce, in a realistic way, the behaviour of the structures. Nonetheless, it is highly time-consuming and consequently requires a high computational cost. In this

regard, pushover analysis is a practical tool, presenting a good trade-off between computational burden and accuracy of the results (Endo et al., 2015; Roca et al., 2010).

5.5. Conclusion

In order to assess the San Agustin church, two types of analysis are presented in Chapter 5: a nonlinear time history analysis and a static nonlinear analysis (pushover). The resultant damage state is described in detail and an evaluation of the span openings is done in four points: the impost line of: (A) the transverse arch east; (B) the transverse arch west; (C) the middle section of the barrel vault; (D) the edge of the barrel vault. The main purpose is to better understand the seismic behaviour of the building.

For the dynamic analysis, eight records of real earthquakes were considered. The damages allowed to identify parts of the building, known as macro-elements, that behave almost independently during a seismic event. These parts are very similar to the damages seen in previous events in single nave churches from the 16th century, located in Mexico. Through a comparison of the lateral displacements generated in the higher part of four macro-elements (namely, the south wall under the dome, south wall in the nave, south tower and north tower), it was possible to better understand the impact of the records in the structure. Major displacements were found in the transverse direction (X) for the south tower (0.11%), the south wall (nave) (0.15%), and the north tower (0.43%), due to the signal THEZ. The south wall (dome) presented more deformation for the signal SAPP (0.15%), followed by OXCU and THEZ (0.13%). In the longitudinal direction (Y), the north tower is the macro-element most affected, with a displacement ratio under 0.14%, lower than half of the displacement presented in the same macro-element in the transverse direction for the THEZ record. The highest displacements in the vertical direction (Z) occur at the barrel vault and the groin vault, reaching around 15 mm in the last one. For the classification of the damage, a list of failure mechanisms is presented (based on the literature and considered applicable to the cases of Mexican heritage).

The selected records were characterised by containing frequencies likely to affect structures with low periods. A proof of this aspect is the damage that, at the time, they caused to historical monuments in the country. The magnitudes are M = 7.1 and M = 8.2, with different distances to the epicentre to consider the effect of the site, being the farter OAXM with 380 Km. It is noted that the maximum PGA is presented by the record SCRU (2.93 m/s^2), nevertheless, it was the record THEZ that mostly affected the building, with damages even higher than those resulting from the SCRU record. Thus, it can be stated that a high

PGA does not determine a high demand from a building. In addition, through the plot of the span openings, it is possible to say that the building was subjected to a very sudden deformation since an abrupt opening was obtained.

The damage caused by these records was described in detail and later classified according to the literature (DPCM, 2015; Fuentes et al., 2019). The towers are affected only by the RFPP and THEZ records, showing mechanisms M.27 and M.28. In all cases, the façade presents damages due to the interaction of irregularities in height (M.25). In addition, the records OAXM and THEZ produce damages due to shear behaviour, recognized due to the diagonal cracks developed from the corners of the choir loft window. The lateral walls suffer the following type of damages: 1) due to the interaction of macro-elements with in-plane and in-elevation irregularities (M.25); 2) damages due to the transverse response of the nave (M.5); 3) damages due to the overturning of the presbytery (M.16); and 4) shear mechanisms (M.17), probably induced by the last mechanism. In the case of the barrel vault, for the eight signals, two types of damages can be reported: 1) due to the transverse response of the nave (M.5), producing longitudinal cracks along the barrel vault; and 2) due to the interaction of macro-elements with in-plane and in-elevation irregularities (M.25) (e.g. hinges at the connection with the façade, connection with the dome, connection with the towers, or the changes in the transverse stiffness along the building). The transverse arches exhibit damage mainly in the area of the crown, for the eight records, due to a transverse response (M.13). The failures in the dome (M.14) show the opening of the base with the development of vertical cracks in the meridians in the area of the tension hoop. Although it is part of the mechanism formed in the overturning of the presbytery, the back wall presents localized damage for two records (OXCU and THEZ). Regarding the groin vault, the results for all the analyses show damage and formation of hinges at the crown and perimeter connections (M.18).

The damage occurred during the analysis is consistent with the failures of single nave churches located in the area affected by the earthquakes in September, 2017. These results support the idea of a classification of the damage as a tool not only to preserve and restore but also a tool to study more in depth the possible seismic vulnerability of the Mexican heritage.

From the pushover analyses (four directions: +X, -X, +Y and -Y), it is clear that the transverse direction of the building is the most critical. The pushover analysis in the X positive direction reached the maximum capacity of the building for a load factor equal to 0.11, i.e. 21% lower than the maximum capacity in -X; 39% lower than the maximum capacity in +Y; and 27% lower than the maximum capacity in -Y. The higher capacity occurs to the pushover in the +Y direction, with a load factor equal to 0.18.

The analyses in the transverse direction activate failure mechanisms related to the façade, the lateral walls, the choir loft, the barrel vault, the transverse arches, the dome, and the groin vault. The analyses in the longitudinal direction activate failure mechanisms related to the north tower, the façade, the south wall, the choir loft, the barrel vault, transverse arches, the dome and the groin vault. Thus, it is possible to conclude that the pushover analysis, as a combination of the four directions, is able to reproduce with good accuracy, the failure mechanism obtained through the dynamic analysis.

According to the literature review (Lourenço et al., 2011, 2016; Mendes, 2012), the geometrical features are considered one of the main concerns regarding the difficulties to characterize the seismic behaviour of existing masonry structures. Currently, it is even stated in the codes that the geometrical irregularities, either in plan or in elevation, should carefully be taken in the seismic assessment of an irregular masonry structure. In this case, this aspect is confirmed since many of the damages are originated in areas of interaction of sudden changes in the geometry of the building: e.g. different height in the elements like the façade and the tower; different stiffness in the parts of the building, such as the front of the building (i.e. the compound façade, towers, choir loft) compared to the rest; among others. These damages are very similar to the presented in the single nave churches that suffered damages due to the earthquakes of September 2017.

Chapter 6
Strengthening of San Agustin barrel vault

6.1. Introduction

Barrel vaults are vulnerable elements in Mexican architectural heritage, as noted in the literature (Meli, 2011; Peña & Manzano, 2015). The earthquakes of September 2017 induced significant damages to the vaults of single nave temples such as *San Juan Bautista* in Morelos (**Figure 6-1a**), *La Virgen del Patrocinio*, *San Francisco del Mar*, *Santiago Apostol*, *San Vicente Ferrer* and *La Virgen del Rosario* in Oaxaca (**Figure 6-1b** to **f**). The same effect was seen at the vaults of cloister corridors, as shown in **Figure 6-1h** for the ex-convent of *Santo Domingo de Guzman* in Oaxaca; or, in **Figure 6-1g**, at the corridors of the Augustinian ex-convent of *Malinalco*, in Mexico state. *San Agustin* church, the historical building adopted in this thesis as a case study, is not an exception. During the last decade, the damage

has appeared along the nave, mainly in the earthquake of April 18th, 2014, when some small pieces of plaster from the barrel vault fell during a liturgy, alarming the church members.

Figure 6-1. Damages at barrel vaults due to the earthquakes of September 2017: a) temple of *San Juan Bautista*, Tlayacapan, Morelos (Ojeda, 2017); b) temple of *La Virgen del Patrocinio*, Oaxaca, Oaxaca (TARES, 2017c); c) temple of *San Francisco del Mar*, Juchitan, Oaxaca (TARES, 2017b); d) parish of *Santiago Apostol*, Niltepec, Oaxaca.(TARES, 2017a); e) temple of *San Vicente Ferrer*, Juchitan, Oaxaca (Matías, 2017); f) temple of *La Virgen del Rosario*, Juchitan, Oaxaca (TARES, 2017d); g) corridor of cloister, ex-convent of *Santo Domingo de Guzman*, Tehuantepec, Oaxaca (Sierra, 2017); h) corridor of cloister, Augustinian ex-convent of *Malinalco*, Mexico (Castañares, 2017).

Several techniques are used to repair and strengthening historical barrel vaults. The most common are: 1) injection of cracks with natural lime-based grout; 2) ties to prevent the horizontal displacement of the supports; 3) overlay of composite materials, such as fibre-reinforced polymers (FRP) or textile-reinforced mortar (TRM); 4) stiffening ribs, usually at the extrados of the vault (Nowak & Orłowicz, 2019).

In the case of injection, the recovery of the original state is achieved through the filling of voids and cracks, improving the continuity of the existing material and providing stability and homogeneity to the structure. This procedure increases the shear resistance and improves the in-plane behaviour (Doran et al., 2019; Luso & Lourenço, 2016). In arches and vaults, tie-rods are used to control the horizontal thrusts caused

by permanent and accidental loads. Calderini et al. (2012) performed a study where it is proved, by means of laboratory testing, that the presence of these elements increases the displacement capacity of the structure. It is worth noting that, in that study, the collapse mechanism changes in comparison with the original URM models. Coïsson et al. (2019) performed a dynamic assessment of the work conditions of buildings that were reinforced using tie-rods in order to support the decision-making process for their preservation. Several examples located in Italy, as The *Fontanellato* fortress or the dome of *Madonna dell'Umiltà* in Pistoia, were analysed. In the last years, FRP has been widely studied as a solution for enhancing the characteristics of strength and deformation capacity of structures. Several examples, mainly for the strengthening of URM vaults and arches, can be found in the literature (Anania et al., 2013; Carozzi et al., 2018; Chiozzi et al., 2016, 2017; Corradi et al., 2015; El-Salakawy et al., 2014). Nevertheless, the presence of epoxy adhesives also has many drawbacks, such as damp and thermal compatibility problems, lack of fire resistance, irreversibility, and poor bond to rough masonry surfaces, among others (Kouris & Triantafillou, 2018). TRM systems offer the same benefits as FRP, but the inorganic matrix in TRM, rather than epoxy adhesives, reduces the disadvantages. However, the efficacy of TRM strengthening depends, to a large extent, on the proper in situ application and is affected by the bond strength between the materials (Alecci et al., 2017; De-Santis et al., 2017; De Santis et al., 2019). Stiffeners are usually located at the extrados of the vaults and can be made of different materials like reinforced concrete, masonry, steel sections or glued laminated wood (Nowak & Orłowicz, 2019).

In order to improve the structural performance of the barrel vault of *San Agustin* church, three different reinforcement configurations are suggested: 1) tie-rods at the impost of the transverse arches; 2) reinforcement with TRM at the intrados of the vault; and 3) a combinated masonry stiffener-TRM system at the extrados of the barrel vault. This last technique can be described as masonry stiffeners connected to the extrados of the barrel vault, wrapped with a layer of basalt-stainless steel TRM (KeraKoll, 2017). A similar scheme is presented by Giuriani and Marini (2008) for the vulnerability assessment and strengthening of historic churches in northern Italy after a strong earthquake in the Benaco region in 2004. One of the analysed techniques corresponds to the implementation of lightweight spandrel ribs, a resisting cross-section made of clay mortar reinforced with plaster meshes with a polystyrene core. Anania et al. (2013) study the so-called Ω-wrap technique. This solution is based on the use of composite materials (FRP) applied around a high-resistance mortar core rib at the barrel vault extrados.

In this chapter, the results of six reinforcement configurations are analysed through FEM models and pushover analysis (POA). The different schemes are described as follows:

- Configuration 1: ties at the impost line of the transverse arches

- Configuration 2: masonry stiffener connected to the extrados of the barrel vault through TRM
- Configuration 3: reinforcement at the intrados with TRM
- Configuration 4: a combination of scheme 1 plus scheme 2
- Configuration 5: a combination of scheme 1 plus scheme 3
- Configuration 6: a combination of the first three schemes

The results are compared with the ones obtained from the pushover analyses (POA's) of the URM building in Chapter 5.

6.2. Modelling

The final 3D FEM model (407,022 TE12L elements with 91,953 nodes), described in Chapter 4, was modified to add the elements for each one of the reinforcement schemes. The ties are modelled as 1D elements, namely 3D truss (L6TRU), with a cross-section equal to 8.04 cm^2 and a diameter of 32 mm. Plates are located at the exterior faces of the walls to provide a proper connection with the masonry. The dimensions of the plates are shown in **Figure 6-2a** and **b**. Due to the geometry of the building, in the south wall the plates have a cross shape, while in the north wall only one key is present. The plates are modelled as sheets, namely regular curved shells (T15SH) with a thickness equal to 50 mm. The masonry stiffeners are modelled as structural solids (TE12L). Their location in the building and dimensions are shown in **Figure 6-2c** and **d**. The TRM technique is modelled as reinforcement sheets, namely a reinforcement grid embedded in the solid elements of the stiffener and the barrel vault. **Table 6-1** describes the final characteristics of the models, for the URM and each one of the reinforcement configurations. The material properties for the base model are described in Chapter 4. The properties for the materials employed for the strengthening are defined according to technical information (CVGSA, 2019; KeraKoll, 2017), standards (EN 1996-1-1, 2005; NTC, 2018) and literature (Angelillo et al., 2014; Lourenço, 1996, 1998, 2008, 2009; Vasconcelos, 2005). **Table 6-2** to **Table 6-4** present the mechanical properties assigned to the reinforcement materials.

POA's are performed in four directions (+X, -X, +Y, -Y), following the same approach adopted in Chapter 5. In order to make comparisons, the same three control points are selected to plot the capacity curves for each one of the reinforcement schemes: (CP-1) top of the dome; (CP-2) top of the north tower; and (CP-3) top of the south tower (see **Figure 5-15**).

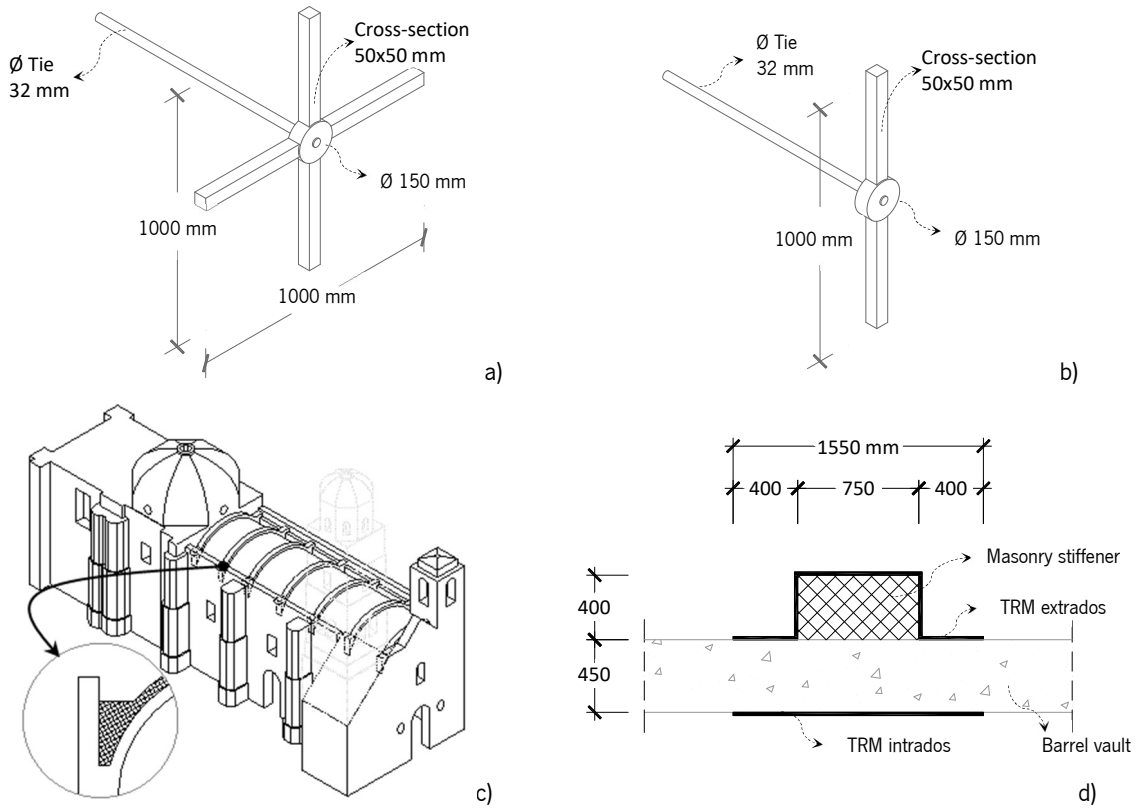

Figure 6-2. a) Dimensions of anchorage plates at the south wall; b) dimensions of anchorage plates at the north wall; c) location of the masonry stiffeners in the building; d) dimensions of the masonry stiffener and TRM (extrados and intrados).

Table 6-1. Type of strengthening technique and number of elements of the strengthened models for the six schemes.

Configuration	3D elements (TE12L)		Ties (L6TRU)	Anchor plates (T15SH)	Embedded reinforcement grid		Total number of	
	Building	Stiffener			Extrados	Intrados	Elements	Nodes
URM model	407,022	-	-	-	-	-	407,022	91,953
1	486,142	-	2	358	-	-	486,502	108,443
2	491,791	14,900	-	-	YES	-	506,691	112,675
3	485,759	-	-	-	-	YES	485,759	125,869
4	491,791	14,900	2	358	YES	-	485,415	148,659
5	491,791	-	2	358	-	YES	492,151	127,479
6	491,791	14,900	2	358	YES	YES	507,051	166,220

TE12L: four-node, three-side isoparametric solid tetrahedron element; L6TRU: a two-node directly integrated truss element; T15SH: three-node triangular isoparametric curved shell element.

Table 6-2. Mechanical properties for the masonry stiffener (M_{Stiff}).

Material	Linear parameters			Compressive parameters		Tensile parameters	
	E (GPa)	w (kN/m³)	v	f_c (MPa)	G_c (N/mm)	f_t (MPa)	G_f (N/mm)
M_{Stiff}	10.4	19.1	0.2	10.4	16.6	1.0	0.02

E: Young's modulus (1000 f_c); w: specific weight; v: Poisson's ratio; G_c: compressive fracture energy; f_t: tensile strength; G_t: tensile fracture energy.

Table 6-3. Mechanical properties for the TRM system.

Material	Linear parameters			Compressive parameters		Tensile Parameters		
	E	w (kN/m³)	t (mm)	f_c (MPa)	ε_c	f_y (MPa)	f_u (MPa)	ε_u
Grid	62 (GPa)	15.5	9	-	-	652	652	0.034
Mortar	15 (MPa)			9.85	0.035	-	-	-

E: Young's modulus; w: specific weight; t: thickness; f_c: compressive strength; ε_c: ultimate compression strain; f_y: yielding tensile strength; f_u: ultimate tensile strength ε_u: ultimate tensile strain.

Table 6-4. Mechanical properties for the steel ties and anchorage plates.

Material	Linear parameters			Tensile parameters		
	E (GPa)	w (kN/m³)	v	f_y (MPa)	f_u (MPa)	ε_u
Steel	200	76	0.3	210	510	0.35

E: Young's modulus; w: specific weight; v: Poisson's ratio; f_y: yielding tensile strength; f_u: ultimate tensile strength; ε_u: ultimate strain.

6.3. Seismic evaluation of the strengthened building

A division of the six configurations is done for this Section: the first three are compared as individual techniques and the last three are presented as the combination of the individual techniques. All the plots are presented in terms of load factor (same scale with a maximum value of 0.24) and displacement in cm (the scale varies according to the direction of the POA). The curves for the URM building are presented in red while the results for the strengthening are plotted in black. A horizontal line with the legend URM_{MAX} indicates the maximum URM capacity value in terms of load factor. The associated failure mechanism is

presented in the bottom of each plot, showing the principal strains (E1) at the ultimate capacity presented in the plot.

6.3.1. Individual strengthening techniques: configurations 1 to 3

The individual strengthening techniques are evaluated in this Section. A description of the individual strengthening techniques is presented in **Table 6-5**. **Table 6-6** presents the results of the eigenvalue analysis considering the frequencies of the calibrated modes selected in Chapter 4. The average frequency variation is equal to 5.1%, which as expected indicate almost no variation of the frequency with the applied strengthening. The only exception is Mode 6, which is involved in the vertical movement of the nave vault and is highly affected by the stiffeners added in configuration 2. **Figure 6-3** to **Figure 6-6** show the capacity curves for each direction of the POA's, namely +X, -X, +Y and -Y, respectively.

Table 6-5. Description of the strengthening configurations 1, 2 and 3.

Configuration	Description
1	Ties at the impost lines of both transverse arches
2	Masonry stiffeners on the extrados of the barrel vault connected through a TRM
3	Reinforcement at the intrados with TRM layers

Table 6-6. Frequencies of the calibrated modes of the URM model and for the strengthening configurations 1, 2 and 3.

Calibrated modes	URM model	Strengthening configuration		
	f_n (Hz)	f_{n1} (Hz)	f_{n2} (Hz)	f_{n3} (Hz)
Mode 1	1.50	1.50	1.53	1.51
Mode 2	1.68	1.68	1.69	1.68
Mode 3	2.36	2.36	2.43	2.37
Mode 6	3.71	3.72	5.62	3.80

In **Figure 6-3** a line at a load factor equal to 0.11 is plotted at the maximum capacity of the building without reinforcement. It shows that the three strengthening configurations increase the capacity of the building in terms of force, nonetheless, it seems that configuration 2 and 3 reduce the ductility, achieving a more brittle behaviour in comparison with configuration 1. In terms of percentage, configuration 1 increases to a load factor equal to 0.16, 47% above the URM; configuration 2 increases to a load factor

equal to 0.20, 83% above the URM; and configuration 3 increases to a load factor equal to 0.18, 62% above the URM.

The principal strains (E1), shown in **Figure 6-3**, describe graphically the failure modes for the +X POA for the strengthening configurations 1, 2 and 3. Configuration 1 exhibits the higher damage, although the mechanisms are similar for the three cases. The damage at the barrel vault reduces with the presence of the masonry stiffeners and TRM at the intrados.

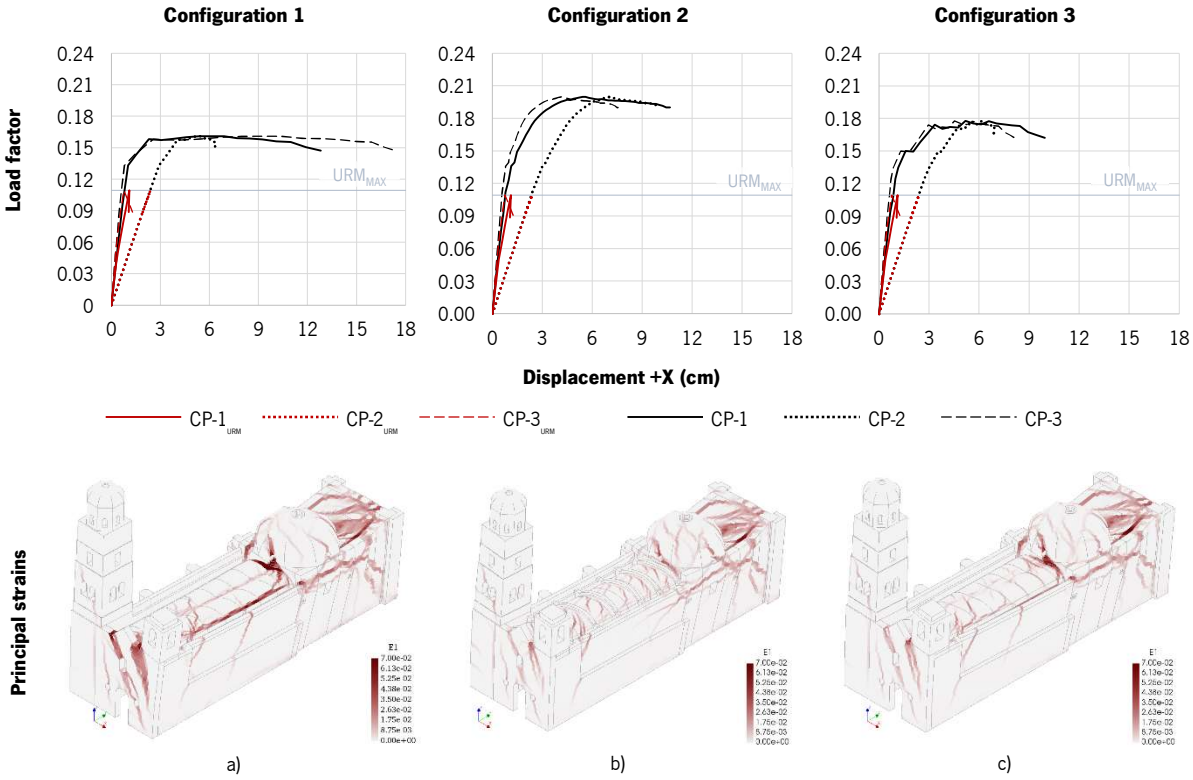

Figure 6-3. Capacity curves and principal strains (E1) for the +X POA. Strengthened configurations a) 1, b) 2 and c) 3.

For the POA's performed for the -X, the increment in the capacity ranges from 22% to 33% above the maximum capacity of the URM building (load factor equal to 0.14). In this direction, configuration 2 is the most favourable for the building in terms of load factor. The maximum increment in the capacity is 33%, the absolute value of the load factor is 0.19, slightly lower than the one reached at the +X POA, making this the critical direction for the strengthened building. According to the comparison of the principal strains (E1), the strengthening configuration 1 shows less damage, nonetheless, configurations 2 and 3 allow higher displacements. It should be noticed that the presence of the buttresses at the north wall decreases the damage extent in comparison with the +X POA's (**Figure 6-4**).

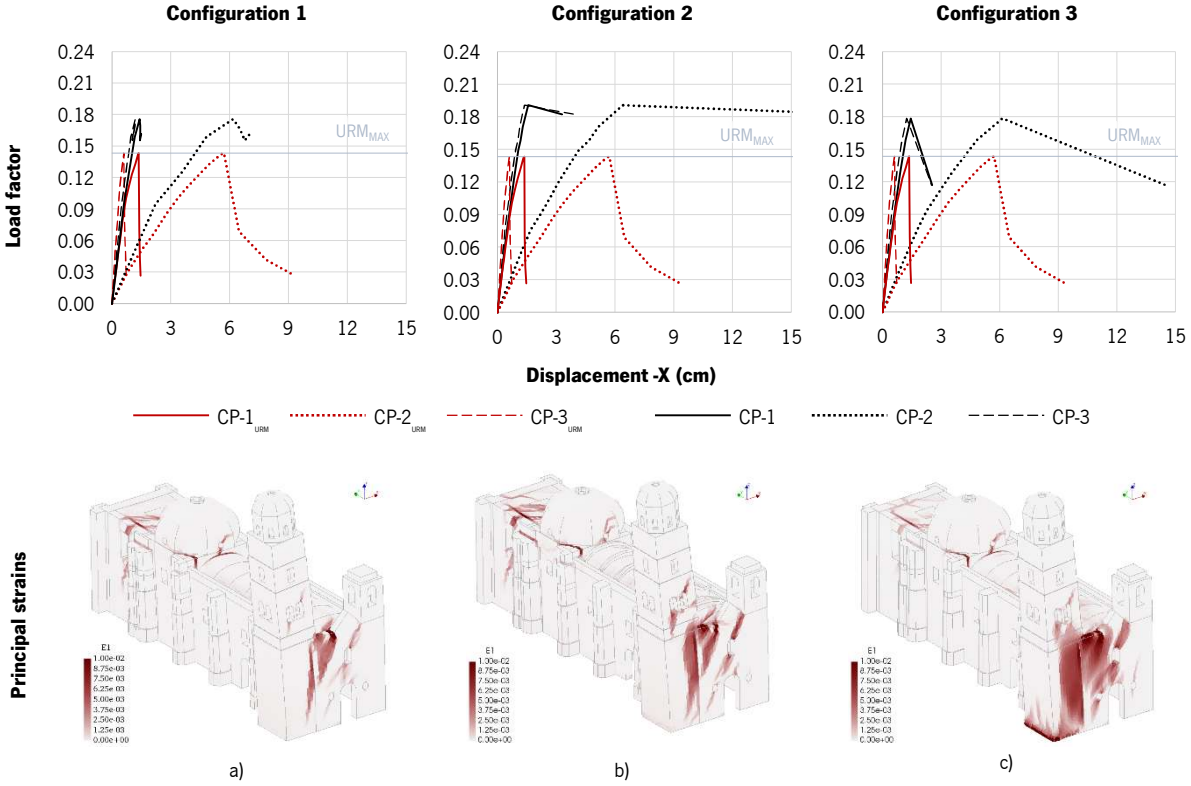

Figure 6-4. Capacity curves for the -X POA. Strengthened configurations a) 1, b) 2 and c) 3.

The three techniques presented in this Chapter influence mainly the response of the building in the transverse direction. Nonetheless, **Figure 6-5** shows that the longitudinal direction of the building is also affected by the intervention. As observed in the analyses for the URM building, the response in the longitudinal direction is mainly governed by the north tower, due to its geometry and slenderness. Indeed, the displacements reached by CP-2 are notably larger than those obtained by CP-1 and CP-3 (**Figure 6-5**). Regarding the load capacity, it is shown that the increments are between 15% and 23% above the load factor of 0.18 (maximum capacity of the URM building), in which the highest value occurs for configuration 3. The cracks are mainly located in the north tower and the presbytery (including the lateral walls and the groin vault). Significant differences cannot be detected in the failure mode of the three configurations.

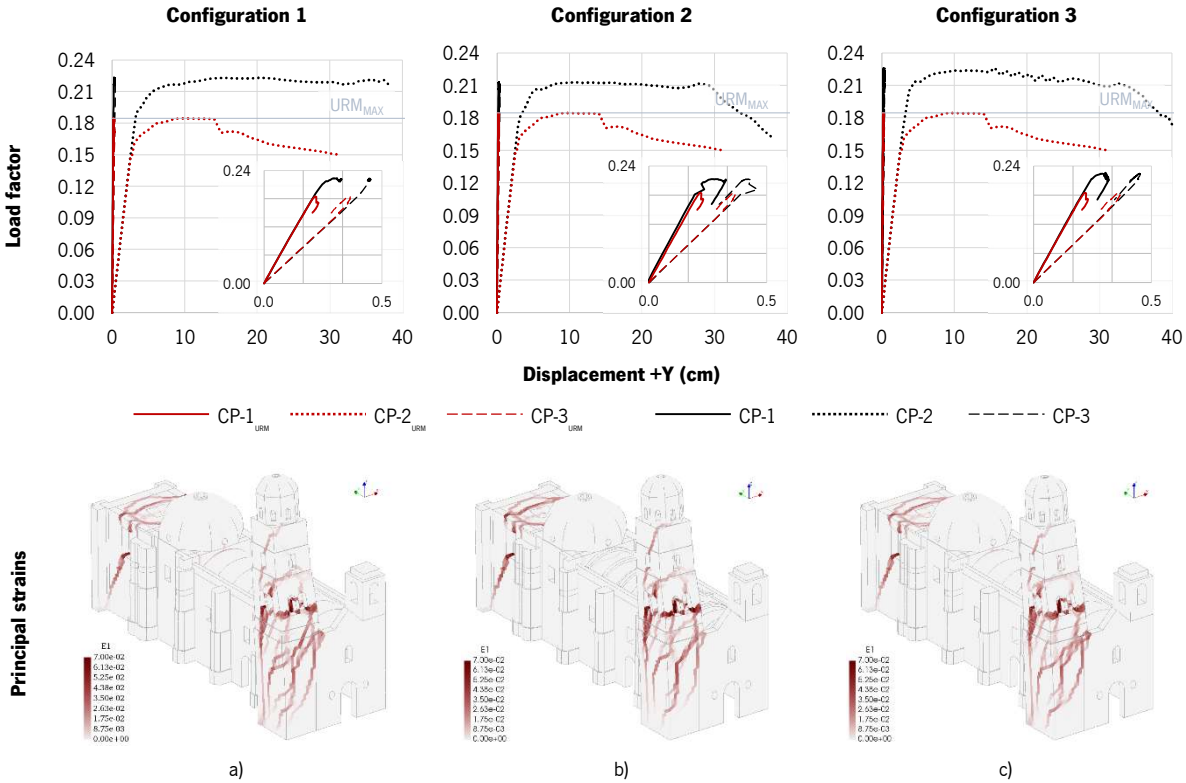

Figure 6-5. Capacity curves for the +Y POA. Strengthened configurations a) 1, b) 2 and c) 3.

As well as in the positive longitudinal direction, the negative (-Y) indicates an increment in the capacity of the building (**Figure 6-6**). Configurations 1 increases the capacity by 30%, configuration 2 by 49% and configuration 3 increases by 21%. The four curves for CP-1 (URM and the three strengthening techniques) show a linear behaviour and very small displacements (lower than 0.3 cm). This is consistent with the shape of the building, considering that the longitudinal direction is the stiffer one. The response in this direction is mainly governed by the out-of-plane behaviour of a macro-element formed by the façade, the south tower, the north tower and a segment of the choir loft. In the case of configuration 2 (strengthening at the extrados of the barrel vault), and although it was possible to continue the analysis for higher displacements, the principal stains reflect the results for deformations similar to configurations 1 and 3. Regarding the type of damage, the geometrical irregularities define three vertical cracks: 1) at the façade; 2) at the south wall; and 3) at the north wall along the connection with the north tower. Another clear crack occurs at the barrel vault, creating the macro-element.

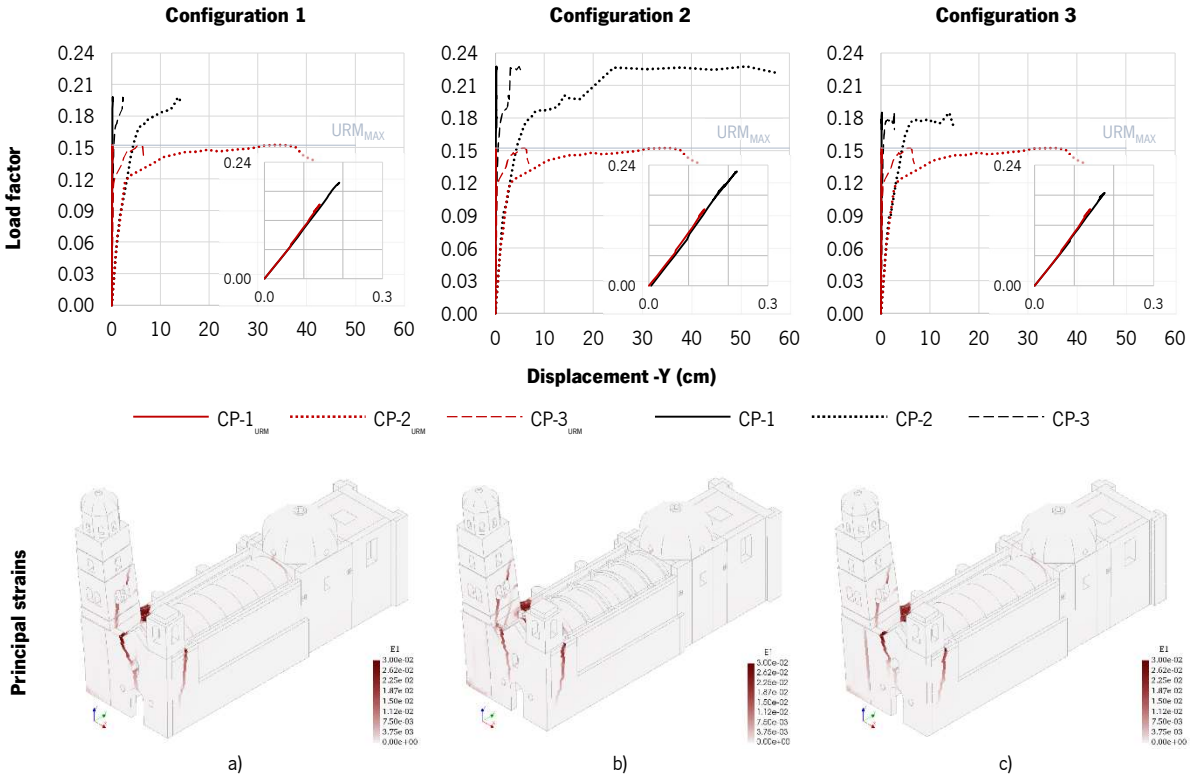

Figure 6-6. Capacity curves for the -Y POA. Strengthened configurations a) 1, b) 2 and c) 3.

6.3.2. Combination of strengthening techniques: configurations 4 to 6

The capacity curves presented hereafter show the comparison between the performance of the URM and the strengthened building for configurations 4 to 6. In order to clarify the adopted interventions, a description of the strengthening configurations is presented in **Table 6-7**.

Table 6-7. Description of the strengthening configurations 4, 5 and 6.

Configuration	Description
4	Ties at the impost lines of both the transverse arches and masonry stiffeners on the extrados of the barrel vault connected through a TRM layer
5	Ties at the impost lines of both the transverse arches and reinforcement at the intrados with TRM layers
6	Ties at the impost lines of both the transverse arches, masonry stiffeners on the extrados of the barrel vault connected through a TRM layer and reinforcement at the intrados with TRM

The frequency values, for the strengthened models 4, 5 and 6, are presented in **Table 6-8**, considering the mode shapes calibrated in Chapter 4. The average frequency variation is equal to 7.1%. Again, the changes in frequencies are minor, except for mode 6, when masonry stiffeners are added.

Table 6-8. Frequencies of the calibrated modes of the URM model and for the strengthening configurations 4, 5 and 6.

Calibrated modes	URM model	Strengthening configuration		
	f_n (Hz)	f_{n4} (Hz)	f_{n5} (Hz)	f_{n6} (Hz)
Mode 1	1.50	1.53	1.5	1.53
Mode 2	1.68	1.69	1.68	1.69
Mode 3	2.36	2.43	2.37	2.44
Mode 6	3.71	5.38	3.81	5.83

Figure 6-7 shows the curves for the +X POA, the maximum increment is reached by configuration 6 with a load factor equal to 0.21, 92% above the URM capacity. In the second place, configuration 4 increases by 87% (load factor rounded to 0.20), while configuration 5 is 76% above the URM capacity (load factor equal to 0.19). The initial stiffness related to CP-1 and CP-3 increase for the three configurations, while for CP-2 does not change significantly. In terms of displacement, the three configurations have a similar behaviour. It is noted that the implementation of the strengthening at the extrados (configurations 4 and 6) increases the capacity in terms of load factor. The principal strains show a similar failure mode. Nonetheless, the use of stiffeners at the extrados reduces the extent of the longitudinal damage at the crown and south haunch of the barrel vault.

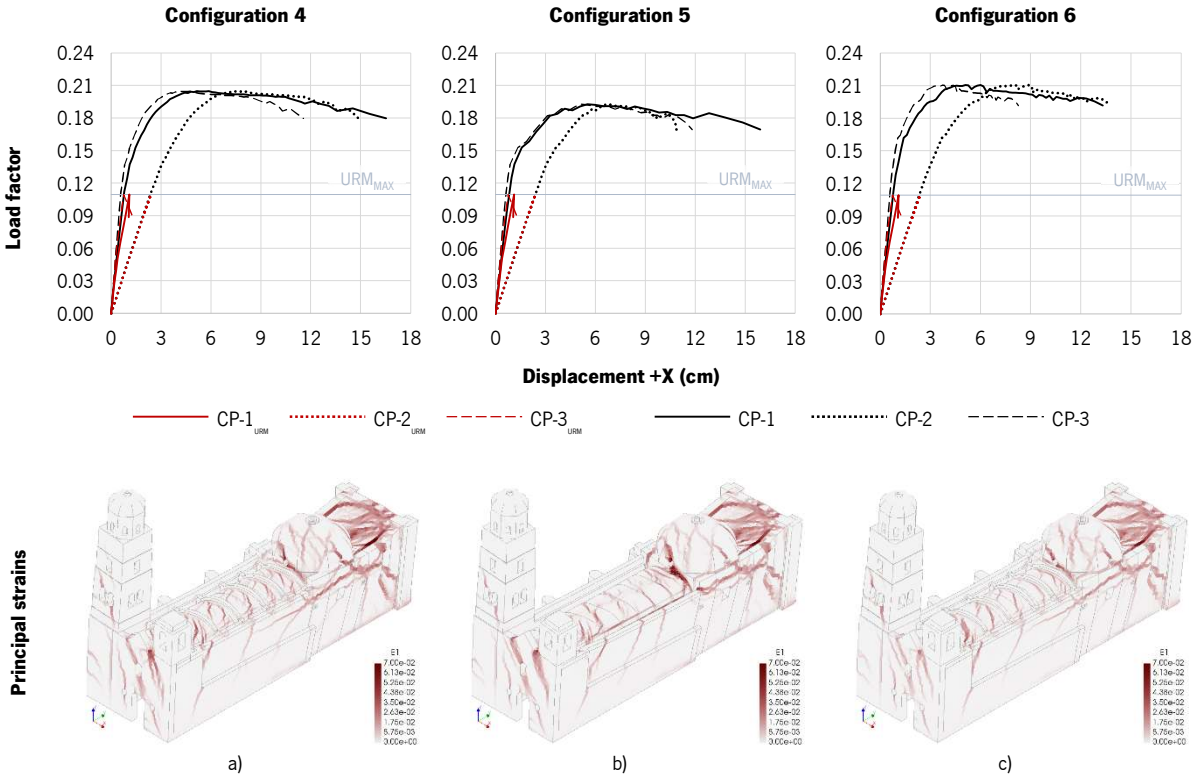

Figure 6-7. Capacity curves for the +X POA. Strengthened configurations a) 4, b) 5 and c) 6.

For the negative transversal direction (-X), **Figure 6-8** shows that configuration 5 presents the maximum increment in terms of load factor, namely 53% (load factor equal to 0.22). Configuration 4 has an increment of 30% and configuration 6 has an increment of 33%. The plotted principal strains (E1) correspond to the ultimate point of the capacity curve. For the three cases (configurations 4, 5 and 6) the damage at the façade and at the presbytery seems to be similar for the three cases.

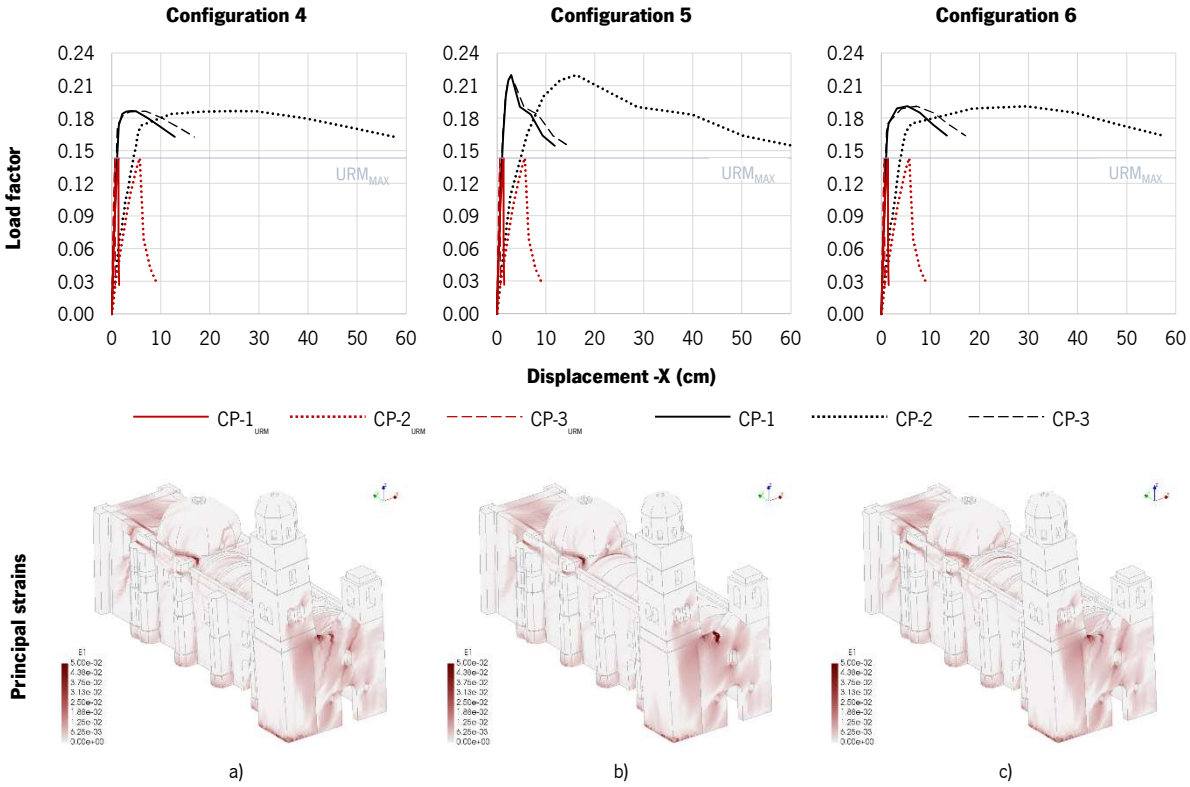

Figure 6-8. Capacity curves for the -X POA. Strengthened configurations a) 4, b) 5 and c) 6.

In contrast to the results of the analyses at the transverse direction, for the longitudinal direction, early cracking does not change significantly due to the strengthening, although the maximum load factor increases for the three configurations. The analysis in the +Y direction is related to the performance of the north tower since CP-1 and CP-3 exhibit very low displacements, in comparison with CP-2 (**Figure 6-9**). For this set of analyses, configuration 5 is the one with the higher increment in the capacity, showing a load factor equal to 0.23 that represents a capacity increment of 27%. A similar increment is provided by configurations 6, equal to 24% above the URM building. Finally, configuration 4 increases only 18% of the capacity. The displacements related to CP-1 and CP-3, reach values lower than 0.5 cm, while CP-2 curves present displacements higher than 40 cm for the three cases. The principal strains (E1) show that the most affected part is the north tower. Severe damage appears at the lower body and the belfry, mainly due to the slenderness of the tower and the in-elevation irregularities between the tower and the rest of the building. Damage also develops at the presbytery. Cracks appear at the lateral walls as well as at the groin vault as a result of a mechanism of rotation of the back wall.

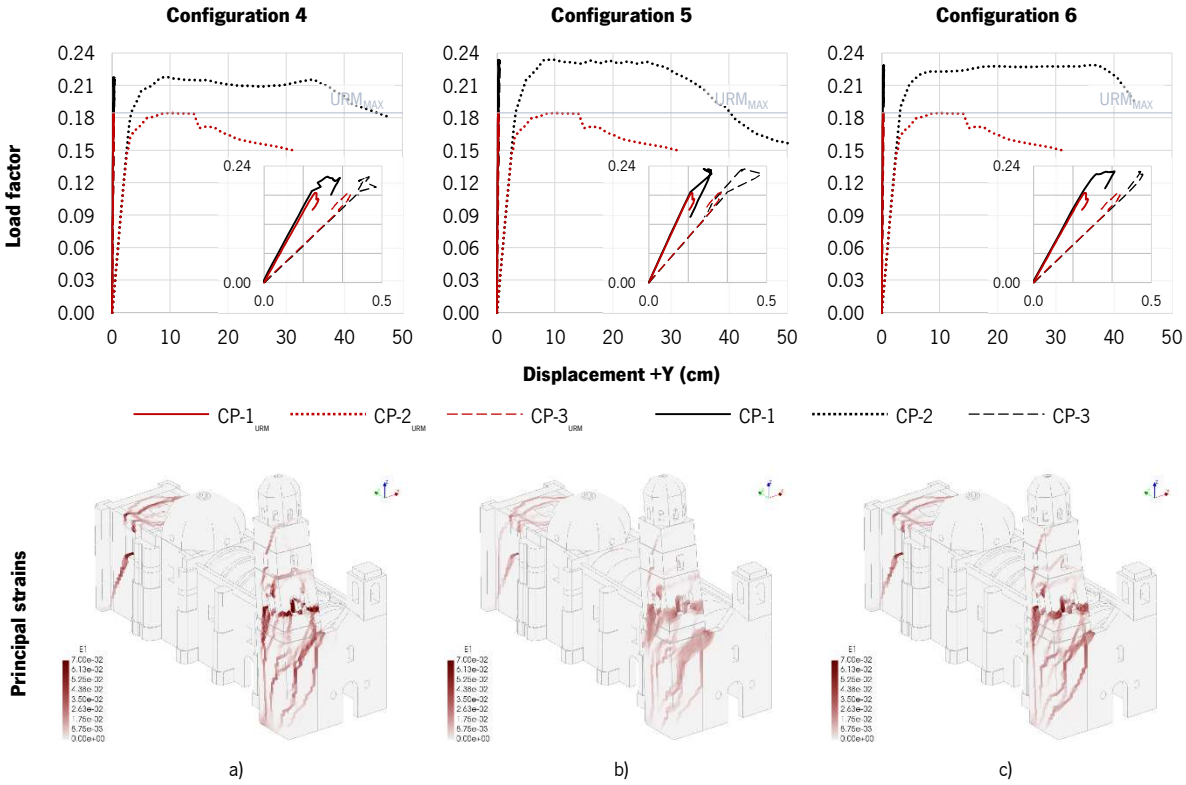

Figure 6-9. Capacity curves for the +Y POA. Strengthened configurations a) 4, b) 5 and c) 6.

In the negative longitudinal direction (-Y), CP-2 and CP-3 curves present the maximum displacement. The CP-1 curve exhibits a linear behaviour with a low displacement, similar to the results obtained by the same curves set for the +Y POA's. The maximum load capacity is presented by configuration 4, with an increment of 57%, with respect to the URM building. For the three configurations, the overturning of the façade and tower are the main failure modes. The post-peak behaviour, shown by the URM curves, follows a quasi-constant load factor of 0.15, with a detachment of the façade from the barrel vault. The presence of reinforcement elements that improve that specific connection increases the capacity. Configuration 6 produces an increment of 50%. However, the peak is followed by a significant drop of capacity, whereas configurations 4 and 5 present a plateau in the response.

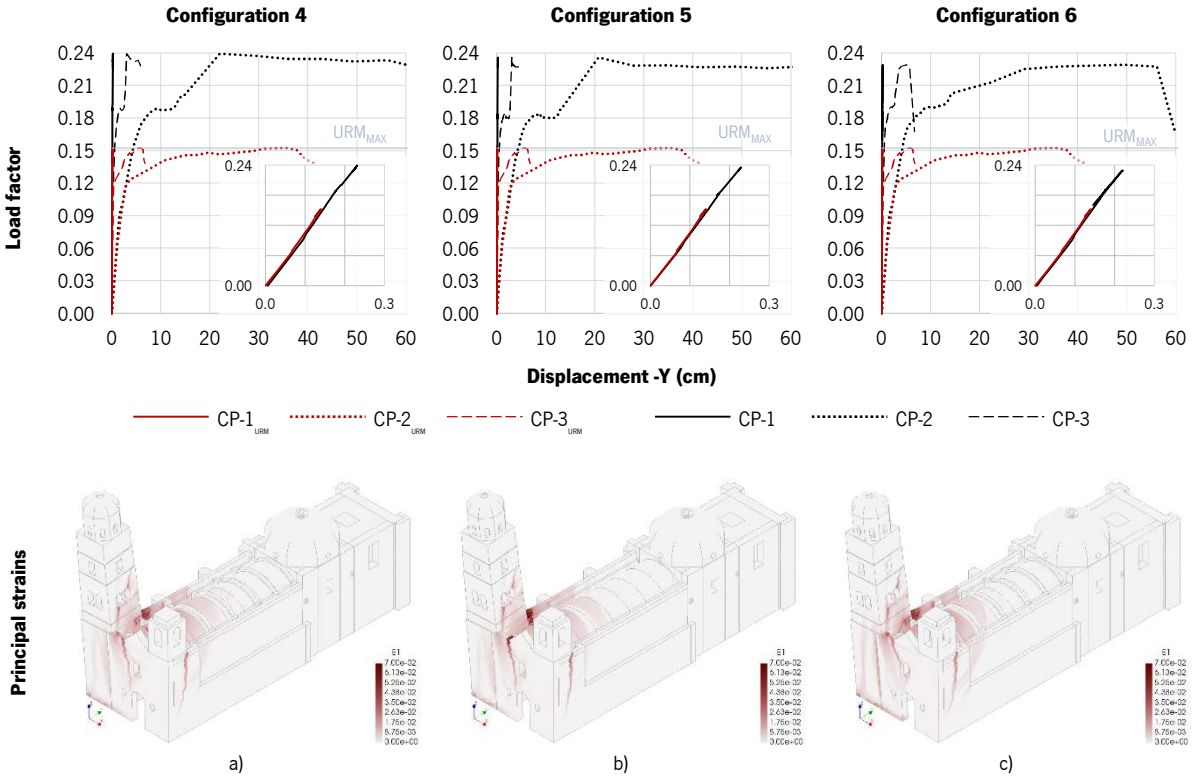

Figure 6-10. Capacity curves for the -Y POA. Strengthened configurations a) 4, b) 5 and c) 6.

6.4. Discussion of the results

Table 6-9 presents the effect of the six strengthening configurations in terms of natural frequencies of the calibrated modes, compared with the frequencies $\boldsymbol{f_n}$ of the URM model, as presented in Chapter 4. The comparison consists of determining the percentage difference of the frequencies for the same mode. Modes 3 and 6 are the most affected in all the cases. These results were expected since modes 1 and 2 are mainly related to the north tower and the strengthening techniques are focused mainly on the barrel vault. The application of the ties in the transverse arches and the strengthening at the intrados of the barrel vault do not modify significantly the frequency modes. On the other hand, as stated above, the presence of the masonry stiffeners at the extrados of the barrel vault changes significantly the frequencies of the modes, mode 6 (vertical mode of the barrel vault) is the most affected one, with increments in the frequency between 44 and 57%.

Table 6-9. Comparison of frequency modes between the URM model and each strengthened model.

Calibrated modes	URM	Strengthening configuration											
	f_n (Hz)	f_{n1} (Hz)	Δf (%)	f_{n2} (Hz)	Δf (%)	f_{n3} (Hz)	Δf (%)	f_{n4} (Hz)	Δf (%)	f_{n5} (Hz)	Δf (%)	f_{n6} (Hz)	Δf (%)
Mode 1	1.50	1.50	-	1.53	2.0	1.51	0.7	1.53	2.0	1.5	-	1.53	2.0
Mode 2	1.68	1.68	-	1.69	0.6	1.68	-	1.69	0.6	1.68	-	1.69	0.6
Mode 3	2.36	2.36	-	2.43	**3.0**	2.37	0.4	2.43	**3.0**	2.37	0.4	2.44	**3.4**
Mode 6	3.71	3.72	0.1	5.62	**51.1**	3.80	2.2	5.38	**44.6**	3.81	2.4	5.83	**56.7**

f_n: numerical frequency; Δf: increment in the frequency value; (-): negligible percentage; significant values highlighted in grey; significant percentages in bold.

Table 6-10 presents a summary of the POA results in terms of load factor (LF). The values in the column (**LF***) were obtained from the analyses carried out for the URM building (see Chapter 5). This comparison consists of determining the increment in the maximum capacity of the building in terms of force, considering the application of each strengthening configuration. The +X direction is the critical one for the URM building, with a LF equal to 0.11. It is, as well, the direction in which the increment of the capacity due to the strengthening is higher, with percentages ranging between 47% and 92%. The additional application of ties (configuration 4) presents an increase of about 5% with respect to strengthening with stiffeners at the extrados of the vault (configuration 2). On the other hand, the additional reinforcement at the intrados with TRM (configuration 6) presents a similar increase of the capacity of the building in the +X direction, with respect to configuration 4. In the case of the -X direction, the increments vary from 22% to 53%. In terms of maximum capacity values configuration 6 is the most effective for the positive direction, while configuration 5 is for the negative one (+X: 92%; -X: 53%). Regarding the longitudinal direction, configuration 5 and 4 present the higher increments: 27% and 57%, positive and negative, respectively. The percentages for **ΔLF** presented in **Table 6-10** show that, as expected, the studied techniques contribute more to the transverse direction than to the longitudinal one. It is notable that for the +Y direction, the variability of the improvement due to the studied configurations is the lowest, with a standard deviation of the increments equal to 4.3.

Table 6-10. URM capacity in comparison with the effect of the six strengthened configurations.

POA	URM	Strengthening configuration												ΔLF STD
	LF*	LF_1	ΔLF_1 (%)	LF_2	ΔLF_2 (%)	LF_3	ΔLF_3 (%)	LF_4	ΔLF_4 (%)	LF_5	ΔLF_5 (%)	LF_6	ΔLF_6 (%)	
+ X	0.11	0.16	47	0.20	83	0.18	62	0.20	87	0.19	76	**0.21**	**92**	17.0
- X	0.14	0.18	22	0.19	33	0.18	24	0.19	30	**0.22**	**53**	0.19	33	11.0
+ Y	0.18	0.22	21	0.21	15	0.23	23	0.22	18	**0.23**	**27**	0.23	24	4.3
- Y	0.15	0.20	30	0.23	49	0.19	21	**0.24**	**57**	0.24	55	0.23	50	14.7

LF: load factor; ΔLF: increment in the load factor; significant values highlighted in bold and grey.

Figure 6-11a presents the results in terms of load factor. The mean load factor of the strengthening techniques is equal to 0.19 and 0.22 in the transverse and longitudinal direction, respectively, which represents an increase of 53% and 35% respect to the URM building. **Figure 6-11b** presents a summary of the results in terms of percentage. As the plot shows, the POA in the +X direction shows the higher increments in the capacity.

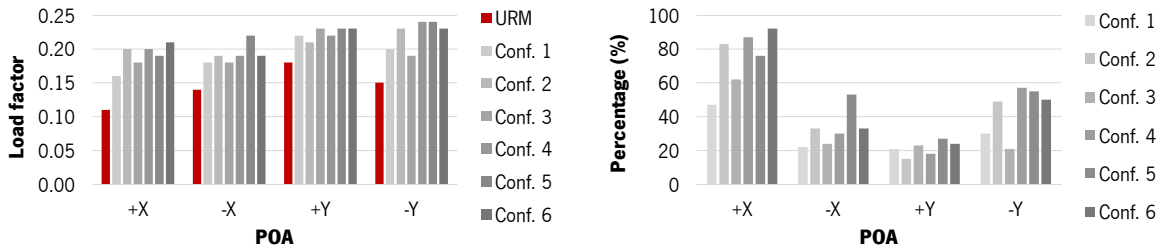

a) b)

Figure 6-11. a) Percentage of increment in the capacity of the strengthened building; b) final load factor due to the strengthened configuration in comparison with the URM building.

The response in each direction, independently of the strengthened configuration, presents the same specific failure mode. The activated mechanisms are not different among the strengthened models. Nonetheless, there are differences in the severity of damages that are also related to the maximum capacities reached for each analysis. **Table 5-3** presents a general list of the mechanisms activated for the analyses in each direction. Based on the graphical results for the principal strains (E1), presented in Section 6.3, the failure mechanisms can be briefly described as follows:

- For the **+X** direction, the global deformation of the building follows mainly the mode 3, which is the first transverse mode shape. This deformation causes damages in several longitudinal elements. There is higher damage in the south wall than in the north wall.
- For the **-X** direction, the deformation follows again mainly mode 3. Similarly, damage occurs at the roofing system and the lateral walls. In this case, the highest damage appears at the north wall.
- For the **+Y** direction, the presbytery suffers out-of-plane rotation, causing damage in the lateral walls (north and south) and the groin vault. Another structural element that suffers damage due to this set of analyses is the north tower, mainly due to the in-plane and in-elevation irregularities.
- For the **-Y** direction, the façade suffers out-of-plane rotation, which also affects the north tower and the connections with the orthogonal elements (lateral walls, choir loft and barrel vault). Independent of this mechanism, the north tower also presents rotation around the level of the belfry.

In general, the transverse arches are damaged in all the analysed scenarios, as well as the dome. Nonetheless, it seems that the arches are most affected by the seismic action in the transverse directions. On the other hand, the north tower seems to be most affected by the seismic action in the longitudinal directions.

Table 6-11. General failure mechanisms activated by the POA for the strengthened building.

Macro-element of San Agustin church	Mechanisms activated in the strengthened building			
	+X	-X	+Y	-Y
North tower	M.27 & M.28	M.27 & M.28	M.27 & M.28	M.27 & M.28
South tower	-	-	-	-
Façade	M.3 & M.25	M.3 & M.25	-	M.1
North lateral wall (nave)	M.5 & M.19	M.5	-	M.1
North lateral wall (dome)	M.5 & M.25	-	-	-
North lateral wall (presbytery)	M.5 & M.6	M.6	M.16	-
South lateral wall (nave)	M.5	-	-	M.1
South lateral wall (dome)	M.5	-	-	-
South lateral wall (presbytery)	-	-	M.16	-
Choir loft	M.29	M.29	-	M.29
Barrel vault	M.5	M.5	M.25	M.1
East transverse arch	M.13	M.13	M.13	M.13
West transverse arch	M.13	M.13	M.13	M.13
Dome	M.14	M.14	M.14	M.14
Presbytery back wall	M.16	M.16	M.16	-
Groin vault	M.18	M.18	M.18	M.18

See Annex D for graphical references.

6.5. Conclusions

The post-disaster surveys and the numerical analyses performed in the previous Chapter demonstrated that the barrel vaults of single nave typical Mexican temples are particularly vulnerable to seismic loading. Thus, six strengthening configurations were identified, based on a literature review, and analysed in order to reinforce this structural element, with specific attention to the *San Agustin* church. The first three schemes were the single techniques: 1) ties at the impost line of both the transverse arches; 2) masonry stiffeners on the extrados of the barrel vault connected through TRM layers; and 3) reinforcement at the intrados of the barrel vault with TRM layers. The other three schemes were combinations of the first three: 4) ties and reinforcement at the extrados; 5) ties and reinforcement at the intrados; and 6) ties, reinforcement at the extrados and reinforcement at the intrados.

Eigenvalue analyses were performed in order to compare the variation of the frequencies for each strengthened configuration. It was notable that the technique that most affects the structural behaviour is the presence of the stiffeners at the extrados of the barrel vault, influencing directly the first vertical mode, namely increasing its frequency by more than 45%. Mode 3, described as the first transversal mode, was also slightly affected. However, the variations reached only a maximum of 3%.

Pushover analyses in the main directions X-X and Y-Y were performed, for six models that represent each strengthening scheme. In order to compare them, the capacity curves were plotted for the same selected control points than for the URM building: CP-1 at the top of the dome; CP-2 at the top of the north tower; and CP-3 at the top of the south tower.

In terms of load factor, the six techniques resulted in an increment of the capacity of the structure. However, for the transverse direction X-X, the maximum capacity is reached for configuration 6, which is the combination of the ties in the transverse arches, the TRM reinforcement at the intrados of the barrel vault and the presence of the masonry stiffeners connected to the extrados of the barrel vault. The highest capacity in longitudinal direction Y-Y occurs for configuration 4, which includes only the ties and the reinforcement at the extrados of the barrel vault. The failure mechanisms were similar to those with no strengthening, with small changes depending on the configuration. Whenever the reinforcement of the barrel vault at the extrados was present, the distribution of the hinges at the crown of the vault changed: instead of a longitudinal and continuous crack, smaller and discontinuous cracks were developed. The X-X analyses are governed by a global transversal response, while the Y-Y direction is characterised by the out-of-plane rotation of the west or east extremes of the building, namely the presbytery or the façade.

It is worth mentioning that the use of a strengthening technique works always for a specific case study. For instance, an external solution should be evaluated when the internal visual appearance of the space is important, such as cases where the intrados of the roofing system is covered with “frescos”. In the analyses performed for San Agustin church, it is notable that only the use of the stiffeners on the extrados increased the capacity of the structure by 83% in the critical direction. It corresponds to a meaningful value, considering the LF (0.20) is higher than the PGA (0.10 g) for the city, reported by the INNEL (2017).

Chapter 7
Final remarks and future works

7.1. Conclusions

During the colonial era, namely between the 16th and 19th century, Mexican architecture evolved featuring a unique combination of the European models commissioned by the new ruling class. Still, a strong contribution of local manpower occurred, which favoured the preservation of the indigenous traditions. This mixture resulted in a peculiar symbiosis of immigrant and local expertise with different tones. Due to the administrative centralization of this influence, the strongest and "purest" impact of the European culture was produced in Mexico City and other relevant centres, while it faded away with distance from those points. The establishment and the following wide diffusion of the Franciscan, Augustinian and Dominican mendicant orders played a significant role in the creation and the evolution of this hybrid style. These orders all contributed for the penetration of the Spanish governance and the organisation of the population. Many cities developed around their convents, as in the case of Morelia, whose centre,

encompassing more than 200 historic buildings, is recognised by the UNESCO (1991) as an outstanding example of urban planning that combines the characteristics of the Spanish Renaissance with the Mesoamerican experience. Among the mendicant orders, Augustinian constructions were characterised by very ambitious projects, with single nave churches reaching between 60 and 70 m in length and more than 13 m in width. Starting from the 16th century, in a short time interval, a large number of convents with very similar geometrical characteristics and architectural features were commissioned by the Augustinians on more than half of the country, many of them in areas with moderate to high seismic hazard. Recent earthquakes demonstrated the vulnerability of such important Cultural Heritage, worsened by an alarming state of neglect and lack of maintenance. Due to the similarity of these churches, a detailed analysis of few representative case studies is likely to be a viable approach to deepen the understanding of their structural behaviour and test the effectiveness of traditional and innovative strengthening techniques. This also allows to generalise the results found. The barrel vault covering the single nave of this type of churches is of particular interest. To study the seismic behaviour of this element, a relevant case study was selected, namely, the temple of San Agustin, dated back to the 16th century and located in the historic centre of Morelia, capital of Michoacán. The church presented visible damage at the barrel vault due to an earthquake on April 18th, 2014, which attracted the attention of scholars, fostering the present work.

The final remarks of this study were divided in three main topics based on the methodology of the research: 1) modelling; 2) assessment; and 3) strengthening. The next subsections point out the most relevant conclusions regarding each topic.

7.1.1. Modelling of the case study

The first task of this work was the development of a detailed numerical 3D FEM model, based on an accurate characterisation of the case study geometry, material properties and structural details. Within this scope, an inspection of the church was performed, encompassing the damage survey. The dynamic properties of the building were estimated through dynamic identification tests under ambient vibration, mainly focused on the barrel vault. Triaxial accelerometers were adopted for the output only acquisition over sixty-one measurement points. Data processing through the ARTeMIS software, using the enhanced frequency domain decomposition method, allowed the identification of eight modes in a range between

1-5 Hz. The first global mode of the church corresponds to a mode in the transverse direction (1.52 Hz). The frequency of the first vertical mode of the barrel vault mode is equal to 3.71 Hz.

The 3D FEM model was developed in the environment of the DIANA software, adopting a macro-modelling approach. The definition of the material properties was based on literature review, codes and technical information. Material properties were calibrated to the results of the dynamic identification test, considering the four modes found relevant, by minimising the difference between numerical and experimental frequencies. To this end, Douglas and Reid method was adopted after a first manual calibration. The agreement between the fine-tuned model's and the experimental mode shapes was then checked through the estimation of the Modal Assurance Criterion (MAC), confirming the accuracy of the model.

It is worth noting that the initial values adopted for the mechanical properties, obtained from European standards and literature, provided a fairly good approximation of the values experimentally measured. This confirms that the existing recommendations are a viable approach to support model generation and analysis when testing data and more precise information are not available.

7.1.2. Seismic assessment of the barrel vault

According to the Mexican code and in order to consider the high seismicity of Mexico, the numerical model of the church was evaluated under eight seismic records collected by the Mexican Seismological System, considering the two horizontal and the vertical components. During these analyses, the building was able to stand an effective peak ground acceleration (PGA_{eff}) up to 0.15 g for the transverse direction. Besides nonlinear time history analyses, static nonlinear pushover analyses (POA) were also performed. As expected, the transverse direction of the building corresponds to the most critical one: a maximum load factor of 0.11 was reached. In the longitudinal direction the lower capacity obtained was equal to 0.15. Comparing the building capacity with the local demand in terms of expected PGA (0.10 g), as reported in the hazard map provided by the INNEL (2017), it is possible to conclude that the building would not collapse due to an expected earthquake, but it presents a low safety factor. The POA in the longitudinal and transverse directions activated different failure mechanisms related to distinct macro-elements of the building. By combining the failure mechanisms for all directions, it was possible to reproduce with good accuracy the damage scenarios obtained through the nonlinear time history analyses. The results of the numerical analyses allowed to conclude that the most seismic vulnerable

structural elements of the church are: 1) the barrel vault, the transverse arches and the dome due to the transverse response of the building; 2) the façade, the presbytery and the groin vault due to the longitudinal response. These scenarios are compatible with the damage identified during the survey. Moreover, the outcomes of both types of analyses are consistent with the failure mechanisms of similar single nave churches located in areas affected by the earthquakes of September 2017. This is likely supporting the reliability of the modelling strategy adopted in the research, which could be replicated for other relevant case studies of the Mexican Heritage. It is worth mentioning that the seismic behaviour of this typology of Mexican churches is strongly affected by the local response of its macro-elements, as well-known in European churches located in seismic areas. However, a classification of the failure mechanisms based on previous studies conducted in Europe does not find a complete correspondence for the Mexican temples, due to their specific geometrical and structural characteristics.

7.1.3. Strengthening of the building

Post-disaster surveys demonstrated that the barrel vaults of typical single nave Mexican temples are particularly vulnerable to seismic loading. The results of the numerical analyses carried out in this study also corroborated it. Thus, six strengthening configurations were defined to improve the seismic behaviour of the church, including the performance of the vault. The first three schemes adopted the following single techniques: 1) ties at the impost line of both the transverse arches; 2) masonry stiffeners on the extrados of the barrel vault connected through textile-reinforced mortar (TRM) layers; and 3) reinforcement at the intrados of the barrel vault with TRM layers. The other three schemes were combinations of the first three: 4) ties and reinforcement at the extrados; 5) ties and reinforcement at the intrados; and 6) ties, reinforcement at the extrados and reinforcement at the intrados.

From the eigenvalue analyses of the different strengthened configurations, it was notable that the stiffeners at the extrados of the barrel vault affected significantly the first vertical mode, changing the frequency value by more than 45%, while the other modes only reached variations around 3%.

In terms of load factor, the six techniques resulted in an increment of the capacity of the structure. However, for the transverse direction, the maximum capacity is reached for configuration 6, which is the combination of the ties in the transverse arches, the TRM reinforcement at the intrados of the barrel vault and the presence of the masonry stiffeners connected to the extrados of the barrel vault. The highest capacity in longitudinal direction occurs for configuration 4, which includes only the ties and the

reinforcement at the extrados of the barrel vault. The failure mechanisms were similar to those with no strengthening, with small changes depending on the configuration. Whenever the reinforcement of the barrel vault at the extrados was present, the distribution of the hinges at the crown of the vault changed: instead of a longitudinal and continuous crack, smaller and discontinuous cracks were developed. The transverse analyses are governed by a global transversal response, while the longitudinal direction is characterised by the out-of-plane rotation of the west or east extremes of the building, namely the presbytery or the façade.

Decision-making on the strengthening technique to be adopted should be evaluated for each case. For example, an external solution should be evaluated when the internal visual appearance of the space is important, such as the cases where the intrados of the vault is covered with frescos. In the analyses performed for San Agustin church, it is notable that, even by using only the stiffeners at the extrados, the capacity of the structure increased by 83% in the most vulnerable direction. This increase is associated with a load factor (0.20) twice as high as the PGA (0.10 g) for the site.

It is also possible to conclude that, in the case of San Agustin church, the application of masonry stiffeners at the extrados of the barrel vault connected through TRM layers (configuration 2) increases the capacity enough to avoid new damages at the barrel vault, without requiring an invasive strengthening at the intrados or ties in the transverse arches, which has visual impact in the inside view of the church.

7.2. Future works

The present thesis aim was to contribute to the preservation of the Mexican cultural heritage from an engineering point of view, by improving the knowledge of the seismic behaviour of a widespread typology of building and assessing the effectiveness of possible strengthening techniques. However, not all the components are considered completely covered. Further research is recommended in order to better understand, protect and tailor appropriate solutions to specific cases. Thus, the following topics are proposed as a future scope for a fruitful continuation of this work:

- Develop a detailed testing campaign to determine the mechanical properties of the endemic materials of this building typology.

- Assess the sensitivity of the seismic capacity to variation in the geometry, contemplating a more ambitious overview of the diversity in the typical single nave churches.
- Carry out dynamic identification testing on more significant cases, focusing not only on the barrel vaults, but also on all the most relevant structural elements.
- Improve the numerical analysis based on time history analysis using more records with different properties (e.g. frequency content, amplitude, duration, etc.), aiming at evaluating the possible occurrence of the new failure mechanisms and damage severity scenarios.
- Increase the detailing on the boundary conditions of the 3D models, namely the surrounding buildings and the convent area, in order to analyse the structural behaviour as a compound.
- Finally, a specific classification of the typical failure mechanisms for the Mexican Heritage, based on real post-earthquake surveys and analytical research, is recommended.

References

Ackerman, J. S. (1949). “ARS Sine Scientia Nihil EST”. Gothic Theory of Architecture at the Cathedral of Milan. *The Art Bulletin*, *31*(2), 84–111.

Aguila, I. (2010). *Iglesia de Santo Domingo, una construcción de los dominicos*. Creative Commons BY-NC. http://www.wikipuebla.poblanerias.com/iglesia-de-santo-domingo-una-construccion-de-los-dominicos/

Alagna, M. (2004). *The Great Fire of London of 1666* (1st ed.). The Rosen Publishing Group, Inc. https://books.google.pt/books?hl=es&lr=&id=KvlgeAfa-EMC&oi=fnd&pg=PA4&dq=london+1666&ots=ykEJ2jzLIW&sig=WYwTo3_Hb9oOu4nzwOFu2CbMzKo&redir_esc=y#v=onepage&q=london 1666&f=false

Alcocer, S. M., Aguilar, G., Flores, L., Bitrán, D., Durán, R., López-Bátiz, O. A., Pacheco, M. A., Reyes, C., Uribe, C. M., & Mendoza, M. J. (1999). *Informes Técnicos - El sismo de Tehuacán del 15 de Junio de 1999*.

Alecci, V., Focacci, F., Rovero, L., Stipo, G., & De Stefano, M. (2017). Intrados strengthening of brick masonry arches with different FRCM composites: Experimental and analytical investigations. *Composite Structures*, *176*, 898–909. https://doi.org/10.1016/j.compstruct.2017.06.023

Alejcasvi. (2009). *Picture: Fachada del Templo de Santa María Tonantzintla*. Publlic Domain. https://commons.wikimedia.org/wiki/File:Fachada_templo_sta_maría_tonantzintla.JPG

Alejo, L. E., Zavala, M., Martínez, G., & Jara, J. M. (2014). Influence of the geometric empirical rules in

the seismic behavior of religious historical buildings. In M. Chávez & F. Peña (Eds.), *9th International Conference on Structural Analysis of Historical Constructions (SAHC2014)* (pp. 1–14).

Alvesgaspar. (2014). *Picture: Main portal of the Museo de História de Madrid, former Real Hospicio de San Fernando*. Creative Commons Attribution-Share Alike 3.0 Unported. https://commons.wikimedia.org/wiki/File:Madrid_May_2014-25a.jpg

Alvesgaspar. (2016). *Picture: St. Vitus Cathedral, Prague*. Creative Commons Attribution-Share Alike 4.0 International. https://commons.wikimedia.org/wiki/File:St_Vitus_Prague_September_2016-21.jpg

Ambriz, A. (2017). *El convento de Cuitzeo*. https://www.youtube.com/watch?v=NR0JdN6nYrU

Anania, L., Badalà, A., & D'Agata, G. (2013). The post strengthening of the masonry vaults by the Ω-Wrap technique based on the use of C-FRP. *Construction and Building Materials*, *47*, 1053–1068. https://doi.org/10.1016/j.conbuildmat.2013.05.012

Angelillo, M., Lourenço, P. B., & Milani, G. (2014). Masonry behaviour and modelling. In M. Angelillo (Ed.), *Mechanics of Masonry Structures* (pp. 1–26). Springer-Verlag Wien. https://doi.org/10.1007/978-3-7091-1774-3_1

Animas, H., Pacheco, J., & Ortiz, J. Á. (2015). Assessment of the Structural Health of Heritage Constructions Based on the Changes of Frequency. In H. Barros, A. Loja, C. Ferreira, J. I. Barbosa, J. M. Adam, M. Fragiacomo, & A. R. Marí (Eds.), *International Conference on Recent Advances in Rehabilitation and Sustainability of Structures (RehabStructures 2015)* (pp. 1–18). https://www.researchgate.net/publication/277555847

Anual. (2010). *Picture: Fachada a plaza de San Francisco del edificio del Ayuntamiento de Sevilla*. Creative Commons Attribution-Share Alike 4.0 International. https://commons.wikimedia.org/wiki/File:Ayuntamiento_sevilla_2010_002.jpg

Autorino, S. (1994). *Memory of Islam : Culture and Politics in Sixteenth-century Religious Architecture of Mexico and Peru*. Massachusetts Institute of Technology.

Ayuntamiento de San Pedro Cholula. (2020). *Casa Del Caballero Águila*. San Pedro de Cholula. http://turismospcholula.mx/casa-caballero#

Badillo-Almaraz, H., Orduña-Bustamante, A., Quintero-Sifuentes, O., & Orozco-Rojas, J. (2019). Assessment of the Structural Damage on the Former San Agustin Temple Using Numerical Modelling. In *Structural Analysis of Historical Constructions. RILEM Bookseries* (Vol. 18, pp. 938–946). Springer. https://doi.org/10.1007/978-3-319-99441-3_101

Bailey, G. A. (2003). *Between Renaissance and Baroque: Jesuit Art in Rome, 1565-1610*. University of Toronto Press.

Barrett, A. A. (2020). III The Great Fire. In *Rome Is Burning* (pp. 57–113). Princeton University Press. https://www.degruyter.com/document/doi/10.1515/9780691208503-008/html

Bianchini, N., Mendes, N., & Lourenço, P. B. (2020). Seismic evaluation of Bagan heritage site (Myanmar): The Loka-Hteik-Pan temple. *Structures*, *24*(December 2019), 905–921. https://doi.org/10.1016/j.istruc.2020.01.020

Bothara, J., & Brzev, S. (2011). *A tutorial: Improving the seismic performance of stone masonry buildings* (A. Charleson (Ed.); 1st ed.). Earthquake Engineering Research Institute.

Brenišínová, M. (2016). Sixteenth-century Mexican Architecture : Transmission of Forms and Ideas

between the Old and the New World. *HISTORIE — OTÁZKY — PROBLÉMY*, *2*(12), 183–192.

Brincker, R., Zhang, L., & Andersen, P. (2001). Modal identification of output-only systems using frequency domain decomposition. *Smart Materials and Structures*, *10*(3), 441–445.

Bury, J. B. (1976). The Stylistic Term "Plateresque." *Journal of the Warburg and Courtauld Institutes*, *39*, 199–230. https://www.jstor.org/stable/751139

Cabrales Barajas, L. F. (2015). La ciudad imaginada: el paisaje neoclásico de Guadalajara y sus productores. *Investigaciones Geográficas*, *86*(86), 82–97. https://doi.org/10.14350/rig.42074

Cabrera, J. (2011). *Templos novohispanos de Valladolid/Morelia. Historia y teoría de su dimensionamiento estructural*.

Calderini, C., Lagomarsino, S., Rossi, M., Decanio, G., Mongelli, M. L., & Roselli, I. (2012). Seismic Behaviour of Masonry Arches with Tie-Rods : Dynamic Tests on a Scale Model. *15 WCEE*.

Carozzi, F. G., Poggi, C., Bertolesi, E., & Milani, G. (2018). Ancient masonry arches and vaults strengthened with TRM, SRG and FRP composites: Experimental evaluation. *Composite Structures*, *187*(October 2017), 466–480. https://doi.org/10.1016/j.compstruct.2017.12.075

Castañares, J. (2017). *Picture: convento agustino de Malinalco*. 19/S: El Dolor y La Esperanza. https://www.jornada.com.mx/2017/09/26/estados/036n1est

CCSEM - Committee on Culture, Science, E. and M. (2014). *Europe's endangered heritage*. source.

Chanfón Olmos, C. (1996). *Fundamentos teóricos de la restauración*. Facultad de Arquitectura, UNAM.

Chauvet, R. P. F. (1966). El convento mexicano y su función social. *Artes de México*, *86/87*, 10–11.

Chávez, M. M., & Meli, R. (2007). Ensaye en mesa vibradora de un templo típico colonial. *XVI Congreso Nacional de Ingeniería Sísmica*.

Chávez, M. M., & Meli, R. (2010). Ensaye En Mesa Vibradora De Un Templo Típico Colonial: Evaluación De Dos Esquemas De Refuerzo. *XVII Congreso Nacional de Ingeniería Estructural*, *55*, 1–17.

Chiozzi, A., Milani, G., Grillanda, N., & Tralli, A. (2016). An adaptive procedure for the limit analysis of FRP reinforced masonry vaults and applications. *American Journal of Engineering and Applied Sciences*, *9*(3), 735–745. https://doi.org/10.3844/ajeassp.2016.735.745

Chiozzi, A., Milani, G., & Tralli, A. (2017). Fast Kinematic Limit Analysis of FRP-Reinforced Masonry Vaults. II: Numerical Simulations. *Journal of Engineering Mechanics*, *143*(9), 04017072. https://doi.org/10.1061/(ASCE)EM.1943-7889.0001268

Circolare n. 7. (2019). Circolare 21 gennaio 2019, n. 7 Istruzioni per l'applicazione dell'«Aggiornamento delle "Norme tecniche per le costruzioni"». In *Gazzetta Ufficiale della Repubblica Italiana* (Vol. 35). Ministero delle infrastrutture e dei trasporti.

Coïsson, E., Collini, L., Ferrari, L., Garziera, R., & Riabova, K. (2019). Dynamical Assessment of the Work Conditions of Reinforcement Tie-Rods in Historical Masonry Structures. *International Journal of Architectural Heritage*, *13*(3), 358–370. https://doi.org/10.1080/15583058.2018.1563231

Collinson, P., Ramsay, N., & Sparks, M. (1995). *A history of Canterbury Cathedral*. Oxford University Press, Oxford.

Compean, M. (2015). *Exploring Mexican Hybrid Baroque : New Perspectives on Colonial Architectural Sculpture by*. Carleton University.

Contreras, M. (2019). *Picture: Casa de la Marquesa is an ancient building located in the World Heritage*

Site "Historic centre of Santiago de Querétaro." Creative Commons Attribution-Share Alike 4.0 International License. https://commons.m.wikimedia.org/wiki/File:Casa_de_la_Marquesa_en_Querétaro.jpg

Cook, D., Van Orden, A., Reyes, J., Oh, S., Balasubramanian, R., Carpio, J., & Townsend, H. (2000). Atmospheric Corrosion in Marine Environments along the Gulf of México. In S. Dean, G. Delgadillo, & J. Bushman (Eds.), *Marine Corrosion in Tropical Environments* (pp. 75-75–23). ASTM International. https://doi.org/10.1520/STP13555S

Corradi, M., Borri, A., Castori, G., & Coventry, K. (2015). Experimental Analysis of Dynamic Effects of FRP Reinforced Masonry Vaults. *Materials*, *November*, 8059–8071. https://doi.org/10.3390/ma8125445

Cotilla-Rodríguez, M. O., Córdoba-Barba, D., & Núnez-Cornú, F. J. (2019). Caracterización Sismotectónica de México. *Revista Geográfica de América Central*, *2*(63), 103–139. https://doi.org/10.15359/rgac.63-2.4

CVGSA. (2019). *Documento de declaração de desempenho No: 02CVG121119*.

De-Santis, S., Carozzi, F. G., de Felice, G., & Poggi, C. (2017). Test methods for Textile Reinforced Mortar systems. *Composites Part B: Engineering*, *127*, 121–132. https://doi.org/10.1016/j.compositesb.2017.03.016

De Santis, S., Roscini, F., & de Felice, G. (2019). Strengthening of Masonry Vaults with Textile Reinforced Mortars. In R. Aguilar, D. Torrealva, S. Moreira, M. A. Pando, & L. F. Ramos (Eds.), *Structural Analysis of Historical Constructions. RILEM Bookseries* (Vol. 18, pp. 1539–1547). Springer, Cham. https://doi.org/10.1007/978-3-319-99441-3_165

Delgado, C. (2012). *Picture: Cathedral of St. Mary, Segovia, Spain.* Creative Commons Attribution-Share Alike 3.0 Unported. https://commons.wikimedia.org/wiki/File:Catedral_de_Santa_María_de_Segovia_-_01.jpg

Deth, K. (2016). *Picture: Front view of Cathedral-Basilica of Our Lady of the Pillar in Zaragoza, Spain*. Creative Commons Attribution-Share Alike 4.0 International. https://commons.wikimedia.org/wiki/File:Catedral-Basílica_de_Nuestra_Señora_del_Pilar_(Front).jpg

DIANA. (2020). *DIANA Finite Element Analysis. Release 10.4* (10.4). DIANA FEA bv. https://dianafea.com/

Doglioni, F., Moretti, A., & Petrini, V. (1994). *Le chiese e il terremoto* (Lint Editoriale Associati (Ed.)). Trieste.

Doran, B., Yuzer, N., Aktan, S., Oktay, D., & Ulukaya, S. (2019). Numerical Modeling of Traditional Masonry Walls Strengthened with Grout Injection. *International Journal of Architectural Heritage*, *14*(10), 1517–1532. https://doi.org/10.1080/15583058.2019.1618970

Douglas, B., & Reid, W. (1982). Dynamic tests and system identification of bridges. *Journal of the Structural Division*, *108*(10), 2295–2312.

DPCM - Direttiva del Presidente del Consiglio dei Ministri. (2015). *Direttiva del Ministro dei beni e delle attività culturali e del turismo Aggiornamento della direttiva del 12 dicembre 2013 "Procedure per la gestione delle attività di messa in sicurezza e salvaguardia del patrimonio culturale in caso di emergenze deriva*. Gazzetta n. 169 del 23 luglio 2015. Gazzetta Ufficiale della Republica Italiana.

Dudley, C. J. (2010). *Canterbury Cathedral: Aspects of Its Sacramental Geometry*. Xlibris Corporation.

Ecelan. (2004). *Picture: La Aljafería - Sala del trono - Techumbre. Artesonado en La Aljafería de Zaragoza*. Creative Commons Attribution-Share Alike 3.0 Unported. https://commons.wikimedia.org/wiki/File:La_Aljafería_-_Sala_del_trono_-_Techumbre.JPG

El-Salakawy, T. S., Kamal, O. A., El-Hariri, O. R., & Hamdy, G. A. (2014). Experimental Investigation for Masonry Vaults/Walls Strengthened Using Different Techniques. *International Journal of Civil Engineering and Technology*, *5*(12), 354–365.

Elyamani, A., & Roca, P. (2018). A review on the study of historical structures using integrated invetigation activities for seismic safety assessment. Part II: Model updating and seismic analysis. *Cultura Científica*, *4*(1), 29–51. https://doi.org/10.5281/zenodo.1048243

EN - Encyclopaedia Britannica. (2020). *Ring of Fire*. Encyclopaedia Britannica, Inc. https://www.britannica.com/place/Ring-of-Fire

EN 1996-1-1. (2005). *Eurocode 6: Design of masonry structures – Part 1-1: General rules for reinforced and unreinforced masonry structures*. European Committee for Standardization.

Endo, Y., Pela, L., Roca, P., da Porto, F., & Modena, C. (2015). Comparison of seismic analysis methods applied to a historical church struck by 2009 L'Aquila earthquake. *Bulletin of Earthquake Engineering*, *13*(12), 3749–3778. https://doi.org/10.1007/s10518-015-9796-0

Escobar, J. (2017). Baroque Spain. Architecture and Urbanism for a Universal Monarchy. In A. Payne (Ed.), *Renaissance and Baroque Architecture: Vol. I* (pp. 1–27). John Wiley & Sons, Inc.

Espejel, R. (2015). *Templo de San Agustín*. http://www.espejel.com/templo-de-san-agustin/

Ewins, D. J. (2000). *Modal testing: theory, practice and application*. Research Studies Press LTD.

Farlex. (2012). Muslim architecture. In *Illustrated Dictionary of Architecture*. https://encyclopedia2.thefreedictionary.com/Muslim+architecture

Fernández Fernández, Í. (1999). *Historia de México*.

Fierro Gossman, R. (2014). *Grandes casas de México*. La Casa de Campo de Don Manuel González En Chapingo. https://grandescasasdemexico.blogspot.com/2014/01/la-casa-de-campo-de-don-manuel-gonzalez.html

Fierro Gossman, R. (2020). *Picture: Casa del Marqués del Apartado en Relox y Cordobanes*. Grandes Casas de México. https://grandescasasdemexico.blogspot.com/2020/08/casa-del-marques-del-apartado-en-relox.html

Flores Marini, C. (1966). La arquitectura de los conventos en el siglo XVI. *Artes de México*, *86/87*, 5–10.

Forbes Mexico. (2021). *Los 8 sismos más catastróficos en la historia de México*. https://www.forbes.com.mx/los-8-sismos-mas-catastroficos-en-la-historia-de-mexico/

Fradkin, P. L. (2006). *The Great Earthquake and Firestorms of 1906. How San Francisco nearly destroyed itself*. University of California Press, Ltd.

Fuentes, D. D., Baquedano Julià, P. A., D'Amato, M., & Laterza, M. (2019). Preliminary Seismic Damage Assessment of Mexican Churches after September 2017 Earthquakes. *International Journal of Architectural Heritage*, *September 2017*, 1–21. https://doi.org/10.1080/15583058.2019.1628323

García, N., & Meli, R. (2008). On Structural Bases for Building the Mexican Convent Churches From the Sixteenth Century. *International Journal of Architectural Heritage*, *3*(1), 24–51.

https://doi.org/10.1080/15583050701842344

García, N., & Peña, F. (2014). Mexican Ribbed Vaults of the Sixteenth Century: Origin and Structural Behavior. *Structural Analysis of Historical Constructions*, *October*, 14–17. https://doi.org/10.13140/2.1.1632.5127

Garitan, G. (2015). *Picture: View from north-east of Reims Cathedral (High Gothic)*. Creative Commons. Attribution-Share Alike 4.0 International. https://commons.wikimedia.org/wiki/File:ReimsCathedral0116.jpg

Giuriani, E., & Marini, A. (2008). Experiences from the Northern Italy 2004 earthquake: Vulnerability assessment and strengthening of historic churches. In D'Ayala & Fodde (Ed.), *6th International Conference on Structural Analysis of Historic Construction (SAHC08)* (pp. 1–12).

GOB MX. (2016). *Picture: Palacio del Conde de Buenavista*. Museo Nacional de San Carlos. https://www.archivo.cdmx.gob.mx/vive-cdmx/post/museo-nacional-de-san-carlos

Gobierno de México. (2018). *Ex Convento de San Agustín. Jonacatepec, Morelos*. https://restauracionpatrimonio.cultura.gob.mx/multimedia/detalle/62

Google Maps. (2019). *Antiguo Templo de Christ Church*. Antiguo Templo de Christ Church Street View. https://www.google.com/maps/@19.4333483,-99.1500613,3a,75y,114.44h,179t/data=!3m8!1e1!3m6!1sAF1QipMZCx8PP5652imamtPseXuW9u8Dd11INOKkBaPr!2e10!3e11!6shttps:%2F%2Flh5.googleusercontent.com%2Fp%2FAF1QipMZCx8PP5652imamtPseXuW9u8Dd11INOKkBaPr%3Dw203-h100-k-no-

Google Maps. (2021). *Casa Castiello*. Casa Castiello Street View. https://www.google.com/maps/@20.6747608,-103.3626578,3a,75y,19.09h,87.4t/data=!3m6!1e1!3m4!1s1P5-DiKYNJ2ijSvxm5CGZQ!2e0!7i16384!8i8192

Gordon, J. (2007). *Picture: Techo del Salón de Embajadores de los Reales Alcázares de Sevilla*. Creative Commons Attribution 2.0 Generic. https://commons.wikimedia.org/wiki/File:Embajadores_1.jpg

Gringer. (2009). *Picture: SVG version of File:Pacific_Ring_of_Fire.png*. Public Domain. https://commons.wikimedia.org/wiki/File:Pacific_Ring_of_Fire.svg

HA - Hidden Architecture. (2018). *Capilla abierta de Teposcolula*. Journal Atlas. http://hiddenarchitecture.net/capilla-abierta-de-teposcolula/

Hamid, A. A., Mahmoud, A., & El Magd, S. A. (1994). Strengthening and repair of unreinforced masonry structures: state-of-the-art. *10th Int. Brick and Block Masonry Conference*, *2*, 485–497.

Hermans, P. (2016). *Picture: Nederlands, Stadhuis van Oudenaarde, België*. Creative Commons Attribution-Share Alike 4.0 International, 3.0 Unported, 2.5 Generic, 2.0 Generic and 1.0 Generic. https://commons.wikimedia.org/wiki/File:Oudenaarde_stadhuis_25-9-2016_09-52-11.JPG

Hernandez, L. (2019). *Atotonilco el Grande*. https://www.youtube.com/watch?v=jqTo4pvCC8M

Historia Civil. (2019). *Picture: Museo Nacional de Historia (Castillo de Chapultepec)*. Construcción Civil. Castillo de Chapultepec. https://historiacivil.wordpress.com/2019/12/22/castillo-de-chapultepec/

Huerta, S. (1998). Mecánica de las bóvedas de la catedral de Gerona. *Las Grandes Bóvedas Hispanas, Madrid 19–23 Mayo de 1997*, 53–65.

Huerta, S. (2002). The medieval "scientia" of structures: the rules of Rodrigo Gil de Hontañón. *Towards*

a History of Construction. Between Mechanics and Architecture, 567–585. http://oa.upm.es/540/

Ibarra-Sevilla, B. (2013). De las grecas a las bóvedas de crucería del siglo XVI, técnicas de construcción y de cantería de los pueblos indígenas de México. *Informes de La Construcción*, *65*(Extra-2), 65–80. https://doi.org/10.3989/ic.13.013

ICOMOS/ISCARSAH. (2003). *Recommendations for the analysis, conservation and structural restoration of Architectural Heritage* (Issue June, pp. 3–6).

IIE - Instituto de Investigaciones Eléctricas, & CFE - Comisión Federal de Electricidad. (2017). *PRODISIS v4.1* (4.1). https://www2.ineel.mx/prodisis/es/prodisis.php

INAH TV. (2017). *Ex convento de Actopan, Hidalgo. Huellas de la evangelización*. https://www.youtube.com/watch?v=ceRvyl7_vsc

INEEL- Instituto Nacional de Electricidad y Energías Limpias. (2017). *PGA Map*. PRODISIS Online, OpenStreetMap Contributors (CC BY-SA 2.0). https://www2.ineel.mx/prodisis/es/prodisis.php

INEEL-Instituto Nacional de Electricidad y Energías Limpias. (2017). *Manual de Diseño de Obras Civiles–Diseño por Sismo*.

Jebulon. (2012). *Picture: Detail of the main facade of the Palace of San Telmo, nowadays the seat of the presidency of the Andalusian Autonomous Government (Junta de Andalucia), Seville, Spain*. Creative Commons CC0 1.0 Universal Public Domain Dedication. https://commons.wikimedia.org/wiki/File:Palacio_San_Telmo_facade_Seville_Spain.jpg

Jentges. (2010). *Picture: Catedral Nueva de la Asunción de la Virgen*. Creative Commons Attribution. https://commons.wikimedia.org/wiki/File:Salamanca_Catedral.JPG

Jimenez, J. I., Villarreal, J. I., Centeno, M. R., Gonzalez, B. G., Correa, J. J. G., Acevedo, C. R., & Salazar, I. S. (1999). Tehuacan, Mexico, Earthquake of June 15, 1999. *Seismological Research Letters*, *70*(6), 698–704. https://doi.org/10.1785/gssrl.70.6.698

Karanikoloudis, G., Lourenço, P. B., Alejo, L. E., & Mendes, N. (2020). Lessons from Structural Analysis of a Great Gothic Cathedral: Canterbury Cathedral as a Case Study. *International Journal of Architectural Heritage*, 1–30. https://doi.org/10.1080/15583058.2020.1723736

KeraKoll. (2017). *GeoSteel Grid 200*.

KINEMETRICS. (2013). *KINEMETRICS. Advancement through innovation*. https://kinemetrics.com/

KINEMETRICS. (2019). *Strong Motion Analyst (SMA)*. https://kinemetrics.com/wp-content/uploads/2017/04/datasheet-software-strong-motion-analyst-sma.pdf

Kirakofe, J. B. (1995). Architectural Fusion and Indigenous Ideology in Early Colonial Teposcolula. The Casa de la Cacica: A Building at the Edge of Oblivion. *Anales Del Instituto de Investigaciones Estéticas*, *17*(66), 45. https://doi.org/10.22201/iie.18703062e.1995.66.1730

Kita, A., Cavalagli, N., & Ubertini, F. (2019). Temperature effects on static and dynamic behavior of Consoli Palace in Gubbio, Italy. *Mechanical Systems and Signal Processing*, *120*, 180–202. https://doi.org/10.1016/j.ymssp.2018.10.021

Klingner, R. E. (2006). Behavior of masonry in the Northridge (US) and Tecomán–Colima (Mexico) earthquakes: Lessons learned, and changes in US design provisions. *Construction and Building Materials*, *20*(4), 209–219. https://doi.org/10.1016/j.conbuildmat.2005.08.024

Kouris, L. A. S., & Triantafillou, T. C. (2018). State-of-the-art on strengthening of masonry structures with textile reinforced mortar (TRM). *Construction and Building Materials*, *188*, 1221–1233.

https://doi.org/10.1016/j.conbuildmat.2018.08.039

Krauze, E. (2013). *Prologo. La ciudad de los palacios: crónica de un patrimonio perdido.* Letras Libres. https://www.letraslibres.com/espana-mexico/historia/guillermo-tovar-teresa-cronista-la-ciudad-los-palacios

Kubler, G. (1983). *Arquitectura mexicana del siglo XVI*. Fondo de Cultura Económica.

Linares Garcia, A. (2010). *Picture: View of the cupola of the Capilla del Rosario in Puebla, Mexico*. Creative Commons Attribution-Share Alike 4.0 International, 3.0 Unported, 2.5 Generic, 2.0 Generic and 1.0 Generic License. https://commons.wikimedia.org/wiki/File:CupolaRosarioPuebla3.JPG

Lomnitz, C., & Castaños, H. (2006). Earthquake hazard in the valley of Mexico: entropy, structure, complexity. In *Earthquake Source Asymmetry, Structural Media and Rotation Effects* (pp. 347–364). Springer.

López-Doncel, R., Wedekind, W., Leiser, T., Molina-Maldonado, S., Velasco-Sánchez, A., Dohrmann, R., Kral, A., Wittenborn, A., Aguillón-Robles, A., & Siegesmund, S. (2016). Salt bursting tests on volcanic tuff rocks from Mexico. *Environmental Earth Sciences*, *75*(3), 212. https://doi.org/10.1007/s12665-015-4770-3

López, E., & Biosca, T. (2012). *Picture: Templo del Hospital, Acámbaro, Estado de Guanajuato, México*. Creative Commons Atribución 2.0 Genérica. https://es.wikipedia.org/wiki/Archivo:Templo_del_Hospital,_Acámbaro,_Estado_de_Guanajuato,_México_.jpg

Lourenço, P. B. (1996). *Computational strategies for masonry structures* (Vol. 70, Issue 08) [PhD Thesis, Delft University of Technology]. https://doi.org/ISBN 90-407-1221-2

Lourenço, P. B. (1998). Experimental and numerical issues in the modelling of the mechanical behaviour of masonry. In P Roca, J. L. González, E. Oñate, & P. B. Lourenço (Eds.), *Structural analysis of historical constructions II* (pp. 57–91). International Center for Numerical Methods in Engineering.

Lourenço, P. B. (2008). Structural Masonry Analysis: Recent Developments and Prospects. In M. Masia, V. Bokan-Bosiljkov, & V. Bosiljkov (Eds.), *14th International Brick and Block Masonry Conference (14IBMAC)* (p. 16). http://hdl.handle.net/1822/17176

Lourenço, P. B. (2009). Recent Advances in Masonry Modelling: Micromodelling and Homogenisation. In U. Galvanetto & M. H. Ferri Aliabadi (Eds.), *Multiscale Modeling In Solid Mechanics: Computational Approaches* (pp. 251–294). Imperial College Press.

Lourenço, P. B., Mendes, N., Costa, A. A., & Campos-Costa, A. (2016). Methods and Challenges on the Out-Of-Plane Assessment of Existing Masonry Buildings. *International Journal of Architectural Heritage*, *11*(1). https://doi.org/10.1080/15583058.2017.1237114

Lourenço, P. B., Mendes, N., Ramos, L. F., & Oliveira, D. V. (2011). Analysis of Masonry Structures Without Box Behavior. *International Journal of Architectural Heritage*, *5*(4–5), 369–382. https://doi.org/10.1080/15583058.2010.528824

Luna, M. (2019). *Picture: Casas abandonadas*. Casas Abandonadas En El Centro Histórico Generan Inseguridad. https://www.elsoldemorelia.com.mx/local/casas-abandonadas-en-el-centro-historico-generan-inseguridad-3940853.html

Luso, E., & Lourenço, P. B. (2016). Experimental characterization of commercial lime based grouts for stone masonry consolidation. *Construction and Building Materials*, *102*, 216–225. https://doi.org/10.1016/j.conbuildmat.2015.10.096

Maldonado, F. (2019a). *Picture: Casas abandonadas*. Casas Abandonadas En El Centro Histórico Generan Inseguridad. https://www.elsoldemorelia.com.mx/local/casas-abandonadas-en-el-centro-historico-generan-inseguridad-3940853.html

Maldonado, F. (2019b). *Picture: Casas abandonadas*. En Riesgo 200 Inmuebles Del Centro Histórico de Morelia. https://www.elsoldemorelia.com.mx/local/en-riesgo-200-inmuebles-del-centro-historico-de-morelia-3935035.html%0A

Martínez, G., Roca, P., Caselles, O., Clapés, J., & Barbat, A. H. (2009). Matrices de Probabilidad de daño para la catedral de Mallorca, España. In SMIS (Ed.), *XVII Congreso Nacional de Ingeniería Sísmica* (p. 17).

Martinez Ramos, M. A. (2012). *Picture: Vista frontal de rectoria*. Creative Commons Attribution-Share Alike 3.0 Unported License. https://commons.wikimedia.org/wiki/File:Edificio_de_rectoria_de_la_Universidad_Autónoma_Chapingo.JPG

Masciotta, M. G., & Ramos, L. F. (2019). Dynamic identification of historic masonry structures. In *Long-term Performance and Durability of Masonry Structures* (pp. 241–264). Elsevier. https://doi.org/10.1016/B978-0-08-102110-1.00008-X

Masciotta, M. G., Ramos, L. F., Lourenço, P. B., & Vasta, M. (2017). Damage identification and seismic vulnerability assessment of a historic masonry chimney. *Annals of Geophysics*, *60*(4).

Masciotta, M. G., Roque, J. C. A., Ramos, L. F., & Lourenço, P. B. (2016). A multidisciplinary approach to assess the health state of heritage structures: The case study of the Church of Monastery of Jerónimos in Lisbon. *Construction and Building Materials*, *116*, 169–187. https://doi.org/10.1016/j.conbuildmat.2016.04.146

Mathias, S. (2013). *Picture: Sagrario Metropolitano*. Creative Commons Attribution-Share Alike 3.0 Unported. https://commons.wikimedia.org/wiki/File:Arte.JPG

Matías, P. (2017). *Picture: Templo de San Vicente Ferrer*. El Terremoto No Perdona Ni a Los Templos; Afectó a 325 de Oaxaca. https://pagina3.mx/2017/11/el-terremoto-no-perdona-ni-a-los-templos-afecto-a-325-de-oaxaca/

McCallum, A. (2006). *Picture: Canterbury Cathedral UK from the south-west*. Creative Commons Attribution-Share Alike 4.0 International. https://commons.wikimedia.org/wiki/File:Canterbury-cathedral-wyrdlight.jpg

Meli, R. (2011). *Los conventos mexicanos del siglo XVI: construcción, ingeniería estructural y conservación* (UNAM (Ed.); 1st ed.). Porrúa.

Meli, R., & Peña, F. (2004). On elastic models for evaluation of the seismic vulnerability of masonry churches. In C. Modena, P. B. Lourenço, & P. Roca (Eds.), *Structural Analysis of Historical Constructions* (pp. 1121–1132). Taylor & Francis.

Mendes-Victor, L., Oliveira, C. S., Azevedo, J., & Ribeiro, A. (Eds.). (2008). *The 1755 Lisbon earthquake: revisited* (Vol. 7). Springer Science & Business Media.

Mendes, N. (2012). *Seismic Assessment of Ancient Masonry Buildings : Shaking Table Tests and Numerical Analysis*. PhD Thesis, University of Minho.

Mexch. (2008). *Picture: Casa de los Muñecos*. Creative Commons Attribution-Share Alike 3.0 Unported License. https://commons.wikimedia.org/wiki/File:Casa_muñecos_puebla.JPG

Niell, P. B., & Sundt, R. A. (2015). Architecture of Colonizers/Architecture of Immigrants: Gothic in Latin America from the 16th to the 20th Centuries. *Postmedieval: A Journal of Medieval Cultural Studies*, *6*(3), 243–257. https://doi.org/10.1057/pmed.2015.23

Nowak, R., & Orłowicz, R. (2019). Selected problems of failures and repairs of historic masonry vaults. *MATEC Web of Conferences*, *284*, 05008. https://doi.org/10.1051/matecconf/201928405008

NTC. (2018). Norme tecniche per le costruzioni. In *Italian Technical Norms for Constructions.*

Nuñez Gaona, A. (2015). *Comportamiento estructural del templo de San Agustín en Morelia, Michoacán*. Thesis, Universidad Michoacana de San Nicolás de Hidalgo.

Nuñez Gaona, A. (2018). *Riesgo sísmico del templo de San Agustín en Morelia, Michoacán*. MsC Thesis, Universidad Michoacana de San Nicolás de Hidalgo.

Ojeda, A. (2017). *Picture: Convento de San Juan Bautista, recinto histórico afectado en el municipio de Tlayacapan, Morelos. Es uno de los 14 inmuebles de la Ruta de los Conventos*. Destrucción En La Ruta de Los Conventos. https://www.eluniversal.com.mx/especiales/cultura/2017/09/28/1005252/nota/1005625/0/destruccion-en-la-ruta-de-los-conventos

Orellana, M. De. (1966). Conventos del siglo Dieciseis. *Artes de México*, *86/87*.

Peña, F., & Chávez, M. M. (2016). Seismic Behavior of Mexican Colonial Churches. *International Journal of Architectural Heritage*, *10*(2–3), 332–345. https://doi.org/10.1080/15583058.2015.1113341

Peña, F., Cruz, C. E., & García, N. (2016). Comparison of seismic behaviour of façades of colonial churches with and without bell towers. *Brick and Block Masonry – Trends, Innovations and Challenges*, 275–282. https://www.researchgate.net/publication/305681602

Peña, F., & Manzano, J. (2015). Dynamical Characterization of Typical Mexican Colonial Churches. In I. N. Psycharis, S. J. Pantazopoulou, & M. Papadrakakis (Eds.), *Seismic Assessment, Behavior and Retrofit of Heritage Buildings and Monuments. Computational Methods in Applied Sciences* (Vol. 37, pp. 297–319). Springer, Cham. https://doi.org/10.1007/978-3-319-16130-3_12

Pérez-Gavilán, J. J., Aguirre, J., & Ramírez, L. (2018). Sismicidad y seguridad estructural en las construcciones: lecciones aprendidas en México. *Salud Pública de México*, *60*(Supl.1), 41. https://doi.org/10.21149/9300

Piñón, A. (2014). *Picture: Christ Church*. Christ Churh, Riesgosa, Pese a Su Recuperación; El Universal. https://archivo.eluniversal.com.mx/cultura/2014/christ-church-riesgosa-pese-a-recuperacion-1061353.html

Ramírez-Cisneros, J., Lozano, J., Ferrer-Toledo, H. O., Rojas-Palacios, J., Vázquez-Rosas, R., & Mijares-Arellano, H. (2012). Dynamic Behavior of Puebla City Cathedral. In Sociedade Portuguesa de Engenharia Sismica (SPES) (Ed.), *15th World Conference on Earthquake Engineering (15WCEE)* (pp. 1–10).

Ramírez, R., Mendes, N., & Lourenço, P. B. (2019). Diagnosis and Seismic Behavior Evaluation of the Church of São Miguel de Refojos (Portugal). *Buildings*, *9*(6), 138. https://doi.org/10.3390/buildings9060138

Rene, P. (2017). *Picture: Palacio de Cortés antes del sismo*. Creative Commons Attribution-Share Alike 4.0 International License. https://commons.wikimedia.org/wiki/File:Palacio_de_Cortés_2017.jpg

Reyes, C., Zepeda, O., Gutiérrez, C., Durán, R., Domínguez, L., Mendoza, M. J., Alcocer, S. M., Durán,

R., Echavarria, A., Leonardo, F., López, O. A., Pacheco, M. A., De la Torre, O., Bitrán, D., Colorado, J. A., & García, N. (2003). *Informes técnicos - El sismo de Tecomán, Colima del 21 de enero de 2003 (Me 7.6)*. www.cenapred.unam.mx

Rhoda, R., & Burton, T. (2012). *Which tectonic plates affect Mexico?* Geo-Mexico; the Geography and Dynamics of Modern Mexico. https://geo-mexico.com/?p=6277%0A

Roca, Pere, Cervera, M., Gariup, G., & Pela, L. (2010). Structural analysis of masonry historical constructions. Classical and advanced approaches. *Archives of Computational Methods in Engineering*, *17*(3), 299–325. https://doi.org/10.1007/s11831-010-9046-1

Roca, Pere, Lourenço, P. B., & Gaetani, A. (2019). *Historic Construction and Conservation: Materials, Systems and Damage* (1st ed.). Routledge.

Rodríguez López, G. (2006). *Picture: Palacio de Gobierno de Michoacán, en Morelia (Michoacán's Government Palace in Morelia)*. Public Domain. https://commons.wikimedia.org/wiki/File:Morelia_-_Palacio_de_Gobierno.jpg

Ruiz Razura, A., & Fregoso Torres, J. E. (2020). *La Casa Cañedo : Un palacio en Guadalajara* (Editorial Universitaria (Ed.)). Universidad de Guadalajara.

Sahakian, V. J., Melgar, D., Quintanar, L., Ramírez-Guzmán, L., Pérez-Campos, X., & Baltay, A. (2018). Ground motions from the 7 and 19 september 2017 tehuantepec and Puebla-Morelos, Mexico, earthquakes. *Bulletin of the Seismological Society of America*, *108*(6), 3300–3312. https://doi.org/10.1785/0120180108

Sánchez Pérez, T. (2007). Lecciones aprendidas del terremoto de M é xico de 1985. *Encuentro Regional Sobre Análisis Costo – Beneficio*.

Sarlis, N. V., Skordas, E. S., Varotsos, P. A., Ramírez-Rojas, A., & Flores-Márquez, E. L. (2018). Natural time analysis: On the deadly Mexico M8.2 earthquake on 7 September 2017. *Physica A: Statistical Mechanics and Its Applications*, *506*, 625–634. https://doi.org/10.1016/j.physa.2018.04.098

Scacco, J., Salazar, G., Bianchini, N., Mendes, N., Cullimore, C., & Jain, L. (2019). Seismic assessment of the church of Carmo Convent. In P. B. Lourenço, P. Flores, & S. Clain (Eds.), *Congress on Numerical Methods in Engineering (CMN2019)* (pp. 1–16).

Schaefer, W. K. (2014). *Ocuituco, Edo. Mor. MÉXICO "EX CONVENTO DE SANTIAGO APÓSTOL" 1 Parte*. https://www.youtube.com/watch?v=MteF-vUVRqc

Schönle, A. (2021). 2-Lessons of the Fire of Moscow in 1812. In *Architecture of Oblivion: Ruins and Historical Consciousness in Modern Russia* (pp. 46–72). Cornell University Press. https://doi.org/10.1515/9781501756771-005

Segundo, S. (2009). *Picture: Fachada Sur de El Escorial*. Creative Commons Attribution-Share Alike 4.0 International, 3.0 Unported, 2.5 Generic, 2.0 Generic and 1.0 Generic. https://commons.wikimedia.org/wiki/File:Escorial-sur.jpg#filelinks

Servicio Geológico Mexicano. (2017). *Sismología de México*. Riesgos Geológicos. https://www.sgm.gob.mx/Web/MuseoVirtual/Riesgos-geologicos/Sismologia-de-Mexico.html

Sierra, S. (2017). *Picture: Casa de Cultura en la edificación dominica del siglo XVI*. Tehuantepec En Medio de Los Escombros.

Soria, F. J., Alfaro, F. H., & Limones, C. A. (2011). Urban and architectural reuse of the former Chapingo Hacienda: Sustainable criteria for the conservation of built heritage. *WIT Transactions on the Built*

Environment, *118*(April), 173–184. https://doi.org/10.2495/STR110151

SRD - Statista Research Department. (2016). *The worst natural hazards of the 21st century, by death toll (in Spanish)*. https://es.statista.com/estadisticas/567843/las-peores-catastrofes-naturales-del-siglo-xxi-por-numero-de-muertes/

SSN - Servicio Sismológico Nacional (México). (2021). *Catálogo de Sismos*. https://doi.org/10.21766/SSNMX/EC/MX

SSN - Servivio Sismológico Nacional (México). (2020). *Mapas de sismicidad anual*. http://www.ssn.unam.mx/sismicidad/mapas-de-sismicidad-anual/

Suárez, G., Caballero-Jiménez, G. V., & Novelo-Casanova, D. A. (2019). Active Crustal Deformation in the Trans-Mexican Volcanic Belt as Evidenced by Historical Earthquakes During the Last 450 Years. *Tectonics*, *38*(10), 3544–3562. https://doi.org/10.1029/2019TC005601

SVS. (2019). *ARTeMIS Modal, Release 6.0.2.0*. Structural Vibration Solutions.

Taleb, R., Bouriche, F., Remas, A., Boukri, M., & Kehila, F. (2012). Use of Ambient and Forced Vibration Tests to Evaluate Seismic Properties of an Unreinforced Masonry Building Rehabilitated by Dampers. In Sociedade Portuguesa de Engenharia Sismica (SPES) (Ed.), *15th World Conference on Earthquake Engineering (15WCEE)* (pp. 1–10).

Tango. (2014). *Picture: Catedral de Murcia, Región de Murcia, España.* Creative Commons Attribution-Share Alike 4.0 International. https://commons.wikimedia.org/wiki/File:Murcia_Catedral1_tango7174.jpg

TARES. (2017a). *Picture: Parroquia de Santiago Apóstol*. https://es-la.facebook.com/taresmx/photos/a.1685814315026145/1950747815199459/?type=3&theater%0A

TARES. (2017b). *Picture: San Francisco del Mar*. https://es-la.facebook.com/taresmx/photos/a.1685814315026145/1956325387975035/?type=3&theater

TARES. (2017c). *Picture: Templo de la Virgen del Patrocinio en la Ciudad de Oaxaca*. El Rescate y Conservación de Inmuebles Históricos Continúa. https://www.facebook.com/taresmx/photos/a.1685814315026145/1963628483911392/?type=3&theater

TARES. (2017d). *Picture: Templo de la Virgen del Rosario*. Rescate Del Inmueble Al Realizare Apuntalamientos En Estructura. https://es-la.facebook.com/taresmx/photos/a.1685814315026145/1965783287029245/?type=3&theater

Thelmadattar, L. (2008). *Picture: Colegio de Minería (College of Mining) building on Tacuba street in the historic Centro of Mexico City*. Public Domain. https://commons.wikimedia.org/wiki/File:ColegioMineriaDF.JPG

Tovar de Teresa, G. (1990). *La ciudad de los palacios: Crónica de un patrimonio perdido* (E. Krauze & J. E. Iturriga (Eds.); 3rd ed.). Vuelta.

Turismo Tlaxcala. (2020). *Picture: Basilica de Ocotlan*. https://turismotlaxcala.com/Atractivos/img_atractivos/Basilica-de-Ocotlan-Galeria8.jpg

UNAM. (2017). *Zona sísmica y vulcanismo en México*.

http://uapas1.bunam.unam.mx/sociales/zona_sismica_y_vulcanismo_en_mexico/

UNESCO. (1991). *15COM XV - Inscription: Historic Centre of Morelia (Mexico)*. https://whc.unesco.org/en/list/585

UNESCO. (2013a). *Historic Centre of Morelia: Map of the World Heritage property*. https://whc.unesco.org/en/list/585

UNESCO. (2013b). *Historic Centre of Morelia*. https://whc.unesco.org/en/list/585/

UNESCO. (2020a). *Mexico - Properties inscribed on the World Heritage List*. https://whc.unesco.org/en/statesparties/mx/

UNESCO. (2020b). *UNESCO World Heritage Centre - Interactive Maps*. World Heritage List. https://whc.unesco.org/en/interactive-map/?search=&id_states=mx

USGS. (1996). *Picture: The key principle of plate tectonics*. Public Domain. https://commons.wikimedia.org/wiki/File:Plates_tect2_en.svg

Vasconcelos, G. F. M. (2005). *Experimental investigations on the mechanics of stone masonry: Characterization of granites and behavior of ancient masonry shear walls*. PhD Thesis, University of Minho.

Von Simson, O. G. (1988). *The Gothic cathedral: origins of Gothic architecture and the medieval concept of order* (Princeton University Press (Ed.); Vol. 106). Bollingen Foundation.

Waldinger, M. (2013). Colonial Missionaries and Long Run Development in Mexico. *London School of Economics*, *1*.

Wallfisch, B. (2016). *Yuriria Guanajuato Pueblo Mágico*. https://www.youtube.com/watch?v=wYfwtz3fsSc

Werner, B. (2009). *Picture: Assisi, San Francesco*. Public Domain. https://commons.wikimedia.org/wiki/File:Assisi_San_Francesco_BW_1.JPG

Willis, R. (1845). *The architectural history of Canterbury Cathedral*. Longman.

Wyrobisz, A. (1980). La ordenanza de Felipe II del año 1573 y la construcción de ciudades coloniales españolas en la América. *Estudios Latinoamericanos*, *7*, 11–34.

Yin, L., Li, X., Zheng, W., Yin, Z., & Song, L. (2019). Fractal dimension analysis for seismicity spatial and temporal distribution in the circum-Pacific seismic belt. *Journal of Earth System Science*, *128*(1), 1–7. https://doi.org/10.1007/s12040-018-1040-2

Zamora, E. (2009). *Picture: Fachada del palacio de Hernán Cortés*. Creative Commons Attribution-Share Alike 4.0 International, 3.0 Unported, 2.5 Generic, 2.0 Generic and 1.0 Generic License. https://commons.wikimedia.org/wiki/File:2006_03_17_Cuernavaca_Casa_de_Cortés_1.JPG

Zavala, J. F. (2019). *Picture: El oratorio de las beatas de santa Rosa de Viterbo en Querétaro*. https://eloficiodehistoriar.com.mx/2019/09/30/el-oratorio-de-las-beatas-de-santa-rosa-de-viterbo-en-queretaro/

Zavala, M., Alejo, L. E., Martínez, G., & Rojas, R. (2014). Influencia de la Proporción Áurea en el Comportamiento Estructural de Edificios Históricos de Tipo Religioso, en la ciudad de Morelia, Michoacán. In Sociedad Mexicana de Ingeniería Estructural (Ed.), *XIX Congreso Nacional de Ingeniería Estructural (CNIE 2014)* (pp. 1–13).

Annex A
Seismic records and response spectra

A.1. OAXM. Oaxaca, Mexico.

Table A - 1. Characteristics of the OAXM earthquake.

Description	Horizontal component (X)	Horizontal component (Y)	Vertical component (Z)
t_{total} (s)	167	167	167
t_{input} (s)	30	30	30
PGA (g)	0.28	0.15	0.09
Sa_{max} (g)	1.37	0.67	0.37
T (s)	0.34	0.26	0.16
t_{eff} (s)	5.3	5.3	5.3
PGA_{eff} (g)	0.10	0.11	0.04

t_{total}: total duration of the record; t_{input}: duration of the input; PGA: peak ground acceleration; Sa_{max}: maximum spectral acceleration; T: period of the structure related to Sa_{max}; t_{eff}: effective time of the analysis; PGA_{eff}: effective peak ground acceleration.

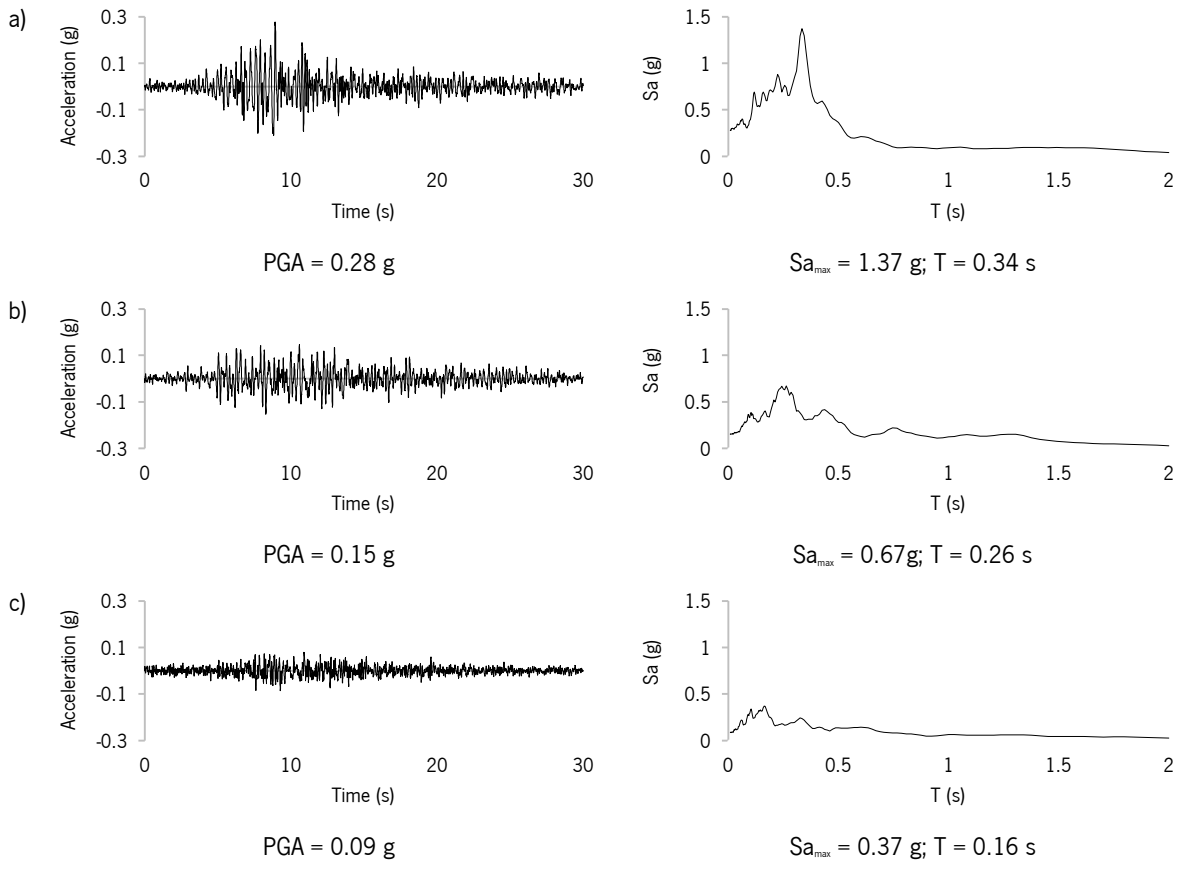

Figure A - 1. Components and response spectra for the input OAXM: a) horizontal (X); b) horizontal (Y); and c) vertical (Z).

A.2. OXCU. Oaxaca, Mexico.

Table A - 2. Characteristics of the OXCU earthquake.

Description	Horizontal component (X)	Horizontal component (Y)	Vertical component (Z)
t_{total} (s)	165	165	165
t_{input} (s)	35	35	35
PGA (g)	0.12	0.20	0.06
Sa_{max} (g)	0.73	1.08	0.21
T (s)	0.45	0.43	0.34
t_{eff} (s)	4.1	4.1	4.1
PGA_{eff} (g)	0.07	0.11	0.03

t_{total}: total duration of the record; t_{input}: duration of the input; PGA: peak ground acceleration; Sa_{max}: maximum spectral acceleration; T: period of the structure related to Sa_{max}; t_{eff}: effective time of the analysis; PGA_{eff}: effective peak ground acceleration.

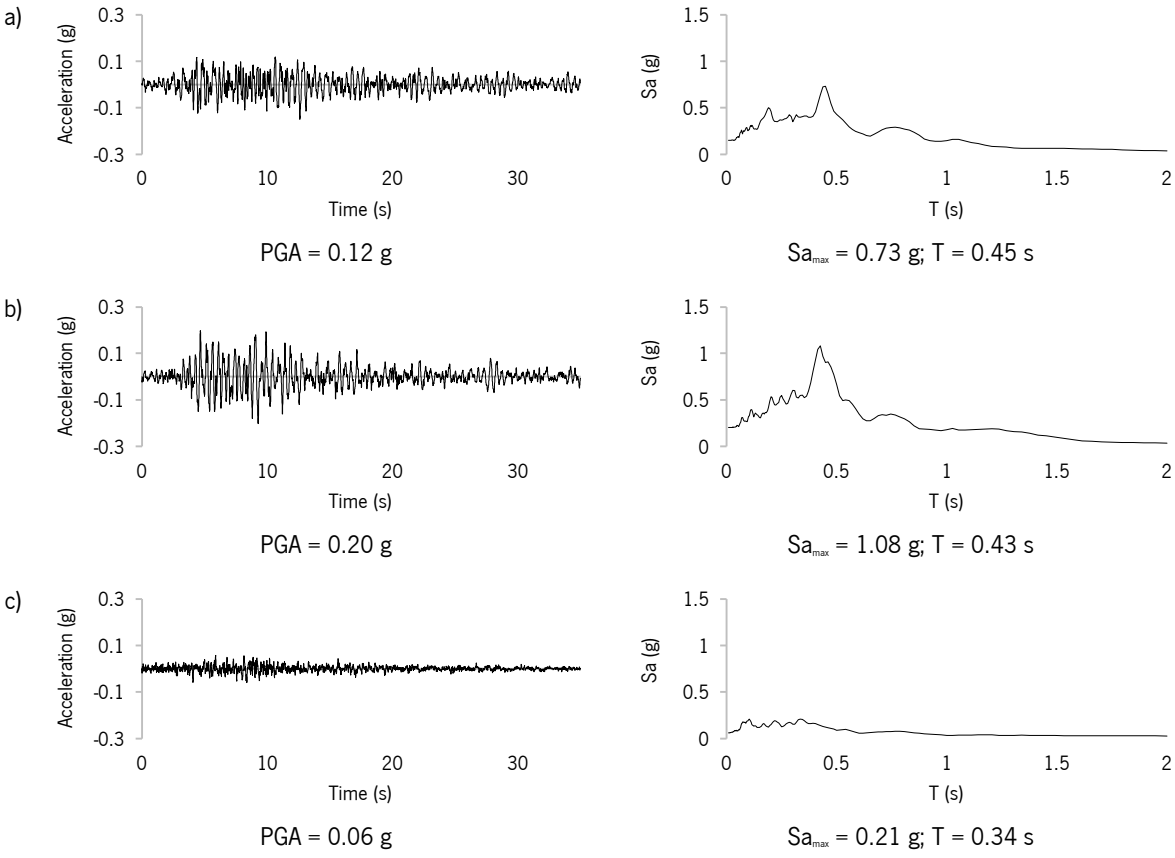

Figure A - 2. Components and response spectra for the input OXCU: a) horizontal (X); b) horizontal (Y); c) vertical (Z).

A.3. OXJM. Oaxaca, Mexico.

Table A - 3. Characteristics of the OXJM earthquake.

Description	Horizontal component (X)	Horizontal component (Y)	Vertical component (Z)
t_{total} (s)	173	173	173
t_{input} (s)	33	33	33
PGA (g)	0.25	0.29	0.17
Sa_{max} (g)	0.99	1.25	0.51
T (s)	0.31	0.37	0.37
t_{eff} (s)	2.5	2.5	2.5
PGA_{eff} (g)	0.07	0.06	0.09

t_{total}: total duration of the record; t_{input}: duration of the input; PGA: peak ground acceleration; Sa_{max}: maximum spectral acceleration; T: period of the structure related to Sa_{max}; t_{eff}: effective time of the analysis; PGA_{eff}: effective peak ground acceleration.

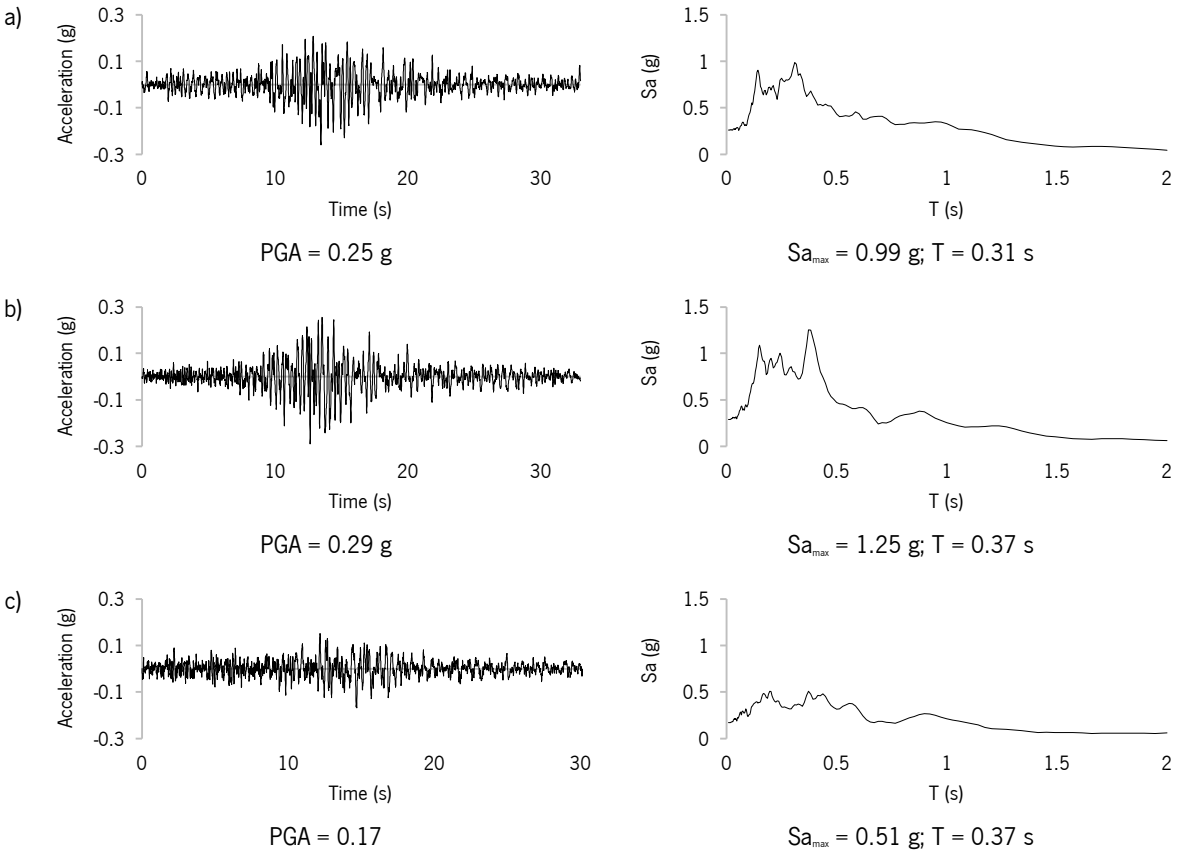

Figure A - 3. Components and response spectra for the input OXJM: a) horizontal (X); b) horizontal (Y); c) vertical (Z).

A.4. OXXO. Oaxaca, Mexico.

Table A - 4. Characteristics of the OXXO earthquake.

Description	Horizontal component (X)	Horizontal component (Y)	Vertical component (Z)
t_{total} (s)	194	194	194
t_{input} (s)	25	25	25
PGA (g)	0.21	0.22	0.08
Sa_{max} (g)	0.93	0.87	0.26
T (s)	0.43	0.35	0.26
t_{eff} (s)	2.2	2.2	2.2
PGA_{eff} (g)	0.06	0.05	0.03

t_{total}: total duration of the record; t_{input}: duration of the input; PGA: peak ground acceleration; Sa_{max}: maximum spectral acceleration; T: period of the structure related to Sa_{max}; t_{eff}: effective time of the analysis; PGA_{eff}: effective peak ground acceleration.

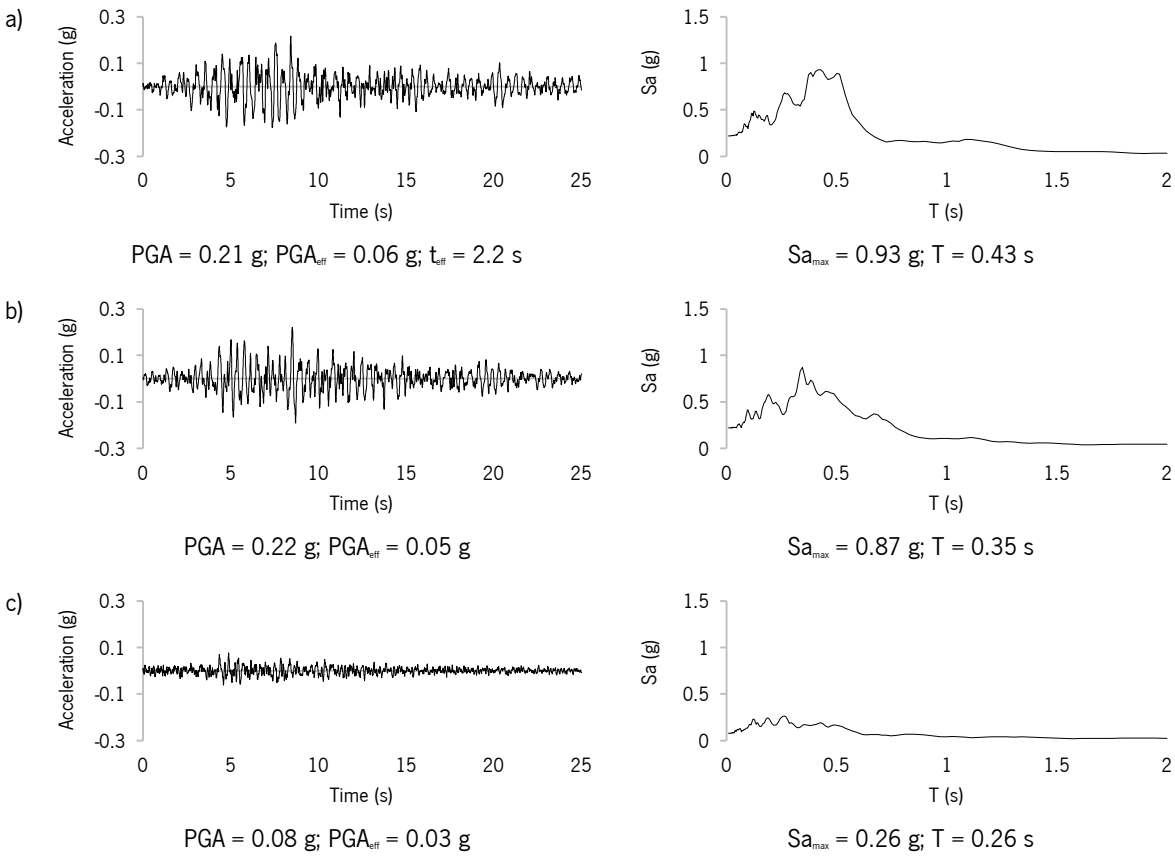

Figure A - 4. Components and response spectra for the input OXXO: a) horizontal (X); b) horizontal (Y); c) vertical (Z).

A.5. SAPP. Puebla, Mexico.

Table A - 5. Characteristics of the SAPP earthquake.

Description	Horizontal component (X)	Horizontal component (Y)	Vertical component (Z)
t_{total} (s)	73	73	73
t_{input} (s)	30	30	30
PGA (g)	0.20	0.20	0.06
Sa_{max} (g)	1.06	1.02	0.22
T (s)	0.56	0.44	0.20
t_{eff} (s)	8.1	8.1	8.1
PGA_{eff} (g)	0.06	0.07	0..06

t_{total}: total duration of the record; t_{input}: duration of the input; PGA: peak ground acceleration; Sa_{max}: maximum spectral acceleration; T: period of the structure related to Sa_{max}; t_{eff}: effective time of the analysis; PGA_{eff}: effective peak ground acceleration.

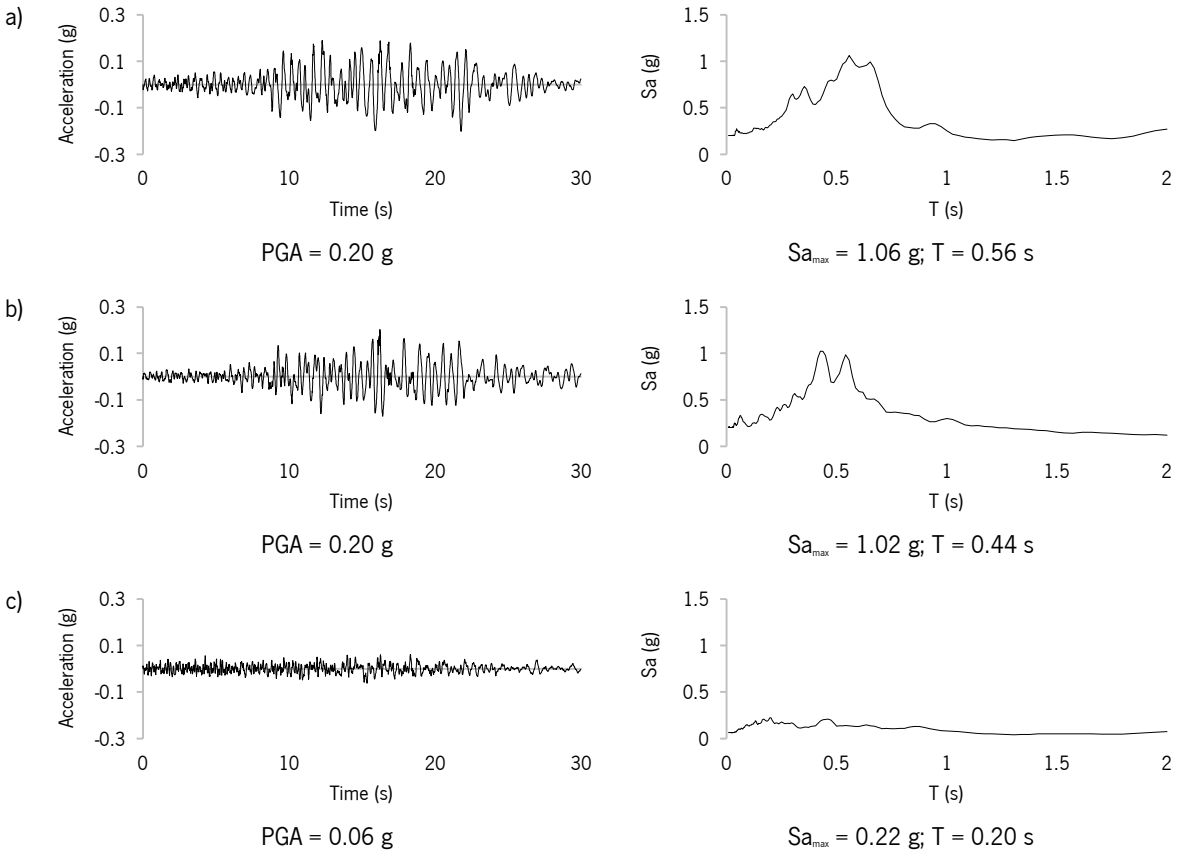

Figure A - 5. Components and response spectra for the input SAPP: a) horizontal (X); b) horizontal (Y); c) vertical (Z).

A.6. SCRU. Oaxaca, Mexico.

Table A - 6. Characteristics of the OAXM earthquake.

Description	Horizontal component (X)	Horizontal component (Y)	Vertical component (Z)
t_{total} (s)	179	179	179
t_{input} (s)	30	30	30
PGA (g)	0.25	0.25	0.30
Sa_{max} (g)	0.79	0.79	0.93
T (s)	0.13	0.12	0.07
t_{eff} (s)	11.9	11.9	11.9
PGA_{eff} (g)	0.14	0.14	0.30

t_{total}: total duration of the record; t_{input}: duration of the input; PGA: peak ground acceleration; Sa_{max}: maximum spectral acceleration; T: period of the structure related to Sa_{max}; t_{eff}: effective time of the analysis; PGA_{eff}: effective peak ground acceleration.

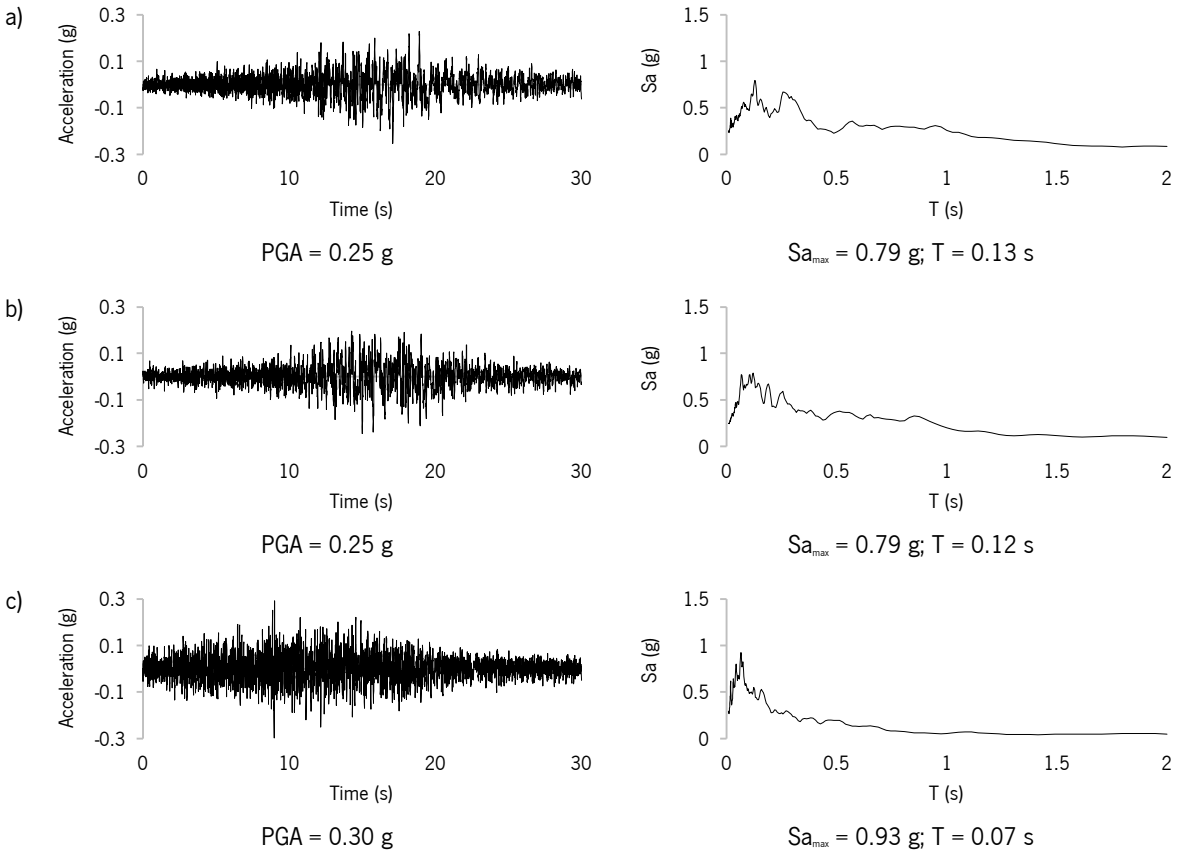

Figure A - 6. Components and response spectra for the input SCRU: a) horizontal (X); b) horizontal (Y); c) vertical (Z).

A.7. RFPP. Puebla, Mexico.

Table A - 7. Characteristics of the OAXM earthquake.

Description	Horizontal component (X)	Horizontal component (Y)	Vertical component (Z)
t_{total} (s)	94	94	94
t_{input} (s)	33	33	33
PGA (g)	0.12	0.19	0.08
Sa_{max} (g)	0.49	0.88	0.34
T (s)	0.03	0.03	0.02
t_{eff} (s)	13.9	13.9	13.9
PGA_{eff} (g)	0.10	0.12	0.07

t_{total}: total duration of the record; t_{input}: duration of the input; PGA: peak ground acceleration; Sa_{max}: maximum spectral acceleration; T: period of the structure related to Sa_{max}; t_{eff}: effective time of the analysis; PGA_{eff}: effective peak ground acceleration.

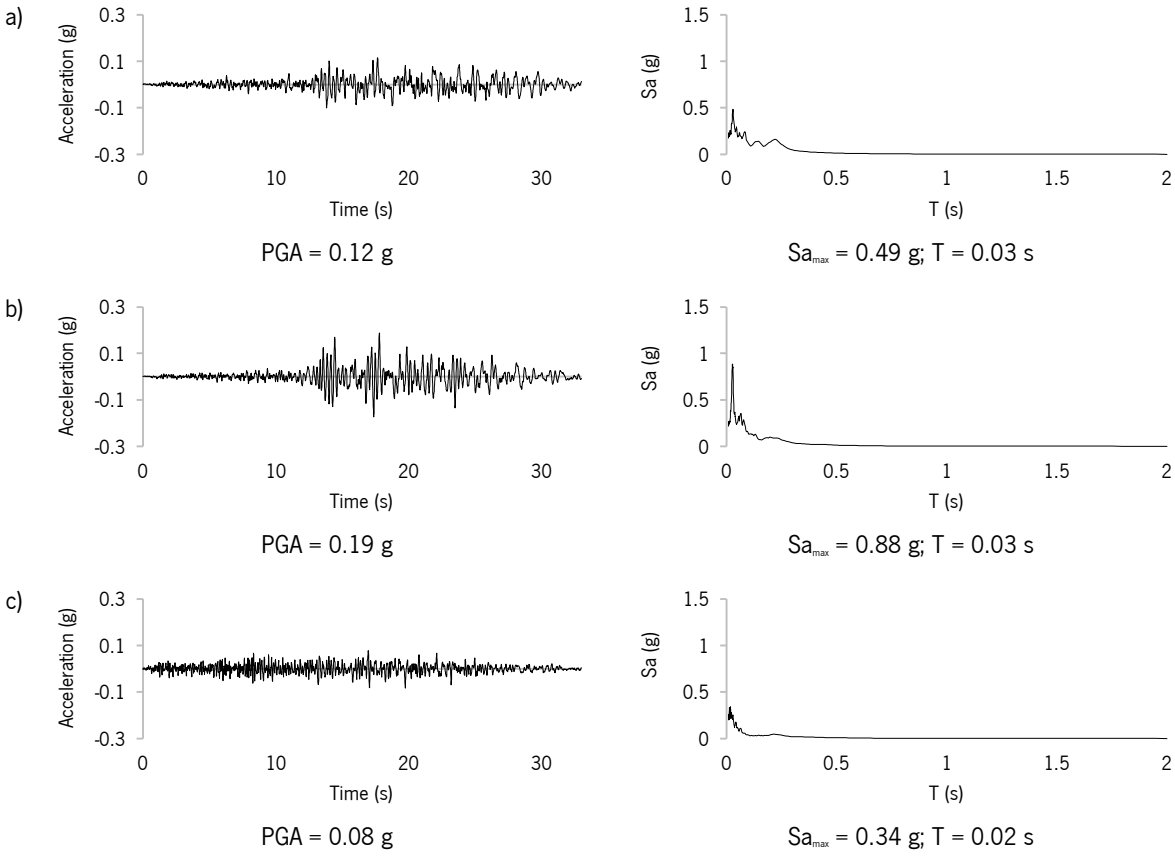

Figure A - 7. Components and response spectra for the input RFPP: a) horizontal (X); b) horizontal (Y); c) vertical (Z).

A.8. THEZ. Puebla, Mexico.

Table A - 8. Characteristics of the THEZ earthquake.

Description	Horizontal component (X)	Horizontal component (Y)	Vertical component (Z)
t_{total} (s)	128	128	128
t_{input} (s)	28	28	28
PGA (g)	0.17	0.15	0.04
Sa_{max} (g)	0.67	0.45	0.20
T (s)	0.03	0.04	0.02
t_{eff} (s)	4.4	4.4	4.4
PGA_{eff} (g)	0.15	0.04	0.03

t_{total}: total duration of the record; t_{input}: duration of the input; PGA: peak ground acceleration; Sa_{max}: maximum spectral acceleration; T: period of the structure related to Sa_{max}; t_{eff}: effective time of the analysis; PGA_{eff}: effective peak ground acceleration.

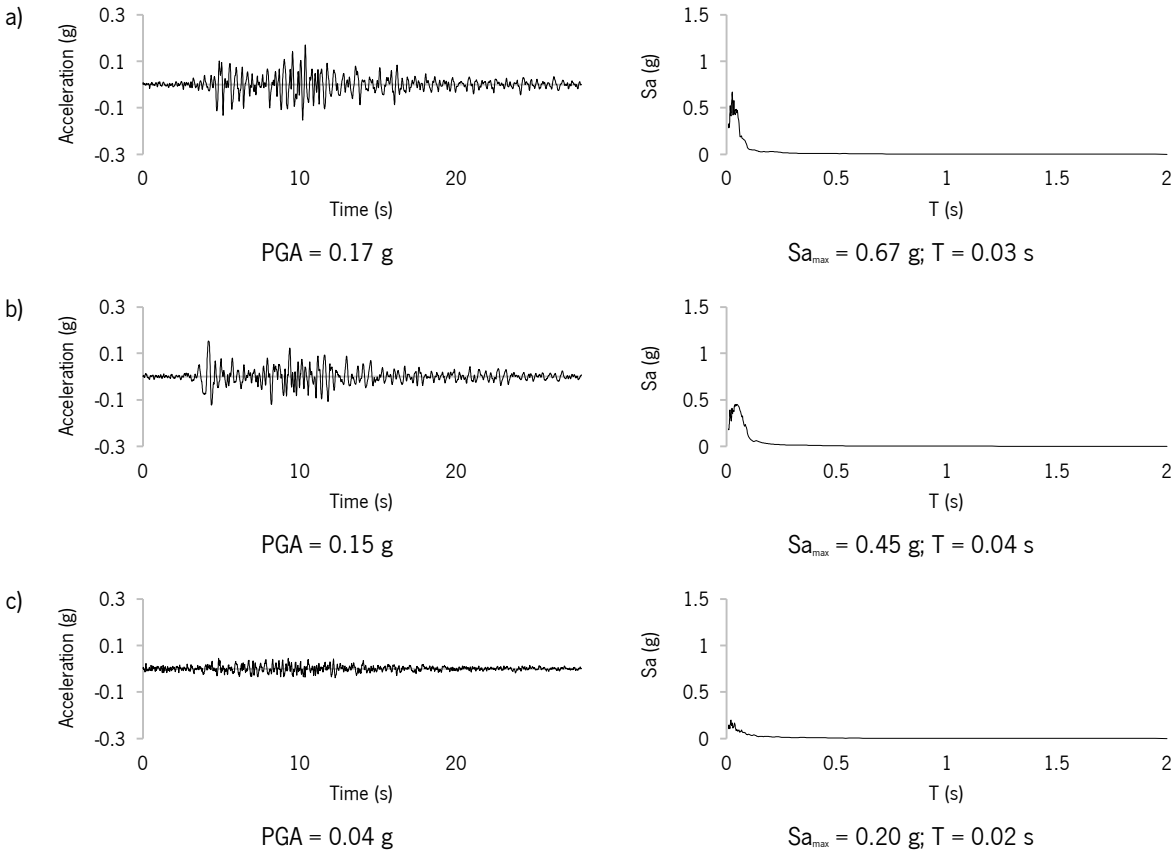

Figure A - 8. Components and response spectra for the input THEZ: a) horizontal (X); b) horizontal (Y); c) vertical (Z).

Annex B
Reports of damage NLDA

Figure B - 1 indicates the nomenclature used in the description of the damage. The lateral walls were divided into three areas: nave, dome area and presbytery. The figures presenting the results in terms of principal strains are scaled to $\varepsilon = 0.03$, for the eight cases, in order to make a comparison among them. Nonetheless, **Table B - 1** shows the maximum results for each case.

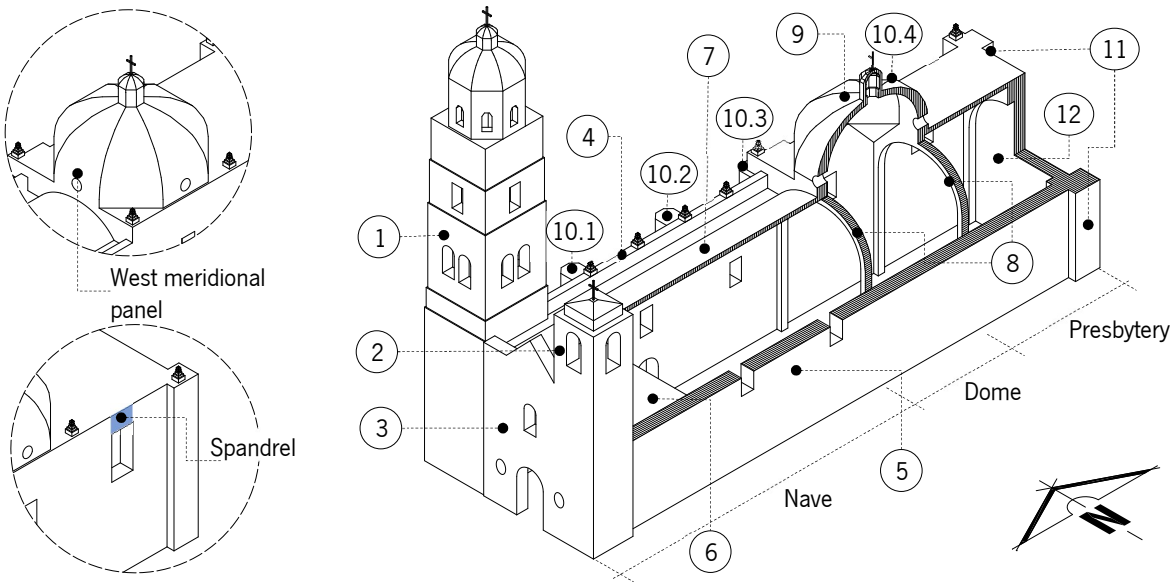

Figure B - 1. Nomenclature used in the description of the damage: 1) north tower; 2) south tower; 3) main façade; 4) north wall; 5) south wall; 6) choir loft; 7) barrel vault; 8) east and west transverse arch; 9) dome; 10) buttresses (1) to (4); 11) presbytery buttresses; 12) presbytery back wall; 13) groin vault.

Table B - 1. Maximum response in terms of principal strains (E1) and maximum crack width (Ecw1) for the eight signals.

Max. response	Earthquake							
	OAXM	**OXCU**	**OXJM**	**OXXO**	**SAPP**	**SCRU**	**RFPP**	**THEZ**
$E1_{max}$	0.0206	0.0482	0.0217	0.0398	0.0746	0.0375	0.0324	0.0628
$Ecw1_{max}$	5.8	15.8	5.3	10.5	24.3	11.26	10.69	13.91

$E1_{max}$: maximum principal strains; $Ecw1_{max}$: maximum crack width (mm).

1. OAXM earthquake. Oaxaca, Mexico

Principal strains (E1)

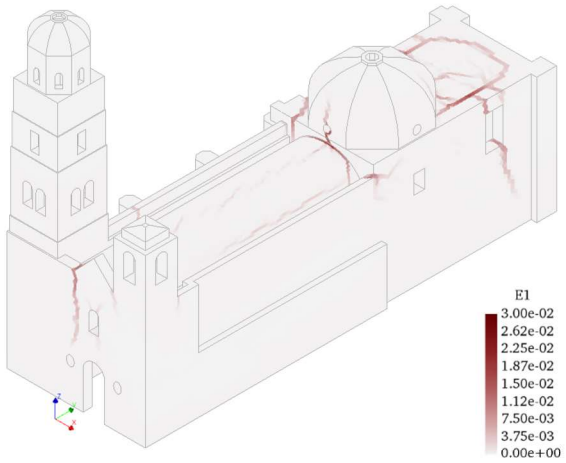

Failure mechanisms

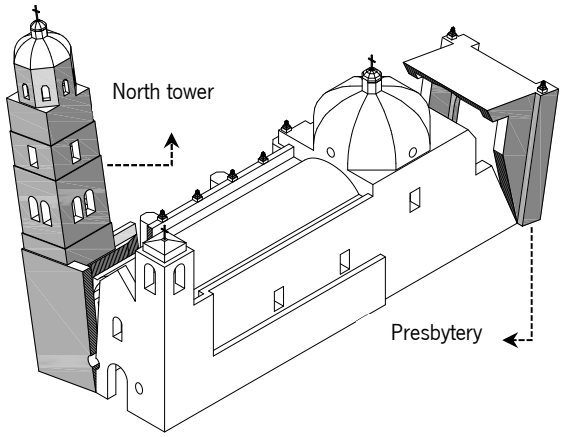

Part of the building	Description of the damage	$E1_{max}$	$Ecw1_{max}$
North tower	No damage	-	-
South tower	No damage	-	-
Façade	Vertical crack (≈ 10.5 m) starting at the north base of pediment to the oval window	0.0161	3.7
	Vertical crack (≈ 3 m) starting at the south base of the pediment	0.0063	1.4
	Diagonal cracks at the corners of the choir loft window	0.0025	0.6
North wall	Vertical crack (≈ 6.5 m) at the connection with the buttresses (1) and (3)	0.0047	0.9
	Diagonal crack (≈ 65°) at the presbytery	0.0143	5.4
South wall	Vertical crack (≈ 3 m) starting at the connection with the south tower	0.0035	0.7
	Horizontal damage at the connection with the dome	0.0131	3.0
	Diagonal crack (≈ 70°) at the presbytery	0.0097	2.9
Choir loft	Damage at the connections with the longitudinal walls	0.0076	1.5
	Crack perpendicular to the façade	0.0013	0.4
Barrel vault	Longitudinal continues crack at the south haunch (extrados)	0.0031	0.4
	Longitudinal not continues hinges at the crown area (both at the extrados and intrados)	0.0124	1.6
	Transversal damage starting at the connection with the north tower	0.0206	2.5
	Transverse crack at the connection with the façade and the south tower	0.0205	2.5
	Transverse crack at the connection with the dome	0.0206	2.9
Transverse arches	Cracks at the intrados of the crown	0.0197	4.8
Dome	Vertical cracks at the east, west and southeast meridional panels	0.0166	4.4
	Damage at the southeast meridional panel and pendentive	0.0069	2.3
	Damage at the northwest corner of the base	0.0094	2.6
Groin vault	Damage at the connection with the perimetral walls and along the crowns at the intrados	0.0179	5.8

$E1_{max}$: maximum principal strains related to the corresponding damage; $Ecw1_{max}$: maximum crack width related to the corresponding damage (mm).

2. OXCU earthquake. Oaxaca, Mexico

Principal strains (E1)

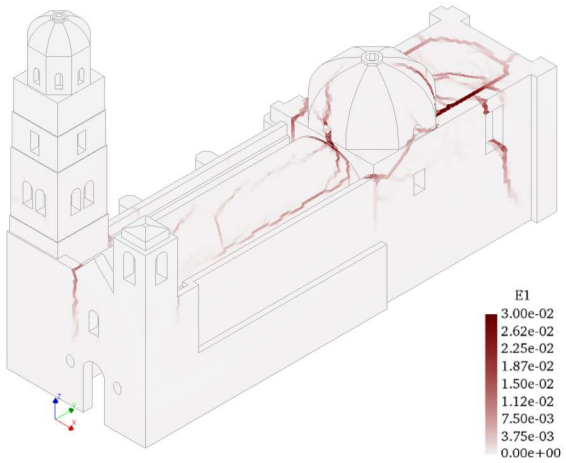

Failure mechanisms

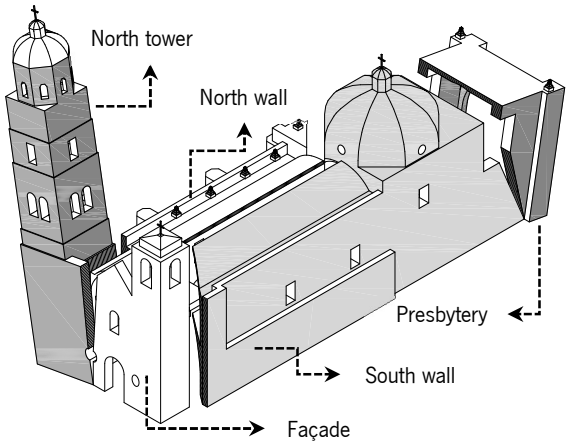

Part of the building	Description of the damage	$E1_{max}$	$Ecw1_{max}$
North tower	No damage	-	-
South tower	No damage	-	-
Façade	Vertical crack (≈ 10.5 m) starting at the north base of pediment to the oval window	0.0197	4.0
North wall	Vertical crack (≈ 9 m) at the connection with the north tower	0.0115	2.3
	Vertical crack (≈ 3.5 m) at the connection with the buttresses (1)	0.0021	0.5
	Diagonal crack (≈ 65°) at the presbytery	0.0109	4.1
South wall	Vertical crack (≈ 5 m) starting at the connection with the south tower	0.0063	1.3
	Horizontal damage at the connection with the dome	0.0192	4.4
	Diagonal crack (≈70°) at the presbytery	0.0171	5.6
	Internal damage at the spandrel of the presbytery	0.0170	5.4
Choir loft	Damage at the connections with the longitudinal walls	0.0094	1.9
Barrel vault	Longitudinal continues crack at the south haunch (extrados)	0.0095	1.2
	Longitudinal not continues hinges at the crown area (extrados and intrados)	0.0148	2.0
	Diagonal crack (≈45°) at the west half of the vault	0.0166	2.3
	Transverse damage starting at the connection with the north tower	0.0053	0.7
	Transverse crack at the connection with the façade and the perimeter of the south tower	0.0194	2.7
	Transverse crack at the connection with the dome	0.0381	4.3
Transverse arches	Cracks at the intrados of the crown of the west arch	0.0440	12.3
	Cracks at the intrados of the crown of the east arch	0.0205	6.1
Dome	Diagonal cracks at the east and west meridional panels	0.0232	5.8
	Severe damage at the southeast meridional panel and pendentive	0.0436	12.2
Groin vault	Damage at the connection with the perimetral walls and along the crowns at the intrados	0.0482	15.8

$E1_{max}$: maximum principal strain related to the corresponding damage; $Ecw1_{max}$: maximum crack width related to the corresponding damage (mm).

3. OXJM earthquake. Oaxaca, Mexico

Principal strains (E1)

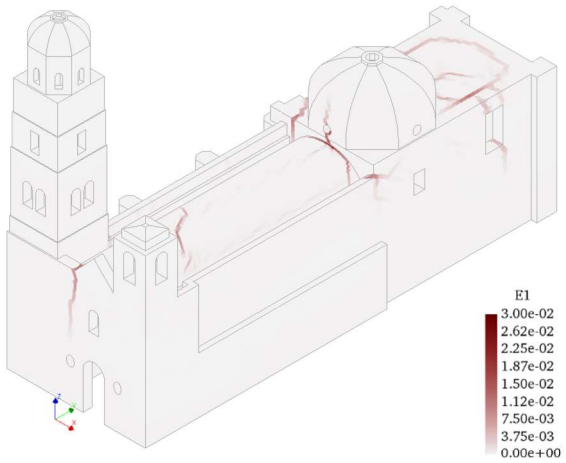

Failure mechanisms

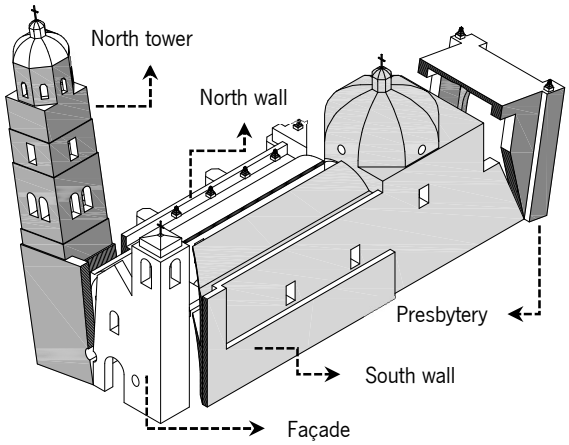

Part of the building	Description of the damage	$E1_{max}$	$Ecw1_{max}$
North tower	No damage	-	-
South tower	No damage	-	-
Façade	Vertical crack starting at the north base of pediment to the oval window	0.0192	3.2
North wall	Vertical crack (≈ 8 m) at the connection with the north tower	0.0103	1.5
	Vertical crack (≈ 3.5 m) at the connection with the buttresses (3)	0.0083	2.13
	Diagonal cracks (≈ 70°) at the presbytery	0.0049	1.9
South wall	Vertical crack at the change of thickness (≈ 4 m)	0.0014	0.3
	Horizontal damage at the connection with the dome	0.0109	2.8
	Diagonal cracks (≈70°) at the presbytery	0.0048	1.4
Choir loft	Damage at the connections with the longitudinal walls	0.0103	2.0
Barrel vault	Longitudinal continues crack at the south haunch (extrados)	0.0063	0.9
	Longitudinal not continues hinges at the crown area (intrados)	0.0110	1.4
	Diagonal cracks (≈ 45° to 60°) at the west half	0.0173	2.2
	Transverse crack at the connection with the façade and the perimeter of the south tower	0.0188	2.6
	Transverse crack at the connection with the dome	0.0217	2.9
Transverse arches	Cracks at the intrados of the crown of the west arch	0.0206	4.9
	Cracks at the intrados of the crown of the east arch	0.0159	4.7
Dome	Diagonal cracks at the east and west meridional panels	0.0171	4.7
	Severe damage at the northwest corner of the base and pediment	0.0083	2.13
Groin vault	Damage at the connection with the perimetral walls and along the crowns at the intrados	0.0118	3.8

$E1_{max}$: maximum principal strain related to the corresponding damage; $Ecw1_{max}$: maximum crack width related to the corresponding damage (mm).

4. OXXO earthquake. Oaxaca, Mexico

Principal strains (E1)

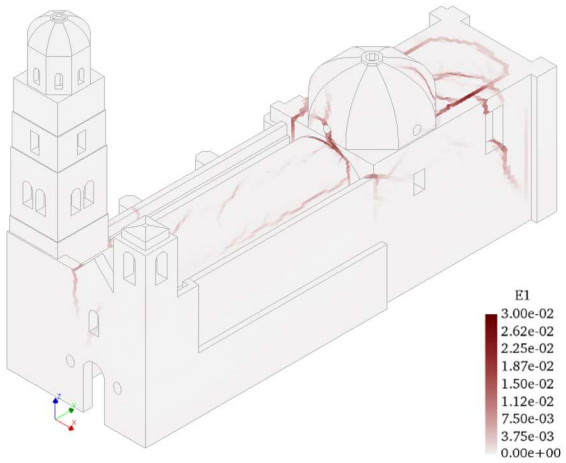

Failure mechanisms

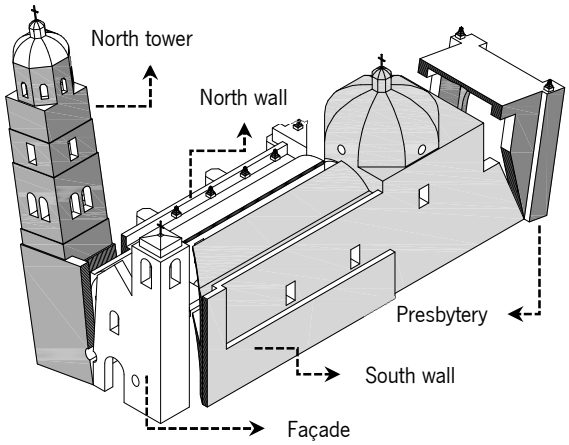

Part of the building	Description of the damage	$E1_{max}$	$Ecw1_{max}$
North tower	No damage	-	-
South tower	No damage	-	-
Façade	Vertical crack (≈ 6.5 m) starting at the north base of pediment to the oval window	0.0135	2.1
	Diagonal cracks at the corners of the choir loft window	0.0026	0.6
North wall	Vertical crack (≈ 8 m) at the connection with the north tower	0.0129	2.2
	Vertical crack (≈ 4.5 m) at the connection with the buttresses (1)	0.036	0.7
	Diagonal crack (≈ 70°) at the presbytery	0.0052	2.1
South wall	Vertical crack (≈ 4 m) at the change of thickness	0.0022	0.5
	Horizontal damage at the connection with the dome	0.0111	3.1
	Diagonal crack (≈70°) at the presbytery	0.0113	3.8
Choir loft	Damage at the connections with the longitudinal walls	0.0100	1.9
Barrel vault	Longitudinal continues crack at the south haunch (extrados)		
	Longitudinal damage formed by diagonal parallel cracks (≈ 30°) at the crown area (extrados and intrados)	0.0110	1.4
	Transverse crack at the connection with the façade and the perimeter of the south tower	0.0144	2.0
	Transverse crack at the connection with the dome	0.0192	2.9
Transverse arches	Cracks at the intrados of the crown of the west arch	0.0398	10.5
	Cracks at the intrados of the crown of the east arch	0.0180	5.3
Dome	Cracks at the east and west meridional panels	0.0241	5.8
	Damage at the southeast meridional panel and pendentive	0.0117	3.3
	Damage at the northwest corner of the base and pediment	0.0082	2.4
Groin vault	Damage at the connection with the perimetral walls and along the crowns at the intrados	0.0268	8.9

$E1_{max}$: maximum principal strain related to the corresponding damage; $Ecw1_{max}$: maximum crack width related to the corresponding damage (mm).

5. SAPP earthquake. Oaxaca, Mexico

Principal strains (E1)

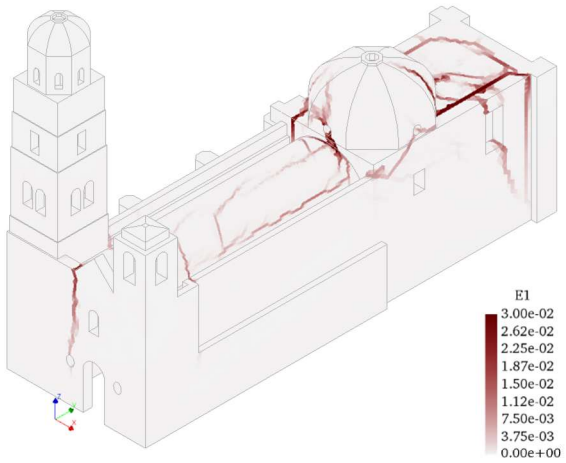

Failure mechanisms

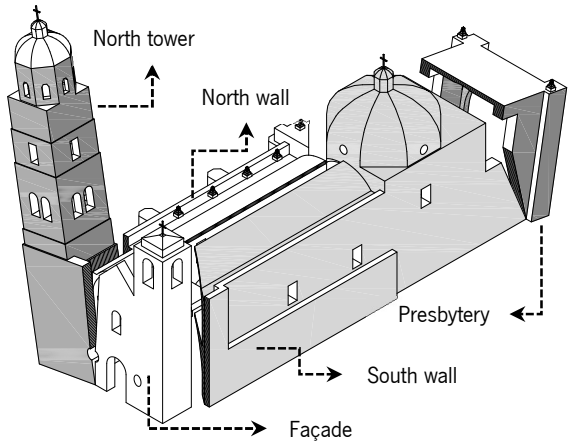

Part of the building	Description of the damage	$E1_{max}$	$Ecw1_{max}$
North tower	No damage	-	-
South tower	No damage	-	-
Façade	Vertical crack (≈ 13.5 m) starting at the north base of pediment to the oval window	0.0295	6.1
North wall	Vertical crack (≈ 9.5 m) at the connection with the north tower	0.0138	2.1
	Vertical crack (≈ 3.5 m) at the connection with the buttresses (1)	0.0010	0.2
	Horizontal damage at the base of the dome	0.0218	3.3
	Horizontal damage at the top of buttress (4)	0.0018	0.5
	Diagonal crack (≈ 75°) at the presbytery	0.0063	2.4
South wall	Vertical crack (≈ 10.5 m) at the change of thickness	0.0137	2.8
	Horizontal damage at the connection with the dome	0.0101	2.8
	Diagonal crack (≈ 70°) at the presbytery	0.0152	4.7
	Vertical crack (≈ 16 m) at the connection with the back wall of the presbytery	0.0462	8.6
Choir loft	Damage at the connections with the longitudinal walls	0.0114	2.2
Barrel vault	Longitudinal continues crack at the south haunch (extrados)	0.0109	1.3
	Longitudinal not continues cracks at the crown area (extrados and intrados)	0.0237	2.8
	Diagonal cracks (≈ 30° to 60°) at the west half	0.0123	1.5
	Transverse crack at the connection with the façade and the perimeter of the south tower	0.0229	3.1
	Transverse crack at the connection with the dome	0.0549	7.6
Transverse arches	Cracks at the intrados of the crown of the west arch	0.0604	17.5
	Cracks at the intrados of the crown of the east arch	0.0206	6.1
Dome	Diagonal cracks at the east and west meridional panels	0.0503	12.9
	Severe damage at the southeast meridional panel and pendentive	0.0611	14.9
	Damage at the northwest corner of the base	0.0289	8.1
Groin vault	Damage at the connection with the perimetral walls and along the crowns at the intrados	0.0746	24.3

$E1_{max}$: maximum principal strain related to the corresponding damage; $Ecw1_{max}$: maximum crack width related to the corresponding damage (mm).

6. SCRU earthquake. Oaxaca, Mexico

Principal strains (E1)

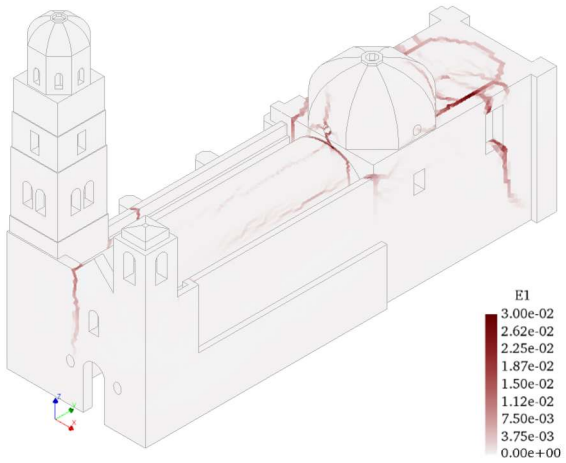

Failure mechanisms

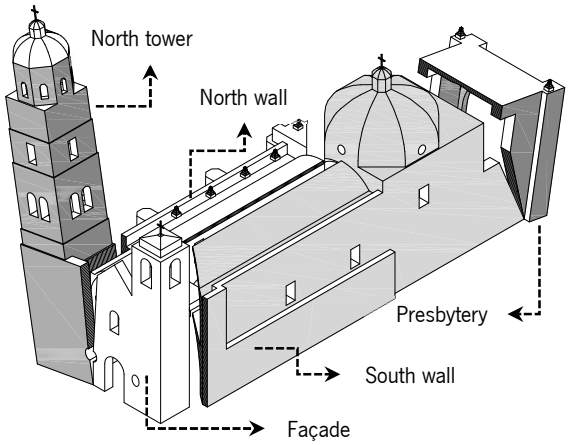

Part of the building	Description of the damage	$E1_{max}$	$Ecw1_{max}$
North tower	No damage	-	-
South tower	No damage	-	-
Façade	Vertical crack (≈11 m) starting at the north base of pediment to the oval window	0.0176	3.7
North wall	Vertical crack (≈ 10 m) at the connection with the north tower	0.0136	2.1
	Vertical crack (≈ 11.5 m) at the connection with the buttresses (1)	0.153	3.0
	Horizontal damage at the base of the dome	0.0078	2.0
	Diagonal crack (≈ 65°) at the presbytery	0.0100	3.2
South wall	Vertical crack (≈ 7 m) at the change of thickness	0.0031	0.6
	Horizontal damage at the connection with the dome	0.0120	2.8
	Diagonal crack (≈ 70°) at the presbytery	0.0199	7.1
Choir loft	Damage at the connections with the longitudinal walls	0.0084	1.6
Barrel vault	Longitudinal continues crack at the south haunch (extrados)	0.0051	0.7
	Longitudinal hinges at the crown area (extrados and intrados)	0.0144	1.9
	Diagonal crack (≈ 60°) at the west half	0.0230	3.1
	Transverse crack at the connection with the façade and the perimeter of the south tower	0.0177	2.4
	Transverse crack at the connection with the dome	0.0300	3.3
Transverse arches	Cracks at the intrados of the crown of the west arch	0.0194	4.5
	Cracks at the intrados of the crown of the east arch	0.0201	6.0
Dome	Diagonal cracks at the east and west meridional panels	0.0174	4.8
	Severe damage at the southeast meridional panel and pendentive	0.0201	5.3
	Damage at the northwest corner of the base	0.0119	3.3
Groin vault	Damage at the connection with the perimetral walls and along the crowns at the intrados	0.0345	11.3

$E1_{max}$: maximum principal strain related to the corresponding damage; $Ecw1_{max}$: maximum crack width related to the corresponding damage (mm).

7. RFPP earthquake. Oaxaca, Mexico

Principal strains (E1)

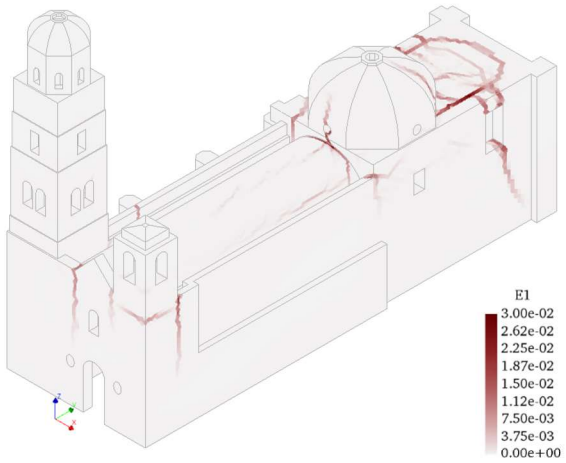

Failure mechanisms

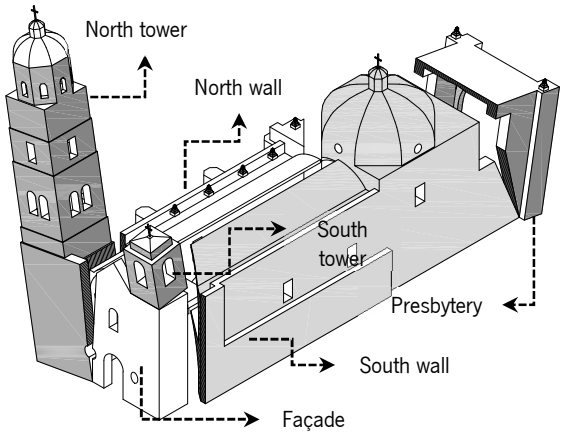

Part of the building	Description of the damage	$E1_{max}$	$Ecw1_{max}$
North tower	No damage	-	-
South tower	No damage	-	-
Façade	Vertical crack (≈ 9.5 m) starting at the north base of pediment to the oval window	0.0179	3.0
	Vertical crack (≈ 5 m) starting at the south base of pediment	0.0077	1.8
	Horizontal crack at the base of the south tower	0.0071	1.9
North wall	Vertical crack (≈ 5 m) at the connection with the north tower	0.0071	1.27
	Vertical crack (≈ 11 m) at the connection with the buttresses (1)	0.0124	2.5
	Diagonal crack (≈ 70°) at the presbytery	0.0242	8.1
South wall	Vertical crack (≈ 9.5 m) starting at the connection with the south tower	0.0228	4.6
	Horizontal damage at the base of the south tower	0.0071	1.9
	Horizontal damage at the connection with the dome	0.0151	3.5
	Diagonal crack (≈70°) at the presbytery	0.0214	7.1
Choir loft	Damage at the connections with the longitudinal walls	0.0081	1.6
Barrel vault	Longitudinal continues crack at the south haunch (extrados)	0.0039	0.5
	Longitudinal not continues damage at the crown area (extrados and intrados)	0.0156	2.0
	Diagonal crack (≈ 50°) at the west half of the vault	0.0107	1.4
	Transversal crack starting at the connection with the north tower	0.0181	2.7
	Transverse crack at the connection with the façade and the perimeter of the south tower	0.0184	2.7
	Transverse crack at the connection with the dome	0.0321	3.6
Transverse arches	Cracks at the intrados of the crown of the west arch	0.0188	5.2
	Cracks at the intrados of the crown of the east arch	0.0233	5.3
Dome	Diagonal cracks at the east and west meridional panels	0.0201	5.2
	Damage at the southeast meridional panel and pendentive	0.0192	5.1
	Damage at the northwest corner of the base	0.0104	2.9
Groin vault	Damage at the connection with the perimetral walls and along the crowns at the intrados	0.0345	11.3

$E1_{max}$: maximum principal strain related to the corresponding damage; $Ecw1_{max}$: maximum crack width related to the corresponding damage.

8. THEZ earthquake. Oaxaca, Mexico

Principal strains (E1)

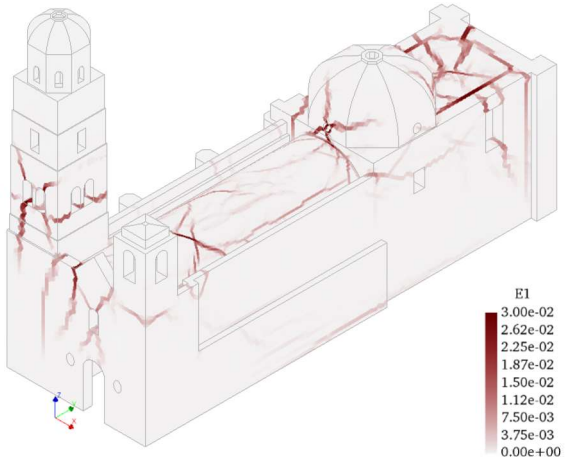

Failure mechanisms

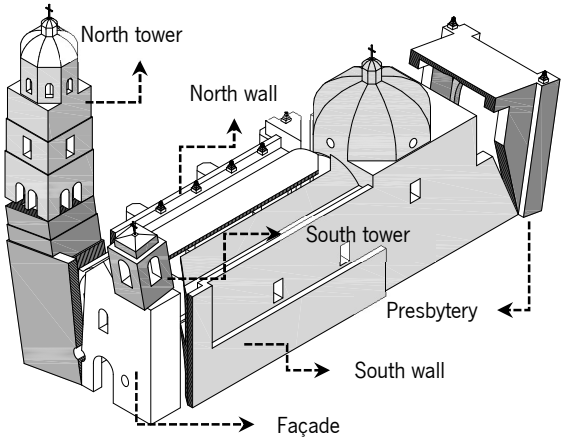

Part of the building	Description of the damage	$E1_{max}$	$Ecw1_{max}$
North tower	Horizontal and diagonal damage at the belfry	0.0398	12.5
	Vertical cracks at the east and west face of the tower	0.0262	10.2
South tower	No damage	-	-
Façade	Vertical crack (≈ 14 m) at the connection with the north tower	0.0175	3.7
	Vertical crack (≈ 9.5 m) starting at the north base of pediment	0.0306	7.2
	Diagonal cracks at the corners of the choir loft window	0.0118	2.9
	Horizontal damage at the base of the south tower	0.0064	2.1
North wall	Vertical cracks at the nave, at the connections with the tower and buttresses (1), (2) and (3)	0.0061	1.5
	Damage at the area under the dome	0.0400	3.8
	Diagonal crack (≈ 70°) at the presbytery	0.0238	8.7
South wall	Vertical crack (≈ 9.5 m) at the change of thickness	0.0071	1.6
	Horizontal damage at the base of the south tower	0.0068	1.9
	Horizontal damage along the base of the wall (nave to presbytery)	0.0042	1.3
	Horizontal damage under the area of the dome	0.0136	4.2
	Diagonal crack (≈ 70°) at the presbytery	0.0170	5.4
	Vertical crack (≈ 17 m) at the connection with the back wall of the presbytery	0.0569	8.8
Choir loft	Damage at the connections with the longitudinal walls	0.0125	2.4
Barrel vault	Longitudinal continues crack at both haunches (extrados)	0.0154	2.0
	Longitudinal damage at the north springer (intrados)	0.0081	1.0
	Spread diagonal cracks at the crown area (extrados and intrados)	0.0235	3.0
	Transverse crack at the connection with the façade and the perimeter of the south tower	0.0614	7.6
	Transverse crack at the connection with the dome	0.0297	4.4
Transverse arches	Cracks at the intrados of the crown of the west arch	0.0297	7.7
	Cracks at the intrados of the crown of the east arch	0.0314	9.4

	Cracks at the base on the pillars of the arches	0.0045	1.3
Dome	Diagonal cracks at the east and west meridional panels	0.0616	11.7
	Horizontal damage under the windows at north and south meridional panels	0.0062	1.6
	Damage at the northeast and southeast meridional panel and pendentive	0.0134	4.3
Groin vault	Damage at the connection with the perimetral walls and along the crowns at the intrados	0.0425	13.9
Back wall of the presbytery	Vertical crack (≈ 15 m) closed to the north buttress	0.0249	8.6

$E1_{max}$: maximum principal strain related to the corresponding damage; $Ecw1_{max}$: maximum crack width related to the corresponding damage (mm).

Annex C
Graphical results NLDA and POA

C.1. Non lineal dynamic analysis (NLDA)

C.1.1. OAXM. Oaxaca, Mexico.

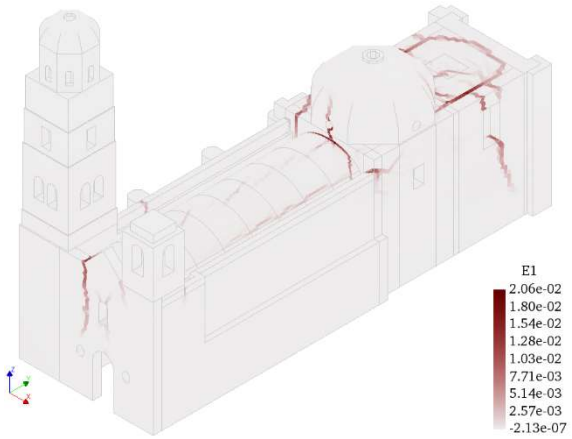

Principal strains E1

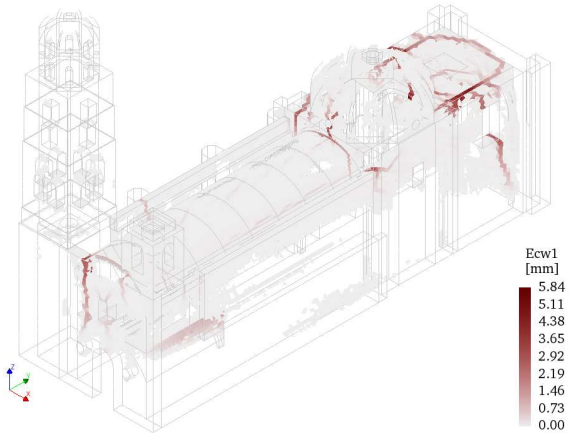

Crack width Ewc1

Plan view of the roof (extrados)

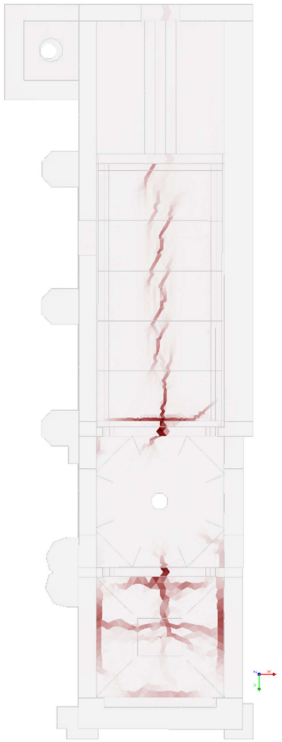

Plan view of the roof (intrados)

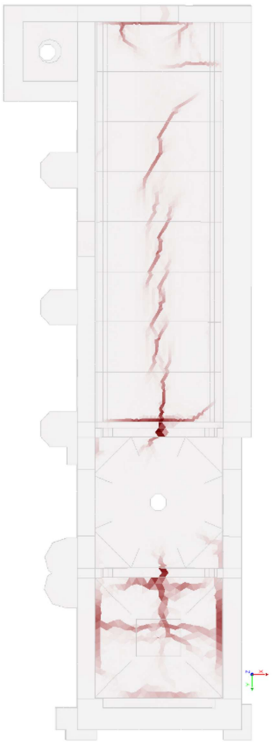

Plan view of the roof (intrados)

Note: choir loft removed.

Figure C - 1. Damage caused by the OAXM record.

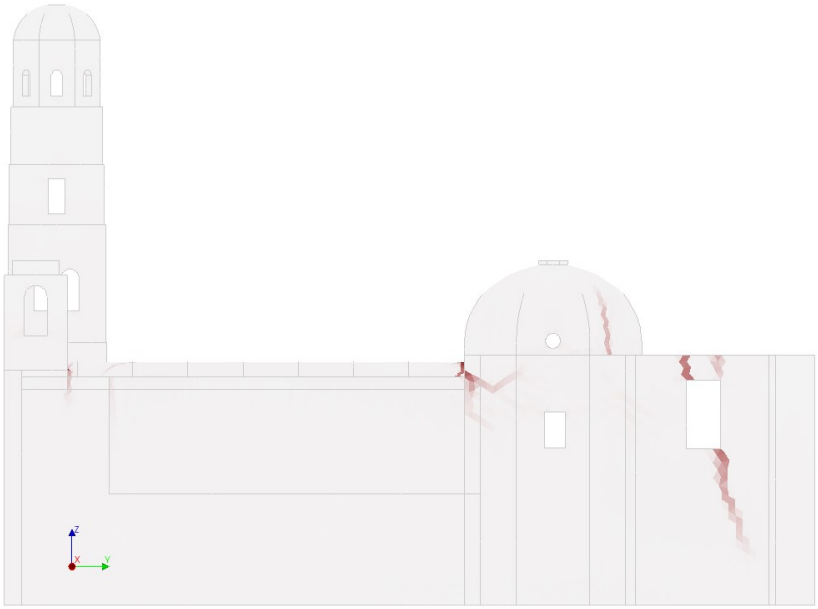

South elevation. Principal strains E1

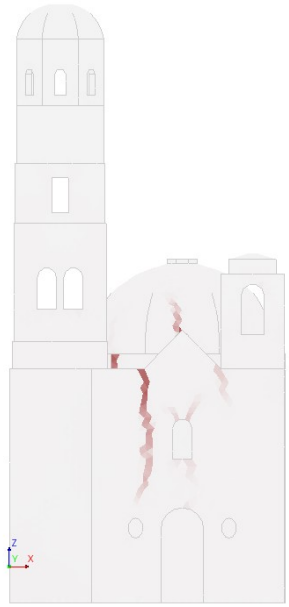

West Elevation. Principal strains E1

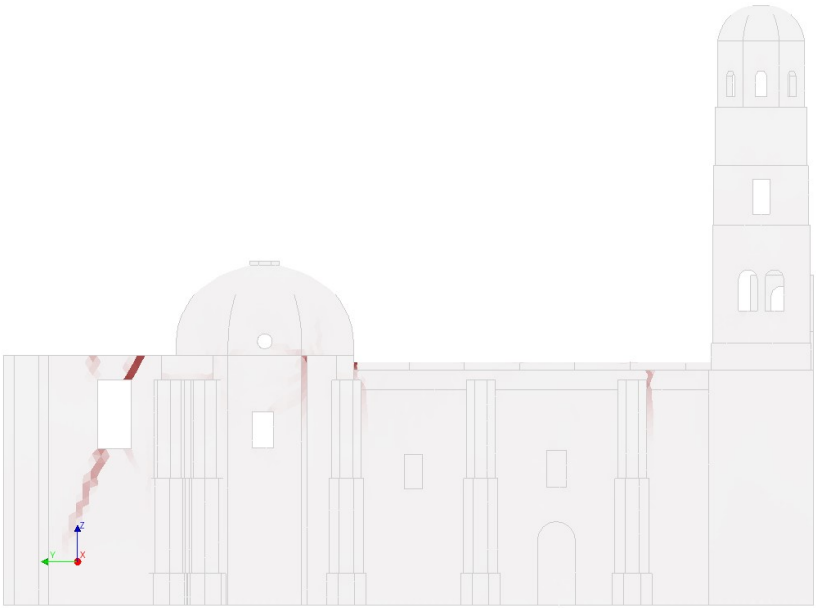

North elevation. Principal strains E1

East Elevation. Principal strains E1

Figure C - 2. Damage caused by the OAXM record.

C.1.2. OXCU. Oaxaca, Mexico.

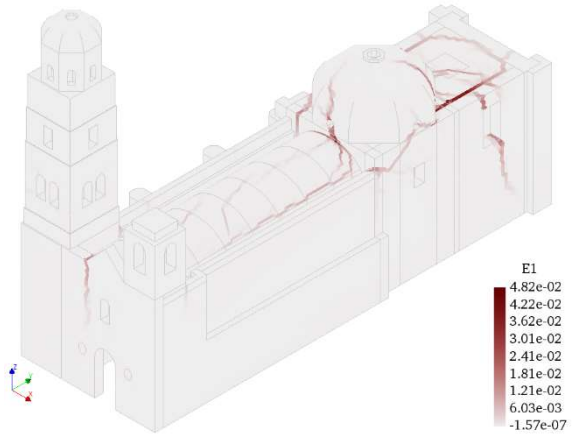

Principal strains E1

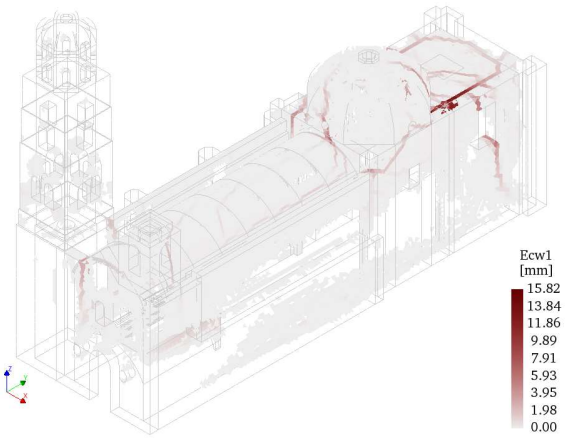

Crack width Ewc1

Plan view of the roof (extrados)

Plan view of the roof (intrados)

Plan view of the roof (intrados)

Note: choir loft removed.

Figure C - 3. Damage caused by the OXCU record.

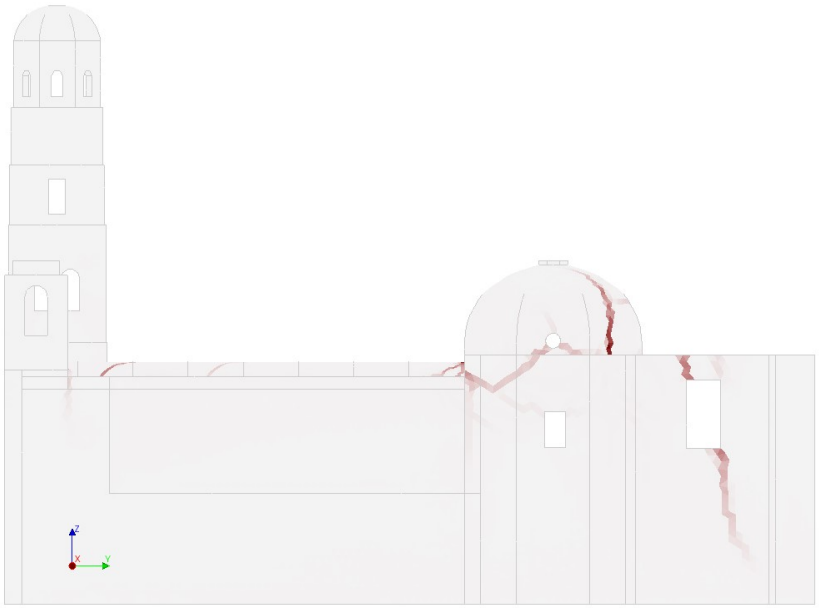

South elevation. Principal strains E1

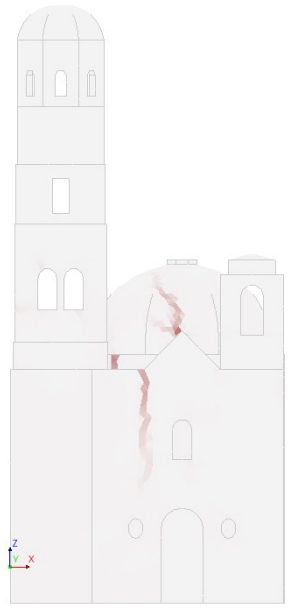

West Elevation. Principal strains E1

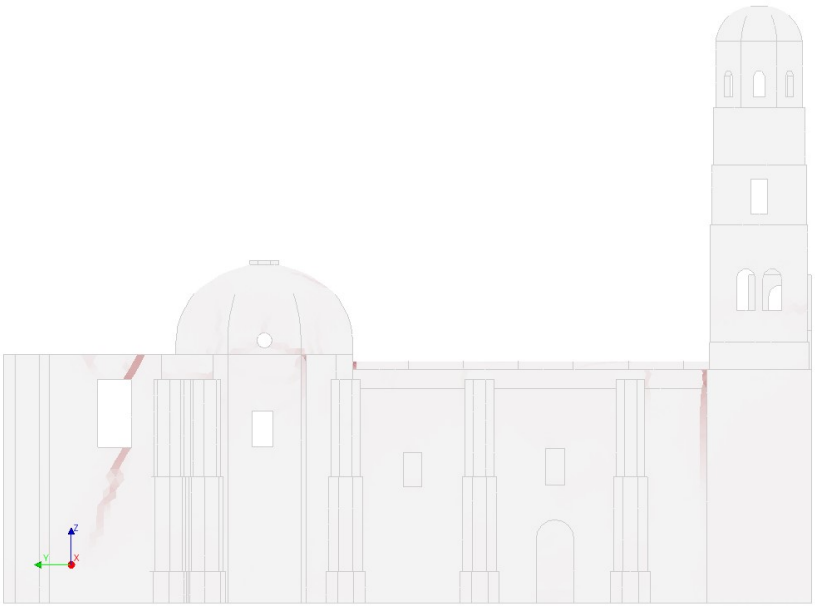

North elevation. Principal strains E1

East Elevation. Principal strains E1

Figure C - 4. Damage caused by the OXCU record.

C.1.3. OXJM. Oaxaca, Mexico.

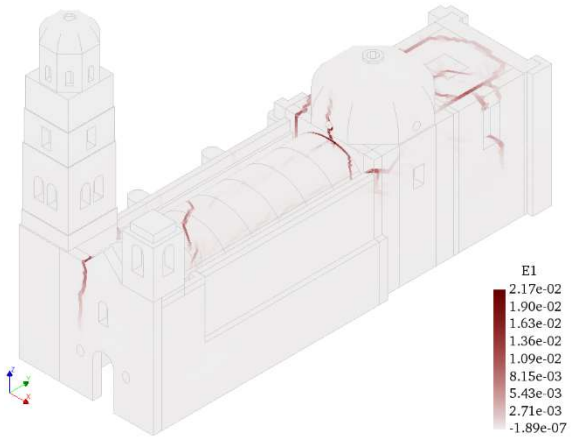

Principal strains E1

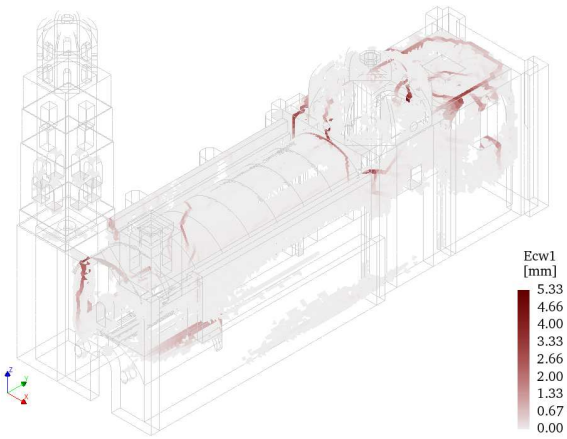

Crack width Ewc1

Plan view of the roof (extrados)

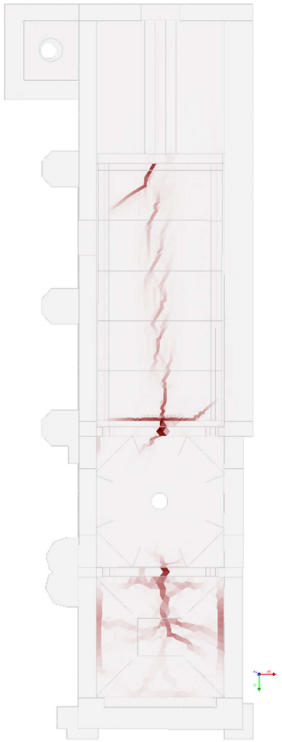

Plan view of the roof (intrados)

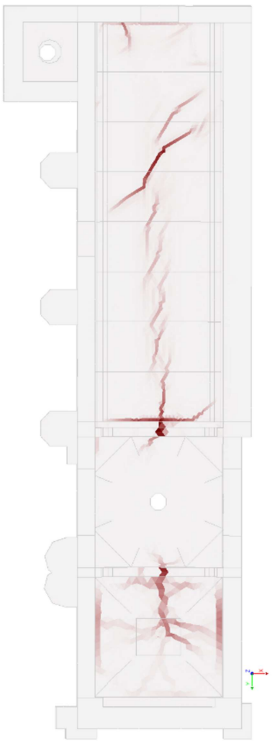

Plan view of the roof (intrados)

Note: choir loft removed.

Figure C - 5. Damage caused by the OXJM record.

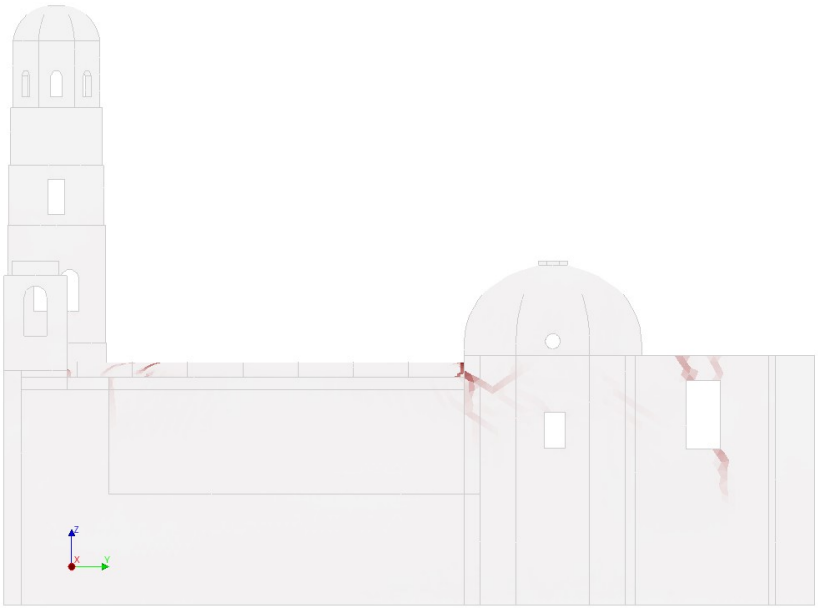

South elevation. Principal strains E1

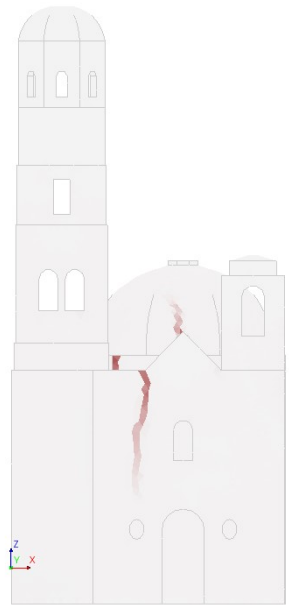

West Elevation. Principal strains E1

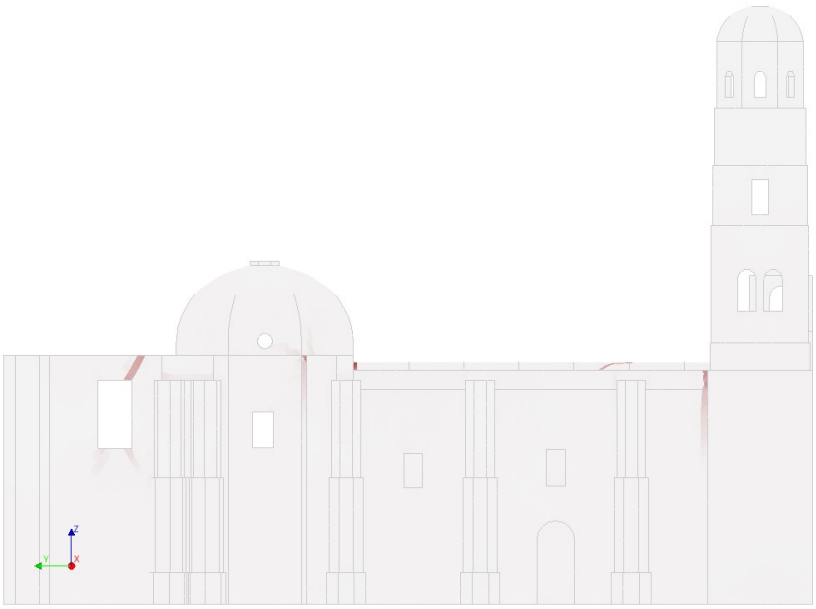

North elevation. Principal strains E1

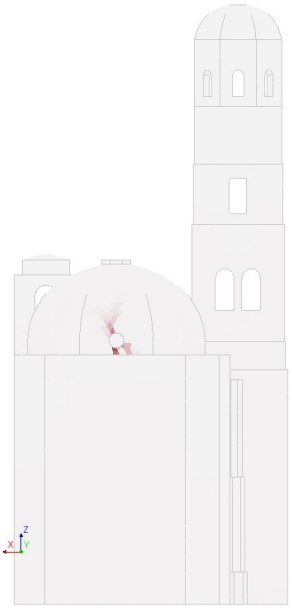

East Elevation. Principal strains E1

Figure C - 6. Damage caused by the OXJM record.

C.1.4. OXXO. Oaxaca, Mexico.

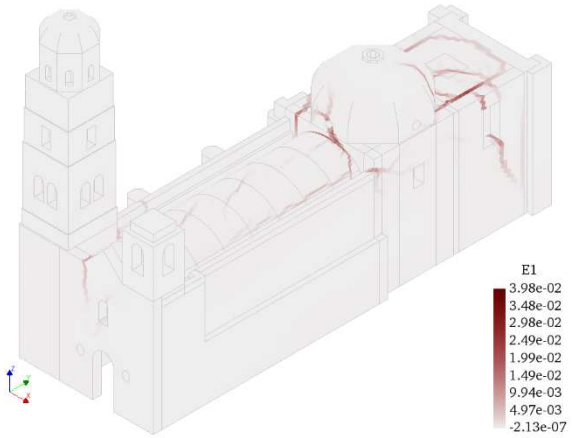

Principal strains E1

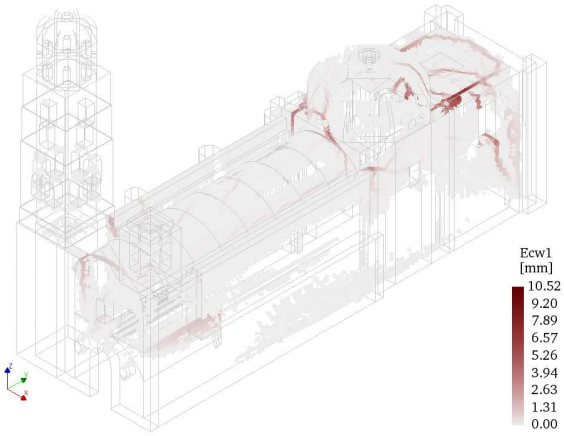

Crack width Ewc1

Plan view of the roof (extrados)

Plan view of the roof (intrados)

Plan view of the roof (intrados)

Note: choir loft removed.

Figure C - 7. Damage caused by the OXXO record.

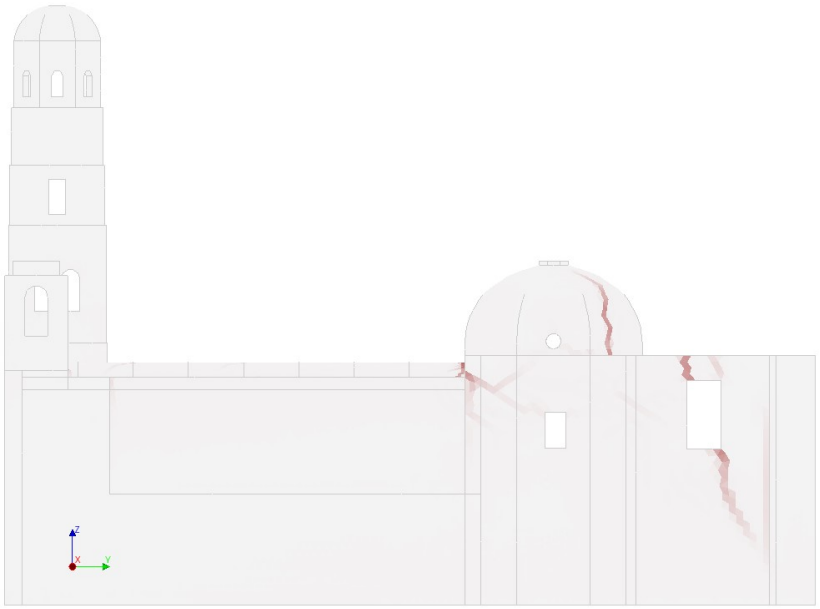

South elevation. Principal strains E1

West Elevation. Principal strains E1

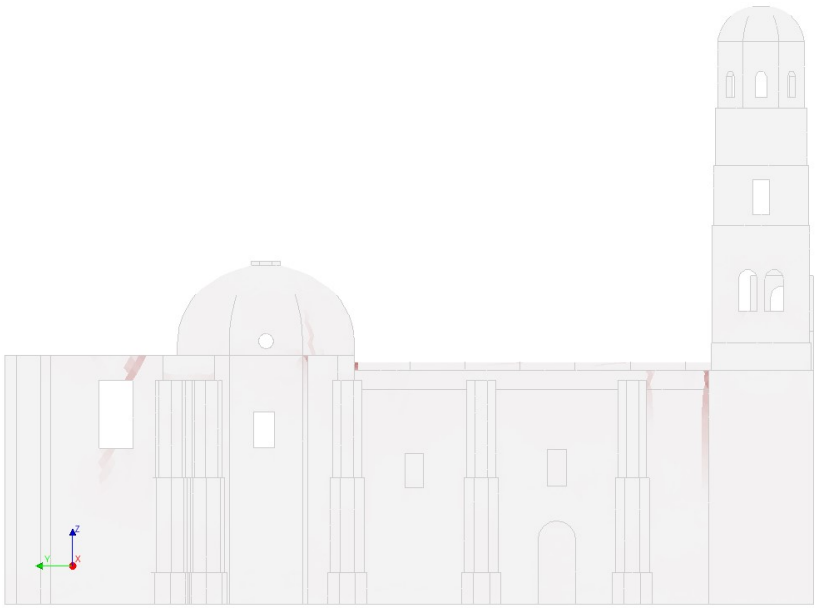

North elevation. Principal strains E1

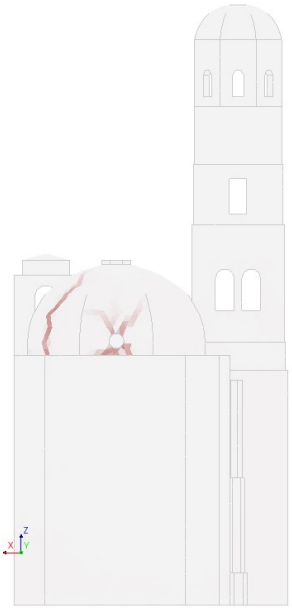

East Elevation. Principal strains E1

Figure C - 8. Damage caused by the OXXO record.

C.1.5. SAPP. Puebla, Mexico.

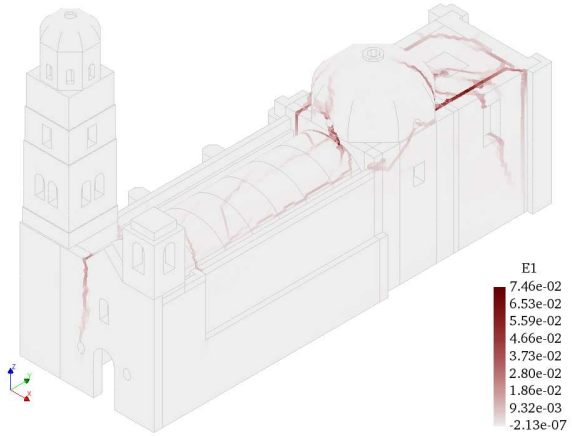

Principal strains E1

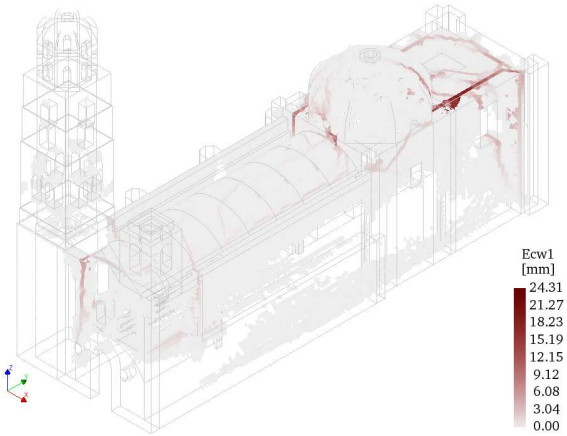

Crack width Ewc1

Plan view of the roof (extrados)

Plan view of the roof (intrados)

Plan view of the roof (intrados)

Note: choir loft removed.

Figure C - 9. Damage caused by the SAPP record.

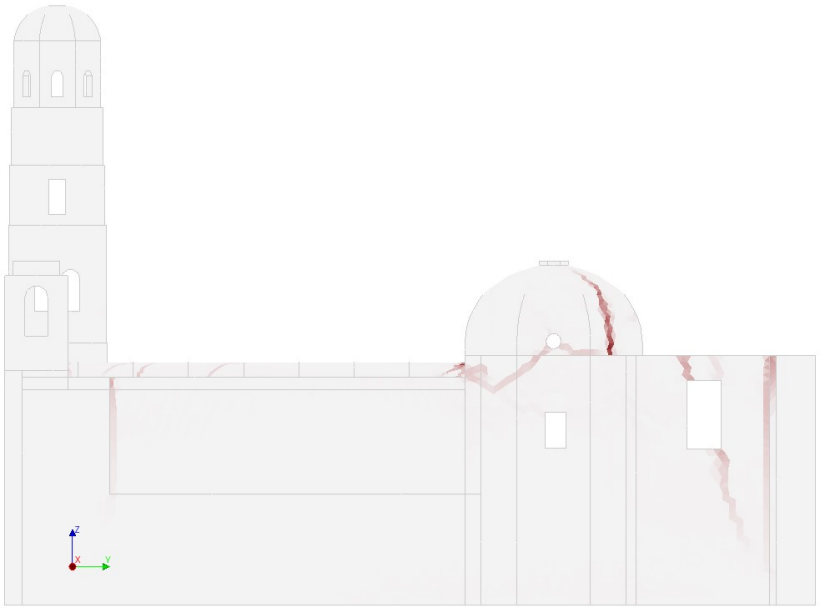

South elevation. Principal strains E1

West Elevation. Principal strains E1

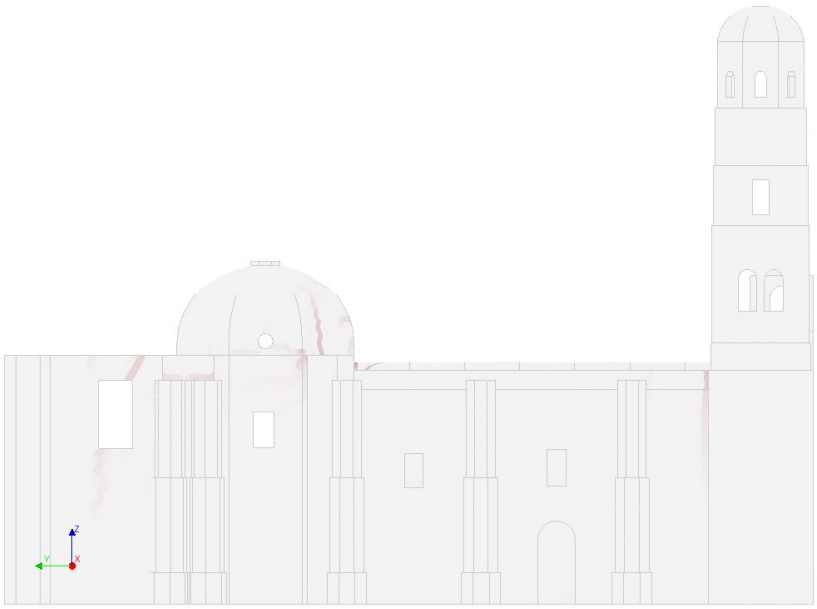

North elevation. Principal strains E1

East Elevation. Principal strains E1

Figure C - 10. Damage caused by the SAPP record.

C.1.6. SCRU. Oaxaca, Mexico.

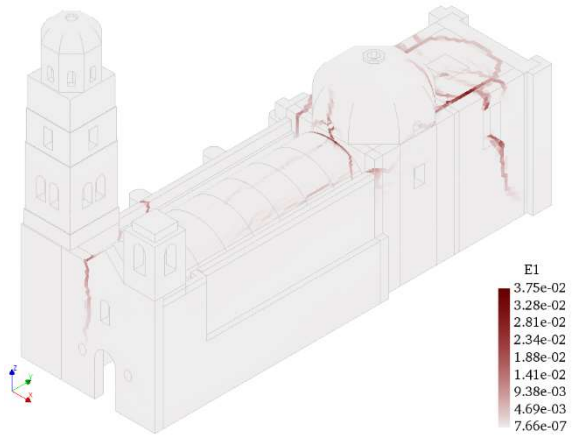

Principal strains E1

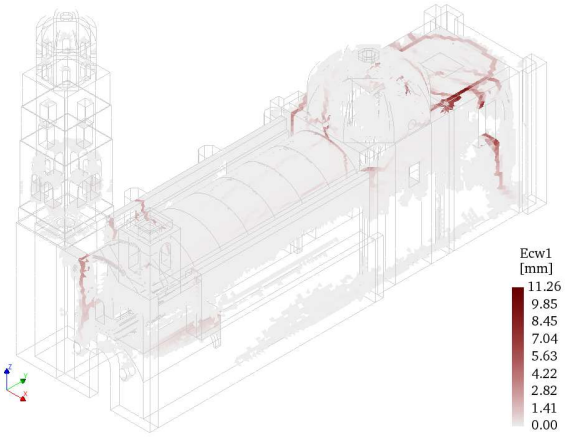

Crack width Ewc1

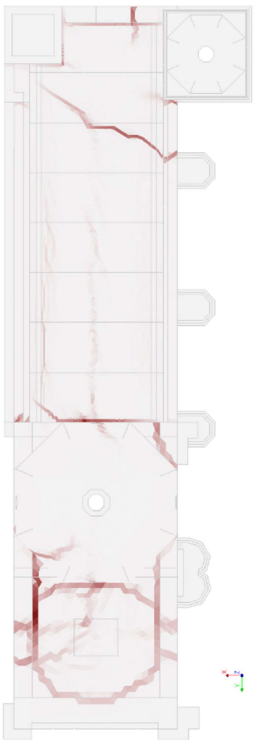

Plan view of the roof (extrados)

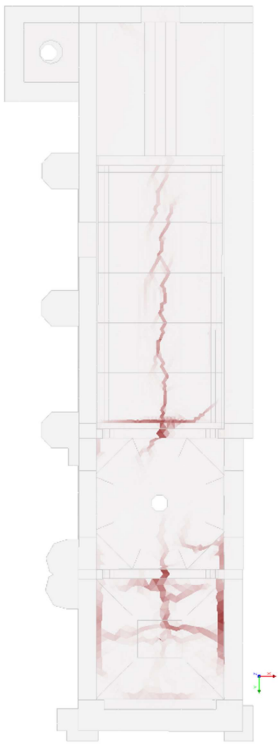

Plan view of the roof (intrados)

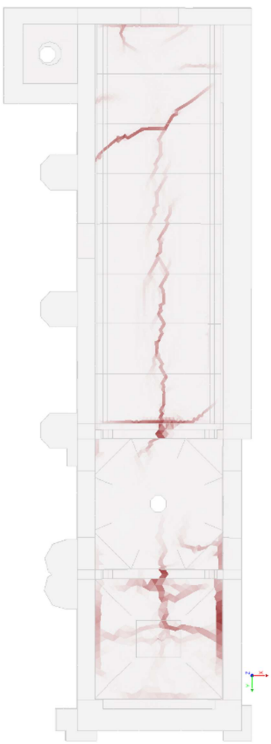

Plan view of the roof (intrados)

Note: choir loft removed.

Figure C - 11. Damage caused by the SCRU record.

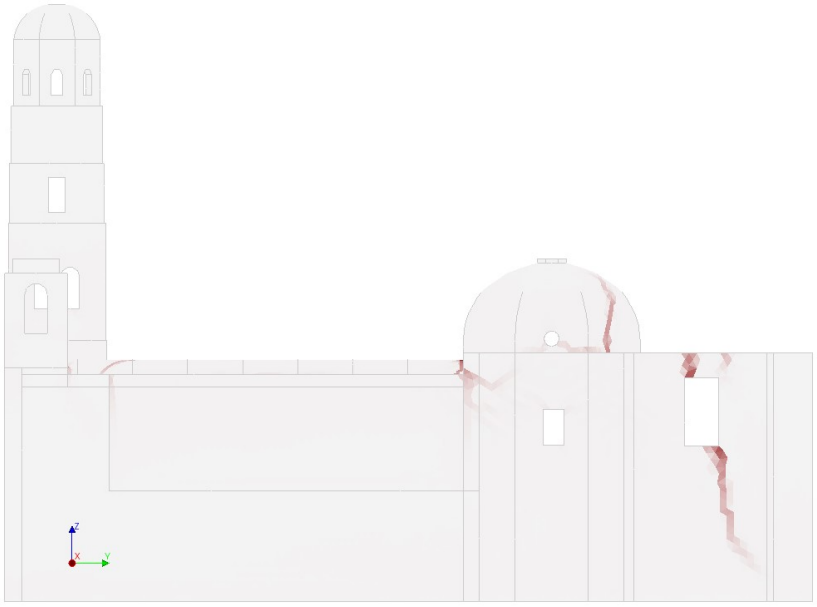

South elevation. Principal strains E1

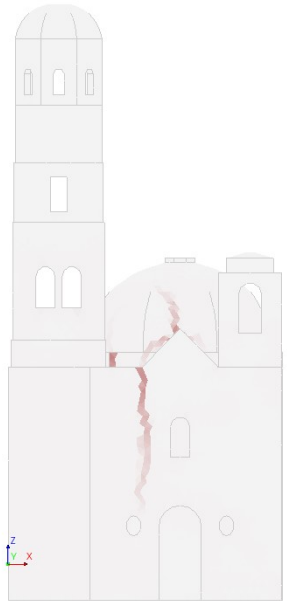

West Elevation. Principal strains E1

North elevation. Principal strains E1

East Elevation. Principal strains E1

Figure C - 12. Damage caused by the SCRU record.

C.1.7. RFPP. Puebla, Mexico.

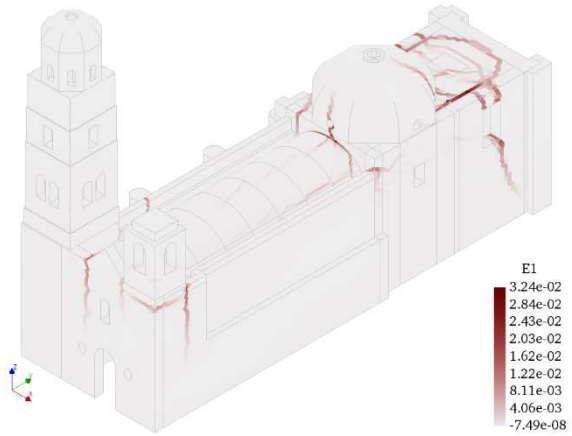

Principal strains E1

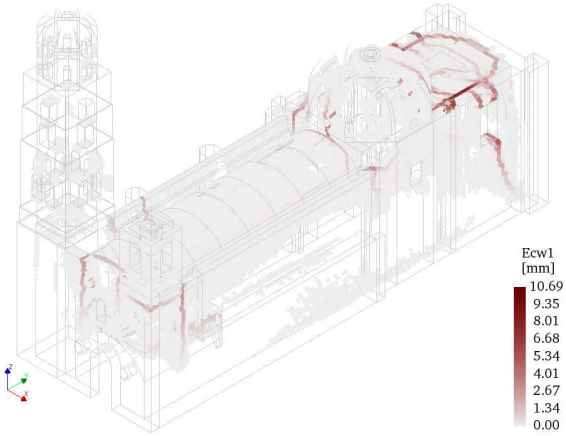

Crack width Ewc1

Plan view of the roof (extrados)

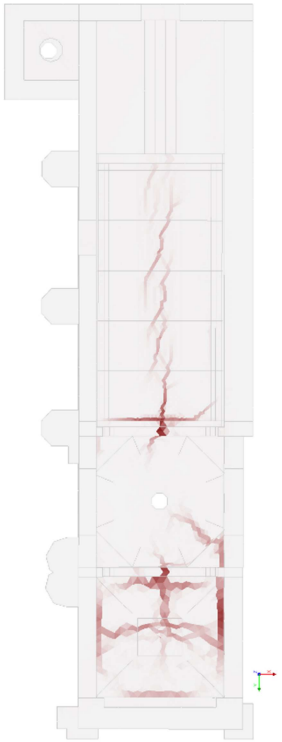

Plan view of the roof (intrados)

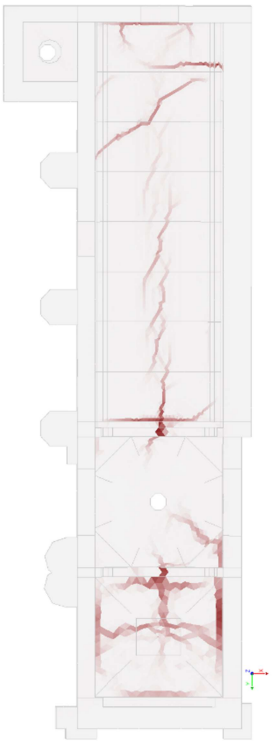

Plan view of the roof (intrados)

Note: choir loft removed.

Figure C - 13. Damage caused by the RFPP record.

South elevation. Principal strains E1

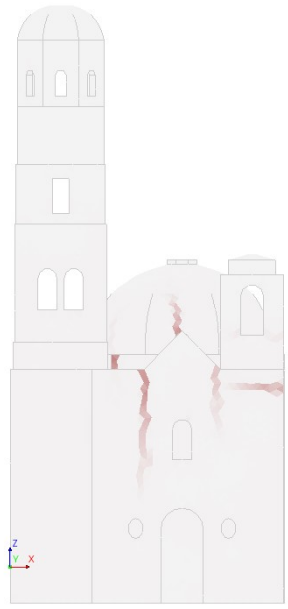

West Elevation. Principal strains E1

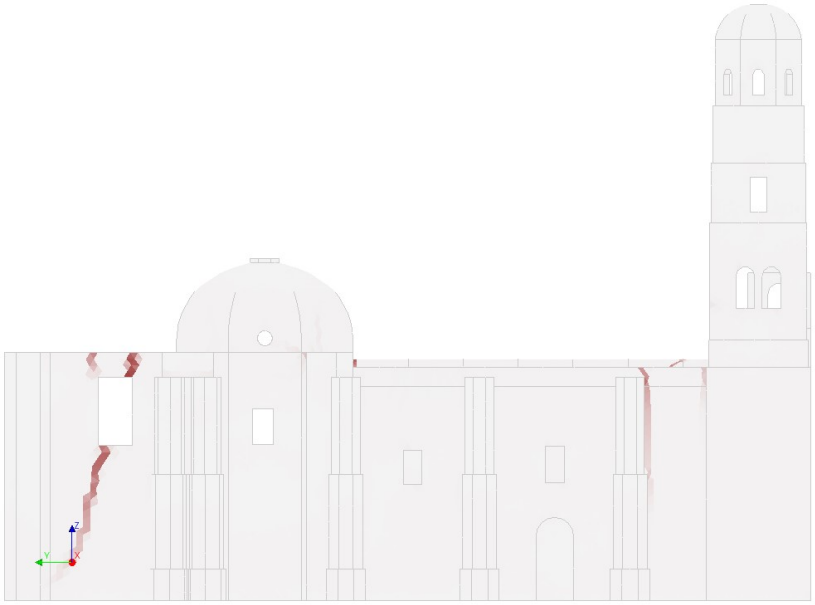

North elevation. Principal strains E1

East Elevation. Principal strains E1

Figure C - 14. Damage caused by the RFPP record.

C.1.8. THEZ. Puebla, Mexico

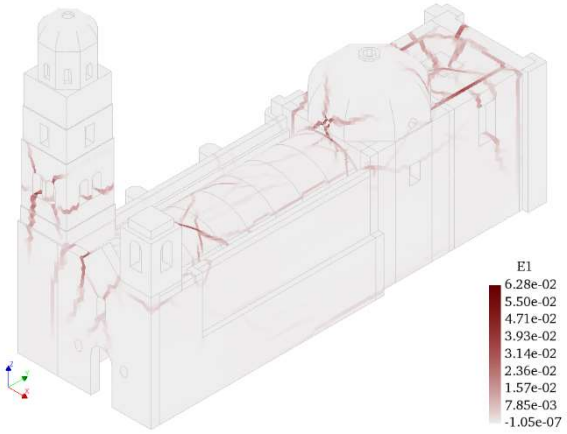

Principal strains E1

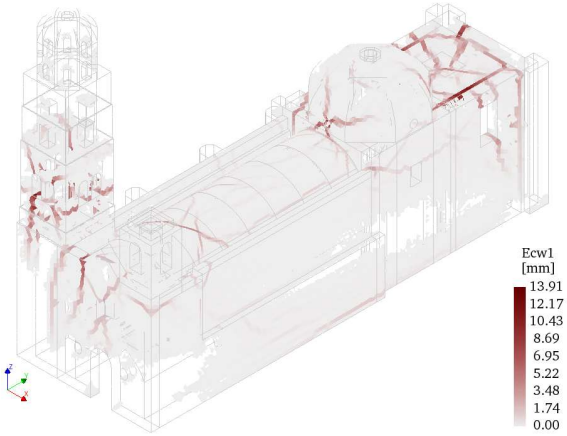

Crack width Ewc1

Plan view of the roof (extrados)

Plan view of the roof (intrados)

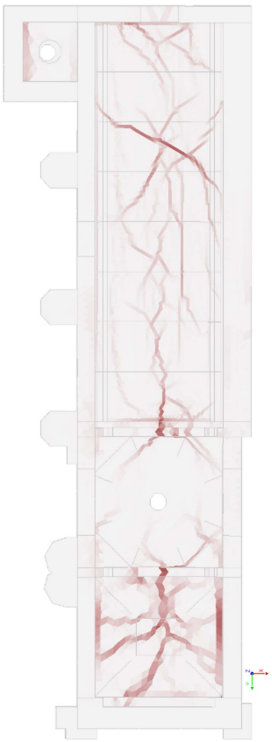

Plan view of the roof (intrados)

Note: choir loft removed.

Figure C - 15. Damage caused by the THEZ record.

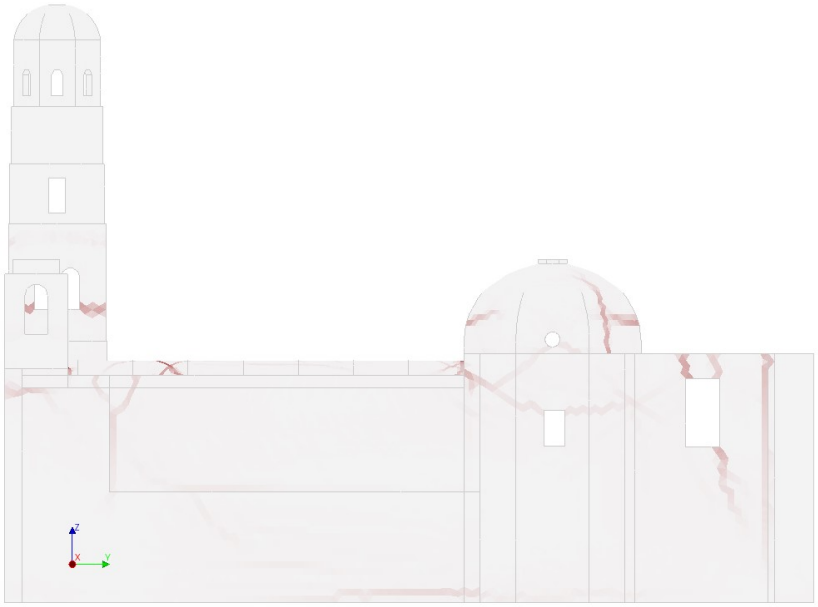

South elevation. Principal strains E1

West Elevation. Principal strains E1

North elevation. Principal strains E1

East Elevation. Principal strains E1

Figure C - 16. Damage caused by the THEZ record.

C.2. Pushover analysis (POA)

C.2.1. Pushover +X

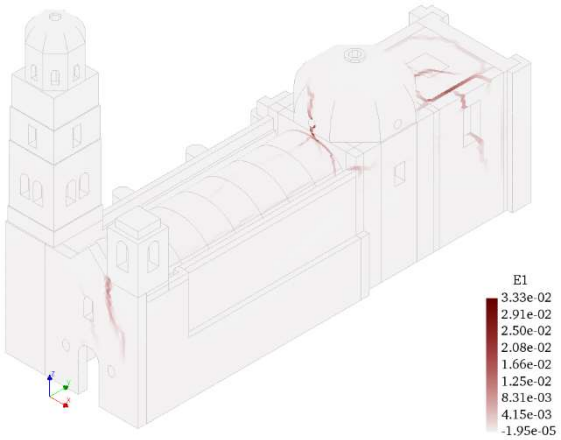

Principal strains E1

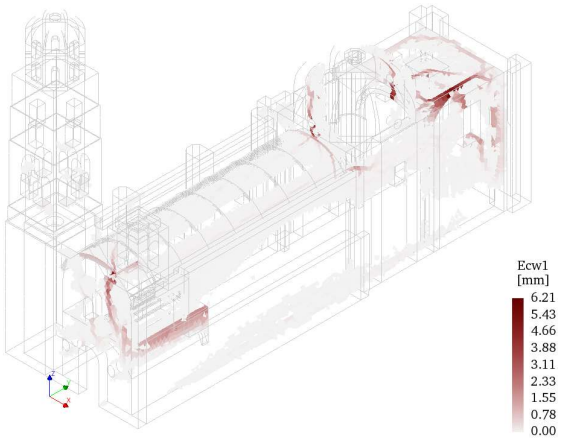

Crack width Ewc1

Plan view of the roof (extrados)

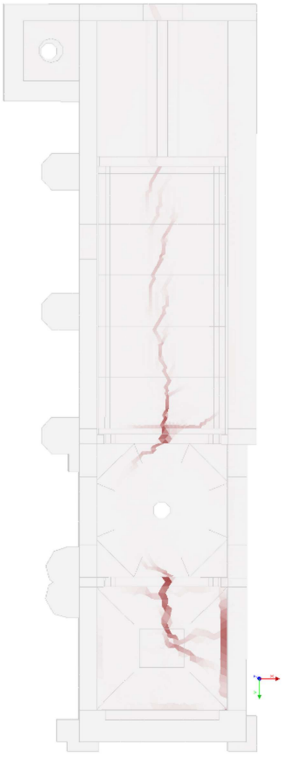

Plan view of the roof (intrados)

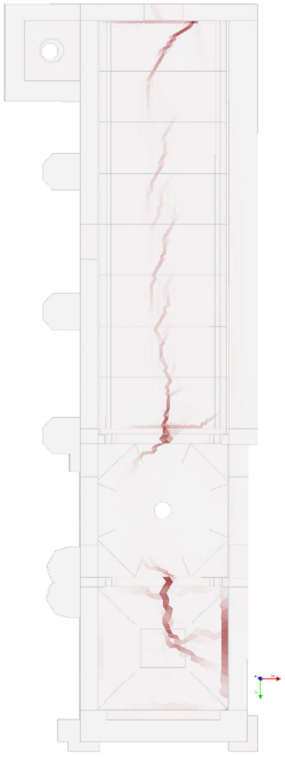

Plan view of the roof (intrados)

Note: choir loft removed.

Figure C - 17. Post-peak damage state caused by the Pushover analysis +X.

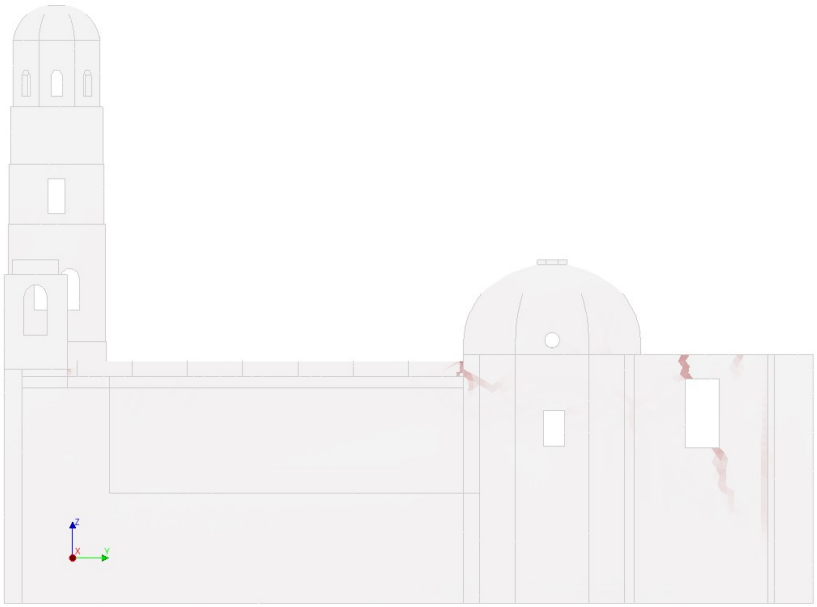

South elevation. Principal strains E1

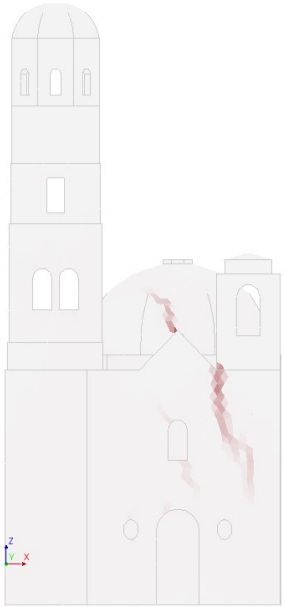

West Elevation. Principal strains E1

North elevation. Principal strains E1

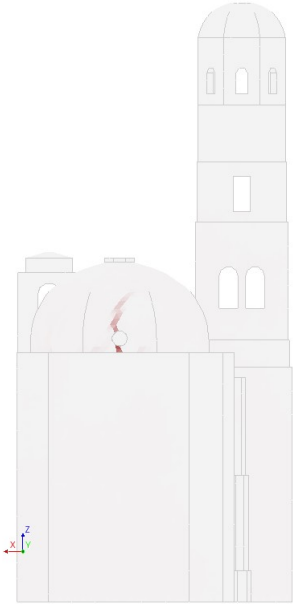

East Elevation. Principal strains E1

Figure C - 18. Post-peak damage state caused by the Pushover analysis +X.

C.2.2. Pushover -X

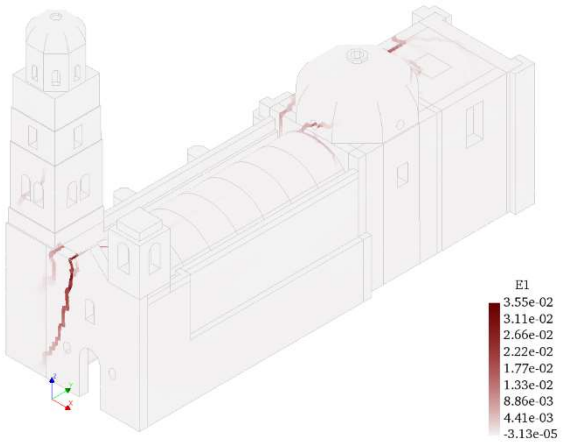

Principal strains E1

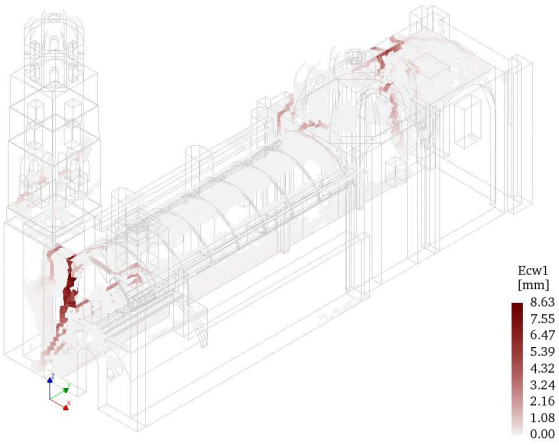

Crack width Ewc1

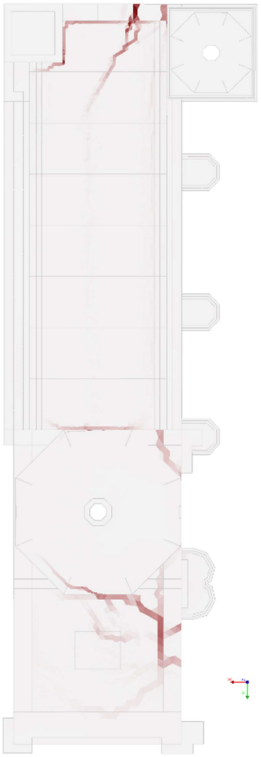

Plan view of the roof (extrados)

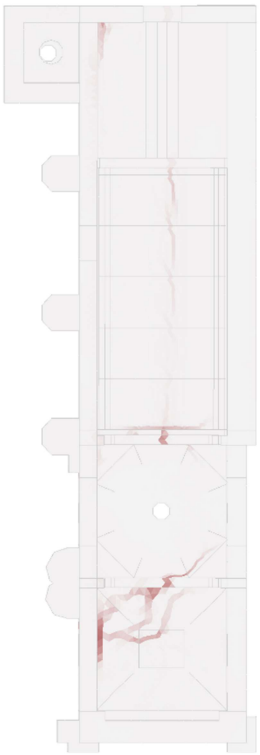

Plan view of the roof (intrados)

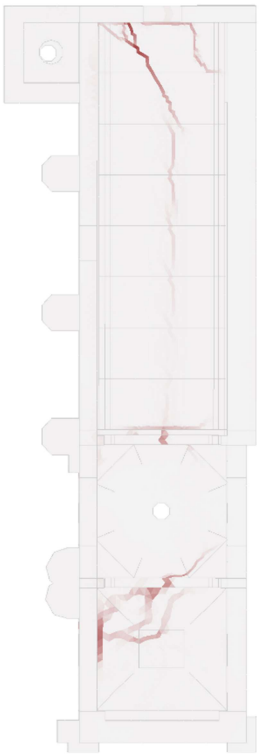

Plan view of the roof (intrados)

Note: choir loft removed.

Figure C - 19. Post-peak damage state caused by the pushover analysis -X.

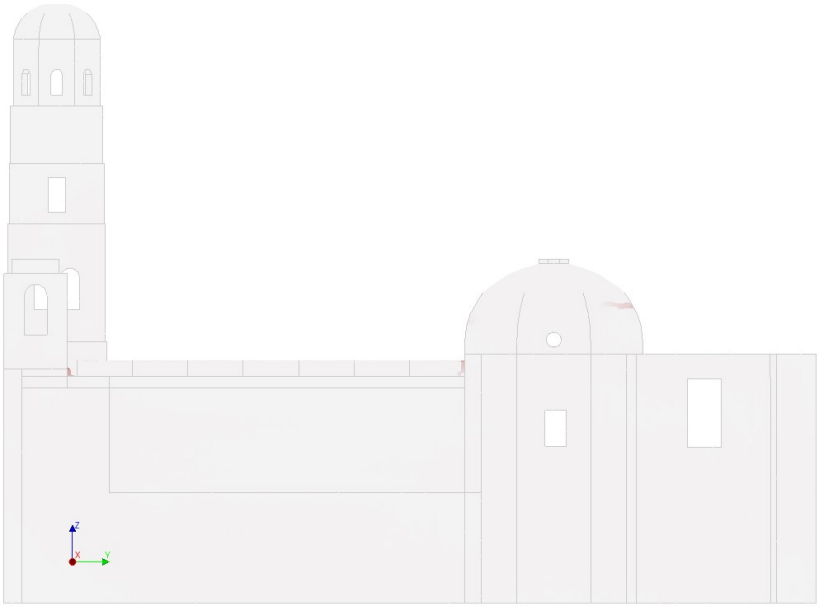

South elevation. Principal strains E1

West Elevation. Principal strains E1

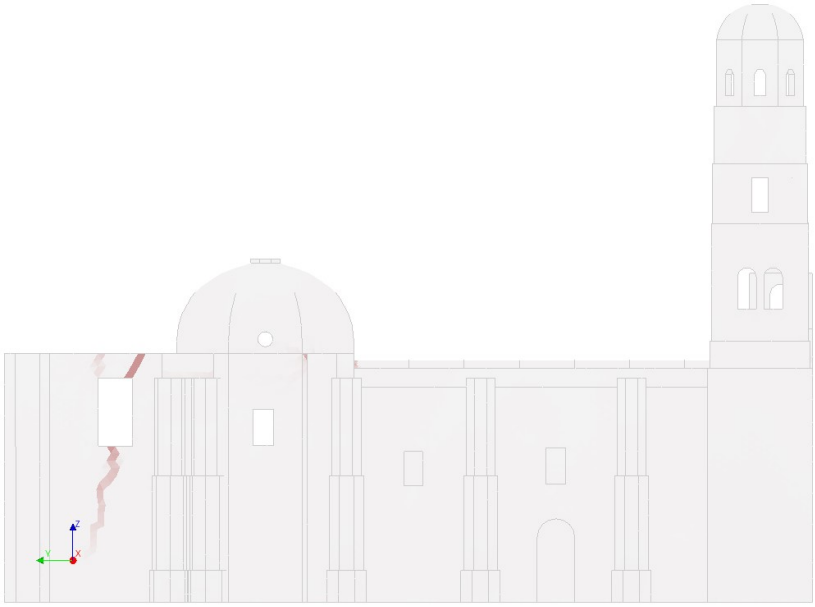

North elevation. Principal strains E1

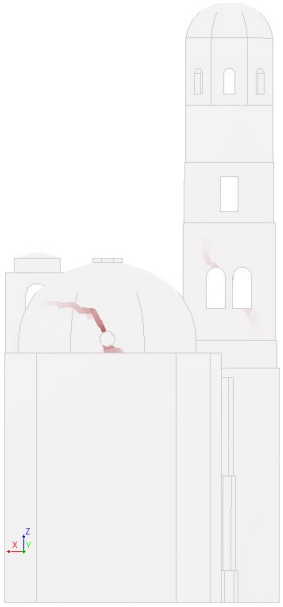

East Elevation. Principal strains E1

Figure C - 20. Post-peak damage state caused by the pushover analysis -X.

C.2.3. Pushover +Y

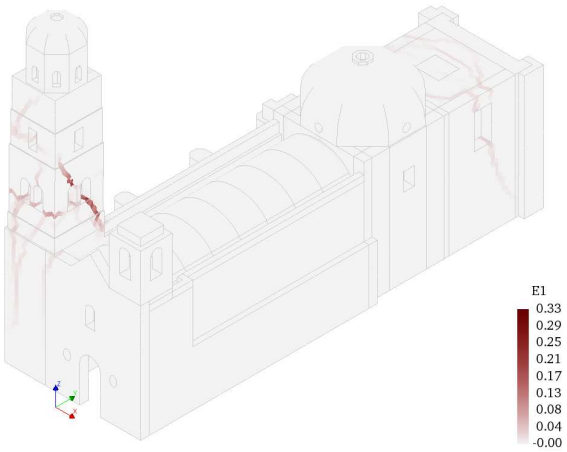

Principal strains E1

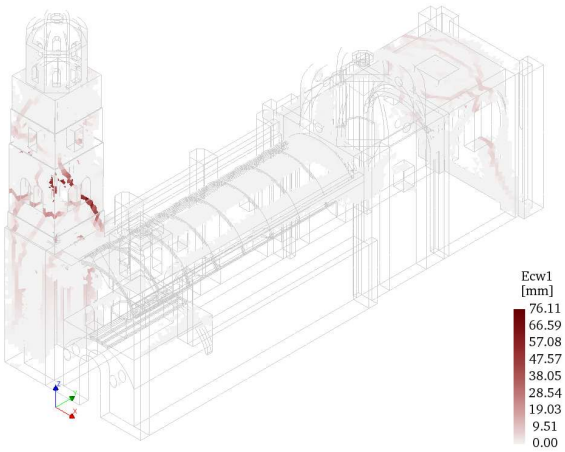

Crack width Ewc1

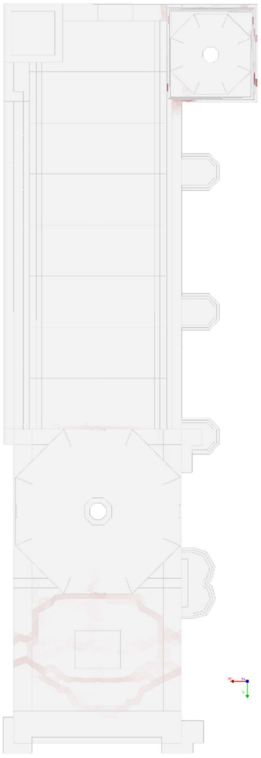

Plan view of the roof (extrados)

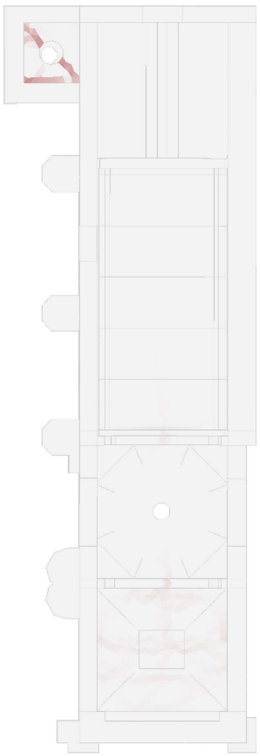

Plan view of the roof (intrados)

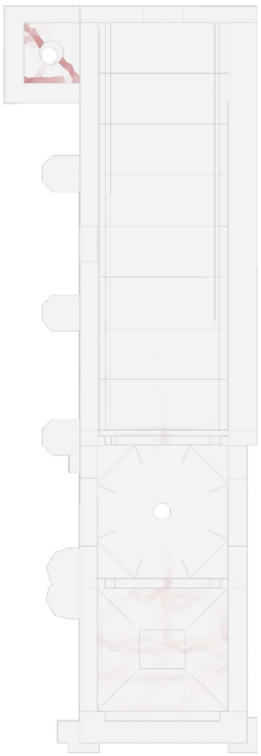

Plan view of the roof (intrados)

Note: choir loft removed.

Figure C - 21. Post-peak damage state caused by the pushover analysis +Y.

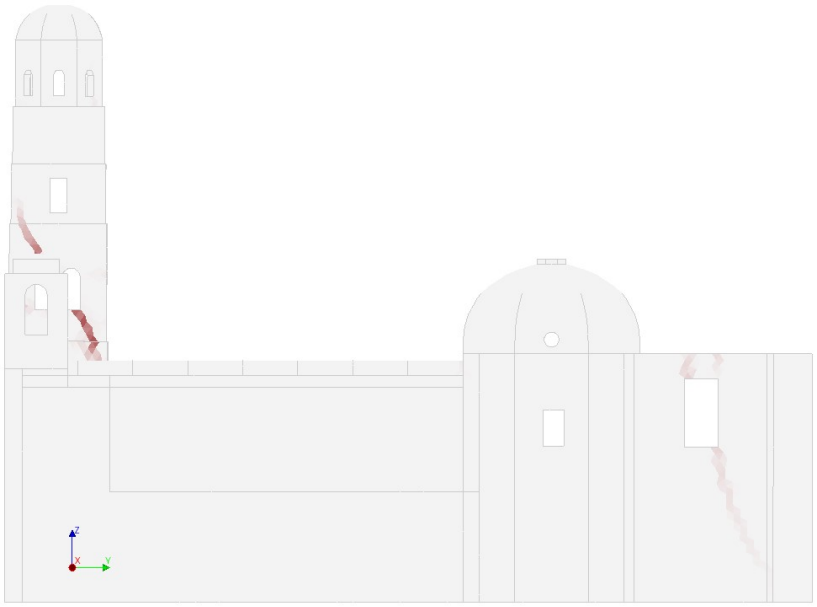

South elevation. Principal strains E1

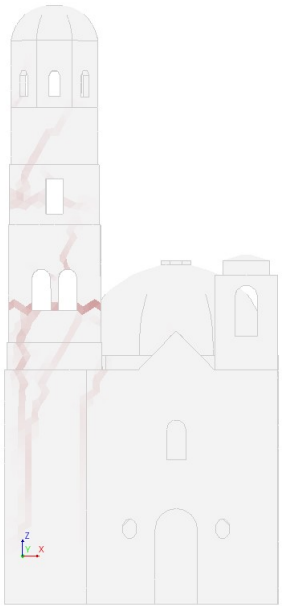

West Elevation. Principal strains E1

North elevation. Principal strains E1

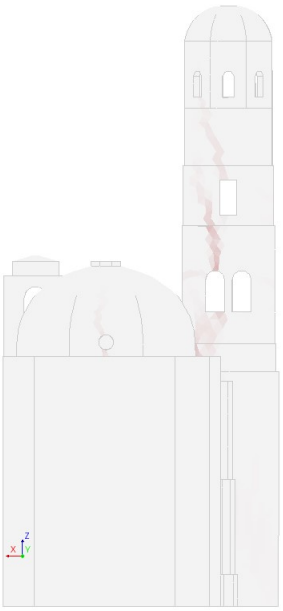

East Elevation. Principal strains E1

Figure C - 22. Post-peak damage state caused by the pushover analysis +Y.

C.2.4. Pushover -Y

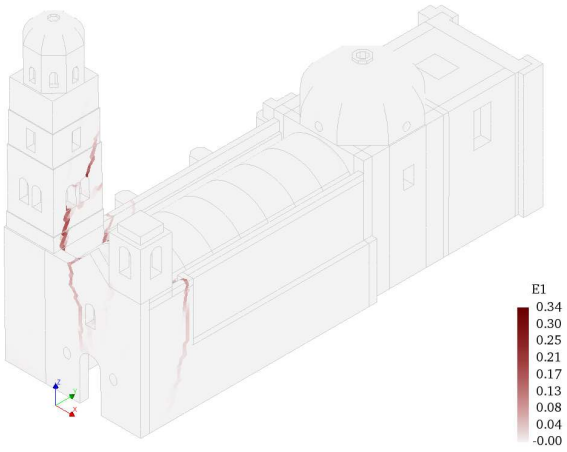

Principal strains E1

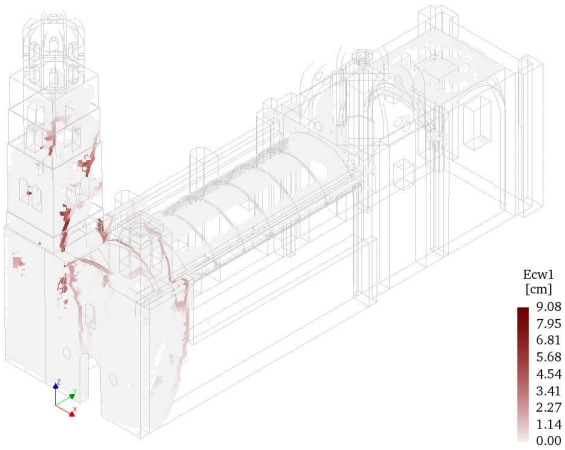

Crack width Ewc1

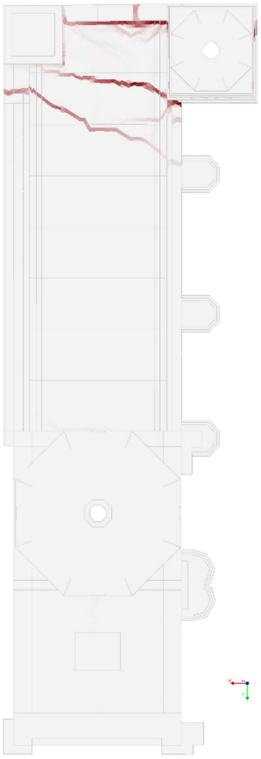

Plan view of the roof (extrados)

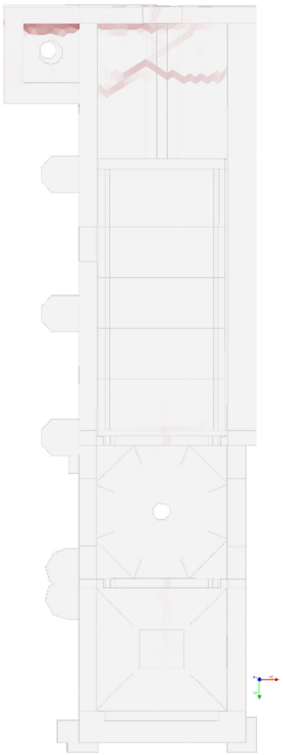

Plan view of the roof (intrados)

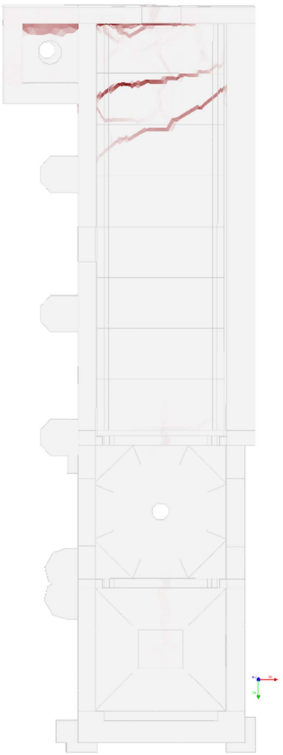

Plan view of the roof (intrados)

Note: choir loft removed.

Figure C - 23. Post-peak damage state caused by the pushover analysis -Y.

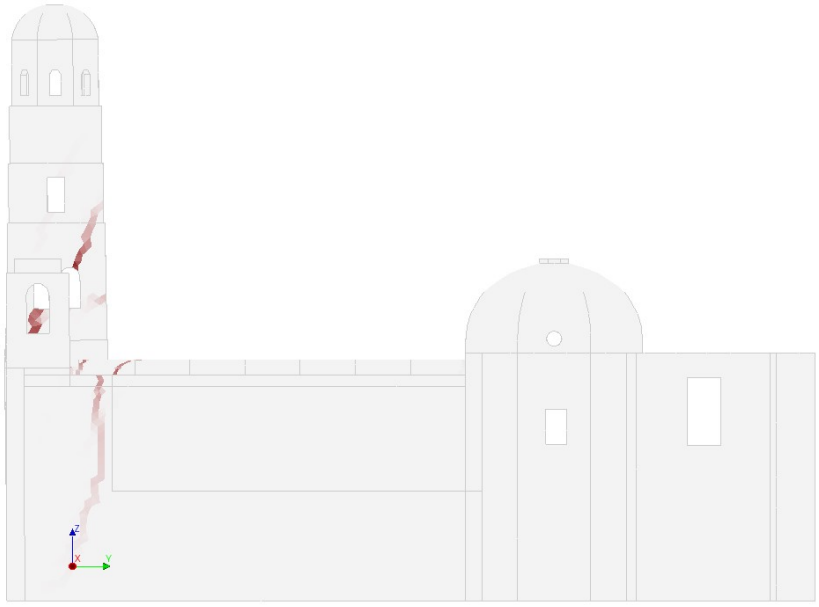

South elevation. Principal strains E1

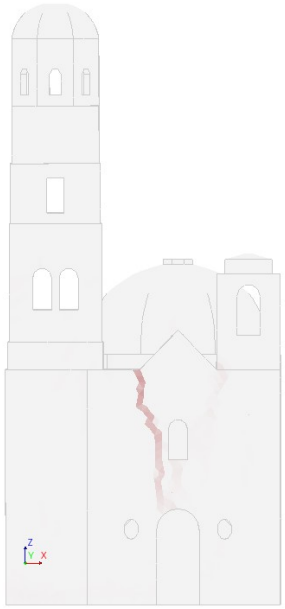

West Elevation. Principal strains E1

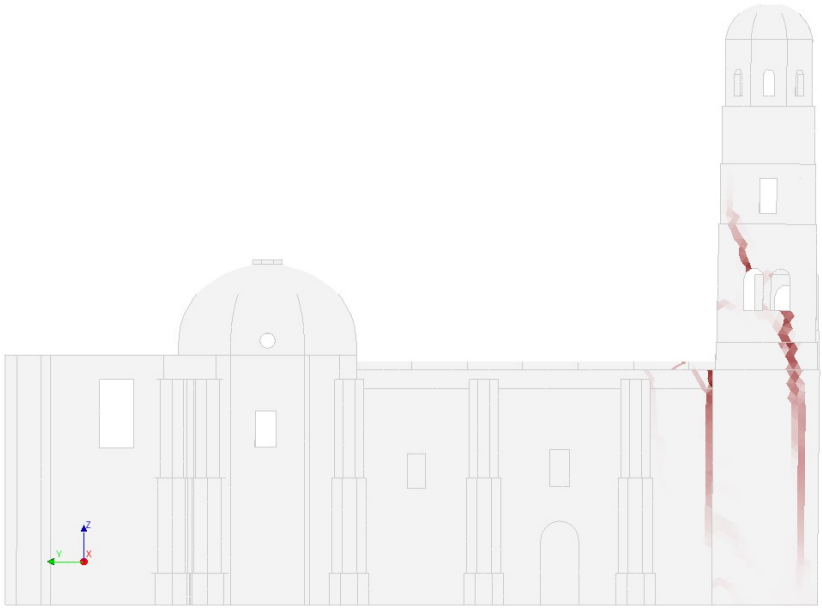

North elevation. Principal strains E1

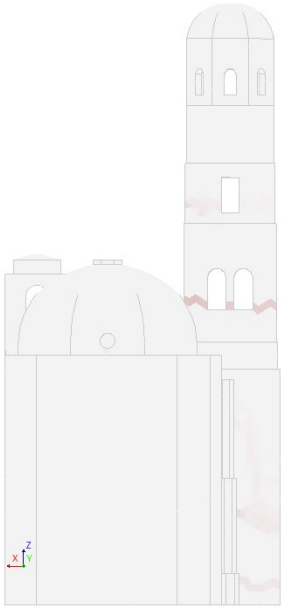

East Elevation. Principal strains E1

Figure C - 24. Post-peak damage state caused by the pushover analysis -Y.

Annex D
Typical failure mechanisms for Mexican churches

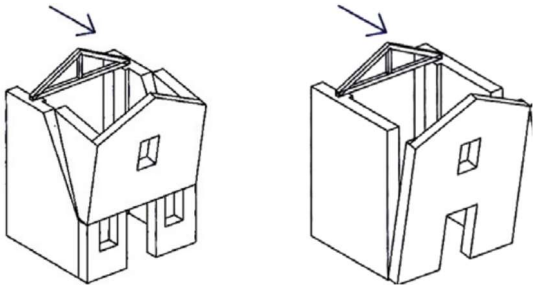

Figure D - 1. M.1 Overturning of the façade (DPCM, 2015).

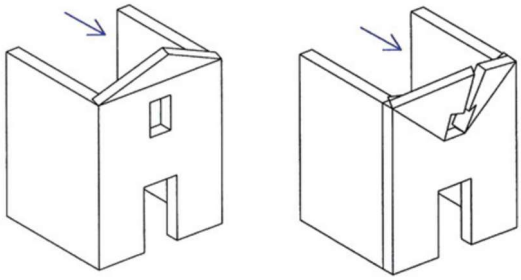

Figure D - 2. M.2 Mechanisms in the pediment of the façade (DPCM, 2015).

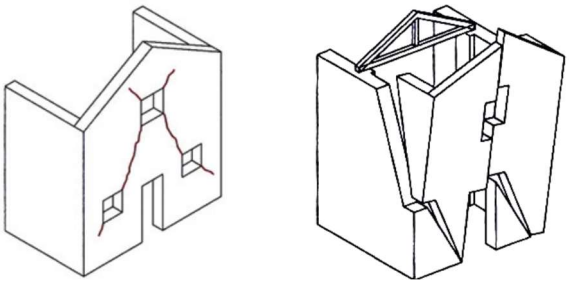

Figure D - 3. M.3 In-plane mechanisms in the façade (DPCM, 2015).

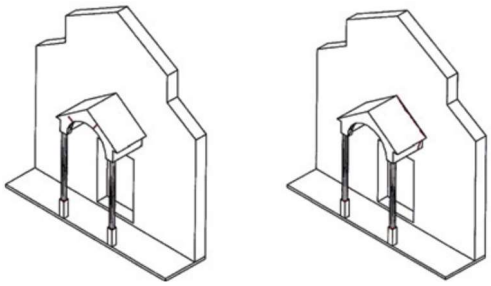

Figure D - 4. M.4 Prothyrum and nartex (DPCM, 2015).

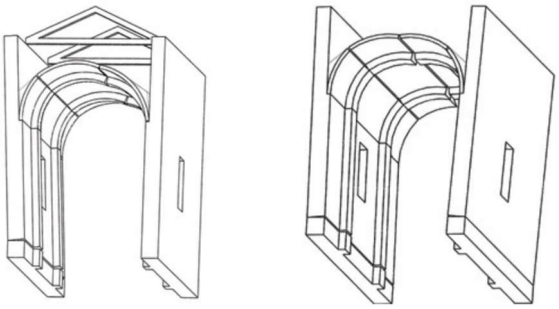

Figure D - 5. M.5 Transverse response of the nave (DPCM, 2015).

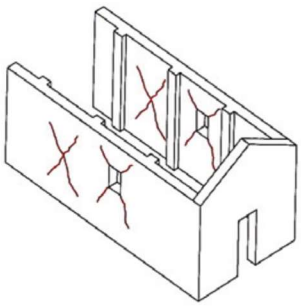

Figure D - 6. M.6 Shear mechanisms in lateral walls (DPCM, 2015).

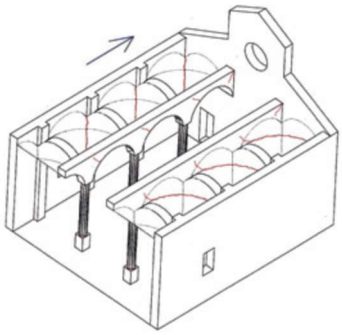

Figure D - 7. M.7 Longitudinal response of the colunnade (DPCM, 2015).

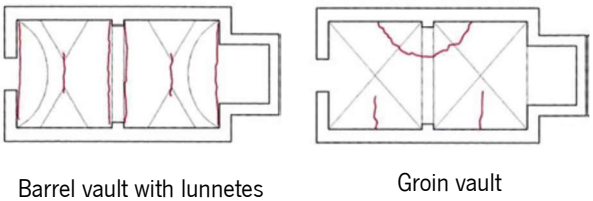

Figure D - 8. M.8 Vaults of the central nave (DPCM, 2015).

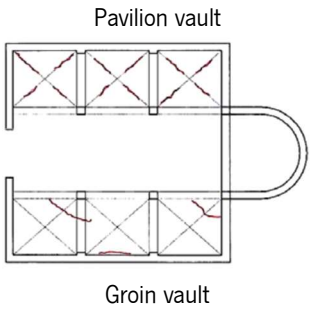

Figure D - 9. M.9 Vaults of the lateral naves (DPCM, 2015).

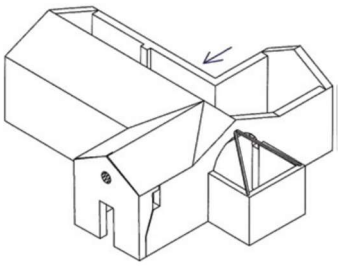

Figure D - 10. M.10 Overturning of the end walls of the transept (DPCM, 2015).

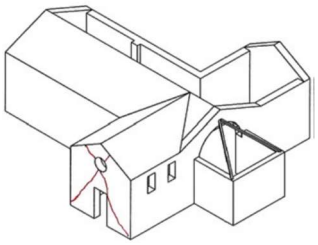

Figure D - 11. M.11 Shear mechanisms in the walls of the transept (DPCM, 2015).

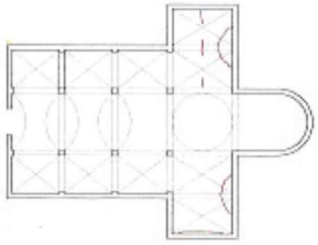

Figure D - 12. M.12 Vaults of the transept (DPCM, 2015).

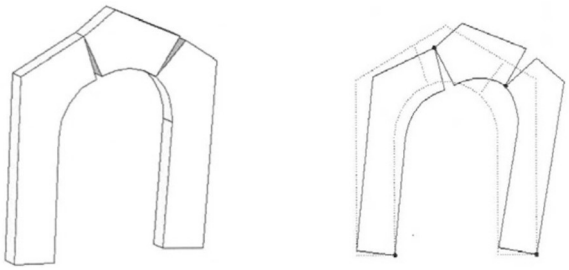

Figure D - 13. M.13 Transverse arch (DPCM, 2015).

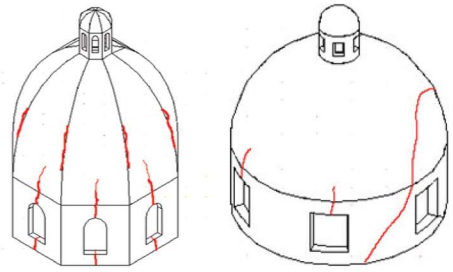

Figure D - 14. M.14 Dome and drum (DPCM, 2015).

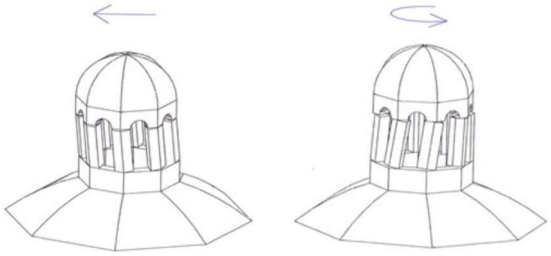

Figure D - 15. M.15 Lantern (DPCM, 2015).

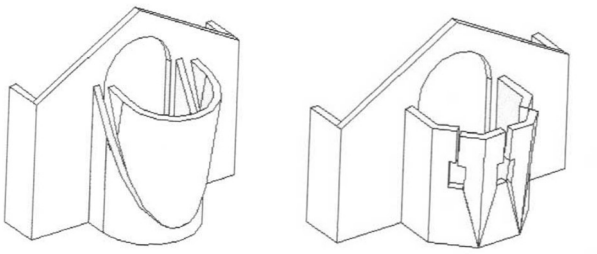

Figure D - 16. M.16 Overturning of the presbytery or apse walls (DPCM, 2015).

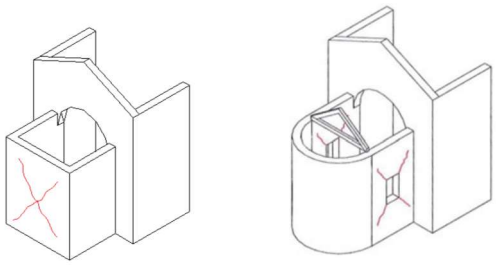

Figure D - 17. M.17 Shear mechanisms in the walls of the presbytery or apse (DPCM, 2015).

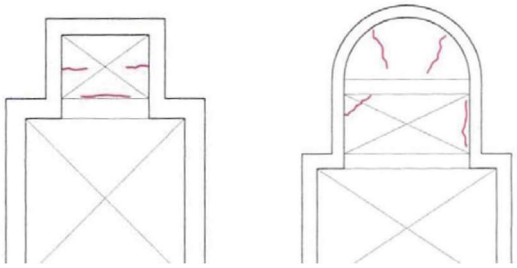

Figure D - 18. M.18 Vaults of the presbytery or apse (DPCM, 2015).

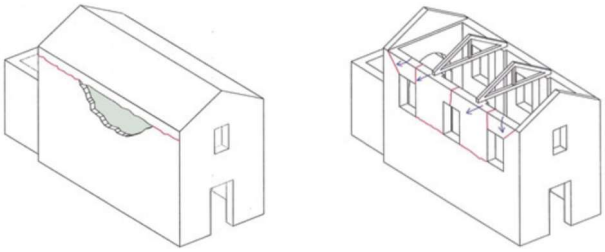

Figure D - 19. M.19 Roof elements: nave (DPCM, 2015).

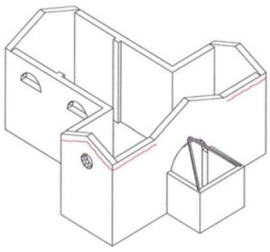

Figure D - 20. M.20 Roof elements: transept (DPCM, 2015).

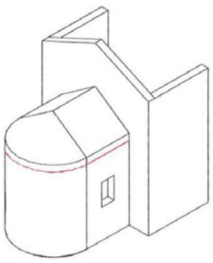

Figure D - 21. M.21 Roof elements: apse (DPCM, 2015).

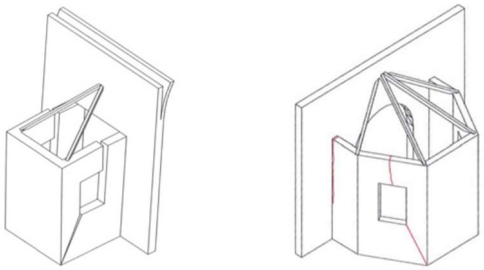

Figure D - 22. M.22 Overturning of the chapels (DPCM, 2015).

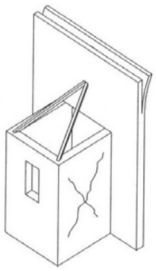

Figure D - 23. M.23 Shear mechanisms in the chapels (DPCM, 2015).

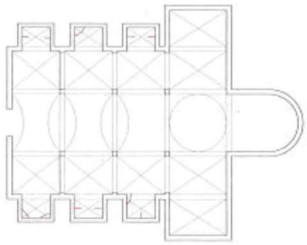

Figure D - 24. M.24 Vaults of the chapels (DPCM, 2015).

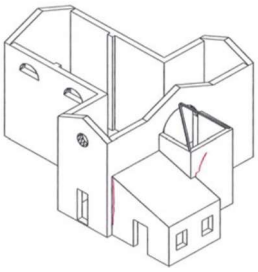

Figure D - 25. M.25 Irregularity interactions (DPCM, 2015).

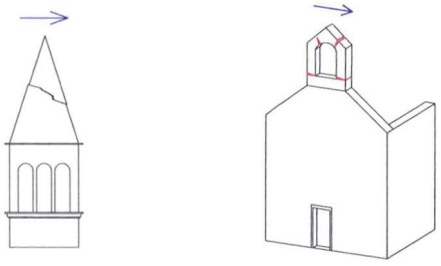

Figure D - 26. M.26 Exterior volumes (gable, pinnacles, statues) (DPCM, 2015).

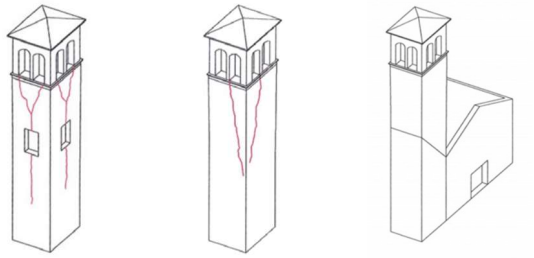

Figure D - 27. M.27 Bell tower (DPCM, 2015).

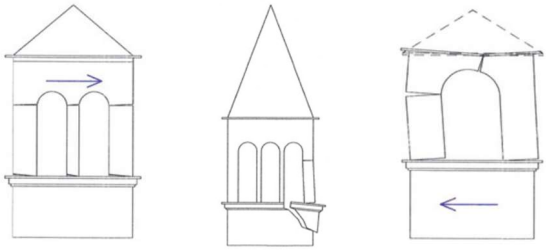

Figure D - 28. M.28 Belfry (DPCM, 2015).

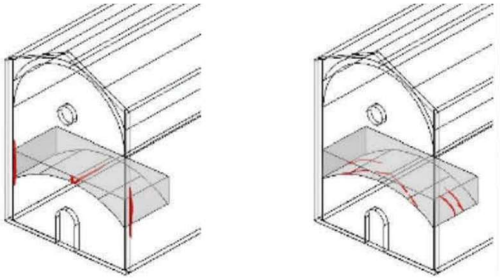

Figure D - 29. M.29 Choir loft (Fuentes et al., 2019)

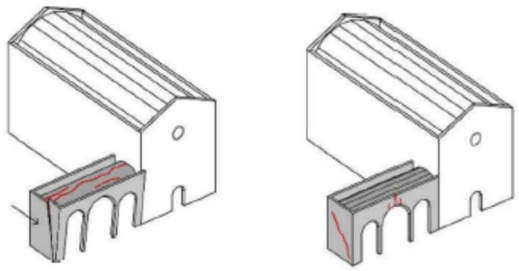

Figure D - 30. M.30 Open chapel (Fuentes et al., 2019).